THE POTENTIAL OF HIGH RESOLUTION PALAEOCLIMATE RECONSTRUCTION FROM ARCTICA ISLANDICA

Laura Foster

A Thesis Submitted for the Degree of PhD
at the
University of St. Andrews

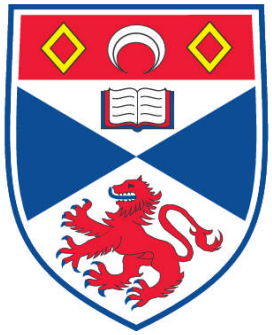

2007

The potential of high resolution palaeoclimate reconstruction from *Arctica islandica*.

Laura Foster

Submitted for the degree of Doctor of Philosophy,

School of Geography and Geosciences,

University of St. Andrews.

18th June 2007

“Fool: Canst tell how an oyster makes his shell?

KING LEAR: No.

Fool: Nor I neither; but I can tell why a snail has a house.”

King Lear

I, Laura Foster, hereby certify that this thesis, which is approximately 65,000 words in length, has been written by me, that it is the record of work carried out by me and that it has not been submitted in any previous application for a higher degree.

Date Signature of candidate

I was admitted as a research student in October 2003 and as a candidate for the degree of Doctor of Philosophy in October 2003; the higher study for which this is a record was carried out in the University of St Andrews between 2003 and 2007.

Date Signature of candidate

I hereby certify that the candidate has fulfilled the conditions of the Resolution and Regulations appropriate for the degree of Doctor of Philosophy in the University of St Andrews and that the candidate is qualified to submit this thesis in application for that degree.

Date Signature of supervisor

A Unrestricted

In submitting this thesis to the University of St Andrews I understand that I am giving permission for it to be made available for use in accordance with the regulations of the University Library for the time being in force, subject to any copyright vested in the work not being affected thereby. I also understand that the title and abstract will be published, and that a copy of the work may be made and supplied to any bona fide library or research worker, that my thesis will be electronically accessible for personal or research use, and that the library has the right to migrate my thesis into new electronic forms as required to ensure continued access to the thesis. I have obtained any third-party copyright permissions that may be required in order to allow such access and migration.

Date Signature of candidate

ABSTRACT

The potential of *Arctica islandica*, a long lived marine bivalve with a lifespan of over 300 years, to reconstruct a high resolution (sub-annual) climate record is explored in this thesis. Fluctuations in trace element and isotopic data from live-collected specimens from Irvine Bay, NW Scotland are compared to instrumental (particularly temperature) data.

X-ray absorption spectroscopy data demonstrate the coordination state of Sr and Mg within the shell. These are consistent with models in which Sr substitutes ideally for Ca in aragonite, and Mg is bound predominantly to organic molecules.

Sr/Ca incorporation may be influenced by changes in the crystal nucleation, propagation and growth rate as well as vital effects. However any effect of seawater temperature on Sr/Ca incorporation was obscured by these other factors. Mg concentration is not a linear function of a single environmental variable or organic content within the shell, indicating that Mg uptake is biologically mediated.

Ba variation shows sporadic increases (of >500% above baseline) in both shells, the timing of which is similar between the prismatic layer and umbo region. The maxima are, however, not synchronous between the two shells analysed. The controls on Ba uptake require further research, but low Ba/Ca may reflect Ba/Ca concentrations within the seawater.

Aliquots taken from cod otoliths show that micromilling has negligible effect on $\delta^{18}O$. The range of reconstructed temperature from $\delta^{18}O$ profiles *Arctica islandica* shows good agreement with the sea surface temperature data from the nearby Millport marine station to within 2.1 °C. However, both the interannual and intra-annual variation appears to be sensitive to changes in temporal resolution resulting from

changes in growth rates. Modelling of $\delta^{18}O$ highlights dependence on changes in temporal resolution of the sampling, in addition to temperature and salinity. Results from the radiocarbon pilot study show that *Arctica islandica* is a suitable archive for changes in radiocarbon associated with anthropogenic ^{14}C fluxes.

ACKNOWLEDGEMENTS

This PhD would have not been possible without a great deal of support from many people. Firstly I would like to thank my supervisors Dr. N. Allison and Dr. A. Finch. I am extremely grateful for their support, insight, and encouragement. Secondly, to Dr. C. Andersson Dahl who provided a warm welcome to the Bjerknes centre in Bergen, and who always assisted with my never ending list of questions! I would also like to thank Egil Erichsen who as well as providing guidance on the SEM also provided help that extended beyond his lab.

I have acknowledged a number of people whom assisted me at the end of various chapters, but I would like to reiterate my thanks to them. These include Andy Smith who provided assistance with Mg EXAFS analysis at SR Daresbury station 3.4; Angus Calder, University of St. Andrews who helped with preparation of samples and analysed numerous XRD samples; Andy Mackie, University of St. Andrews for sectioning and polishing the many *Arctica islandica* samples; Richard Hinton and John Craven at the Edinburgh ion probe; Hans Høie at the University of Bergen who provided extensive assistance with the micromill and in particular the sampling of otoliths; Ole Tumyr, Hildegunn Almelid, Jan Kosler and especially Claudia Kruber (who helped even when she had her own PhD to submit!) for their invaluable assistance in the ICP-MS laboratory at the University of Bergen; also to Rune Søraas, Ulysses Ninnemann and Jonathan Wynn for invaluable assistance with analysis of samples in the mass spectrometer; and Tanya Ertunç and Pauline Gulliver from SUERC radiocarbon laboratory who provided invaluable assistance. In addition, I would like to thank Philippa Ascough, and Michael Bird for their helpful comments and insights during my thesis. I also want to thank my fellow students, who helped to make my time at St. Andrews and Bergen much more fun and interesting.

There are many others who also provided assistance so I apologise for not including their names and hope they accept my heartfelt gratitude for their assistance. I also wish to thank Suenje Dallmeier-Tiessen, not only for her professional help in much improving this thesis, but also her continuing friendship and support, and in particular those occasions where she made dinner after late nights in the laboratory. I would also personally like to thank my mum for supporting her daughter in leaving her city job to do something that was in her heart. Finally to Oliver and the menagerie of animals- in particular B&F- who provided support with smiles (and more than once practical assistance) especially when things seemed hopelessly lost, and provided some much needed hot chocolate at these times!

I would also like to thank colleagues at the University of Bangor for allowing me to use some of their shells from their *Arctica islandica* archive and I extend my gratitude to the crew and my fellow scientists of the research ships of the Marion Dufresne, Prince Madog, RV Håkon Mosby and G.O. SARS.

This project was supported by an array of funding bodies including the University of St. Andrews lapsed bursary, EU Marie Curie Training Fellowship (EVK2-GH-00-57123-10), ion microprobe grant (no. IMP223/0504), NERC grant (allocation no. 981.0402), Daresbury SRS grants (41339 and 45027), QRA New Researcher's Award, Marine Studies Postgraduate Award, and Fife Council.

TABLE OF CONTENTS

LIST OF FIGURES

LIST OF TABLES

CHAPTER 1: INTRODUCTION.

Abstract

Arctica islandica is a long lived marine bivalve, which has the potential to provide an archive of palaeoenvironmental conditions. The organism produces aragonite with annual growth bands, which can be used to construct high-resolution multi-shell chronologies using sclerochronology (a method akin to dendrochronology). This chapter outlines key questions that this thesis will address and introduces the key concepts used in the thesis, including the biology of the organism as well as a description of the main sampling site, Irvine Bay, UK.

1.1 Introduction

Reconstructing past environmental conditions is crucial for understanding variations within the environmental system and for modelling changes. Instrumental measurements are limited to approximately the last 50 years (particularly within the marine system), but the use of archives such as marine sediments, ice cores and tree rings can provide reconstructions at much longer time scales. The use of such archives however hinges on whether proxies (such as stable isotopes and trace elements) are used appropriately, and whether their incorporation into such archives is fully understood. Projects such as MARGO (Multiproxy Approach for the Reconstruction of the Glacial Ocean surface) that used different proxies from foraminifera e.g. $\delta^{18}O$, alkenones and Mg/Ca to reconstruct sea surface temperature (SST), highlighted how different proxies can differ when used to reconstruct a single environment factor. The exploration of different proxies for SST, has however, allowed the application of such proxies to become better understood (Kucera *et al.*, 2005).

High resolution, long-term palaeoclimate archives are particularly important to resolve intra-annual and multi-annual variation, which can then provide information on the timing of events, and therefore improve understanding of systems e.g. lead-lag, feedback mechanisms and teleconnections within the climate system. Low-resolution sampling can however result in the loss of such detail and thus, there is a need for high-resolution climate reconstruction to test climate models, and understand variability in past systems. High resolution sampling (compared to lower resolution "bulk" sampling) has also highlighted that many systems, e.g. corals and speleothems, are far more complex on micron scales and hence the extension of macroscopic sampling to meaningful high-resolution reconstruction is not trivial (e.g. Finch *et al.*, 2001; Allison *et al.*, 2005). However, high resolution palaeoenvironmental

reconstruction is crucial to understanding past environmental fluctuations and thus understanding the behaviour of proxies is important if they are to be used to obtain estimates of seasonal and multi-annual climate variations and ultimately to refine our understanding of the climate system.

The deposition of calcium carbonate (particularly aragonite and calcite) by corals (e.g. Lea *et al.*, 1989; Gischler *et al.*, 2005), sclerosponges (e.g. Fallon *et al.*, 2005; Rosenheim *et al.*, 2005) speleothems (e.g. Finch *et al.*, 2003b; Fairchild *et al.*, 2006), otoliths (e.g. Kalish, 1989; Surge and Walker, 2005) and molluscs (e.g. Dodd and Crisp, 1982; Stecher *et al.*, 1996; Takesue and van Geen, 2004) have been studied as potential high-resolution palaeoarchives. These materials provide a chronology through the deposition of growth increments, which can be used to provide an estimate of age with respect to time of death. The composition of these materials is dominated by calcium, oxygen and carbon but many other elements are present at minor (>100 ppm) or trace (<100 ppm) levels.

Bivalves have been used for palaeoenvironmental reconstruction, particularly at higher latitudes where few high resolution marine records are available. Thus, they represent a valuable archive, providing *in situ* records of environmental conditions. Stable isotopes (e.g. oxygen and carbon) and trace element (e.g. Sr, Mg and Ba) have been frequently used for environmental reconstruction (e.g. Klein *et al.*, 1996b; Hart and Blusztajn, 1998; Schöne *et al.*, 2004b; Schöne *et al.*, 2005a). However, the underlying controls, particularly of the trace elements, in such studies are less established than for other systems.

The present thesis aims to gain a better understanding of the potential of *Arctica islandica*, a marine bivalve, to reconstruct palaeoenvironmental conditions. *A. islandica* is an excellent species to study since the organism reaches ages >200 years

depositing annual growth checks throughout its lifespan (e.g. Schöne *et al.*, 2005a). Therefore, it is possible to determine accurately when fluctuations of isotopes (both stable and radiogenic), trace elements and organic compounds occurred. *A. islandica* can in principle act as a high resolution (sub-annual) climate archive (e.g. Jones, 1980; Bennett *et al.*, 1982; Murawski *et al.*, 1982; Witbaard, 1997; Schöne *et al.*, 2005a).

1.1.1 Applications of A. islandica to reconstruct environmental conditions

The use of oxygen isotopes to reconstruct temperature is perhaps one of the most widely applied environmental proxies. Seawater temperature can be reconstructed using the empirically derived equation of $\delta^{18}O$ incorporation in aragonite molluscs of Grossman and Ku (1986) providing the initial $\delta^{18}O$ of the water is known (or can be estimated). This equation has been applied successfully to reconstruct temperature from $\delta^{18}O$ incorporation in *A. islandica* studies (e.g. Weidman *et al.*, 1994; Witbaard *et al.*, 1994; Schöne *et al.*, 2004c; Schöne *et al.*, 2005a; Schöne *et al.*, 2005b). Incorporation of $\delta^{13}C$ is, however, more complex, and may be controlled by a combination of dissolved inorganic carbon within the water and metabolically derived carbon (e.g. Borchardt, 1985; Tanaka *et al.*, 1986; McConnaughey, 1989; Klein *et al.*, 1996a; McConnaughey *et al.*, 1997; Lorrain *et al.*, 2005).

An independent assessment of the accuracy of $\delta^{18}O$ as a palaeoenvironmental proxy within *A. islandica* can be made by using a well-characterised site, such as that at Irvine Bay, SW Scotland. Regular sea surface temperature data, have been collected at a nearby marine sampling station for >50 years.

Trace elements incorporated into the shell of *A. islandica* (Table 1.1) also have the potential to reconstruct climate by using inorganic precipitation models (such as the Sr/Ca vs. temperature calibration by Kinsman and Holland, 1969). This model has been widely applied to sequentially grown aragonites such as speleothems (e.g. Finch *et al.*, 2003b), corals (e.g. Beck *et al.*, 1992; Mitsuguchi *et al.*, 1996; Beck *et al.*, 1997) as well as bivalves (e.g. Hart and Blusztajn, 1998) for climate reconstructions. However, the incorporation of trace elements in bivalves is very poorly understood and a number of different controls are cited within the literature, including taxon, ontogeny, concentrations of elements in the ambient water, physiology, shell mineralogy and architecture (e.g. Carriker *et al.*, 1991; Carriker *et al.*, 1996; Lazareth *et al.*, 2003; Gillikin *et al.*, 2005a; Gillikin *et al.*, 2006). Note that by calling upon biological controls for trace element partitioning (such as taxon, physiology etc), these authors are implying that bivalves (including *A. islandica*) do not comply with simple inorganic precipitation models. The different results for trace elements (even within bivalves) suggest that the trace element uptake into the shell is complex and there is a need for further research (e.g. Putten *et al.*, 2000; Lazareth *et al.*, 2003; Takesue and van Geen, 2004; Tripati *et al.*, 2004; Gillikin *et al.*, 2005a).

This present study of *A. islandica* explores quantitative fluctuations in the trace elements and couples these data to experiments designed to explore how the two trace elements, Sr and Mg are hosted within the shell. Understanding how elements are hosted is crucial for determining whether thermodynamic equations such as those of Kinsman and Holland (1969) are applicable i.e. the element is ideally hosted and thus substitutes randomly for Ca; or whether they are hosted in other phases e.g. discrete phases (e.g. $SrCO_3$) or organics, in which the thermodynamics would differ.

1.1.2 Key questions to be addressed

A comprehensive overview of the potential of *A. islandica* is developed through the thesis, with each chapter tackling a particular question relevant for understanding the potential of the bivalve as an archive for palaeoenvironmental conditions (as highlighted in Figure 1.1). This "ground-truthing" of modern *A. islandica* is crucial to exploit the potential of ancient *A. islandica*, such as those from the nearby Clyde Beds (~11,500-14,000 calendar years BP (Peacock *et al.*, 1977)).

- Chapter 1 will introduce *A. islandica* including the biology and the use of sclerochronology. Background details on the main sampling site, Irvine Bay, UK, will be presented as well as initial characterisation of the samples.

- Chapter 2 uses X-ray absorption spectroscopy (XAS) to analyse how Sr and Mg are hosted within the shell of *A. islandica* i.e. whether they are ideally substituted in aragonite or hosted by e.g. organics. The exchange models applied to palaeotemperature reconstructions assume that the metal (e.g. Sr) substitutes ideally (i.e. randomly for Ca in aragonite).

- Chapter 3 presents quantitative analysis of the prismatic layer of the umbo using Secondary Ion Mass Spectrometry (SIMS). The data show how trace elements fluctuate over time. Measurement of two shells (228 and 248); live-collected at the same time allows comparison of timing of fluctuations and magnitude. This provides an indication of whether changes are dominated by external factors or by internal mechanisms (e.g. vital effects).

- Chapter 4 continues with quantitative analysis in the same two shells but within the prismatic layer of the outer shell using LA-ICPMS (Laser Ablation-Inductively Coupled Plasma Mass Spectrometry) and solution-ICPMS. LA-ICPMS like SIMS provides an *in situ* sampling technique but with larger spot sizes (40 μm vs. 10 μm) and deeper sampling pits ~200-250 μm (compared to <20 μm with the ion probe). However, LA-ICPMS is more widely available with the larger spots sizes being more appropriate to the faster growing outer shell. Solution-ICPMS provided an independent verification of the concentrations measured by LA-ICPMS. A comparison of the two areas of the shells provides information on the controls on the uptake of trace elements and the reproducibility.

- Chapter 5 discusses whether drilling and micromilling (due to the heat and stress generated) influences $\delta^{18}O$ composition of aragonite. $\delta^{18}O$ data are used as a temperature proxy (see Chapter 6), and therefore, it is important to demonstrate that the sampling methods do not modify the composition of aragonite. This is crucial as it underpins whether such samples can potentially provide accurate temperature reconstructions. A selection of *A. islandica* shells was used to measure the percentage conversion of aragonite to calcite. Aragonite otoliths, from cod grown under stable temperatures in a laboratory tank, were used to examine if the conversion affects the measured $\delta^{18}O$.

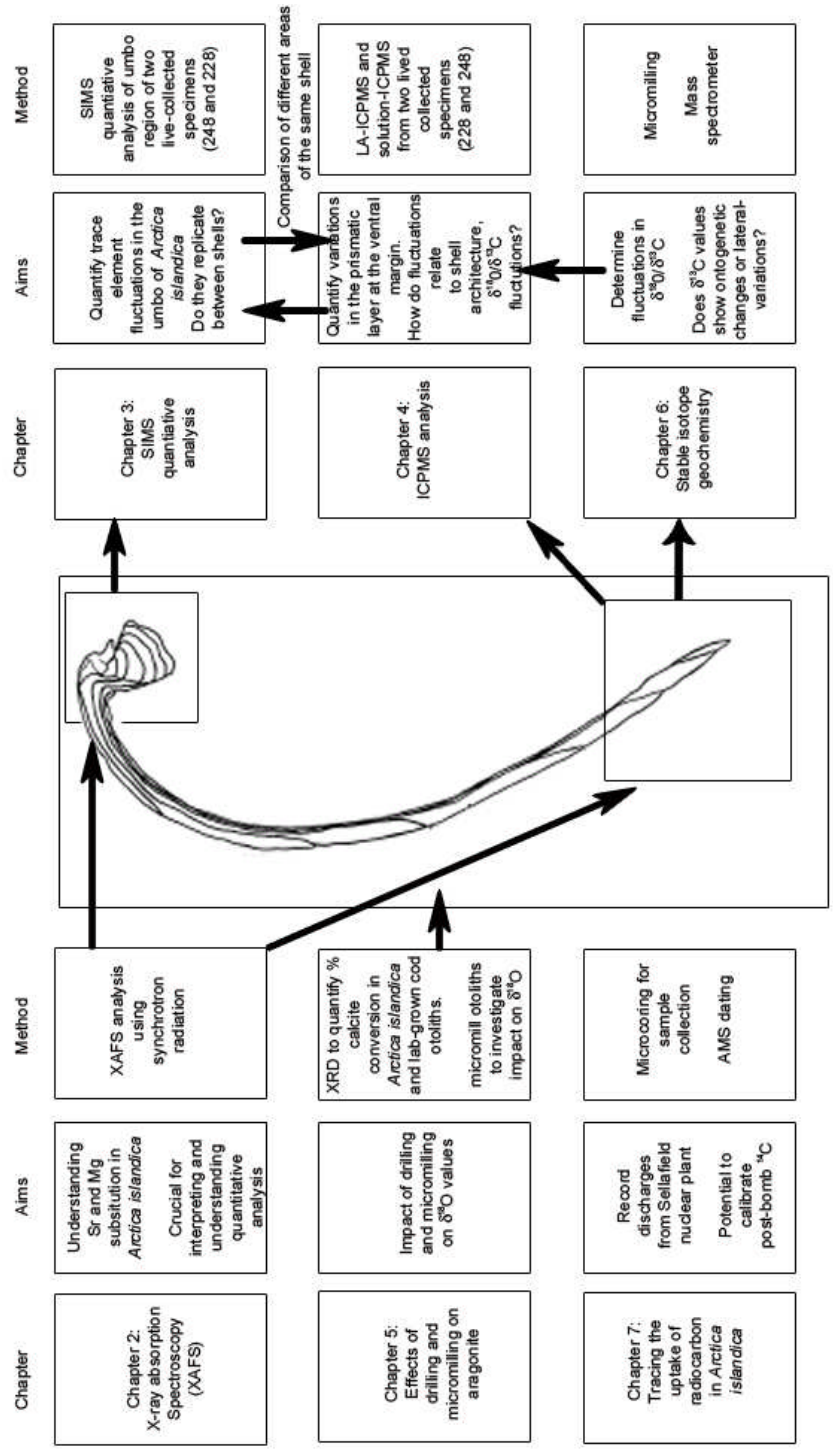

Figure 1.1: Outline of chapters and key questions tackled in each chapter. The arrows indicate how the different techniques provide a multi-faceted approach. For example, XAFS data feeds into the interpretation of the analysis of the prismatic layer in umbo and outer shell layer. Schematic of *A. islandica* taken from Witbaard (1997).

- Chapter 6 examines stable isotope data ($\delta^{18}O$ and $\delta^{13}C$) from the same two shells analysed for trace elements (Chapter 3, 4). $\delta^{18}O$ is examined to determine whether it provides an accurate reconstruction of temperature. The controls on $\delta^{13}C$ are also explored. A simple model explores the relative contribution of temperature and salinity on $\delta^{18}O$ incorporation and investigates how changes in the temporal resolution of the sampling, influence the $\delta^{18}O$ profile. In addition, samples were taken laterally across a single band to measure changes of $\delta^{13}C$, which may be indicative of changes within the Extrapallial Fluid (EPF) as the shell is deposited.

- Chapter 7 is a preliminary study on the ^{14}C fluctuations in *A. islandica* from Irvine Bay, which may be affected by both radiocarbon from nuclear weapons testing in the 1950s as well as discharge from the Sellafield nuclear plant that lies ~150 km south of Irvine Bay.
- Chapter 8 collates the findings and compares data from the prismatic layer measured in both the umbo and outer shell layer of the two shells from Irvine Bay. Data from the $\delta^{18}O$ record, trace element analysis (SIMS and ICPMS), XAS and SEM (Scanning Electron Microscopy) are used to conclude the potential of *A. islandica* for environmental reconstruction.

1.2 Background introduction to *A. islandica*

A. islandica originates from the Cretaceous period and is the now only living species of its genus (Lutz *et al*., 1982). It is known by a number of common names including 'Icelandic cyprina', 'ocean quahog', 'mahogany clam' and 'black clam' (Witbaard, 1997). It is found from the shallow sub-tidal zone to water depths of over 400 m (Nicol, 1951). Its geographical distribution is poorly constrained although it is found on both sides of the North Atlantic continental shelf at latitudes of 35-70˚N. It is usually found at the sediment/water interface (Witbaard, 1997) but can bury several centimetres for periods of up to 24 days (Taylor, 1976) and survive extreme hypoxia (Theede *et al.*, 1969; Oeschger, 1990). *A. islandica* survives on a wide range of substrates, from fine sediments to sand and gravel (Witbaard and Bergman, 2003).

A. islandica generally spawn between June and November, depending on geographical location, with August-October being the most common (Loosanoff, 1953). The larvae can survive up to 60 days in the water column. The recruitment however is very sporadic, with the age distribution from a population in Iceland showing that recruitment increased at approximately 20 year intervals (Thórarinsdóttir, 1990). Once settled on the seabed, *A. islandica* is generally immobile (unless affected by storm surges etc) and hence the environmental data encoded within the shells of live-collected specimens usually relates to the location in which they are found.

The width of the growth bands typically shows a sigmoidal growth curve, with a maximum between 3-7 years with sexual maturity reached around 10-13 years (Thompson *et al.*, 1980b). After this, growth is considerably reduced although annual bands are deposited even in old age (Ropes *et al.*, 1984). The animals can reach ages of >90 years (e.g. Thompson *et al.*, 1980a; Murawski *et al.*, 1982; Kraus *et al.*, 1992)

with specimens >360 years old being reported (Schöne *et al.*, 2005a). The shell extension rate is highly dependent on the local conditions, with those from the Fladen Ground, North Sea showing a slower shell growth rate but greater longevity than those in Irvine Bay. The disparity in growth rates have been attributed to differences in water temperature, sex ratios (with the females being larger than the males), grain size and food supply (Fritz, 1991). Witbaard *et al.* (2003) demonstrated that during years of poor growth, the copepod population was high; suggesting the copepods heavily influences the benthic food supply, and thus growth rate of *A. islandica*.

1.2.1 Morphological and compositional characteristics

A. islandica grows from the tooth/hinge area with three aragonite layers: the prismatic layer, the nacre and the thin myostracum that separates the two. In addition, a periostracum forms on the outside of the shell, which changes from yellowish-brown in young shells to black in older specimens. The composition of the periostracum and the bulk shell determined by X-ray Fluorescence (XRF) is given in Table 1.1. This is discussed in further detail later in the chapter (within section 1.4.1).

The morphology of the shell is shown on Figure 1.2. The line of sectioning (the line of maximum growth) used for shell preparation during this thesis together with maximum growth axis is shown. Deposition of aragonite at the outer margin of the prismatic layer produces a concentric growth pattern (the growth bands), with a gradual thickening of the nacre. The growth lines in nacre do not correspond to those in the prismatic layer. However, the bands formed in the prismatic layer can be traced from the ventral margin to the umbo where they form a condensed record of the depositional increments (Murawski *et al.*, 1982). The umbo has fewer disturbance

bands and is less susceptible to short term environmental events (Thompson *et al.*, 1980a; Richardson, 2001).

The terminology used for the growth bands is confusing, so the nomenclature used throughout this thesis is as outlined in Figure 1.2, with the growth band delimited by what is referred to as the annual "termination band" or annual growth check. The growth edge refers to the most recently deposited material in the prismatic layer (i.e. material within both the umbo and outer shell layer). Quantitative analyses were only taken in the prismatic region within both the umbo and the outer shell layer, i.e. no analyses were carried out in the nacre (or in the myostracum) with the exception of the XAS analyses.

During the growth of the shell, calcification occurs from the extrapallial fluid (EPF), an enclosed space between the mantle and inner shell surface (Figure 1.3). The EPF contains proteins and polysaccharides with its composition different from both the ambient seawater and the shell aragonite (during both periods of growth and non-growth) (Wada and Fujinuki, 1976; Hendry *et al.*, 2001).

During periods of slow growth, growth checks form. These include both annual growth checks and daily growth bands (Schöne *et al.*, 2004). Lutz and Rhoads (1977) hypothesised that daily growth checks originate from increased concentration of the organic matrix, caused by anaerobic-related dissolution of previously deposited calcium carbonate. During anaerobic periods, calcium carbonate may in fact act as a buffer (Crenshaw and Neff, 1969; Taylor and Brand, 1975; Gordon and Carriker, 1978), resulting in periodic shell dissolution (e.g. Dugal, 1939; Wada and Fujinuki, 1976; Richardson, 2001). In other words, the lack of oxygen causes the production of acid (H^+), which is then buffered by the dissolution of the $CaCO_3$ shell. However, increases in the secreted organic matrix or cessation of the calcium carbonate

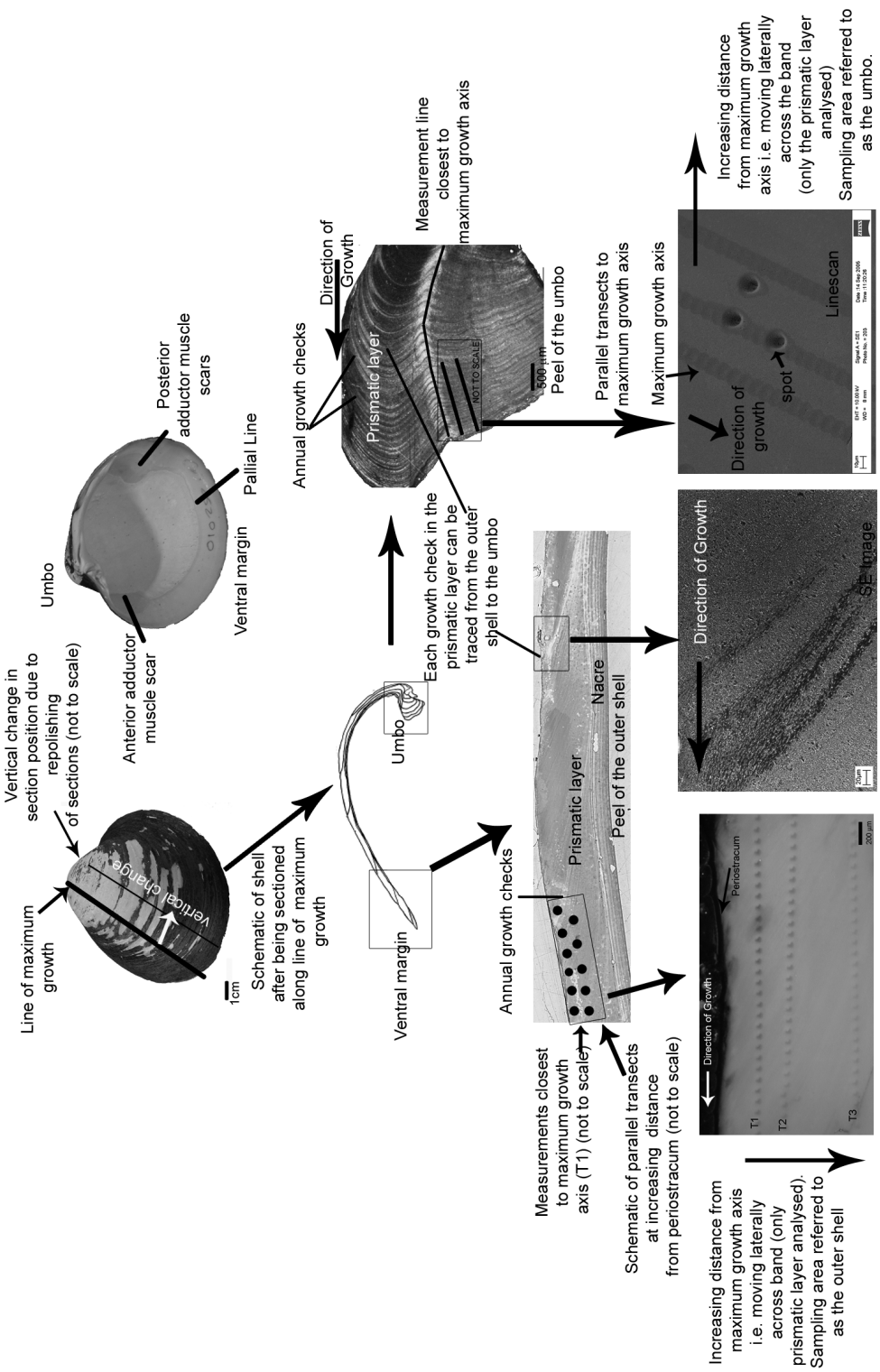

Figure 1.2: Schematic of the morphology of *A. islandica*, together with sampling regime using shell peels, secondary electron images and reflected light micrograph (from different shells). *A. islandica* sketch (not to scale) adapted from Witbaard (1997).

%	Na_2O	MgO	Al_2O_3	SiO_2	P_2O_5	SO_3	Cl	K_2O	CaO	TiO_2	MnO	Fe_2O_3	LOI
Periostracum	0.51	0.39	0.98	11.30	0.10	0.05	0.18	0.18	12.56	0.32	0.01	1.90	71.5

(ppm)	V	Cr	Mn	Fe	Ni	Cu	Zn	Br	Rb	Sr	Y	Zr	Ba	Ce	Pr	Nd	Hf	Pb	Th	U
Arctica islandica (389) outer margin	<LoD	<LoD	14	42	<LoD	<LoD	<LoD	12	<LoD	1190	<LoD	<LoD	16	<LoD	<LoD	<LoD	<LoD	<LoD	<LoD	<LoD
Arctica islandica (389) umbo region	<LoD	<LoD	11	72	4	<LoD	<LoD	19	<LoD	1191	<LoD	<LoD	16	<LoD	<LoD	<LoD	<LoD	<LoD	<LoD	<LoD

Table 1.1: Composition of *A. islandica* determined by X-ray fluorescence (XRF) for periostracum (live collected specimen from Irvine Bay) and prismatic layer (shell 389 used in present study). LOI= Loss on Ignition. Limits of detection (LoD) are typically 2-3 ppm. V, Cr, Cu, Rb, Y, Zr, Ce, Pr, Nd, Hf, Pb, Th, U all below LoD. Further details on the instrument and technique are available at http://www.st-andrews.ac.uk/~acc/MAS.htm

deposition would also increase the organic content, without requiring dissolution (Lutz and Rhoads, 1980).

The presence of an annual growth check in *A. islandica* has been shown by a number of researchers, using a number of methods including mark and recapture (Bennett *et al*., 1982; Murawski *et al*., 1982; Jones, 1980; Weidman and Jones, 1994) and isotope measurements $\delta^{18}O$, $\delta^{13}C$ and $\Delta^{14}C$ (Witbaard, 1997).

The annual growth checks in *A. islandica* result from either a decrease in temperature (Weidman *et al.*, 1994) or a seasonal minimum in the food supply (Thompson *et al.*, 1980a; Turekian *et al.*, 1982; Witbaard, 1997). However, laboratory experiments have shown that shells can grow even at 2˚C given sufficient food supply (Witbaard, Pers. Comm. 2006) and therefore food supply is likely to be a significant control.

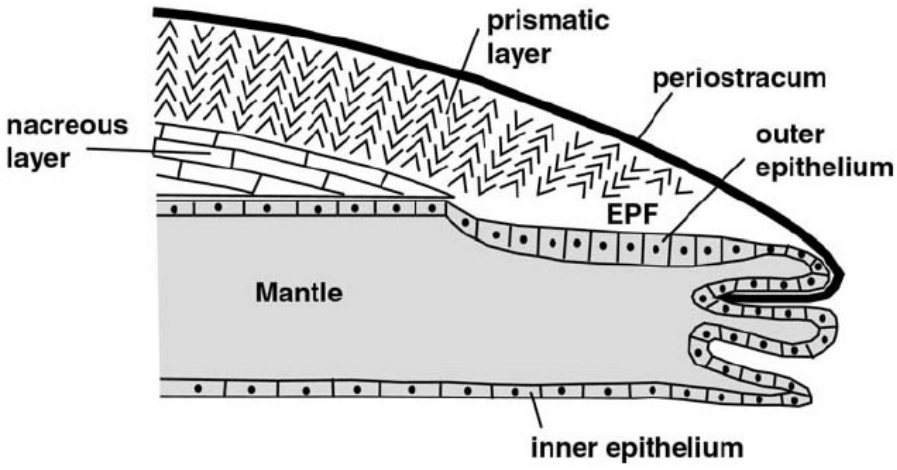

Figure 1.3: Schematic of bivalve section (from Carré *et al.*, 2006). EPF is the Extrapallial Fluid. The myostracum between the prismatic and nacreous layer in *A. islandica* is not shown.

The organism also deposits a growth line when stressed e.g. predator attack, heat shock, abrasion, spawning and storms (Kennish, 1980). However, the discovery of so-called "doublets" in specimens from the Fladen Ground, North Sea has raised questions about our understanding of what determines an annual band (Scourse, Pers. Comm. 2005). "Doublets" refer to where a narrow growth line is deposited before the main growth annual growth check and can be traced to the shell margins. Disturbance lines do not however encircle the shell completely (Richardson, 2001). The cause of these doublets is not known but they are found throughout the shell (including juvenile stages). They may in fact represent one year of good growth followed by one year of very poor growth. Schöne *et al.* (2005b) found that shell growth was interrupted during spawning between early September and mid-November, after which growth recommences, with growth until mid-December in shells taken from the North and Baltic Seas. Such a pattern of growth could therefore give rise to the doublets every year, as juvenile *A. islandica* mimic this reproductive cycle (Thompson *et al.*, 1980b). Hence, juveniles would also have a slower growth period during "pseudo-spawning" phases. An alternative hypothesis is that the doublets form after the growth check has started, but the resuspension of food during the autumn months allows for further growth before the main winter growth check. The uncertainty in the cause of the doublets, increases the uncertainty in age assignment, however the use of $\delta^{18}O$ analysis in Chapter 6 provides further support for the assignment of the annual bands.

1.2.2 Determining annual bands in A. islandica

In order to estimate the age of an *A. islandica* shell, the growth bands are counted. The method first determined by Ropes *et al.* (1984) has not since been greatly

modified. Samples are set in epoxy resin and then sectioned from the umbo to the ventral margin along the line of maximum growth (Figure 1.2) to reveal the growth bands. The sections are then polished to produce a flat surface that is then etched using a weak acid. This enhances the relief by dissolving carbonate causing the organic-rich parts to become relatively prone. In this study 0.1 N HCl was used to etch for 60 s before being rinsed in distilled water. Acetone is then added to the surface of the sample and an acetate peel replica is taken (referred to as a polish). This can then be examined under reflected light, and the annual bands counted. This was the method used during this thesis.

An alternative method has been published by Schöne *et al.* (2005c) in which the section is immersed in a solution of acetic acid, glutardialdehyde and Alcian Blue. Thus, the sample is simultaneously etched with the organic matrix bonded with glutardialdehyde and the Alcian Blue staining the mucopolysaccharides and glucosamides that are enriched near the growth lines (Schöne *et al.*, 2005c). The bands can thus be counted and analysed directly from the shell. However, this method cannot be used for preparing samples for subsequent geochemical analysis.

After trace element analyses, SEM (Scanning Electron Microscopy) was used to determine the position of the growth checks relative to the position of analyses, as well as allowing the study of any changes in the shell architecture.

All these methods allow the age to be calculated by counting the number of growth bands present. If the specimen is live-collected (i.e. the year of death is known), the calendar year of each growth band can be reconstructed. Constructing a chronology in such a way is known as sclerochronology. Sclerochronology can produce multiple-shell records by cross-matching growth bands from different shells.

1.2.3 Sclerochronology

The first step in producing multi-shell records from dead collected samples using sclerochronology is to radiocarbon date each shell to give an approximate guide to the age. The peel is photographed to produce a digitised image and the annual bands are marked with the width of each measured. These measurements are then entered into computer programs such as PAST (http://www.sciem.com), which was developed for dendrochronology, to produce cross-dated time series. Once the ontogenetic growth trend has been removed, the bandwidths can be compared to other shells to see if any similar patterns are present in shells of similar ages. Populations of *A. islandica* respond to environmental stresses in a similar way e.g. during a year of poor food supply, growth will be limited and shells from the same region will show a narrow growth band (e.g. Schöne *et al*., 2003).

Marchitto *et al.* (2000) used seven *A. islandica* shells, collected within ~20 km of each other, from Georges Bank, North Atlantic to produce a 154 year chronology. In the North Sea, Schöne *et al.* (2005c) produced a 121 year chronology for the North Sea with Scourse *et al.* (2006) publishing a 267 year floating chronology from *ca*. 1000-1400 AD. Sclerochronology can thus potentially provide a long time series. However, there is a need to understand what additional data can be extracted from the shell and applied to this chronological framework to reconstruct palaeoenvironment as a function of time.

1.3 Site of research

Irvine Bay on the North-west coast of Scotland (Figure 1.4) provides an ideal sampling location for *A. islandica*. It is close to Millport marine sampling station at which sea surface temperature (SST) measurements are made. Millport is ~22km

north of Irvine Bay and has a daily SST records 1953-1983 and then for every working day from 1983 (P. Barnett, Pers. Comm. 2007). In addition, periodic temperature, salinity, and other environmental data for Irvine Bay itself have been collected. The shallow water site has fast growing *A. islandica*, thus enabling a finer temporal resolution of analysis than those from slower-growing, deeper water sites such as the Fladen Ground, North Sea.

A. islandica samples were collected at 55° 45'N, 4° 54'W by University of Wales, Bangor in May 2001 at a depth of 6 m. Millport and Irvine Bay do not differ greatly hydrographically being affected by the same water masses. Comparison of the intermittent temperature data collected at Irvine Bay at 7 m in a water depth of >30 m (no data was available at 6 m) to that of Millport marine station monthly averages show the latter are representative, with temperature data typically within 1.2 °C (2σ). However, it should be emphasised that Millport data refers to SST measurements, whereas *A. islandica*, a benthic species, was collected at a water depth of 6 m in Irvine Bay. The snapshot data is taken in a water depth of >30 m and thus is not an *in situ* measurement, however the data provides an indication of typical variation in seawater temperatures within this region.

Millport data show that SST typically fluctuate between 13-14 °C in the warmest months (late summer) to 6.5-8 °C in the winter, with water depth <10 m similar to that of Irvine Bay.

Additional sites of research

Additional material was also used from a wide range of sites (Figure 1.5) to address particular issues (outlined in Table 1.2). Synchrotron analysis was carried out on VO5-257-3 from Viking Bank, Northern North Sea to examine changes in the shell,

which occur after the death of the organism. The shell was radiocarbon dated as being modern (i.e. post 1950), (see Chapter 2 for further discussion on this specimen). In addition, XRD samples were taken from specimens from a range of sites; Viking Bank, Northern North Sea; Tjörnes beds, Iceland and Fladen Ground, North Sea.

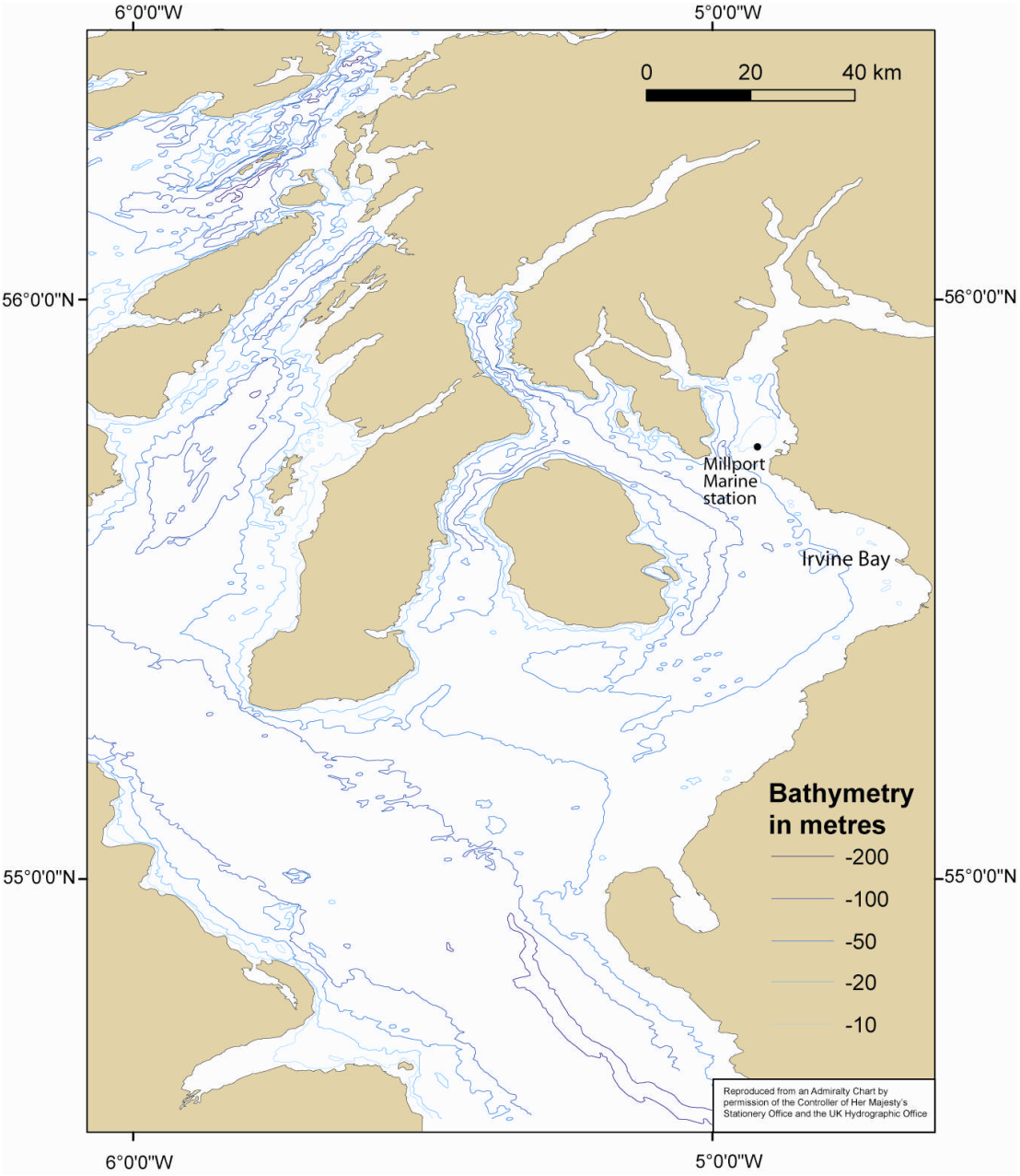

Figure 1.4: Bathymetric map showing Irvine Bay (sampling site) and Millport Marine Station (where sea surface temperature records have been collected for over the last 50 years).

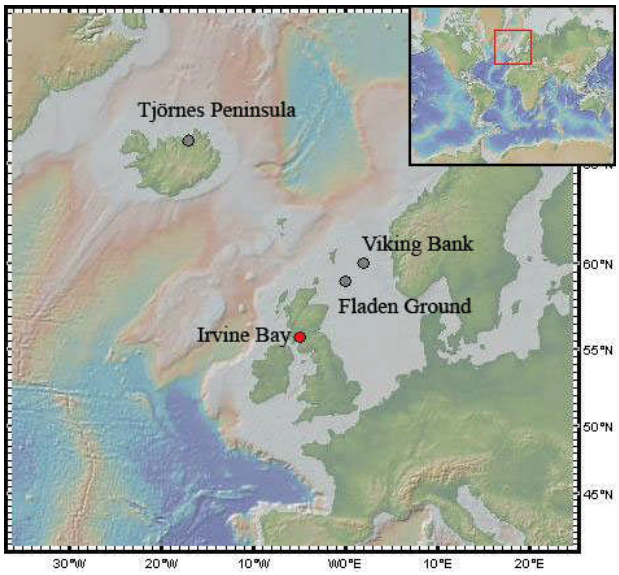

Figure 1.5: Site locations of *A. islandica* specimens used in this study.

Shell name	Location	Latitude	Long	water depth (m)	Live collected?	If Dead collected, estimated age	Age of sample (years) taken from peel	Method and purpose	Chapter
389	Irvine Bay, Irish Sea	55° 45'N	4° 54'W	6	Yes	n/a	47	EXAFS (Sr, Mg), Subsitution of trace elements, ^{14}C	2
VO5-257-3	Viking Bank, North Sea	60° 24'N	2° 20'E	98.3	No	post modern (^{14}C-dated)	n/a	XANES (Mg), XRD milling	2
228	Irvine Bay, Irish Sea	55° 45'N	4° 54'W	6	Yes	n/a	18	SIMS, LA-ICPMS, $\delta^{18}O$, $\delta^{13}C$	3, 4, 6
248	Irvine Bay, Irish Sea	55° 45'N	4° 54'W	6	Yes	n/a	21	SIMS, LA-ICPMS, $\delta^{18}O$, $\delta^{13}C$	3, 4, 6
3.7 Ma	Tjörnes beds, Iceland	66° 00'N	17° 00W	n/a	No	3.7 Ma	n/a	XRD comparison to milled calcite, ^{14}C dating (background sample)	5, 7
VD017	Viking Bank, North Sea	60° 24'N	2° 20'E	98.3	Yes	n/a	n/a	XRD milling	5
313	Irvine Bay, Irish Sea	55° 45'N	4° 54'W	6	Yes	n/a	n/a	XRD milling	5
Dead1	Irvine Bay, Irish Sea	55° 45'N	4° 54'W	From beach	No	unknown	n/a	XRD milling	5
400260	Fladen Ground, North Sea	59° 23'N	0° 30'E	129	Yes	n/a	n/a	XRD milling	5
405	Irvine Bay, Irish Sea	55° 45'N	4° 54'W	6	Yes	n/a	32	$\delta^{18}O$, $\delta^{13}C$	6

Table 1.2: Outline of all *A. islandica* specimens used during this thesis.

1.4 Initial sample characterisation

Initial work to determine the shell composition and structure used XRF and XRD. XRF provided initial quantification of the trace elements to indicate which techniques would be applicable, with XRD providing information on whether *A. islandica* was aragonitic in all areas of the shell (excluding the periostracum).

1.4.1 XRF

X-ray fluorescence (XRF) allows the elemental concentrations of a material to be calculated. Material is bombarded with high-energy X-rays, which can be either absorbed by the atom or scattered through the material. When the former occurs, if the primary X-ray has sufficient energy, electrons are ejected from the inner shells, creating vacancies. However, these vacancies are unstable, with relaxation of the excited atom to ground state occurring when electrons from the outer shells are transferred to the inner shells. This results in energy released in the form of a photon, with an energy equivalent of the difference in the two orbitals involved. This phenomenon is called fluorescence. Each element has electronic orbitals of characteristic energy and hence the energies or wavelengths of the emitted X-rays are used to identify the elements present in the sample, with the intensity of the X-rays indicative of the concentration in the sample.

The emitted X-rays can be detected using an energy dispersive (ED) or wavelength dispersive (WD) detector. ED-XRF, as used here, provides simultaneous detection of multiple elements, focusing all emitted X-rays onto a single detector that analyses the X-rays as a function of energy.

XRF Sample preparation

All samples were analysed on the Spectro-Lab ED XRF instrument at the University of St. Andrews. Two different preparation techniques were used. For the periostracum, where major elements were examined, the periostracum was scraped off the shell surface (a live collected Irvine Bay specimen- not used in other studies). The sample was then powdered and 0.7000 g then mixed with a fixed weight of 50% Lithium Metaborate and 50% Lithium Tetraborate of 2.3000 g. This mixture is fused at 1100 ºC for 20 mins before being cast into a 32 mm diameter glass "bead." A loss on ignition (LOI) is caused by the oxidation and/ or loss of volatiles due to the high fusion temperature. The sum of the LOI and oxides gives a total of 99-100%.

The trace elemental composition was measured in two aliquots of *A. islandica* samples taken from a live-collected shell, 389, from Irvine Bay, Scotland. 389a was taken from the more juvenile part of the shell, incorporating the umbo and early growth of the shell (including nacre), (estimated to be the first ~8-10 years), with 389b from the latter years of growth (including nacre), (estimated to be the last 10-15 years). The shell was powdered by hand approximately 10 g of powdered sample was mixed with 0.2% Polyvinylalcohol binder (Movial). This was then pressed at 12 T into a 32 mm powder pellet.

XRF results and discussion

XRF of the periostracum (Table 1.1) shows that a large proportion (71.5%) of the periostracum consists of volatile components, which are likely to include organic complexes. The composition of the periostracum differed considerably from that of the shell. XRF data from the bulk shell shows that there is little or no difference (with the exception of Fe) in the composition of the material taken from the umbo/juvenile

part of the shell compared to the latter years of growth, suggesting that the composition is relatively homogeneous. At these concentrations, the electron probe microanalyser would have difficulty in detecting changes in trace elements in the shell (such as Sr), but there was sufficient concentration for Sr EXAFS (Extended X-ray Absorption Fine Structure), and for trace elemental analysis using SIMS (Secondary Ionisation Mass Spectrometry) and LA-ICPMS (Laser Ablation- Inductively Coupled Plasma Mass Spectrometry). Further details of these techniques are given in the relevant chapters.

1.4.2 XRD

X-ray Diffraction (XRD) provides information on the structure and phases as well as other structural parameters such as crystallinity, strain and crystal defects. X-ray diffraction peaks are produced by constructive interference of monochromatic beam scattered from each set of lattice planes at a specific angle. The orientation and relative intensity can be used to determine the interplanar spacings of unknown materials. Comparison to known standards (such as ICDD cards (International Centre for Diffraction Data)) allows the compounds to be identified. Mixtures of structures can be analysed with the relative peak height providing quantification by either comparative standards comprising a range of relative concentrations, or through modelling software such as Siroquant^{TM}.

Analysis during this thesis, focused on determining whether aragonite was the only phase that could be detected in *A. islandica*. XRD was used for initial sample characterisation for synchrotron analysis, as well as for understanding how micromilling may change the structure of aragonite (examining *A. islandica* shells and

cod otoliths). The percentage of calcite produced was calculated using Siroquant™ software (see Chapter 5 for further details).

XRD sample preparation

XRD samples were analysed as powders, with randomly orientated grains to ensure all crystallographic directions are "sampled" by the beam. The samples were crushed by hand (under acetone to reduce shear stress on the sample) and then back packed into the holder (no pressure is used as the sample must have randomly orientated grains).

XRD results and discussion

Aragonite was the only phase detected (International Centre on Diffraction Data card 41-1475) within a pristine shell (i.e. live-collected and with the aliquot collected by chipping a section off). The limits of detection of other calcium carbonate (particularly calcite) in an aragonite matrix by XRD are <1% (Finch, unpublished data). However, note that XRD provides no information about materials without long-range crystallographic order such as organic molecules. The XRD findings of aliquots taken from dead-collected specimens e.g. a 3.7 Ma year old specimen, and those sampled by drilling and micromilling are discussed as relevant, with particular emphasis in Chapter 5.

CHAPTER 2: X-RAY ABSORPTION SPECTROSCOPY (XAS).

Abstract

The substitution of trace elements within the shell of *Arctica islandica* is poorly understood, although the manner in which trace elements are hosted provides an indication of whether they are a suitable palaeoenvironmental proxy. Exchange models for trace element substitution in proxies assume that the metal substitutes ideally (i.e. randomly) for Ca in the aragonite. X-ray absorption spectroscopy is an analytical method that allows the substitution of trace elements in solids to be explored. By modelling Sr Extended X-ray Absorption Fine Structure (EXAFS) spectrum of *Arctica islandica*, estimates of the bond distances and the phase angle of electron interaction with the third shell (R_3 and PERCA1 respectively) were determined. These showed that Sr is ideally substituted within *Arctica islandica* (i.e. it is randomly substituting for Ca within the aragonite). Analysis of Mg substitution was limited to the X-ray Absorption Near Edge (XANES) due to the low concentration of Mg within *Arctica islandica* but comparison of the sample to a suite of standards developed by Finch *et al.* (in prep.) show Mg is not hosted within the aragonite, but within organics. Thus, temperature reconstructions using the model of Mg ideally substituted are unlikely to provide accurate temperature reconstructions.

2.1 Introduction

Mollusc shells are 95-99% by weight $CaCO_3$ with the remaining mass being organic molecules (Hare, 1983; Wilbur, 1984; Marin and Luquet, 2004). The organic matrix plays an important role in crystal formation controlling the polymorph, the size, shape and texture (e.g. Herman *et al.*, 1988; Falini *et al.*, 1996; Dietzel *et al.*, 2004; Sato *et al.*, 2006). In biogenic $CaCO_3$ crystals (e.g. bivalves, corals, ammonites), organics do not simply exist between the crystals, but the crystals themselves are composed of densely packed grains, tens of nanometres in diameter, embedded in a thin layer of organic material (Stolarski and Mazur, 2005 and references therein). However, it is not known whether trace elements (Me) such as Sr and Mg in bivalves such as *Arctica islandica* are hosted differently in biogenic calcium carbonate crystals compared to abiogenic crystals used for temperature precipitation studies (e.g. Kinsman and Holland, 1969).

Synchrotron radiation can provide information on whether trace elements are ideally substituted into aragonite i.e. randomly for Ca within the calcium carbonate structure. Temperature reconstructions are based upon the assumption that the metal substitutes ideally, but the metal may also be found in discrete phases e.g. Sr may be present as $SrCO_3$ or within organics, which would have a different partition coefficient (Finch and Allison, 2003). In such cases, reconstructions based on the assumption of ideal substitution will produce erroneous results. However, if the thermodynamics of such a phase e.g. strontianite, were fully understood, this could be applied in the thermodynamic model. However, for phases such as organics, which actually represent a spectrum of phases consisting of both a soluble and insoluble fraction that differ in composition (for a more in-depth description see Marin and Luquet, 2004); the system is very poorly understood.

Kinsman and Holland (1969) showed that Sr substitution in inorganic aragonite decreased linearly with increasing temperatures and this has underpinned its use in palaeotemperature reconstructions. Thermodynamic calculations and inorganic precipitation experiments have shown that Mg substitution in calcite is temperature related (Mucci, 1987; Oomori *et al.*, 1987; Rosenthal *et al.*, 1997). This model has been extended to include aragonite, but Mg substitution in inorganic aragonite seems to be less conclusive. Oomori *et al.* (1987) reported it was not controlled by temperature, with Dietzel *et al.* (2004) finding

> "Mg^{2+} content of aragonite is highly divergent and does not depend on temperature and on Sr^{2+} or Ba^{2+} incorporation. Thus, Mg^{2+} content of the aragonite might be affected by complex adsorption phenomena onto the aragonite crystal surface during precipitation rather than to well-regulated substitution into the crystal lattice."

Thus determining how Sr and Mg are hosted within *A. islandica* can determine their potential for environmental reconstruction. This is key to interpreting the quantitative data from SIMS and ICPMS analysis of the prismatic layer of both the umbo and outer shell layer, which is discussed in the later chapters.

2.2 Introduction to Synchrotron Radiation

Synchrotron radiation (SR) is the electromagnetic radiation (mostly white X-rays) produced by electrons travelling near to the speed of light when they are forced to bend in an arc using strong magnetic fields. SR has a number of unique properties that make it ideal for X-ray absorption spectroscopy (XAS). These include high intensity,

high degree of polarization, high tunability and stability, providing a high signal to noise ratio in XAS data (Newville, 2004). These unique properties have allowed synchrotron radiation facilities to make X-ray absorption measurements at the atomic level, with the history and development of X-ray Absorption Fine structure (XAFS) closely paralleling that of the development of synchrotron facilities (Newville, 2004).

Synchrotron radiation generates an intense, monochromatic beam of X-rays that can be used to measure the XAFS. This can provide information on the electronic configuration, interatomic distances, coordination chemistry and vacant orbitals (Mosselmans, 2005).

2.2.1 Generation of Synchrotron Radiation

Synchrotron radiation is emitted when charged particles travelling at the speed of light, in particular electrons, are forced to move in a circular orbit, causing photons to be emitted as the electron accelerates. The energy of these photons ranges from infrared to energetic (short wavelength) X-rays.

The electrons are generated in the electron gun and then accelerated in a linear accelerator before being transmitted to a circular accelerator (booster synchrotron). Here they are accelerated with the energy reached dependent on the individual machine e.g. 2 GeV at Daresbury, UK. These high-energy electrons are stored in a large outer storage ring. Here they are kept at a constant energy level with the use of RF (Radio Frequency) cavity that receives RF energy and transfers it to electrons as they pass through the cavities. From the storage ring, beamlines process the synchrotron radiation and deliver it to the experimental stations.

Each beamline contains mirrors, which allow some degree of focusing of the radiation. The radiation then passes through the monochromator, which is a double

crystal usually made from Si, which is cooled to maintain an even temperature, to provide high reproducibility and stability (Figure 2.1). Using the Bragg diffraction equation, the monochromator can be adjusted to deliver particular X-ray energy to the sample:

$$n\lambda = 2d \sin\theta$$

Where:

n = is an integer number of wavelengths

λ = wavelength (of monochromatic X-ray beam)

d = distance

θ = angle of diffraction

If the equation can be satisfied for more than one value of n, this can lead to harmonic contamination, as these additional wavelengths do not get absorbed in the same way as the primary beam. The possibility of this type of contamination can be reduced by either changing the angle of the vertical mirror in the beam so it is above the critical angle of the higher harmonics but below that of the desired beam, resulting in them being absorbed, reducing the harmonic content below 0.1% (Mosselmans, 2004). Alternatively by tilting the second crystal to give a slight misalignment can reduce to the harmonics to <1% (Mosselmans, 2004). In other words, these reduce the probability of n being satisfied by values greater than one.

The monochromatic X-radiation then passes through an ion chamber that measures the initial intensity of the beam (I_0) prior to the sample. The chamber consists of two parallel plates (one at high potential) in an inert gas atmosphere. The

current collected off the plate is fed into an amplifier and then a frequency converter to give I_0. In transmission XAS mode, a second identical chamber downstream of the sample measures the intensity of the signal after the sample (I_1). This forms the basis of the XAFS spectrum. However, in all experiments here (with the exception of the strontianite standard) the signal derives from intensity of secondary Sr Kα X-ray fluorescence from the sample. In this case, a multi-element (usually Ge or Si (Li)) solid-state detector is positioned orthogonal to the incident beam (this is to minimise scatter) and measures the fluorescence photons, which are emitted when the outer shell electron drops into a core hole. X-ray fluorescence has the advantage of being able to measure samples that are more dilute but because the signals are smaller than those of the ion chamber readings there is proportionally more electronic noise (Mosselmans, 2005).

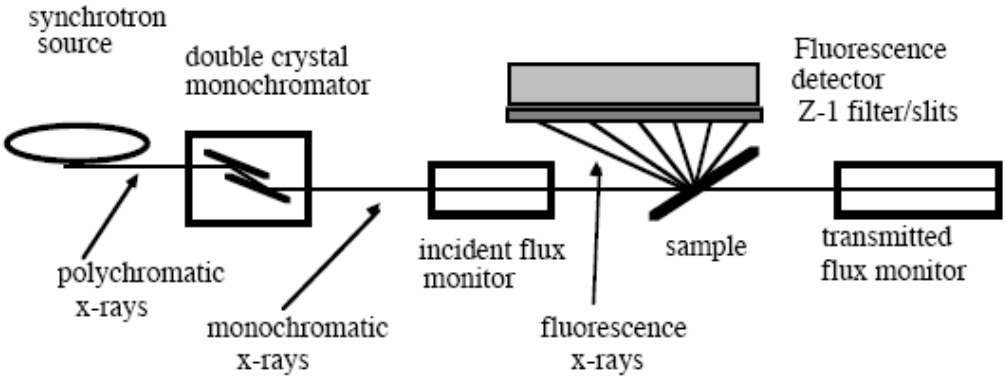

Figure 2.1: Outline of synchrotron experimental station (Bunker, 1997). Note focusing of the beamline with mirrors occurs prior to the X-rays passing through the monochromators (mirrors not shown).

2.2.2 XAFS spectrum

The basis of an XAFS spectrum is the measurement of the interaction of the X-rays with matter as a function of X-ray energy. The interaction involves three processes: elastic scattering, inelastic scattering (Compton) and absorption due to ionisation. This absorption is characterised by Beers formulae:

$I_1 = I_0 e^{(-\mu x)}$

Where:

I_0 = Incident intensity on the sample

I_1 = Exciting intensity i.e. intensity transmitted through the sample

x = Distance travelled through the material or sample thickness

μ = X-ray absorption coefficient of the material

The X-ray absorption coefficient of the material is energy dependent and generally decreases smoothly but has certain discontinuities in its values (Mosselmans, 2004). Measuring the amount of absorption with increasing X-ray energy reveals the so-called absorption edges, where an energy threshold is crossed, which corresponds to the binding energies of K or L electrons in the atom. This occurs when the incident X-ray photon has just enough energy to promote a core electron to a higher unoccupied levels, releasing photoelectrons and leaving one of the core electron levels empty (a so-called core hole). Since every atom has core-level electrons with well-defined binding energies and the X-ray energy of the synchrotron beamline can be tuned to the appropriate absorption edge, the absorption spectrum can be measured. The edge energies relevant to the present study are ~1.31 keV for Mg and ~16.1 keV for Sr.

When the photon energy is low (<30-40 eV of the edge energy) in the near edge region, the photoelectrons populate unfilled bound states, nearly bound state or low-lying continuum states of appropriate symmetry. These spectra are termed X-ray Absorption Near Edge Structure (XANES) or Near Edge X-ray Absorption Fine Structure (NEXAFS). Above this (to about 1000 eV beyond the edge), the Extended X-ray Absorption Fine Structure (EXAFS) region transitions are to continuum states (see Figure 2.2). The XANES and EXAFS regions demonstrate a smooth transition from one regime to the other (Miheliç, 2002). The excited state from the absorption event eventually decays (typically within femtoseconds of the absorption) due to X-ray fluorescence (XRF) and the emission of an Auger electron.

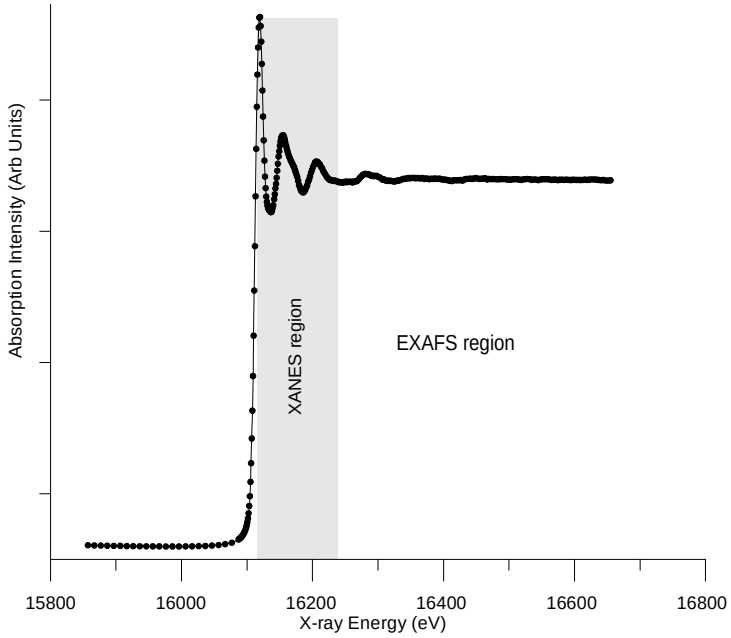

Figure 2.2: XAS spectrum of Sr in *A. islandica*. XANES and EXAFS regions are shown.

XANES region

For XANES, where the electron's kinetic energy is small, the multiple scattering caused by other atoms is significant, making it particularly sensitive to the absolute

position of the edge, the point symmetry (i.e. regular or distorted polyhedra) and the coordination chemistry (e.g. octahedral, tetrahedral coordination). The edge energy correlates with differences in oxidation states of the element since the core electron becomes more tightly bound with increased oxidation (Szulczewski *et al.*, 1997). The XANES spectrum is substantially more complicated to interpret than the EXAFS because it involves multi-electron and multiple scattering interactions. In order to determine the geometrical arrangement of the atoms surrounding the absorbing atom, theoretical multiple scattering calculations can be compared with experimental XANES spectra, but these are applied with limited success in many systems. More typically, XANES studies involve the empirical comparisons of model materials, in which the coordination state is constrained, with a suite of unknowns.

EXAFS region

EXAFS shown on Figure 2.2 shows the oscillatory part of the absorption coefficient above the major absorption edge. This oscillation function $\chi(E)$ is defined as

$$\chi(E) = \frac{\mu(E) - \mu_0(E)}{\Delta \mu_0(E)}$$

Where:

$\mu(E)$ = measured absorption coefficient

$\mu_0(E)$ = smooth background function representing the absorption of an isolated atom

$\Delta\mu_0(E)$ = measured jump in the absorption $\mu(E)$ at the threshold energy E_0.

This oscillation can be calculated (e.g. using a program such as Excurve) for a particular arrangement of atoms to confirm their bond length precise to typically

±0.002 nm, determine the distances, the coordination number to ±1 (if the thermal vibration parameters are known), and species of the neighbors of the absorbing atom. This equation for EXAFS cannot be used for XANES as the number of photoelectrons waves is too low, and the relationship breaks down (Mosselmans, 2004). This is why EXAFS can provide quantitative results, whereas XANES can still only provide semi-quantitative analysis. EXAFS refinement requires the user to know the Debye-Waller factor, which is a measure of the thermal vibration of the central atom in its site. For atoms at room temperatures in single sites, typical Debye-Waller values are ~0.015 $Å^2$ but this increases with temperature (thermal disorder), or if the model averages several non-equivalent crystallographic sites (static disorder). Debye-Waller factors and the coordination numbers are inversely correlated and hence uncertainties in one generate uncertainties in the other. Hence, EXAFS is in practice relatively insensitive to coordination state.

2.3 Method

Two *A. islandica* samples were analysed for Sr and Mg substitution. These were both taken from a live-collected shell 389 from Irvine Bay, Scotland. 389a was taken from the more juvenile part of the shell, incorporating the umbo and early growth of the shell (including the nacre), (estimated to be the first ~8-10 years), with 389b from the latter years of growth (estimated to be the last 10-15 years). An additional shell VO5-257-3, dead-collected, from Viking Bank, Northern North Sea radiocarbon dated as modern (i.e. post-1955) was analysed for Mg substitution, with only the latter years of growth used in the sample. This was to determine if any changes in the substitution occurred after death.

The samples were crushed in an agate mortar and pestle under acetone to achieve a finely ground powder. It is important to gain a homogeneous sample (with no pinholes after mounting) so that the fluorescence signal with respect to I_0 is not distorted (Mosselmans, 2004). Prior to synchrotron analysis, all samples were analysed on an automated Philips PW1050 X-ray diffractometer with Philips WinXRD V2 software at the University of St. Andrews, UK. This is to confirm that the samples are single phase aragonite. Samples were analysed for Sr and Mg coordination at SRS Daresbury Synchrotron facility, Warrington, UK (www.srs.ac.uk/srs), a second-generation light source facility with 2 GeV machine energy. The concentrations of Ba (and U) are too low to permit analysis on the Daresbury beamlines and therefore the substitution of these elements could not be analysed.

2.3.1 Sr analysis

Sample analysis was carried out at station 16.5 with an average beam current of 200 mA. Sr-K edge (~16106 eV) was measured using a spot size <2 mm, achieved through dynamically focused double crystal Si220 monochromator. A vertical focusing pre-mirror is used for harmonic rejection. The sample itself was mounted between adhesive tape, and placed into a letterbox slot on an aluminium plate. This was aligned carefully so the holder did not contaminate the beam measurements. The sample area presented to the beam is ~ 5 x 10 mm. Multiple scans were taken to ensure high signal to noise ratio (~8 cycles). Analysis was started at 15857 eV and extended beyond the edge to an energy corresponding to k=12, residence times were increased from 3 s to 12 s in a manner that was proportional to k^3 (to compensate for loss of signal away from the edge.)

2.3.2 Mg analysis

Analysis was carried out at station 3.4 with an average beam current of 200 mA with increasing residence time away from the K-edge (akin to Sr analysis). Only the XANES part of the spectrum (1280-1380 eV) of Mg K-edge (~1306 eV) was collected due to the weak signal. This was the result of a relatively low X-ray flux and low concentrations of Mg (100-200 ppm) resulting in a too low signal to noise ratio in the EXAFS despite extended count times and high number (>20) of scans. Qualitative interpretation of the substitution of Mg in aragonite is possible by comparison of the spectra to a number of known standards and reference.

The beam was focused with a double crystal Si111 monochromator. The powdered sample was mounted onto carbon tape stuck to an aluminium holder. A number of standards and reference material covering different states of Mg coordination (e.g. Mg in regular octahedral coordination; Mg in distorted octahedral; Mg in distorted 9-fold coordination and Mg in sites with irregular or low symmetry) were analysed as a comparison.

2.4 Data analysis

2.4.1 Sr data analysis

Qualitative analysis of the XANES signal was carried out with manual removal of the background, and comparison to standards of Finch *et al.* (2003a). This provides independent collaboration of the quantitative EXAFS analysis.

EXAFS data analysis was carried out on software provided by SRS Daresbury. Individual cycles were averaged using EXCEL from which text files were exported. Background measurements were removed using SPLINE (Paul Ellis, University of Sydney, 1990). Modelling and refinements of the edge energy (E_f), the thermal

vibration parameters (A_1, A_2 and A_3), the interatomic bond distances of the same shell (R_1, R_2, and R_3) and percentage of Ca in the third shell (PERCA1) (see Finch *et al.*, 2003a for a discussion of how this model was constructed) were carried out with EXCURV98 (Daresbury Laboratories, UK). The refinements were carried out using a single-phase aragonite model developed by Finch *et al.* (2003a), with the initial values those of Sr in aragonite standard (Finch *et al.*, 2003a). The maximum and minimum refinements, and errors were calculated when the average offsets from the optimum values cause a 2.5% increase in the fit index.

In the case of aragonite, nine oxygen atoms form the first shell around the metal ion (Sr or Ca), with six carbon atoms in the second, and six metals atoms in the third shell. Analysis of this third shell is particularly useful as it provides information on whether the third shell is surrounded by Sr or Ca indicative of strontianite and aragonite respectively. This is achieved by inspecting R_3 (the interatomic distance between the central Sr and its nearest metal present in the third shell) and PERCA1 (phase angle of electron interaction with the third shell). R_3 varies from ~4.018± 0.010 Å in aragonite coordination to 4.167± 0.010 Å in strontianite (Finch *et al.*, 2003a) and PERCA1 is scaled to vary from 1 to 0, where 1 represents 6 Sr atoms, and 0 equates to no Sr atoms present in the third shell.

2.4.2 Mg data analysis

Data analysis was carried out manually to remove the background and qualitatively analyse the XANES signal. Comparison of the Mg spectrum to known standards (including those not analysed during this experiment see Finch *et al.* (in prep.)) allowed interpretation of the Mg spectrum. They consist of four types of Mg coordination 1) Mg in a regular octahedral coordination bonded to carbonate

(magnesite, dolomite and calcite); 2) Mg in 9 fold irregular coordination (aragonite) 3) Mg in regular octahedral coordination bonded to silicates and Mg (bentonite, glauconite) 4) Mg in open polycoordinate coordination (organic Mg) (Finch *et al.*, in prep.). In addition, dolomite acted to normalise the K-edge of Mg between analytical sessions (Finch *et al.*, in prep.)

2.5 Results and discussion

2.5.1 XRD results

XRD analysis of all the samples detected aragonite as the only phase (International Centre on Diffraction Data card 41-1475) within the limits of detection (limits of detection for calcite in an aragonite matrix are <1% (Finch, unpublished data)).

2.5.2 Sr results

The XANES profiles of both 389a and 389b (see Figure 2.3) show excellent agreement with that of Sr ideally (i.e. randomly) substituted within the aragonite structure (Finch *et al.*, 2003a). No standard is presently available for Sr substituted in organics and hence the XANES could not be compared with such a material.

The results of the refinements of Sr data using the Finch *et al.* (2003a) structural model are shown in Table 2.1. R_3 is 4.021±0.01 Å (for both samples) fitting with the aragonite structure (defined by standards analysed by Finch *et al. (*2003a)) with PERCA1 showing refinement fit of 1.000±0.09 and 1.012±0.09 for 389a and 389b respectively (PERCA1= 1 represents 6 Sr atoms). The R-factor (fit index) for 389a and 389b was 36.3% and 32.3% respectively for a Sr model (which provides the best fit for the EXAFS data). This is in the typical range described by Finch and

Allison (2003) for modelling of EXAFS. Thus, the model indicates that Sr substitutes randomly within the aragonite lattice. The slight difference in fit index between the two *A. islandica* samples results from differences in the intensity of the beam and the relatively low concentration of Sr in the samples (compared to corals) resulting in a lower signal to noise ratio.

If Sr were hosted by organics in the shell, there would be no long range order in the structure (i.e. no second or third shells), resulting in a poor R-factor (fit index) for the above model. Standard deviations of the modelled values would be high as the structure would be irregular and therefore show no consistent coordination. In particular, the Debye-Waller factors (A_1, A_2, A_3) would increase from values of ~0.03. Therefore, the Sr K-edge XAS data for *A. islandica* indicates that the model of Sr ideally (i.e. randomly) substituted in aragonite.

	A. islandica 389a		*A. islandica* 389b		Aragonite standard		Strontianite standard	
	Refined values	Error	Refined values	Error	Refined values	Error	Refined values	Error
E_f	-8.967	0.24	-8.951	0.22	-2.59	0.28	-3.51	0.26
A_1	0.023	0.001	0.024	0.001	0.022	0.001	0.028	0.001
A_2	0.033	0.006	0.035	0.006	0.038	0.008	0.029	0.005
A_3	0.029	0.003	0.031	0.003	0.028	0.003	0.031	0.003
R_1	2.587	0.004	2.587	0.003	2.583	0.004	2.632	0.004
R_2	3	0.014	3	0.013	2.981	0.019	3.023	0.012
R_3	4.021	0.009	4.022	0.009	4.018	0.011	4.166	0.010
PERCA1	1	0.09	1.012	0.09	Fixed to 1		Fixed to 6	
Fit %	36.3		32.3		24		24.2	

Table 2.1: Parameters of the optimum final EXAFS refinements using a single phase aragonite model with aragonite and strontianite standard of *Finch et al.*, (2003a)**.**

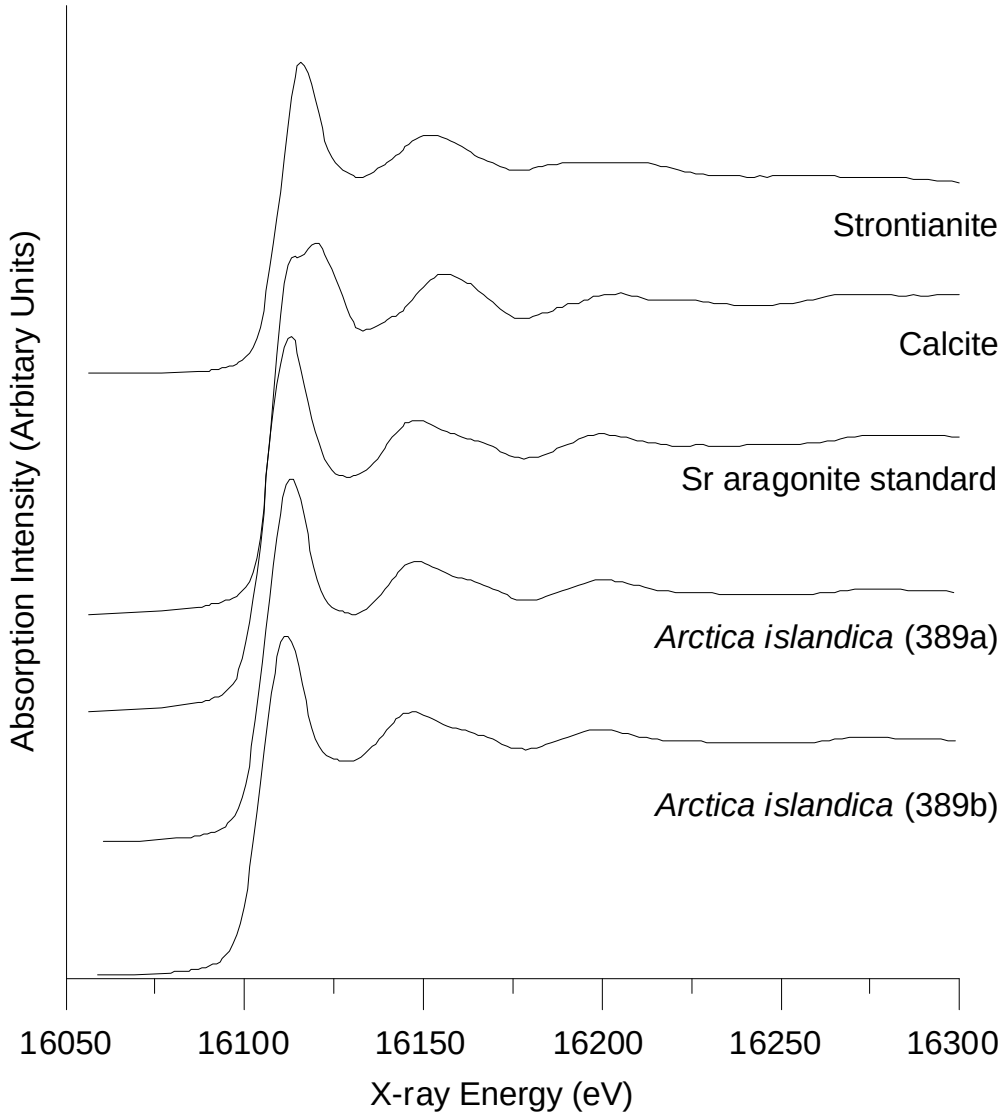

Figure 2.3: XANES profiles of two *A. islandica* samples (from the different sections of the same shell) compared to a Sr in aragonite, calcite and strontianite standard of Finch *et al. (*2003a).

2.5.3 Mg results

Full suites of standards (including those analysed in previous sessions by Finch *et al.* (in prep.)) are shown on Figure 2.4. A full interpretation of the XANES is beyond the present study (due to the complexity of XANES spectrum) but it can be concluded that the XANES of each coordination state can be distinguished. The XANES from *A. islandica*, 389a and 389b, and V05-257-3 are shown on Figure 2.5. The *A. islandica* signal shows a low signal to noise ratio (resulting from the low concentrations of Mg within the sample, typically 100-200 ppm).

Despite being single-phase aragonite to XRD, all three *A. islandica* spectra show no increase in intensity of absorption at ~1330 eV (which indicate Mg hosted in aragonite, Figure 2.4), nor are the spectra indicative of Mg hosted within clays. The latter shows that Mg in the shell does not result from the uptake of Mg-rich clays. Comparison to the organic standard shows the best fit suggesting that Mg in *A. islandica* is hosted within organics. 389a however also shows a high point at 1322.5 eV, the position expected for calcite peak. Therefore, residuals of the data of organic standard minus the *A. islandica* data (with backgrounds removed, and data scaled) were examined. This confirmed that Mg showed the best fit with the model in which Mg was hosted solely by the organics and it is not composed of a mixture of organics and calcite. Therefore, the high point at 1322.5 eV results from the low signal to noise ratio.

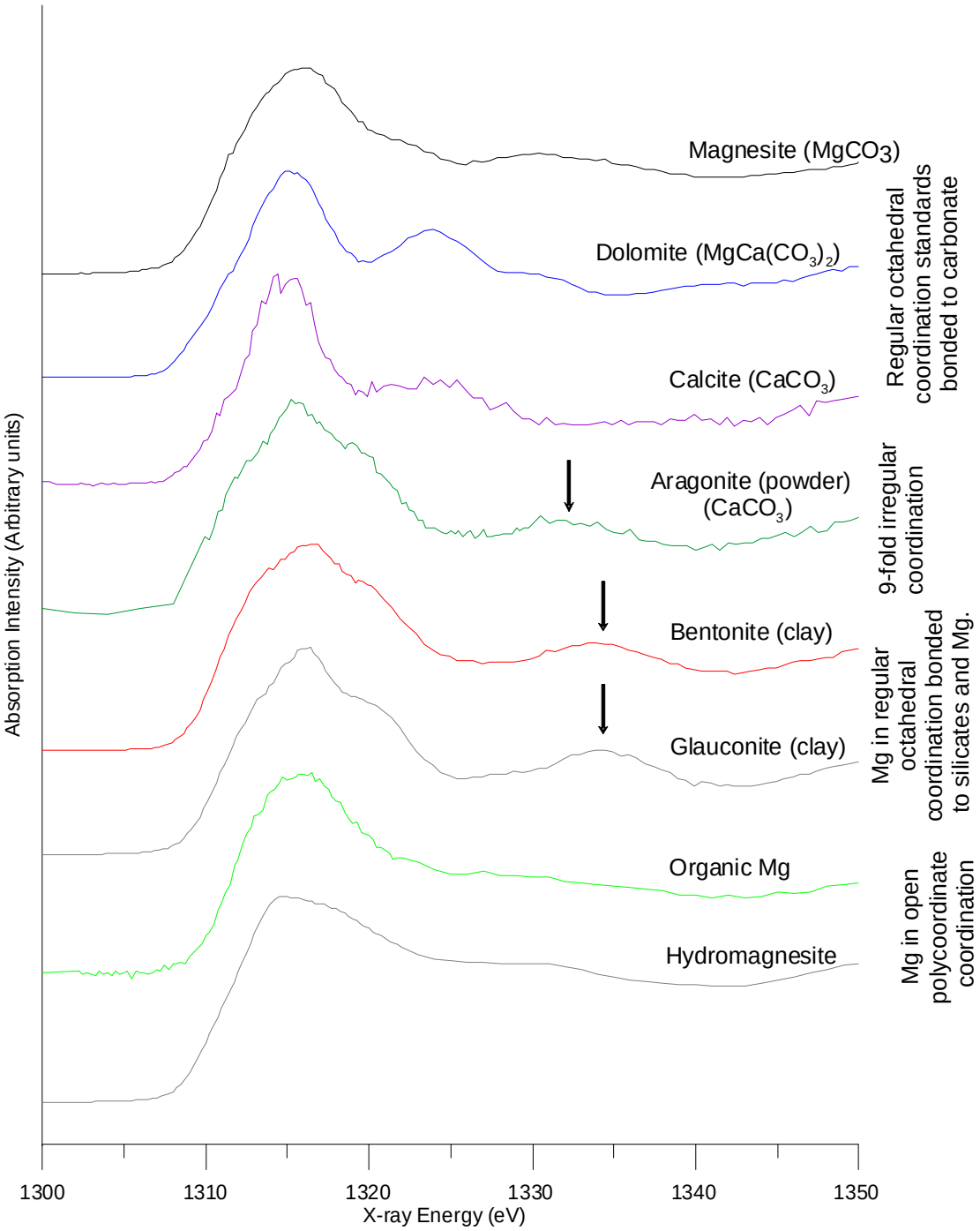

Figure 2.4: XANES of Mg standards. The arrows highlight the resonance of Mg in aragonite at 1332 eV compared to the broad oscillation at 1335 eV when it is hosted in bentonite and glauconite (clays).

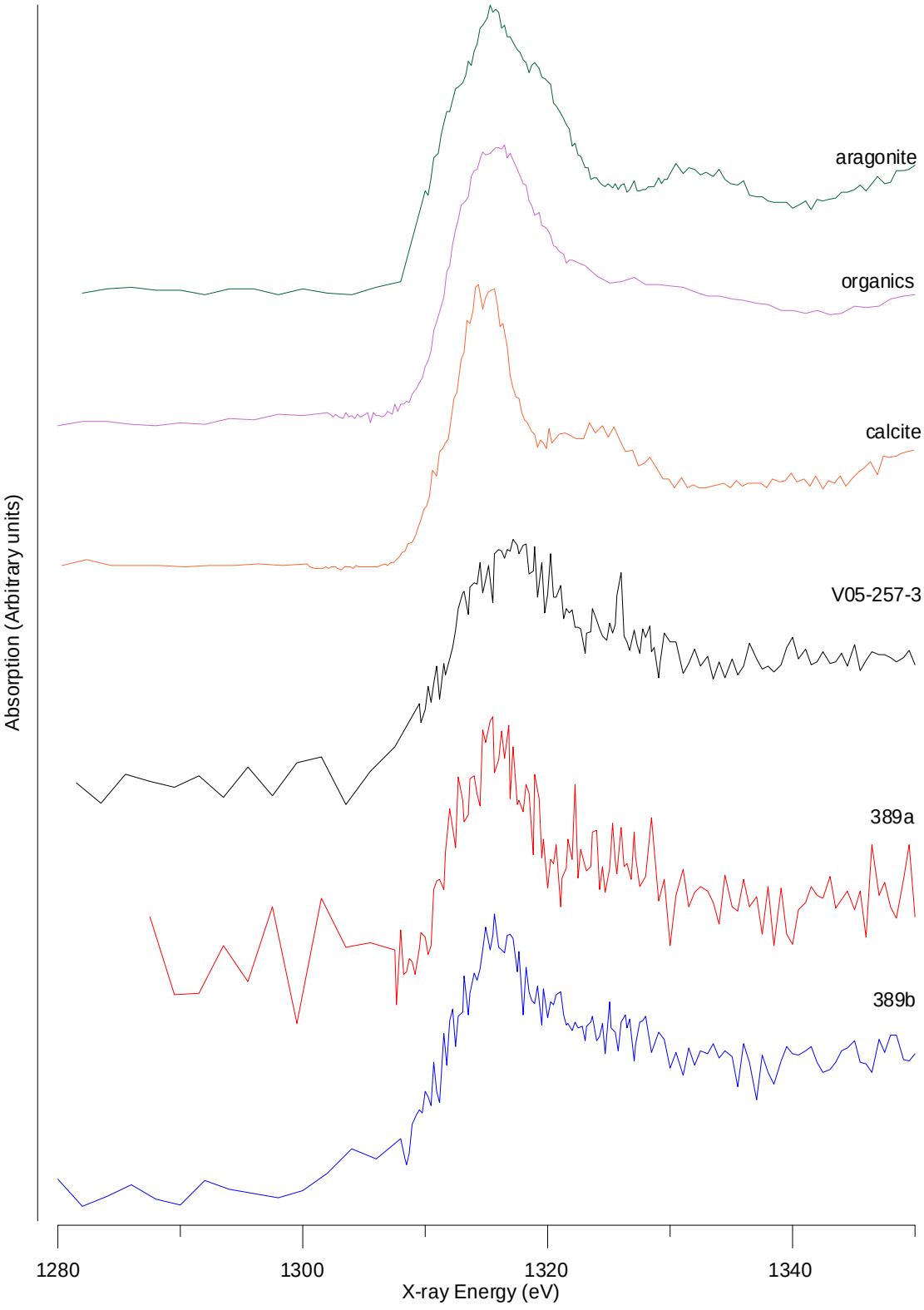

Figure 2.5: XANES of Mg from three *A. islandica* samples; V05-257-3, 389a and 389b with calcite, aragonite and organic standards.

2.6 Conclusion

XANES and EXAFS of Sr are consistent with it being ideally hosted within aragonite, indicating that thermodynamic equations and inorganic temperature experiments such as that of Kinsman and Holland (1969) are applicable. To develop Sr as a proxy, the effects of other factors (e.g. crystal growth rate, propagation and nucleation) need to be investigated. To understand better such effects, quantitative analysis of Sr within *A. islandica* from the prismatic layer found within both the umbo and outer shell layer are presented in the following two chapters.

Mg spectrum was limited to analysis of XANES, but comparison to a suite of standards permitted interpretation of the spectrum. Qualitative comparison of the *A. islandica* spectrum was consistent with Mg hosted by organics. Therefore, palaeoclimate reconstructions using Mg fluctuations in *A. islandica* are unlikely to provide accurate results until the thermodynamics of such a system are more fully understood. However, quantitative analysis of the prismatic layer found within both the umbo and outer shell layer should however provide further details of the behaviour of Mg and provide an insight into the controls on its behaviour, such as whether fluctuations can provide information on organic concentration.

Thus, these findings can provide significant insights into the behaviour and controls of Sr and Mg within *A. islandica* and their potential as palaeoproxies.

Acknowledgements

This work was generously supported with Daresbury SRS grants (41339 and 45027), with additional support from the Marine Studies Postgraduate Award. Personal thanks go to Angus Calder who ran XRD samples and helped with sample preparation and to Andy Smith who provided invaluable assistance at station 3.4

CHAPTER 3: SIMS ANALYSIS: TRACE ELEMENT FLUCTUATIONS WITHIN THE UMBO.

Abstract

The potential for the use of trace elements within the prismatic layer of the umbo of *Arctica islandica* to reconstruct palaeoenvironmental conditions was investigated, analysing two shells (U228 and U248) from Irvine Bay, SW Scotland, UK. The trace elements show high variability within the prismatic layer of the umbo. During latter years of growth, Sr/Ca shows sharp increases within the annual growth check (typically increase of >1.0 mmol/mol) with increases (of ~0.4 mmol/mol) present within the growth bands in the younger part of the shell. Sr/Ca does not obey simple thermodynamic models. The uptake of Sr/Ca during the latter years may be modified by changes in the crystal habit caused by increased organics as well as vital effects. During years of faster growth, crystal growth rate may become increasingly important. In addition, a lateral variation can result in an increase of >25 % towards the lateral margins.

Analysis of Mg/Ca in linescan mode showed evidence of contamination (with high Si values). Although there is some covariation with the annual growth checks, it is unclear whether this is related to increased contamination within these areas (which are likely to be softer and therefore more prone to contamination) or due to increased organics.

Ba/Ca shows sporadic sharp increases in concentrations (over five times the typical value), which could not be attributed to changes to the architecture of the shell, or any known environmental stimulus (e.g. temperature, salinity). The pattern of the Ba/Ca fluctuations is however consistent with the findings of a number of other researchers (e.g. Stecher *et al.*, 1996; Putten *et al.*, 2000; Lazareth *et al.*, 2003; Gillikin *et al.*, 2006).

3.1 Introduction

During the growth of *Arctica islandica*, trace elements are incorporated into the shell during the calcification process occurring within the extrapallial fluid (EPF). Research on the trace elements in bivalve shells has focused mainly on Sr/Ca and Mg/Ca and their potential to reconstruct a temperature record independent of $\delta^{18}O$ which is dependent on salinity estimates (e.g. Hart and Blusztajn, 1998; Takesue and van Geen, 2004), with some research on Ba/Ca as a proxy for palaeoproductivity (e.g. Lazareth *et al*., 2003 Gillikin *et al.*, 2006).

By quantifying changes in trace elements within *A. islandica* shells and combining it with the sclerochronology (i.e. identifying the annual growth checks), it is possible to measure how these fluctuations vary temporally. The typical contents of the shells are 1000-1800 ppm Sr and 50-100 ppm Mg, with *in situ* microanalysis possible using methods such as SIMS (Secondary Ion Mass Spectrometry or ion microprobe) and Laser Ablation Inductively Coupled Plasma Mass Spectrometry (LA-ICPMS). These methods permit higher resolution sampling than is possible with solution-ICPMS. For example in this study the spot size of LA-ICPMS was <60 μm with a depth of ~200-250 μm compared to 500 μm by 2000 μm with a depth of 500 μm for solution-ICPMS. LA-ICPMS and SIMS also has the advantage that fluctuations in geochemistry can be more easily related to changes in shell architecture. In addition, sampling can be adapted or modified during the analysis sessions and hence provides much more dynamic sampling. SIMS, in particular, provides extremely high resolution sampling with a beam size <10 μm and low (ppm) limits of detection.

In *A. islandica*, some research in sclerochronology has focused on the umbo because the growth bands here are less influenced by stress events such as storms and

predator attacks thus providing a more coherent record (Richardson, 2001; Scourse *et al.*, 2006). However much of the work on stable isotopes ($\delta^{18}O$ and $\delta^{13}C$) is carried out in the outer shell prismatic layer because of the limitations of sample size in the umbo (see Figure 1.2 for schematic of the shell regions). SIMS analysis of the umbo can provide a high resolution analysis enabling, in this study, up to 40 analyses per year (~ one per growing week) in the fastest growing part of the umbo (i.e. juvenile), with <10 analyses/yr at the slowest in this study. Thus, the potential use of trace elements within the umbo to reconstruct palaeoenvironmental conditions can be explored.

Data from the prismatic layer of the umbo will compared to the outer shell prismatic layer, sampled using ICPMS (results of ICPMS analyses are shown in the next chapter), to show whether trace element fluctuations are the same in different parts of the prismatic layer despite being deposited at the same time. If they differ it is important to understand why e.g. changes in shell architecture, growth rate or from changes in the biological mediation. Thus by using these two sets of data (see Chapter 8), it provides a much clearer understanding of the controlling factors of trace element uptake and their potential as proxies.

3.1.1 Previous trace element studies of bivalves

Inorganic precipitation experiments on Sr-bearing aragonite have shown that Sr/Ca incorporation is inversely related to temperature (Kinsman and Holland, 1969; Dietzel *et al.*, 2004; Gaetani and Cohen, 2006). Sr/Ca ratios in biogenic aragonite are not significantly altered by salinity in the range of ~10-35 (Drever, 1980; Dodd and Crisp, 1982).

Findings from bivalve research have failed to find one sole control for the uptake of trace elements suggesting that environmental factors do not control Mg/Ca and Sr/Ca concentrations in skeletal carbonate according to simple equations (Mann, 1992). The majority of researchers have found that trace elements are not primarily dependent on temperature, a commonly targeted environmental goal. Lutz (1981) found *Mytilus edulis* (inner nacreous layer) failed to reveal any long-term periodic variations in Sr/Ca and thus concluded temperature was not a controlling factor.

Purton *et al.* (1999) found in *Venericardia planicosta,* an aragonitic mollusc, and the marine gastropod *Clavilithes macrospira* that neither growth rate, calcification rate nor temperature were the sole controlling factors, but rather that metabolic rate governed indirectly by these factors was the likely cause of Sr/Ca variation. Both showed an increased in Sr/Ca with ontogeny even though the gastropod, *Clavilithes macrospira* has, unlike bivalves, linear growth rate through ontogeny. Ontogenetic trends in Sr/Ca have been seen in other gastropods e.g. *Conus ermineus* as well as bivalves such as *Mercenaria mercenaria* (Gillikin *et al.*, 2005a) including *A. islandica* (Tripati *et al.*, 2004).

For *A. islandica* widely ranging results have been reported. Hart and Blusztajn (1998) determined a positive linear relationship between Sr/Ca and temperature from Nantucket Shoals Lightship, Gulf of Maine, where:

TºC= 20.752[Sr/Ca mmol/mol)]-16.0

and applied this relationship to hydrothermal vent clams *Calyptogena magnifica*. This assumes that Sr/Ca uptake is independent of taxa. However, the positive relationship presented is the opposite of the thermodynamic model where Sr/Ca uptake is inversely dependent on temperature (e.g. Kinsman and Holland, 1969). Toland *et al.* (2000) also found Sr/Ca inversely covariant with $\delta^{18}O$ (i.e.

positive with temperature) using *A. islandica* specimens from Cardigan Bay, SE Irish Sea. Epplé (2004) found cyclic variations but concluded that Sr/Ca maximum at the winter growth checks could be used to reconstruct winter seawater temperatures whereas Tripati *et al.* (2004) found that ontogenetic changes were overriding factors. *A. islandica* is unable to tolerate waters with salinities of <16 (Nicol, 1951) and thus Sr/Ca in *A. islandica* should not be strongly influenced by changes in salinity. Thus, there is a need to understand which environmental factors Sr/Ca within *A. islandica* encodes.

There have been fewer studies on Mg/Ca in aragonite bivalves. For Mg/Ca, there is no clear consensus on the controls of uptake in bivalves. Takesue and van Geen (2004) found Mg/Ca in *Protothaca staminea* shells to be significantly correlated with temperature (Mg/Ca was r = 0.71 in one of the four growth increments) but found significant year-to-year variation. Cyclic patterns of Mg/Ca variation through a year's growth have been observed in a number of species such as *Isognomon murchison*, *Mytilus edulis* and *Patella vulgata* (Fuge *et al.*, 1993; Hendry *et al.*, 2001) as well as within *A. islandica* (Toland *et al.*, 2000; Epplé, 2004). The significance of these is however unclear. Quantitative measurements from *A. islandica* may provide further insight into the controls of Mg/Ca fluctuations especially when interpreted in conjunction with the XANES analysis (presented in the previous chapter).

Ba/Ca profiles from both aragonitic (including *A. islandica*) and calcitic bivalves show similar patterns, with low values interspersed with very high Ba/Ca peaks (Bishop, 1988; Stroobants *et al.*, 1991; Stecher *et al.*, 1996; Toland *et al.*, 2000; Epplé, 2004). Large increases in Ba/Ca concentration are typically deposited over short distances and thus have been defined as Ba/Ca peaks in these papers and will be subsequently referred to as Ba/Ca peaks within this thesis.

These Ba/Ca peaks have been generally attributed to phytoplankton blooms production and uptake of barite particles (Stecher *et al.*, 1996; Lazareth *et al.*, 2003; Gillikin *et al.*, 2006). The sporadic increases of Ba/Ca uptake is common not only in bivalves but also in other taxon e.g. corals (Sinclair, 2005). Using *A. islandica* shells, the timing and magnitude of the Ba/Ca peaks can be explored to gain further insight into the controlling mechanism.

Thus in summary, there is a consensus that the uptake of trace elements is not easily attributable to one environmental factor and the controls are complex. Sr/Ca uptake in bivalves has been related to growth rate in a number of publications (Stecher *et al.*, 1996; Takesue and van Geen, 2004; Carré *et al.*, 2006). In the coral *Diploria labyrinthiformis* (brain coral) Goodkin *et al. (*2007) applied a crystal growth rate correction temperature reconstructions from Sr/Ca. Higher crystal growth rate resulted in increased growth entrapment of trace elements (i.e. non-biogenic effect). Such a method, if applied to bivalves, would imply that vital effects do not have a significant influence.

Thus, by using *A. islandica*, key questions on the controls on bivalves can be explored, e.g. temperature effect on incorporation, the timing of the increases, relationship to changes in the shell architecture, lateral heterogeneity, and whether fluctuations are replicated in different shells collected at the same time from the same area. Thus, the potential of trace elements in *A. islandica* as proxies can be explored. Insights into the behaviour of *A. islandica* may not only be applicable to other bivalves but also for other aragonitic systems such as corals.

3.1.2 Rationale of the present study

The present study into *A. islandica* from Irvine Bay, NW Scotland uses the nearby primary instrumental SST (sea surface temperature) dataset collected (almost) daily from Millport marine station (Figure 3.3) and additional intermittent temperature and salinity data collected within Irvine Bay (see Figure 6.3). Comparison of measured fluctuations of trace elements (in particular Sr and Mg) in the prismatic layer of the umbo with SST, allows the potential of trace elements as palaeotemperature proxies to be explored.

3.2 Introduction to SIMS

SIMS (Secondary ion mass spectrometry), also known as ion probe or ion microprobe, works by bombarding the sample surface with high energy ions from a primary ion beam. This causes secondary ions and atoms from the sample to sputter from the surface. These ions can then be passed into a mass spectrometer and their count rates measured. The components of the SIMS can be seen on Figure 3.1 and are described in further detail below.

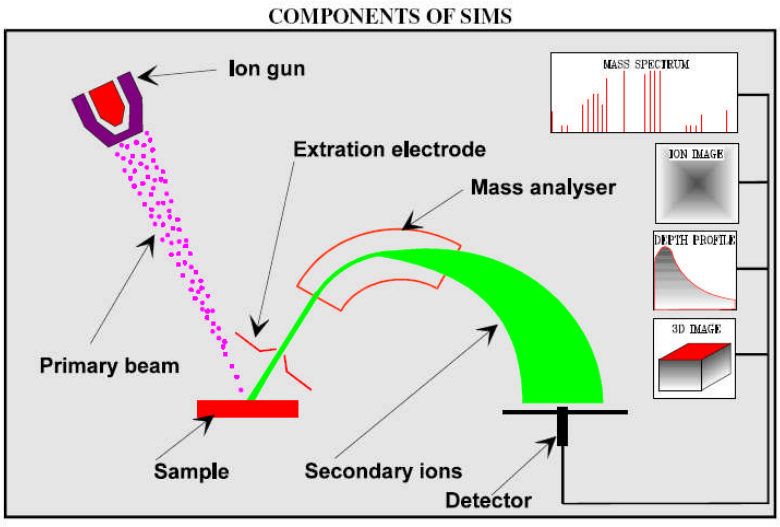

Figure 3.1: Components of SIMS (Craven, 2007).

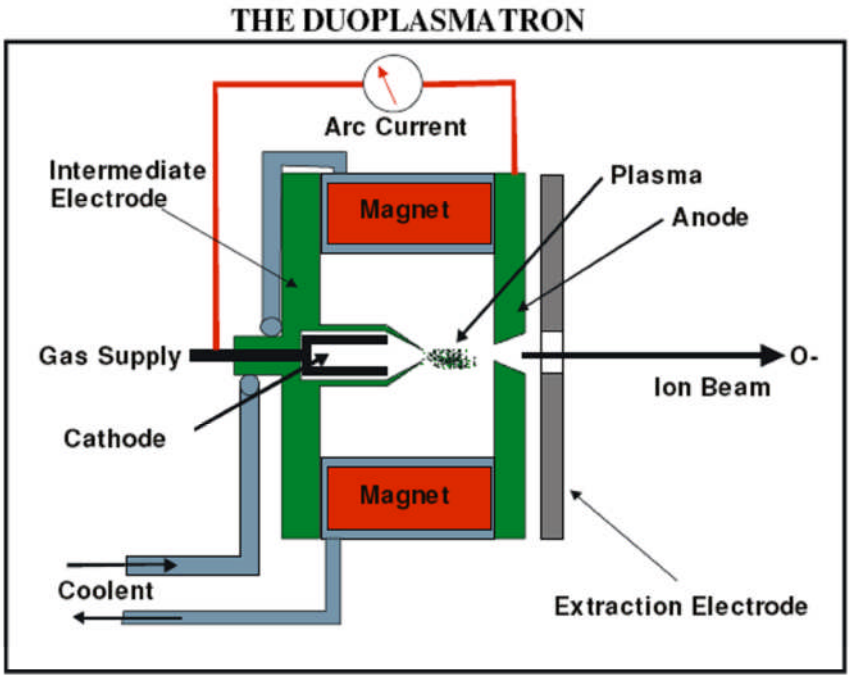

Figure 3.2: Duoplasmatron used to generate ions for the primary beam (Craven, 2007).

The primary ion source can either be a metal gun (typically Cs) or a gas passed through a duoplasmatron (Figure 3.2), producing ions with energies between 1-30 keV. The choice of gas depends on the type of sample to be analysed with oxygen being the most common. O_2 gas can be ionised to produce O^- or O_2^+ ions. The primary ions are then accelerated along the primary ion column, which contains a primary beam mass filter to eliminate impurity species in the beam, e.g. the stainless steel surfaces within a duoplasmatron generate ions such as Cr, Fe and Ni, which would raise the detection limits for these elements (Fleming, 2000).

The sample under high vacuum is bombarded with a primary ion beam, with the sputter rate dependent on the sample material, crystal orientation and the primary beam intensity. Typical sputter rates are 0.5-5 nm/s (Fleming, 2000). Some of these sputtered atoms are ionised, the efficiency of which is termed the ion yield (IY) i.e. the fraction of atoms that become ionised. This is typically <10% (Williams, 1992).

The relationship between the first ionisation potential and secondary ion yield is not simple. It is affected by the element in question, the nature of the matrix and the bombarding beam. For instance the presence of electronegative elements in the matrix or implanted from the primary beam, enhances the positive secondary ion yield (Hinton, 1995). In addition, the physical processes that lead to the formation of secondary ions are poorly understood. Analyses on standards are therefore used to determine a Relative Ion Yield (RIY), which eliminate these effects with secondary ion intensities normalised to a major element (in this study Ca) (Hinton, 1995). The Relative Ion Yield (RIY) normalises to a standard matrix and by matching the matrix of the unknown and standard, matrix effects are minimised (Galuska and Morrison, 1987).

In addition, mass interferences occur when an ion or molecular species has the same nominal mass as the target species to be analysed. Hence counts collected at that mass comprise one or more species e.g. for ^{88}Sr, the $^{44}Ca^{44}Ca$ dimer has the same nominal mass. This can be corrected by closing the mass slits to resolve the different species, which commonly have slightly different masses. The latter method however, reduces the overall counts substantially and hence the precision falls. Greater accuracy can often be achieved by leaving the slits open and estimating the expected relative abundance of the isobaric species by analysis of another entity (A. Finch, Pers. Comm. 2007). For example, in this case, the contribution of $^{44}Ca^{44}Ca^{+}$ to counts at mass 88 can be estimated from direct measurements of the counts for the $^{40}Ca^{40}Ca$ dimer.

3.3 Method

3.3.1 Sample preparation

The shells were live-collected from Irvine Bay, which is close to the marine sampling station at Millport, Isle of Cumbrae (see Section 1.3 for further details). The annual temperature variation of which is shown on Figure 3.3.

The prismatic layer of the umbo of two shells, 228 and 248 (which will be subsequently referred to as U228 and U248 respectively) were prepared by sectioning along the axis of maximal growth (see Figure 1.2), set in Buehler Epo-thin epoxy, and then finely polished to 1 μm.

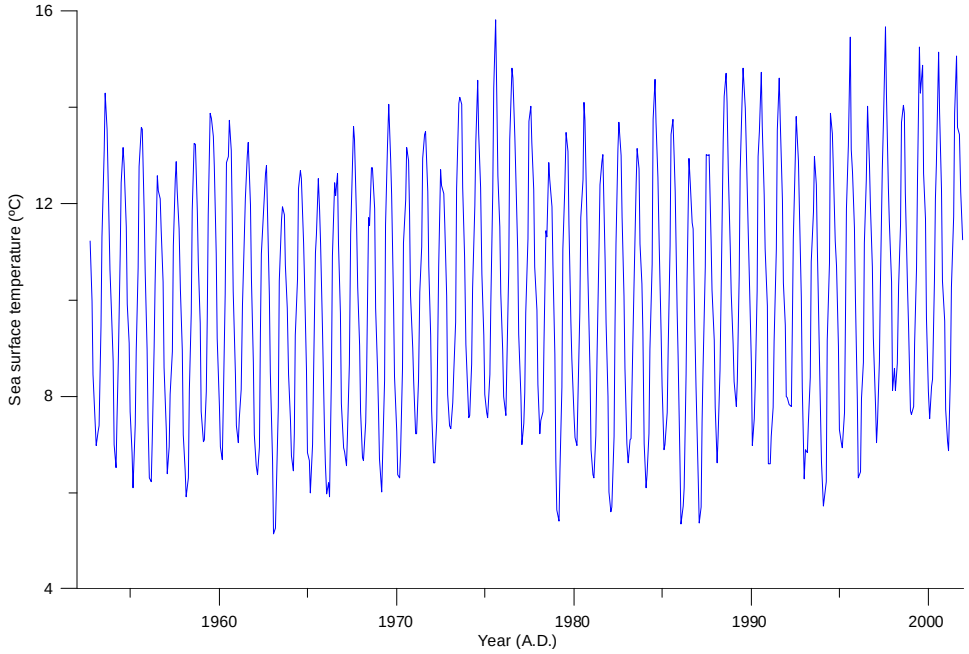

Figure 3.3: Sea surface temperature (using monthly averaged values) at marine sampling station Millport, Isle of Cumbrae, NW Coast of Scotland from 1953-2001. Maximum error is <2 °C for each daily measurement, which is used to provide a monthly average. Prior to 1983, measurements were taken daily but financial cutbacks reduced it to working days only (P. Barnett, Pers. Comm. 2007).

3.3.2 Sample analysis

Analysis was carried out on a Cameca ims-4f ion microprobe in the Department of Geology and Geophysics, University of Edinburgh, UK during one analytical session (one week). Sections were gold-coated and analysed using a 2 nA O^- primary beam, energy offset of 75 eV in spot mode and 0 eV in linescan mode. The imaged field was 25 μm, the field aperture 150 μm and the contrast aperture 150 μm.

The main linescan analyses were made along the line of maximum growth (see Figure 3.4a for schematic), with some linescan analyses moving laterally away from this line of maximum growth to determine laterally variability. U248 (and two short transects on U228) were analysed with a spot size of ~10 μm in both spot and linescan mode, with the secondary ions measured including ^{26}Mg, ^{48}Ca, $^{40}Ca^{40}Ca$, ^{88}Sr and ^{138}Ba. A stepsize of 10 μm was used in linescan mode. ^{40}Ca could not be used to measure Ca due to the large count rates, which would trip the safety circuits on the electron multiplier tubes. Therefore, the less abundant ^{48}Ca isotope is used. Estimates of concentration for each element are made from known natural isotopic abundances. On U228 the main transect measured only ^{48}Ca, $^{40}Ca^{40}Ca$ and ^{88}Sr with a larger spot size of ~30 μm (with stepsize of 10 μm). The count times are shown on Table 3.1 including waiting time (which provided a pre-burn time). Note that the beam spot is significantly larger than the area from which secondary ions are drawn, and hence there is some pre-burn in linescan mode while the instrument analyses adjacent spots. When a 10 μm beam size, there was no pre-burn from the preceding spots, but analysis on U228 when a coarser spot size (30 μm) was used, effectively a pre-burn of 9 s was applied prior to sampling, as a stepscan of 10 μm was used.

Analysis in U248 covered 1986-2001 and in U228 1988-2001, determined from counting the growth bands. Shell 248 and 228 were 21 (1980-2001) and 18 years old (1983-2001) respectively. The earliest years of the shell (~6 years) were not measured due to problems caused by the strong curvature of the umbo within the juvenile section and the narrowing width of the umbo (the linescan consists of a series of straight lines). As the sample was highly polished and gold coated, relating the position to the architecture of the shell was difficult, and resulting in difficulty in keeping the analysis along the maximum growth axis (see Figure 3.4b, c). Thus, analysis was focused on the more mature section of the umbo.

Analysis concentrated on one shell (248) to build up a comprehensive picture of changes in the trace elements Mg/Ca, Sr/Ca and Ba/Ca within the prismatic layer of the umbo using a 10 μm spot size in linescan mode (Figure 3.4b). This meant that in the latter years of growth, each measurement consisted of material deposited over more than one month whereas in the earlier years, analytical resolution was temporally much more detailed covering ~1 week of growth e.g. in 1987 in U248, >40 analysis were carried out per year, this compares to $<10yr^{-1}$ during 2000.

A long transect was taken on the line of maximum growth to examine the interannual variability and any possible changes during ontogeny. The curvature of the shell however made determining the exact positioning of the line of maximum growth difficult, especially during the earliest growth where the shell curvature is greatest. The transect taken closest to the maximum growth axis has, in order to distinguish it from transects taken parallel to it, being referred to as the transect of maximum growth axis. Any deviation from the true maximum growth axis is particularly significant if the trace element deposition is not homogeneous transversely across the same band.

Therefore, multiple parallel linescans were carried out over the latter part of the shell with tracks ~25-100 μm apart, with a few short transects measured ~750 μm from the main transect. These transects explore whether results are reproducible along a band, i.e. whether trace elements concentrations are independent of distance from the maximum growth axis. A number of spot analyses were also taken to check for any evidence of superficial contamination, as the spot analysis provides a depth profile. Additionally, a series of spots were taken along a single annual termination band to measure any lateral changes occurring at the growth check.

A more limited analysis was also carried out on U228, with two short transects (700 μm covering 1997-2000) covering all three elements (Sr, Mg, and Ba) and with one long transect covering 12 years (i.e. 1988-2000) (Figure 3.4c). Only Sr/Ca was analysed in the latter as Sr/Ca has the highest concentration and the most detailed XAFS data of the three elements (see Chapter 2). This allowed the more of the umbo to be analysed, providing a long time series for comparison of Sr/Ca in the two different shells. This allows further evaluation on whether Sr/Ca fluctuations are linked to external forcing mechanisms or driven by internal mechanisms.

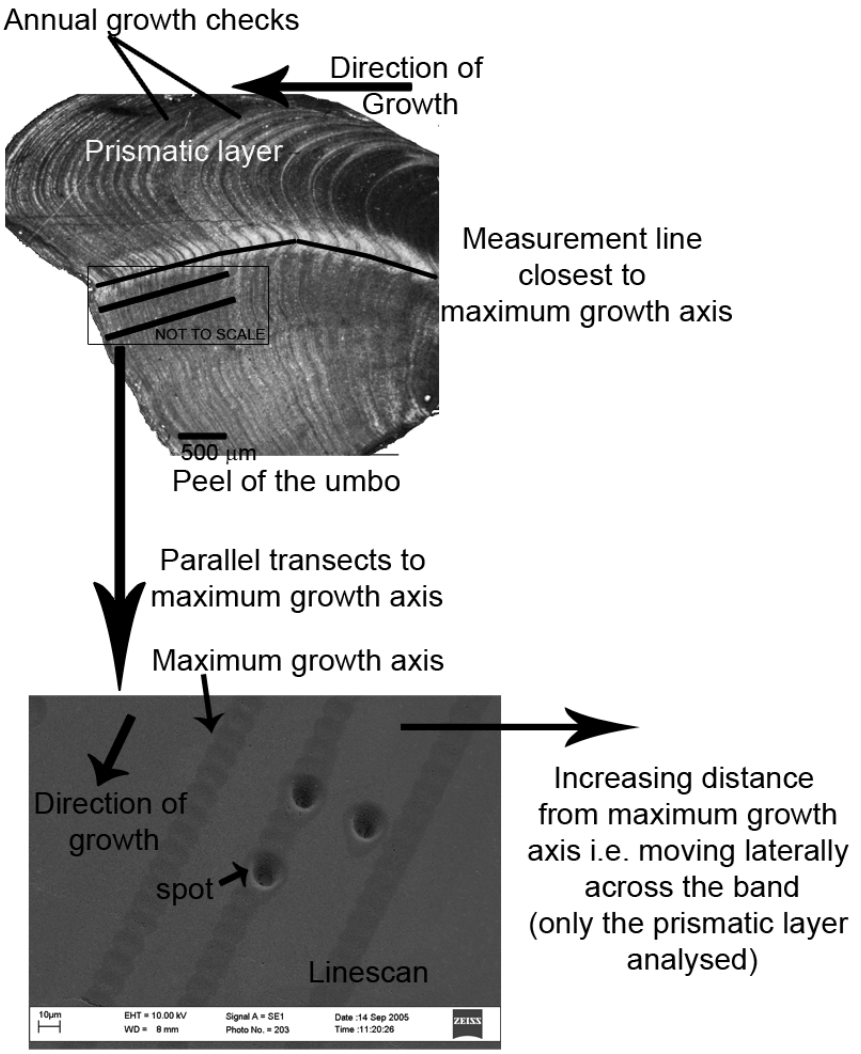

Figure 3.4a: Schematic of sampling within the prismatic layer of the umbo.

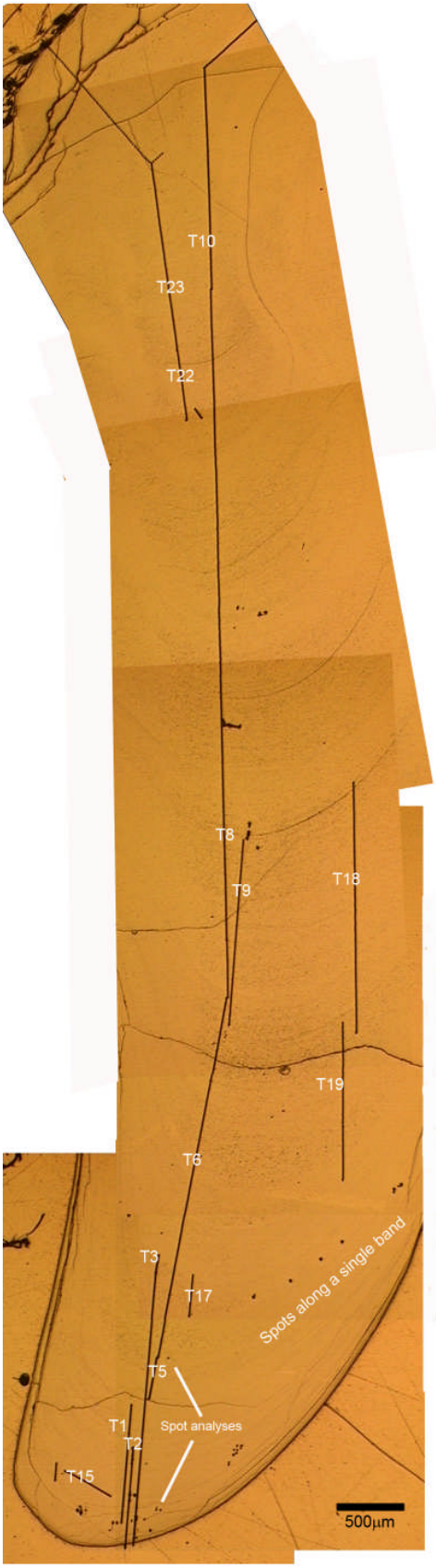

Figure 3.4b: Location of transects and spots analysed in the prismatic layer of the umbo of *A. islandica* specimen 248.

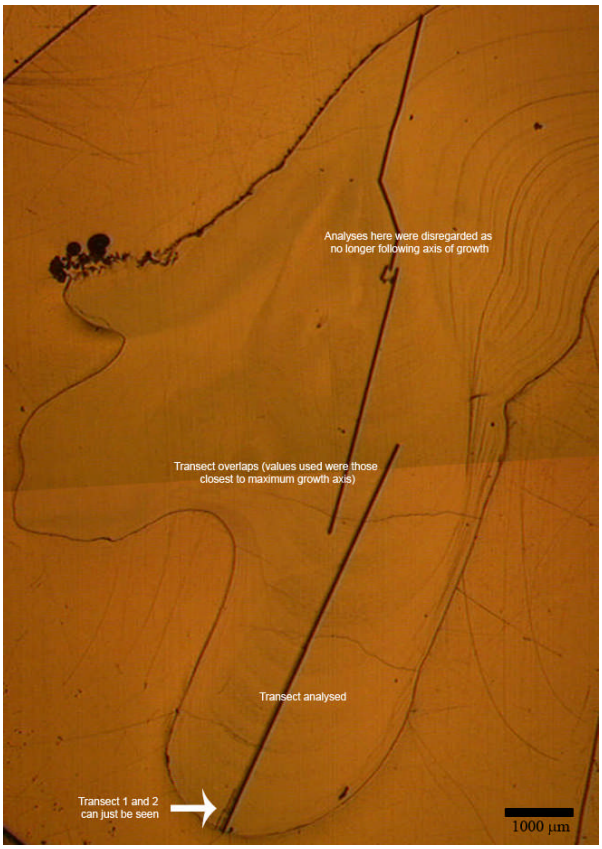

Figure 3.4c: Location of transects analysed on U228 in the prismatic layer of the umbo of *A. islandica* specimen 228.

	U248 linescan (+U228 short transects)	U248 spot mode	U228 (increased spot size)
Wait time	10	5	
^{6}Li	10	5	-
^{10}B	10	5	-
^{26}Mg	5	3	-
^{27}Al	-	2	-
^{30}Si	5	4	-
^{44}Ca	-	2	-
^{48}Ca	5	-	2
^{54}Fe	5	-	-
^{55}Mn	-	20	-
$^{40}Ca^{40}Ca$	2	-	2
^{88}Sr	5	2	5
^{138}Ba	15	15	-
$^{197}Au+^{40}Ca$	-	2	-
^{238}U	-	20	-

Table 3.1: Count times (s) of the isotopes measured for the umbo of shell 248 and shell 228. Wait time provides a burn-in time. Table includes isotopes not considered in the present study (but were given to provide a reference time for each spot cycle).

3.3.3 Data processing

Measurement of possible interference of $^{44}Ca_2$-dimer was carried out by measuring the $^{40}Ca_2$-dimer and using known isotopic abundances to estimate the counts at mass 88 that resulted from $^{44}Ca^{44}Ca$. This was found to contribute <0.2 % of ^{88}Sr counts and was therefore ignored in subsequent calculations.

OKA carbonatite and NCC (Norman Cross calcite) were used as external standards in both linescan and spot mode. The relative ion yields (RIYs) of Mg, Sr

and Ba to Ca were estimated based on the carbonate standard OKA (Ca concentration = 40.04 %). NCC showed greater compositional heterogeneity (see Table 3.2) and hence OKA was chosen as the primary standard. Analyses of Si and Fe were used as a check for contamination in U248 as they are present in polishing media but largely absent from the aragonite.

In spot scan mode collect 15 cycles of data were collected on the same spot, of which the last 10 were averaged (i.e. in effect 400 s of pre-burn are applied before the data are used). Reproducibility of spot analysis was calculated as $2\sigma/\sqrt{n}$ where n is the number of cycles (10) and σ was calculated from the standard deviation from the mean of last 10 cycles. In linescan mode, only one cycle of data is collected before moving onto the next analysis. Spotscan mode allows changes in element to calcium ratios to be measured, this is particularly important for determining any evidence of superficial contamination. Linescan mode, in contrast, allows more data to be collected in the same time interval and the pre-burn is shorter.

OKA was used to calculate concentrations, as calcite is the closest matrix to that of the aragonite matrix of the *A. islandica* shell available, and as discussed earlier was found to be more homogeneous than NCC. However, OKA is a calcite standard and the shell is a mixture of aragonite and organics, hence there is a matrix contrast and potentially a systematic error in the estimates of concentration. The concentrations of the standards, together with typical counts of *A. islandica* (in both linescan and spot mode) are shown in Table 3.2. Precision of standards in linescan mode quoted is the average standard deviation (2σ) measured from multiple analysis of the standard. Reproducibility of the spot was calculated by the typical standard error, calculated by $2\sigma/\sqrt{n}$ where n is the number of cycles for the spot. It was not possible to calculate the reproducibility of linescan measurements on *A. islandica* due

to the heterogeneity of the sample. Estimates of the limit of detection were calculated from the three times the maximum number of counts per second at mass 7 divided by the number of counts per second at the mass of interest (e.g. ^{26}Mg). The limits of detection were 7.1 x 10^{-6} mmol/mol, 1.7 x10^{-4} mmol/mol and 3.6 x10^{-5} mmol/mol for Mg/Ca, Sr/Ca and Ba/Ca respectively.

Contamination check and data filtering

During linescan analysis, positioning of the beam to avoid imperfections was not possible and hence post-analysis data filtering is applied. Counts at mass 28 (nominally Si) and mass 54 (^{54}Fe and $^{27}Al_2^+$) were collected to provide a contamination check, as Si, Fe and Al are not present in high concentrations in bivalve aragonite but present in the polishing media. Analysis within 20 μm of the edge between the shell and epoxy resin were discarded since the edges of the samples attract systematically significant contamination. For U228 linescans, in which only Sr/Ca data were collected, no contamination checks were analysed as initial analysis showed Sr/Ca to be relatively robust when encountering minor pits and surface imperfections. However, analyses on visible cracks in the track were removed since Sr/Ca values are affected when cracks are encountered (data from the present study and Finch *et al.*, 2003b). It is important to check there is no correlation between "contamination indicators" (i.e. Si and Fe) (see Allison and Austin, 2003) and the trace elements analysed which would indicate a dependence on the variations in a profile to variable degrees of contamination.

The distribution of the linescan data points are left-skewed and therefore lognormal data was taken of each data point of Sr/Ca, Mg/Ca and Ba/Ca and plotted against lognormals of Si/Ca and Fe/Ca (Figures 3.5-3.7) to determine if any

covariation could be seen. Lognormal plots of Sr/Ca show no relationship to either contamination indicators (Si/Ca and Fe/Ca). The relationship of lognormal plots of Mg/Ca to Si/Ca and Fe/Ca shows that Mg/Ca is sensitive to contamination, although there is a high degree of scatter, with R^2 values of 0.6 and 0.5 for log(Si/Ca) and log(Fe/Ca) respectively. Ba/Ca shows some evidence of contamination, with log(Ba/Ca) showing R^2 values of 0.1 and 0.2 to log(Si/Ca) and log(Fe/Ca) respectively. Allison and Austin (2003) used t-testing to identify data that shows a strong correlation with the contaminants, however the non-normal distribution and size of the present dataset prohibits this. Measurements of Si/Ca and Mg/Ca show that the contamination can be significant through the dataset. Ba/Ca shows that the correlation with contamination is only at low Ba/Ca. When low Ba/Ca (<0.01 mmol/mol) are excluded, the R^2 values decreases to 0.02 for the log(Ba/Ca) vs log(Si/Ca), with similar decrease for log(Fe/Ca), indicating that only at low Ba/Ca, is the contamination significant.

Spot data provides additional indication of surface contamination. In particular, it allows a better understanding of how many counts are attributable to surface contamination.

During the burn time of spot analysis (typically 15 cycles each lasting 70 s), changes in ratios can occur due to the difference in the relative efficiencies of sputtering between the two. However, an exponential decrease in the first few cycles, suggests that surface contamination is present, with the area from which surface contamination is generated decreasing with depth. Therefore, by examining changes between the first five cycles to those in later cycles should indicate whether there is significant contamination. Comparison to OKA indicates the effects of sputtering, although within a calcite (rather than biogenic aragonite). Three spots analyses are

shown on Figure 3.8, one of the OKA standard and two on *A. islandica* (spot 10 and 15). Spot 10 shows higher Mg/Ca and Sr/Ca than spot 15, with Mg/Ca of 0.0014 and Sr/Ca of 0.054 in the first cycle.

Sr/Ca spot measurements in *A. islandica* show an increase during the cycles (see spot 10 and 15) with the change of similar magnitude to that seen in the OKA standard. There is no exponential decrease during the first few cycles. The range of Sr/Ca measured within the spot data (0.8 mmol/mol to 2.2 mmol/mol) is similar to that of the linescan data (0.7 to 2.6 mmol/mol), indicating that the spot data was representative of the fluctuations measured during linescan analyses. Note the ratios to Ca could not be compared directly, as spot mode is Me/^{44}Ca, and in linescan Me/^{48}Ca, and hence the calculated values in mmol/mol are quoted.

Mg/Ca spot data shows a range of 0.2 to 0.6 mol/mol measured from the last 10 cycles of 15, and the decrease is similar to that seen within the OKA. Mg/Ca in spot 10 and 15 indicate a decrease during the cycles, but the rate of decrease is only slightly different to that in OKA, which can be attributed to the difference in matrices. Significantly, there is no exponential decrease during the first few cycles, which would be indicative of surface contamination. Therefore, this indicates that such measurements are likely to be representative fluctuations in Mg/Ca within the shell rather than superficial contamination.

The highest Mg/Ca measured in spot analyses was 1.0 mmol/mol (spot 2) occurring during the first cycle, with the 10 cycles giving a mean concentration of 0.43 mmol/mol. The decrease during the spot was similar to that seen in spot 10 and 15. In linescan mode however calculated values were typically ranged from 0.3 to 2.0 mmol/mol, with slightly less than 5% of the Mg/Ca data being >2.0 mmol/mol and 0.7% of the data >4 mmol/mol. Thus approximately 13% of the Mg/Ca data in

linescan mode are >1.0 mmol/mol, the maximum initial concentration measured in spot mode. Therefore, if the positioning of the spots had been chosen at random at least one of the spots (statistically 1.25 spots) should have shown values >2 mmol/mol. Linescan data was measured after 30 s whereas in spot mode Mg/Ca was analysed after 10 s i.e. linescan has more burn-in time before it is measured compared to the first cycle in spot mode. The lack of spot measurements showing high Mg/Ca (i.e. >1.0 mmol/mol) appears to be due to the location of the spot analyses. All spot analyses were taken during the latter years of growth, when as Figure 3.12 highlights there are less high Si/Ca values (see Figure 3.4b for positions).

As discussed previously, the plot of the linescan data points for Mg/Ca show that there is a strong correlation between Mg/Ca and the contamination indicators (Si/Ca and Fe/Ca). Comparison of the linescans (Figure 3.12) highlights that the extreme Mg/Ca points >0.03 are generally associated with high Si/Ca (>0.003). Exclusion of the higher Mg/Ca i.e. >1.0 mmol/mol (i.e. the limit of the spot data) shows that R^2 value decreases to 0.2 implying that there is still some correlation between the Mg/Ca and Si/Ca fluctuations. However, some initial exploration of the data can provide preliminary investigation, which can then be explored further in the following ICPMS chapter.

Spot analyses shows a maximum of Ba/Ca of $2x10^{-4}$, which represents 0.014 mmol/mol, with linescan measurements varying from ~0.005 to >0.9 mmol/mol. Spot data 10 and 15 show that Ba/Ca decreases exponentially during the first 1-2 cycles (this is not seen in the OKA standard), suggesting that superficial contamination is present i.e. Ba/Ca counts are relatively stable after the first two cycles (i.e. 140 s). However, in linescan mode, Ba/Ca counts are taken after 57 s and hence not all the superficial contamination will have been removed. Surface

contamination contributes typically 3 x 10^{-5} counts to the overall counts of Ba/Ca in spot mode. Comparison of the timing Ba/Ca and Si/Ca in linescan mode showed significance difference to that of Mg/Ca. By disregarding low Ba/Ca measurements (<1.0 mmol/mol), the correlation between the Ba/Ca and Si/Ca becomes insignificant. Thus, synthesising data from both spot and linescan contamination analyses indicates that contamination may only become significant at low concentrations, but at higher concentrations, the relative contribution of contaminants becomes insignificant. Thus, the effect that contamination has at higher concentrations of Ba/Ca (>0.01 mmol/mol) is minimal.

		OKA		NCC		*Arctica islandica* (U248)	
		Linescan	Spot	Linescan	Spot	Linescan	Spot
Sr	Concentration (ppm)		11967		845	800-2200	800 - 1800
	mmol/mol		13.67		0.96	0.9-2.5	0.9 - 2.1
	Counts (cps)	28,000-32,000	15,000-18,000	2,400-2,800	1500-1600	1,800-2,800	1700-2200
	Reproducibility (%)	0.9%	1.9%	23.5%	1.3%	n/a	2.5%
Mg	Concentration (ppm)		688		2749	100 - 1350*	50 - 140
	mmol/mol		2.83		11.31	0.3-5.5*	0.2 - 0.6
	Counts (cps)	250-300	50-70	1200-1450	200-300	28-40	10-15
	Reproducibility (%)	5.1%	5.1%	8.8%	6.4%	n/a	7.0%
Ba	Concentration (ppm)		1800		29	10* - 300	2-15
	mmol/mol		1.31		0.02	0.007* - 0.95	0.002 - 0.01
	Counts (cps)	600-750	13-18	1.3-1.5	0.4-0.5	0.6-2	0.5-2
	Reproducibility (%)	1.8%	3.5%	10.5%	6.0%	n/a	3.0%
	^{48}Ca Counts in linescan mode	5400-5600		6400-6800		4000-48000	
	^{44}Ca Counts in spot mode		27,000- 32,000		30,000-32,000		27,000-33,000

Table 3.2: Concentrations within standards OKA, NCC and *A. islandica*, together with counts (per second) and calculations of the precision. Reproducibility for the spots was calculated by $2\sigma/\sqrt{n}$ (where n is the number of analyses). Note the higher counts for linescan is because the energy offset was 75 eV during spot mode, thereby reducing the counts. *Calculated concentrations include measurements affected by contamination.

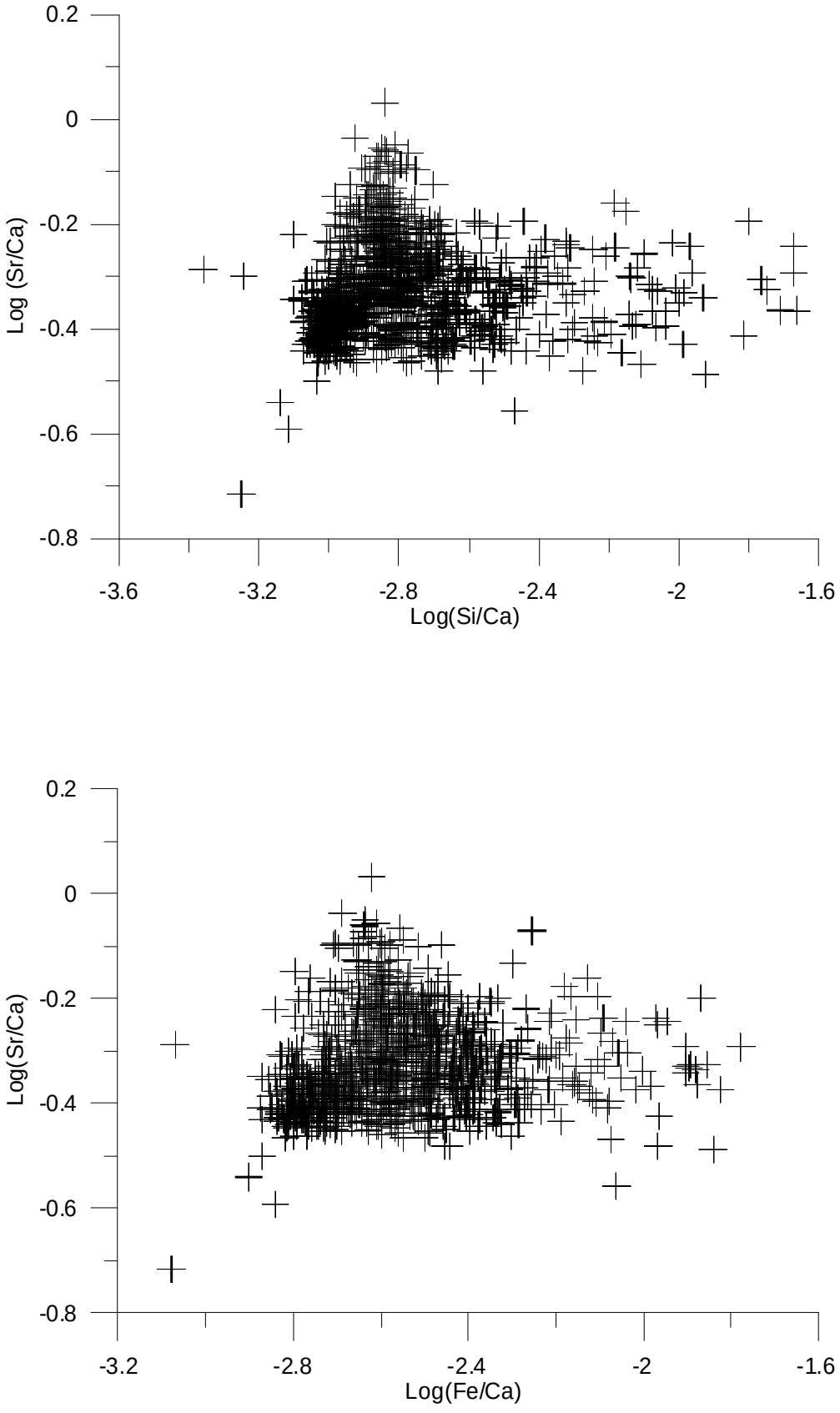

Figure 3.5: Lognormal plot of Si/Ca vs. Sr/Ca and Fe/Ca vs. Sr/Ca for linescan data from the prismatic layer of the umbo of *A. islandica* specimen 248.

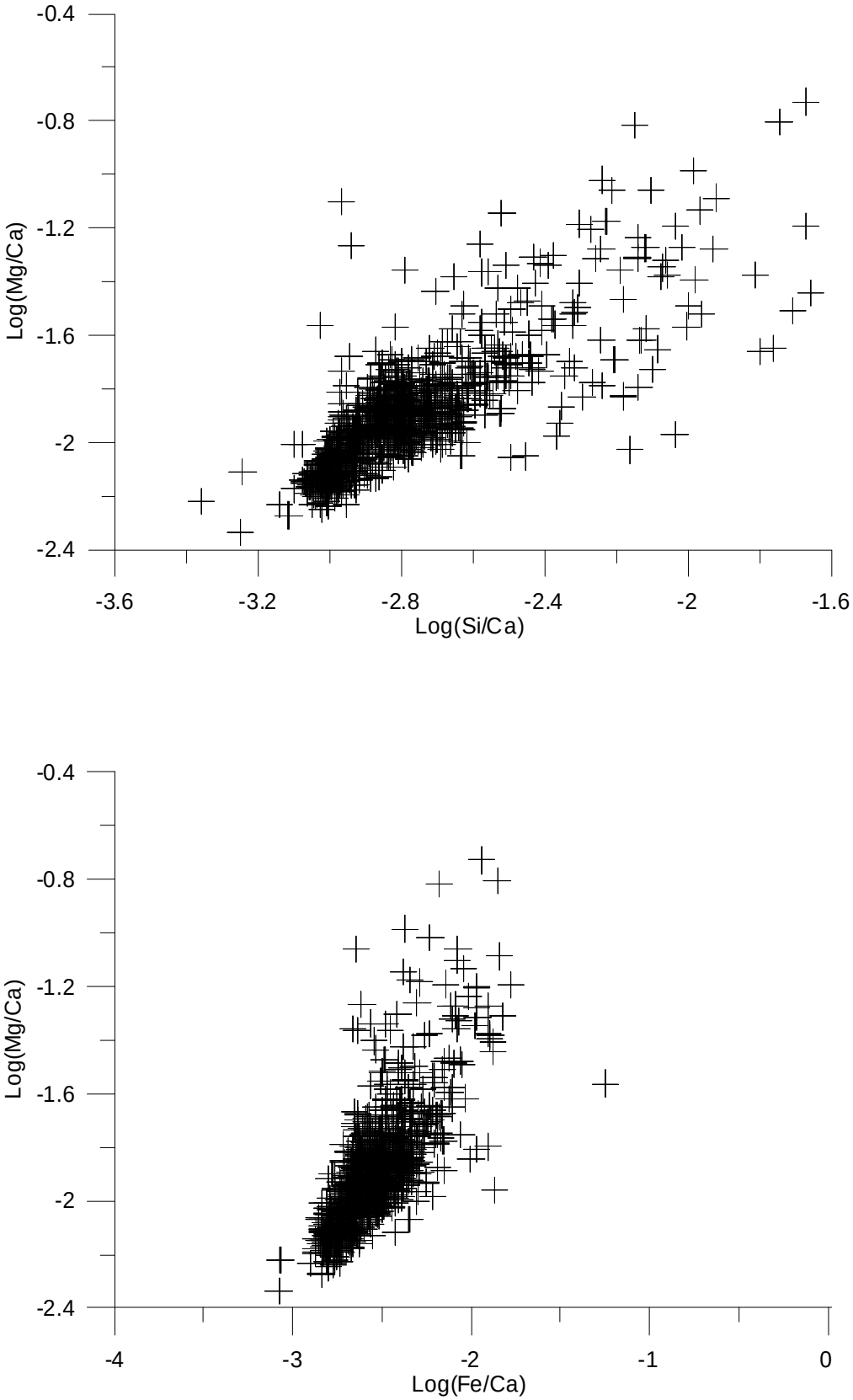

Figure 3.6: Lognormal plots of Si/Ca vs. Mg/Ca and Fe/Ca vs. Mg/Ca from linescan data from the prismatic layer of the umbo of *A. islandica* specimen 248.

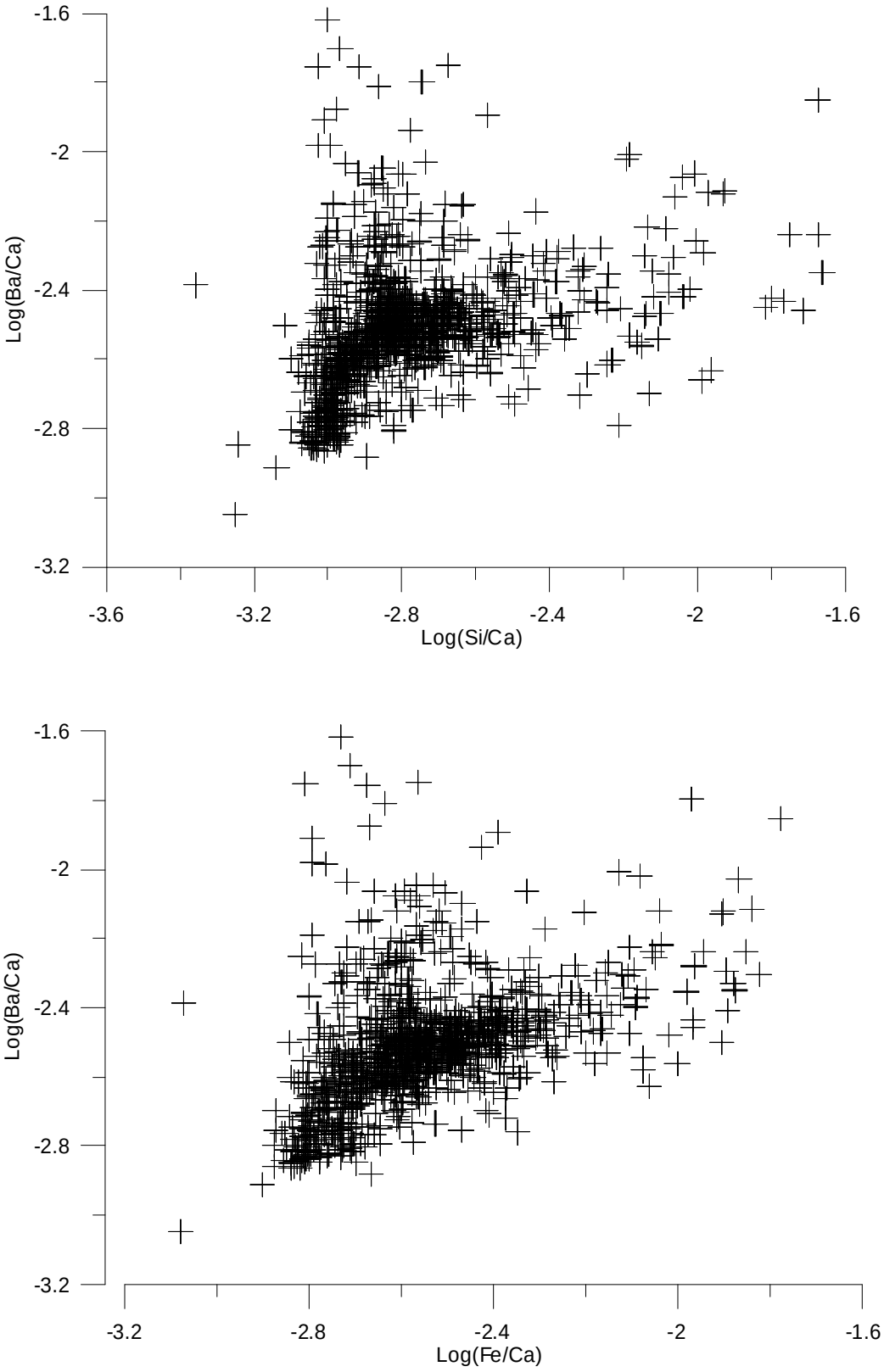

Figure 3.7: Lognormal plots of Si/Ca vs. Ba/Ca and Fe/Ca vs. Ba/Ca from linescan data from the prismatic layer of the umbo of *A. islandica* specimen 248.

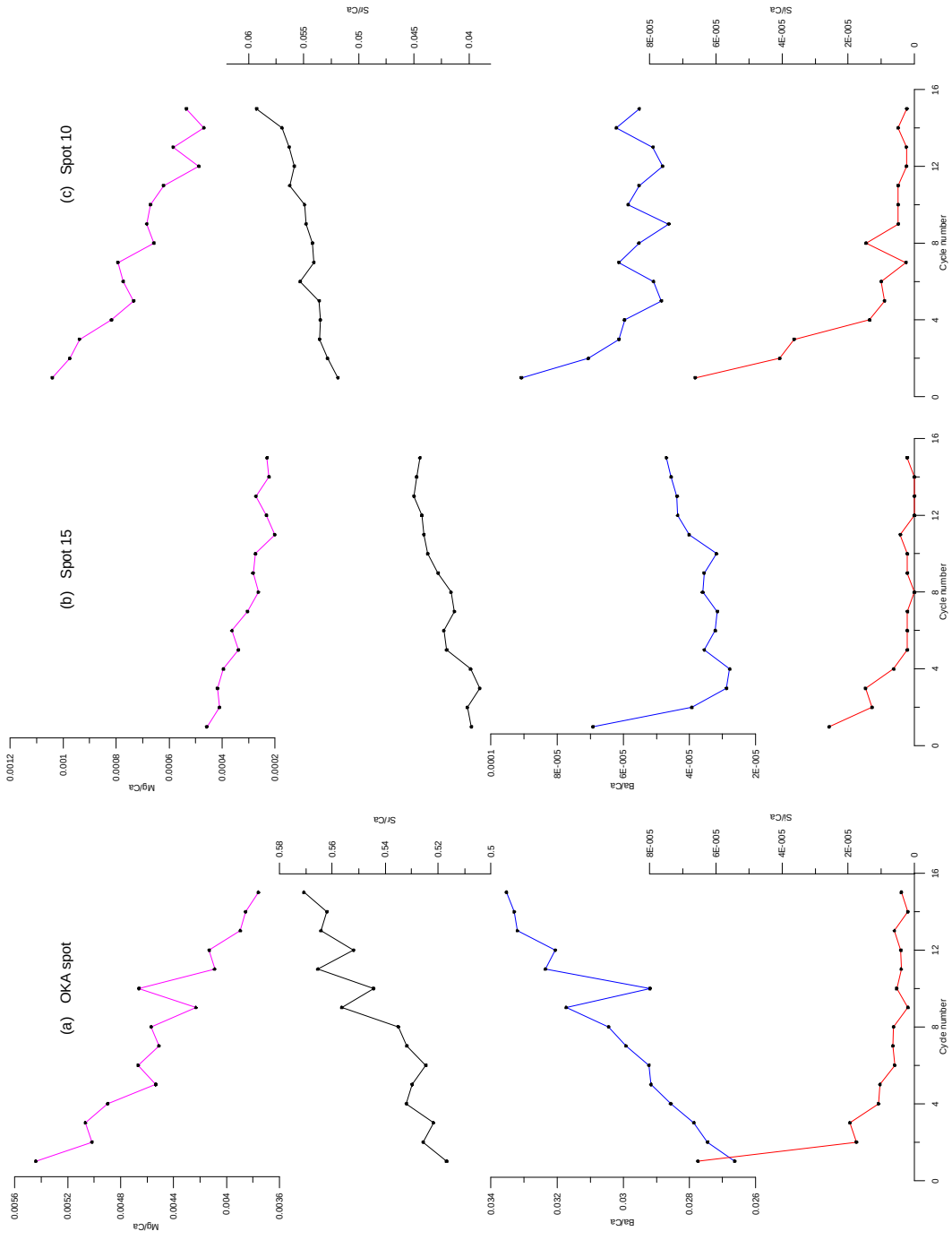

Figure 3.8: Spot analysis through burn cycles of Mg/Ca (magenta line), Sr/Ca (black line), Ba/Ca (blue line), Si/Ca (red line) of (a) OKA (b) spot 10 (c) spot 15. Note all elements show some change during the cycles due to sputtering but it accounts for <20%. Note for spots on *A. islandica* decrease of Mg/Ca counts of ~50% whereas changes Sr/Ca were <25% equivalent to that in the OKA standard. Ba/Ca shows significant decrease in the first two cycles but then is relatively steady.

3.4 Results

All the trace elements vary significantly within the prismatic layer of the umbo; with variations between the elements not occurring synchronously (see Figure 3.9). The results for U248 and U228 of trace element analysis are presented below.

3.4.1 Sr variation in U248

Sr/Ca increases coincide with the annual termination band, typically >1.5 mmol/mol but broadly increasing with age (Figure 3.10). These large increases in Sr/Ca at the annual growth check are deposited over short distances (typically <100 μm) and are defined as Sr/Ca peaks for the remainder of the discussion. The peaks consist of more than one data point (Figure 3.11). In addition, during 1998 a doublet (noted visually) is also recorded with an increase in Sr/Ca of ~2.2 mmol/mol equivalent or greater to those at the annual growth check. During the more juvenile stages of growth, there is increased growth rate (i.e. more shell material is deposited per year in the juvenile years) and within the growth bands there is an increase in Sr/Ca e.g. Such variation intraannually is not seen during the latter years of growth, with variation e.g. in 1993 being <0.2 mmol/mol. While there is significant variation during the growth bands of 1987-1989, particularly in 1988 varies from 0.9 to >1.3 mmol/mol, there is no pattern in the Sr/Ca variation within the growth bands between years. In 1988, the maximum occurs mid-way through the band, but in other years, there is no determinable pattern.

3.4.2 Mg variation in U248

As discussed above, Mg/Ca measurements were affected by contamination that could not be removed by data filtering. Therefore, the interpretation of the Mg/Ca results presented here is limited.

Mg/Ca data showed significantly more contamination during the earliest years of growth and therefore only the last ~7 years have been examined. Mg/Ca peaks exceed 0.8 mmol/mol with the average level being around 0.4 mmol/mol, in addition the peaks with the growth bands are often considerably more than those associated with the annual growth check (i.e. >0.4 mmol/mol) (Figure 3.12).

Prior to 1996, this correlation is much more limited with increases in Mg/Ca occurring independently of Sr/Ca peaks. Mg/Ca varies from 0.4-2 mmol/mol, with single data points exceeding these levels. In order to establish which Mg/Ca were affected by contamination, Si/Ca values were plotted for comparison (Figure 3.14). These show that Si/Ca values were low during the first 1000 μm of measurement, with no extreme Mg/Ca values but after which there is increasing number of high data points for both Si/Ca and Mg/Ca. In addition, there is an increase of ~0.2 mmol/mol, 4300-6700 μm from growth edge, in the Mg/Ca non-extreme values, which is associated with an increase in the average (non-extreme) values of Si. This distance was covered by a single transect (T8). The transects were analysed as a series of straight lines, due to complexity of measuring curved transects, with the direction of measurement changed at the end of each transect to correct for the curvature of the shell. The increase in Mg/Ca and Ba/Ca in T8 is not discernible in the Sr/Ca data, indicating that this increase is due to contamination (Figure 3.13).

In the latter years of growth Mg/Ca increases at the annual termination band as does Sr/Ca, but the relative increases in counts are inconsistent (see Figure 3.13 for increased resolution). While they both co-vary at the annual termination band Mg/Ca increases ~10 μm later than Sr/Ca, suggesting that they have different controls within the termination band.

3.4.3 Ba variation in U248

Ba/Ca increase does not occur at the growth check (as Mg/Ca or Sr/Ca). Ba/Ca varies from 0.02-0.1 mmol/mol, with values typically ~0.02 mmol/mol with sporadic increases exceeding 0.06 mmol/mol (see Figure 3.14). Ba/Ca peaks do not occur every year, nor within the same part of the growth band. There was no correlation between the Ba/Ca and Si/Ca counts at these high points and unlike Mg/Ca high values, high Ba/Ca are analysed during more than one spot, i.e. each peak is made up of typically three or more spots. Therefore, such Ba/Ca increases are not due to contamination.

3.4.4 Lateral variation of the trace elements in U248

Parallel transects on shell U248 were analysed ~60 μm and 750 μm from the maximum growth axis (3800-5000 μm from the growth edge during 1988-1989). A five point running average has been used for all three transects to compensate for any small differences in position in the band analysed. These show significant lateral change (i.e. greater than the estimated error) in the trace elements along individual bands. For Sr/Ca, the profile is very similar but the absolute values increase away from the maximum growth axis (Figure 3.15a) by ~25%. Slight offsets in the position of the Sr/Ca maximal result from differences in shell extension rates, which are highest at the maximum growth line. Mg/Ca does not show a consistent offset between transects despite using a five point running average (Figure 3.15b). Ba/Ca shows an offset at the higher values, but not at the lower ones (Figure 3.15c), however as discussed previously, values <0.01 mmol/mol were significantly affected by contamination. Analysis of a second set of parallel transects taken 25 μm apart (close at the growth edge) (Figure 3.16) again show that the Sr/Ca and Ba/Ca trends

replicate well across the shell, although an offset in the absolute values of ~10%. For Mg/Ca while some points are replicated (with an offset), others are not. This suggests either some of these features are likely to do be due to contamination or Mg/Ca incorporation is very heterogeneous. The replication of some Mg/Ca along the band may reflect the accumulation of contamination along the laminae.

Spot analysis provides further support for the above findings (Table 3.3) with a lateral offset in Sr/Ca, whereas Mg/Ca variation is within error. Ba/Ca shows variation across the termination band, but all values (for spot 16-20) are <0.01 mmol/mol. As previously discussed, where Ba/Ca was <0.01 mmol/mol the effect of contamination is significant.

Spot number	Distance from maximum growth line	Sr/Ca mmol/mol	Mg/Ca mmol/mol	Ba/Ca mmol/mol $x10^{-3}$
16	410	1.06 ± 0.02	0.18 ± 0.02	0.31 ± 0.1
17	680	1.34 ± 0.04	0.17 ± 0.02	11.0 ± 1.2
18	940	1.43 ± 0.04	0.17 ± 0.02	12.0 ± 0.3
19	1100	1.62 ± 0.04	0.21 ± 0.02	5.7 ± 0.2
20	1390	1.57 ± 0.03	0.22 ± 0.02	8.3 ± 0.2

Table 3.3: Lateral variation in concentration of Sr/Ca, Mg/Ca and Ba/Ca in single annual termination band (1993) in the prismatic layer of the umbo of shell 248, with increasing distance from the maximum growth axis. Precision is given as the precision of the mean $2\sigma/\sqrt{10}$ (for 10 cycles) (see method for further details). Note that for Ba/Ca values <0.01 mmol/mol show significant correlation to contamination. Therefore for spot data 16-20 where Ba/Ca is <0.01 mmol/mol, the effect of contamination is significant.

3.4.5 Trace element analysis of U228

Analysis of U228 was limited to two short transects measuring the same elements as U248; with a longer transect measuring only Sr/Ca. The short transects show variation of Sr/Ca 0.9-1.8 mmol/mol and Mg/Ca varying 0.25-0.7 mmol/mol. Both Mg/Ca and Sr/Ca show peaks at the annual termination bands (Figure 3.17) with Mg/Ca also showing peaks within the growth band. These peaks are similar in magnitude or larger than the Mg/Ca peak present at the annual termination band. The largest peak within the growth band is 0.52 ± 0.005 mmol/mol compared to 0.5-0.7 ± 0.005 mmol/mol at the growth check. Ba/Ca varies 0.006-0.018 mmol/mol, and does not correlate with Mg/Ca, Sr/Ca, or the annual termination bands.

Sr/Ca peaks in U228 also occur at the annual bands in the later years of growth (with peaks around 1.7-1.9 mmol/mol), but during the juvenile stages, these highly defined peaks at the termination band are not visible. Instead, there is a broad increase consistently throughout the year. The annual termination bands also become more diffuse and can cover over 150 μm with values up to 1.5 mmol/mol.

3.4.6 Comparison of U228 and U248

Both shells show generally the same pattern of Sr/Ca behaviour, but the increase in Sr/Ca varies. High Sr/Ca is found at the growth checks with Sr/Ca variation within the growth bands occurring in both shells in the younger part of the shell. Both shells also show Sr/Ca increases at the doublet (which was noted visually in both shells) in 1998. The transition from high Sr/Ca peaks at the growth checks to little or no increase of Sr/Ca at the growth check varies significantly between the shells. For example, high Sr/Ca peaks are present in approximately the last 12 years of

growth in U248 can be clearly distinguished whereas in U228 the pattern is more complex with significant variation during the growth band.

Comparison of U228 and U248 (Figure 3.19a with Figure 3.19b highlighting the first 2000 μm measured) shows the range of Sr/Ca concentrations within U228 is less variable. Sr/Ca values in U228 have a maximum which never exceeds 2 mmol/mol, and is >10% less than those of U248 (where the maximum can be >2.4 mmol/mol). Both shells show Sr/Ca peaks at the annual termination band as well as at the doublet in 1998.

In shell 248, during 1998 the outer shell prismatic layer was damaged, but this shows no influence on Sr/Ca in the umbo (see Figure 3.11) (no visual record of the damage was seen in the umbo).

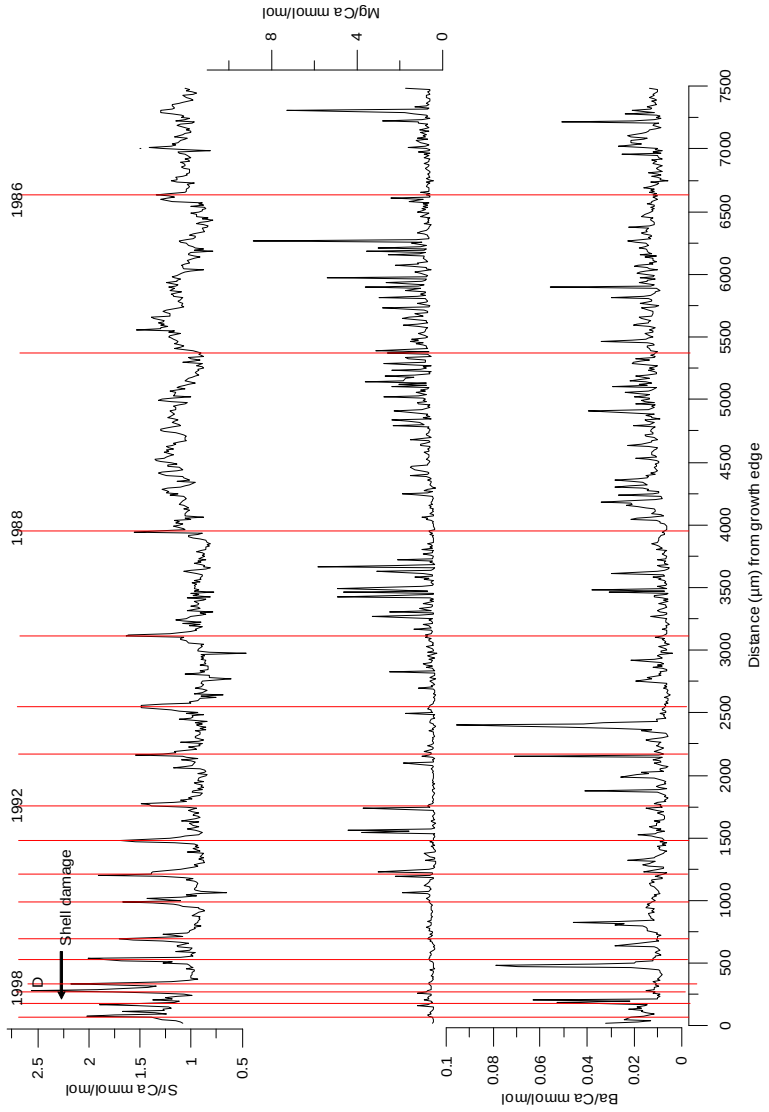

Figure 3.9: Variation of trace elements Sr, Mg and Ba (unfiltered data) in the prismatic layer of the umbo of *A. islandica* specimen 248. The red lines mark the position of the growth checks determined visually for each year (see section 1.2.2). D signifies the presence of a doublet just prior to the main annual growth check. 2σ was 0.9% Sr/Ca, 5.1% Mg/Ca, 1.8 % Ba/Ca (too small to be shown on the figure). Mg/Ca analyses in spot mode with a maximum of 1.0 mmol/mol showed no evidence of contamination, suggesting low concentrations may reflect Mg/Ca fluctuations in the shell, but Mg/Ca shows correlation to Si/Ca indicating that higher Mg/Ca may be subject to contamination. Ba/Ca data below 0.01 mmol/mol showed significant correlation with Si/Ca.

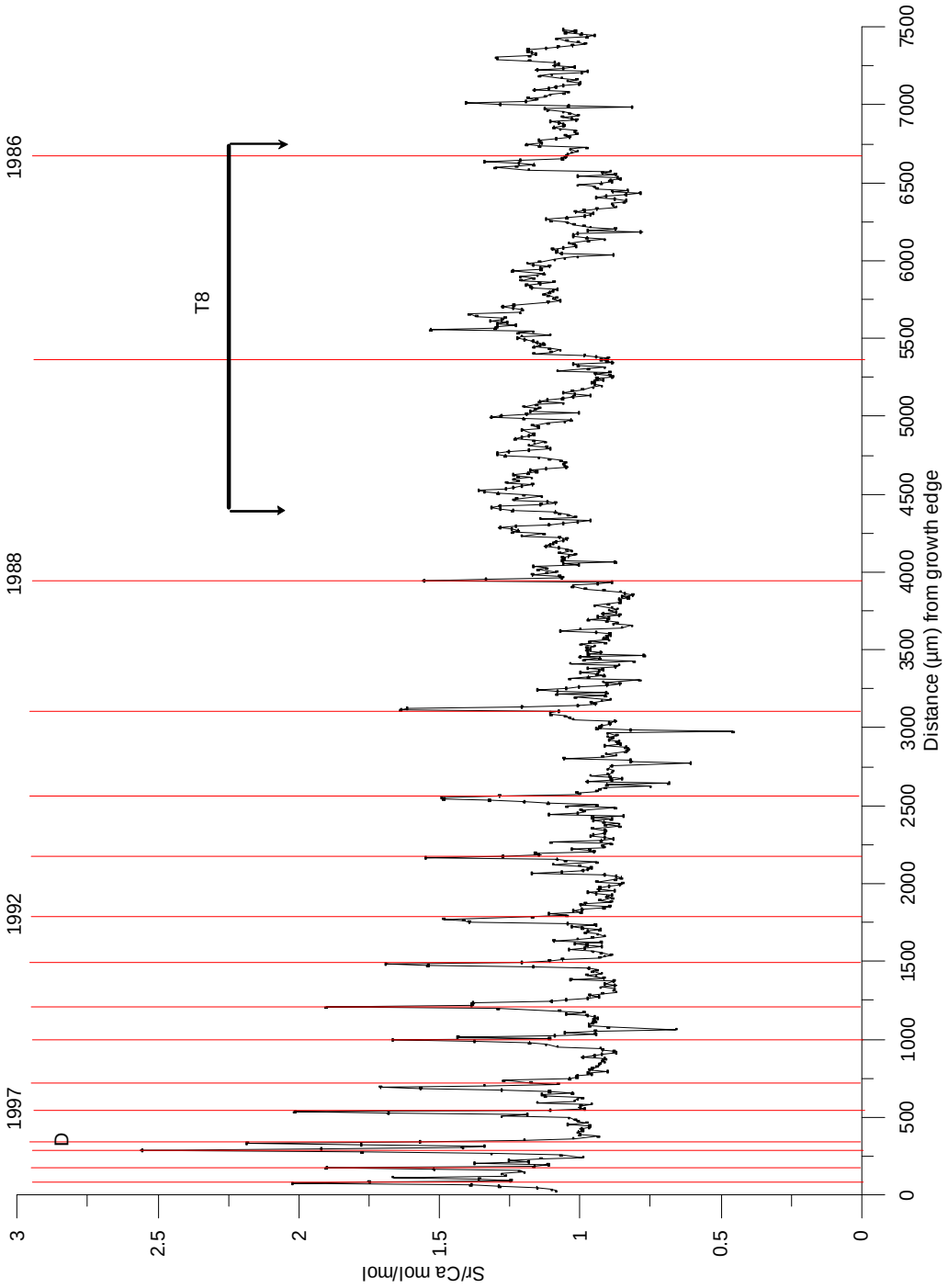

Figure 3.10: Sr/Ca variation in prismatic layer of the umbo of *A. islandica* specimen 248. The red lines mark the position of the growth checks determined visually for each year (see section 1.2.2), D signifies the presence of a doublet just prior to the main annual growth check. 2σ error was too small to be shown (0.9%). T8 refers to a specific transect taken during which low Mg/Ca and Ba/Ca both see elevated concentrations, this cannot be seen in Sr/Ca analysis.

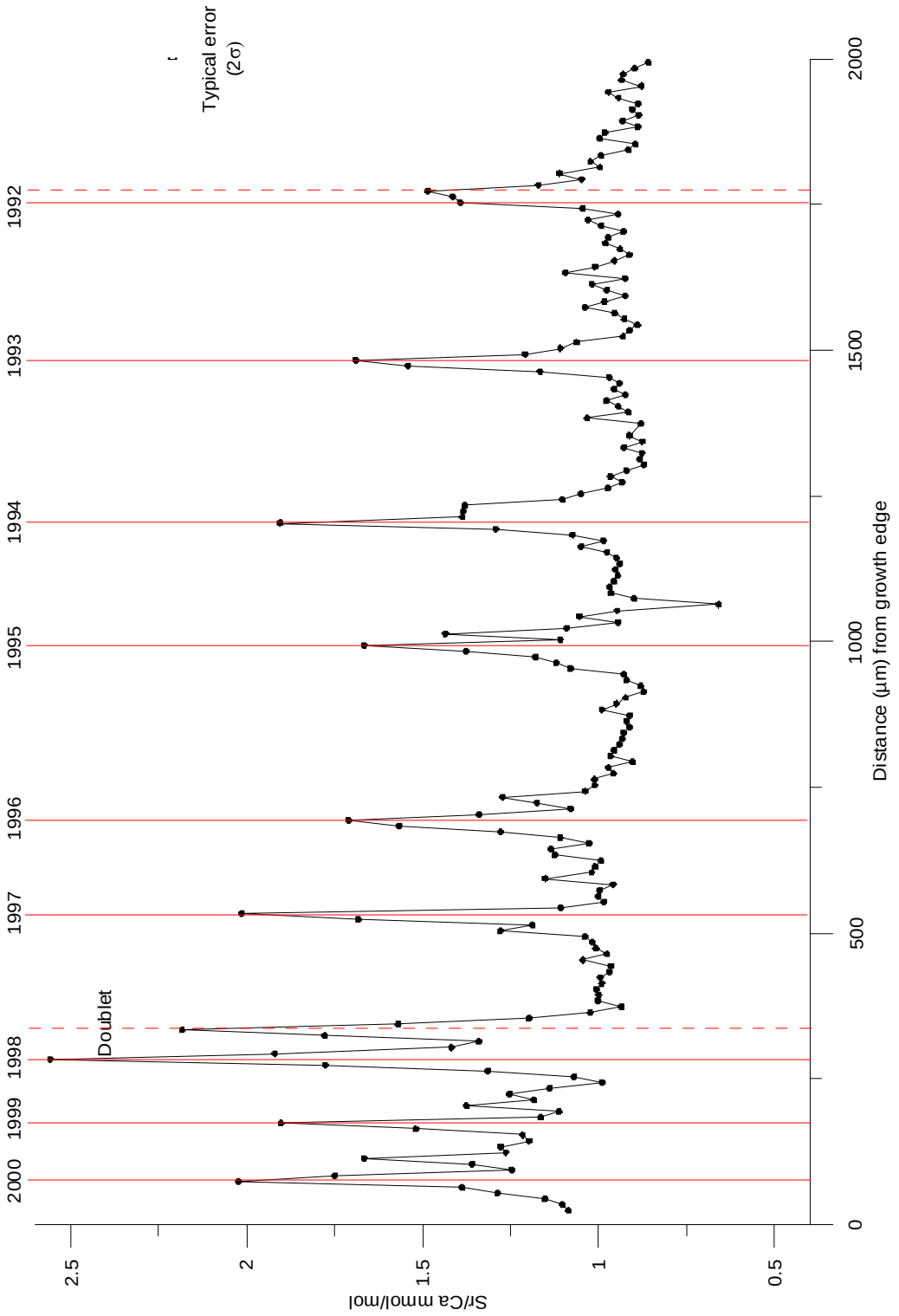

Figure 3.11: Sr/Ca fluctuations within the first 2000 µm of analysis of the prismatic layer of the umbo analysis of *A. islandica* specimen 248. The red lines mark the position of the growth checks determined visually for each year (see section 1.2.2).

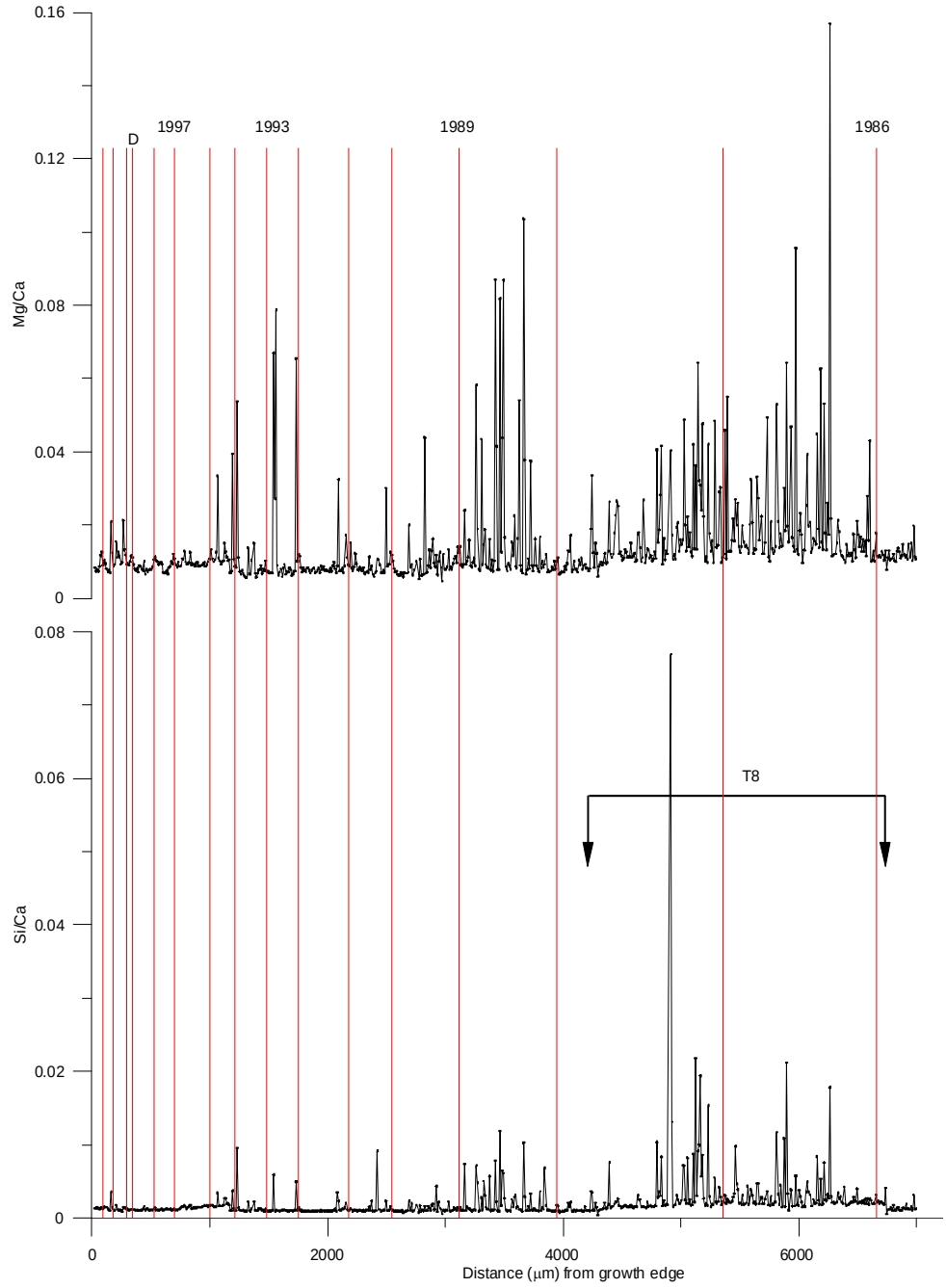

Figure 3.12: Mg/Ca (top) compared with Si/Ca (bottom) data for the prismatic layer of the umbo of *A. islandica* specimen 248. Data shown is not filtered and shows evidence of significant contamination, with correlation with Si/Ca increases. The red lines mark the position of the growth checks determined visually for each year (see section 1.2.2). D signifies the presence of a doublet just prior to the main annual growth check. 2σ on the OKA standard for Mg/Ca was 5.1%.

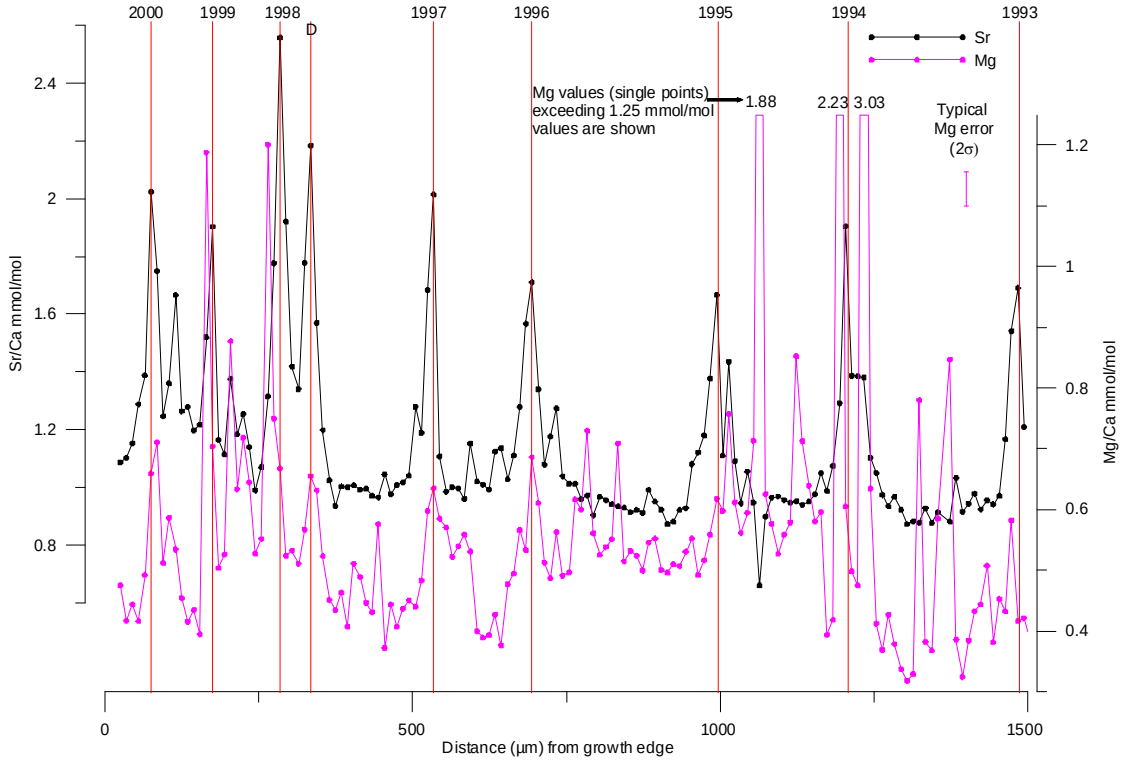

Figure 3.13: Enlargement of Sr/Ca (black) and Mg/Ca (magenta) peaks 0-1500 μm from growth edge (i.e. the most recent period of growth). Note high single values of Mg/Ca start after 1000 μm, which are >1.2 mmol/mol. Mg/Ca shows some agreement with Sr/Ca but peaks after Sr/Ca in the narrowest bands. The red lines mark the position of the growth checks determined visually for each year (see section 1.2.2). D signifies the presence of a doublet just prior to the main annual growth check. Sr/Ca error (2σ) is 0.9% (too small to be shown). Mg/Ca concentrations measured by spot analyses to the maximum concentration measured of 1.0 mmol/mol showed no evidence of superficial contamination, but higher concentrations may be affected by superficial contamination with Mg/Ca linescan data correlating significantly with Si/Ca.

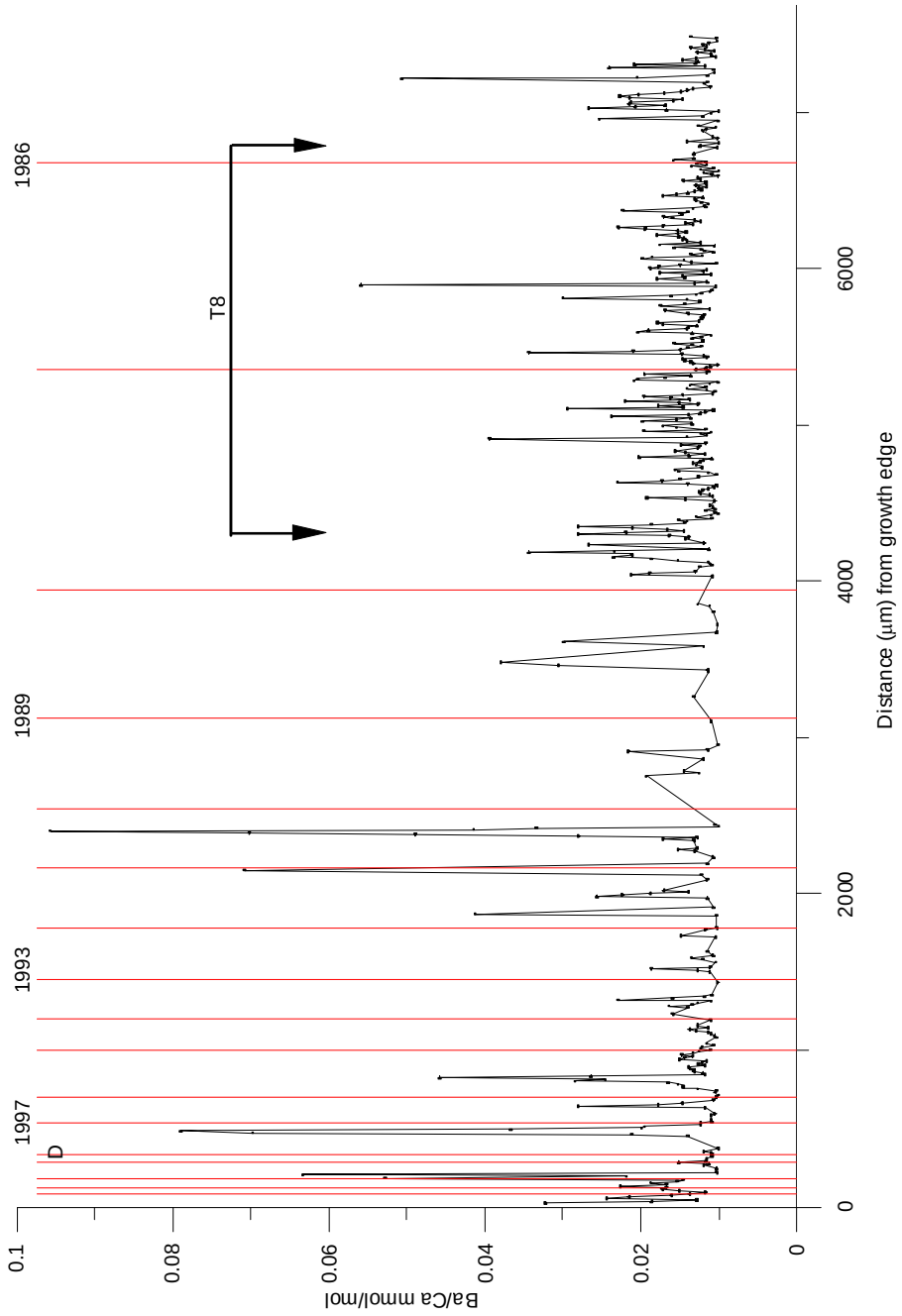

Figure 3.14: Ba/Ca fluctuations in the prismatic layer of the umbo region of *A. islandica* specimen 248. Transect 8 (T8) is highlighted (within which increased concentrations of Ba/Ca were recorded). The red lines mark the position of the growth checks determined visually for each year (see section 1.2.2). D signifies the presence of a doublet just prior to the main annual growth check. 2σ error was 1.8% (too small to be shown). Note that low concentrations Ba/Ca (<0.01 mmol/mol) is sensitive to contamination, and thus is not shown.

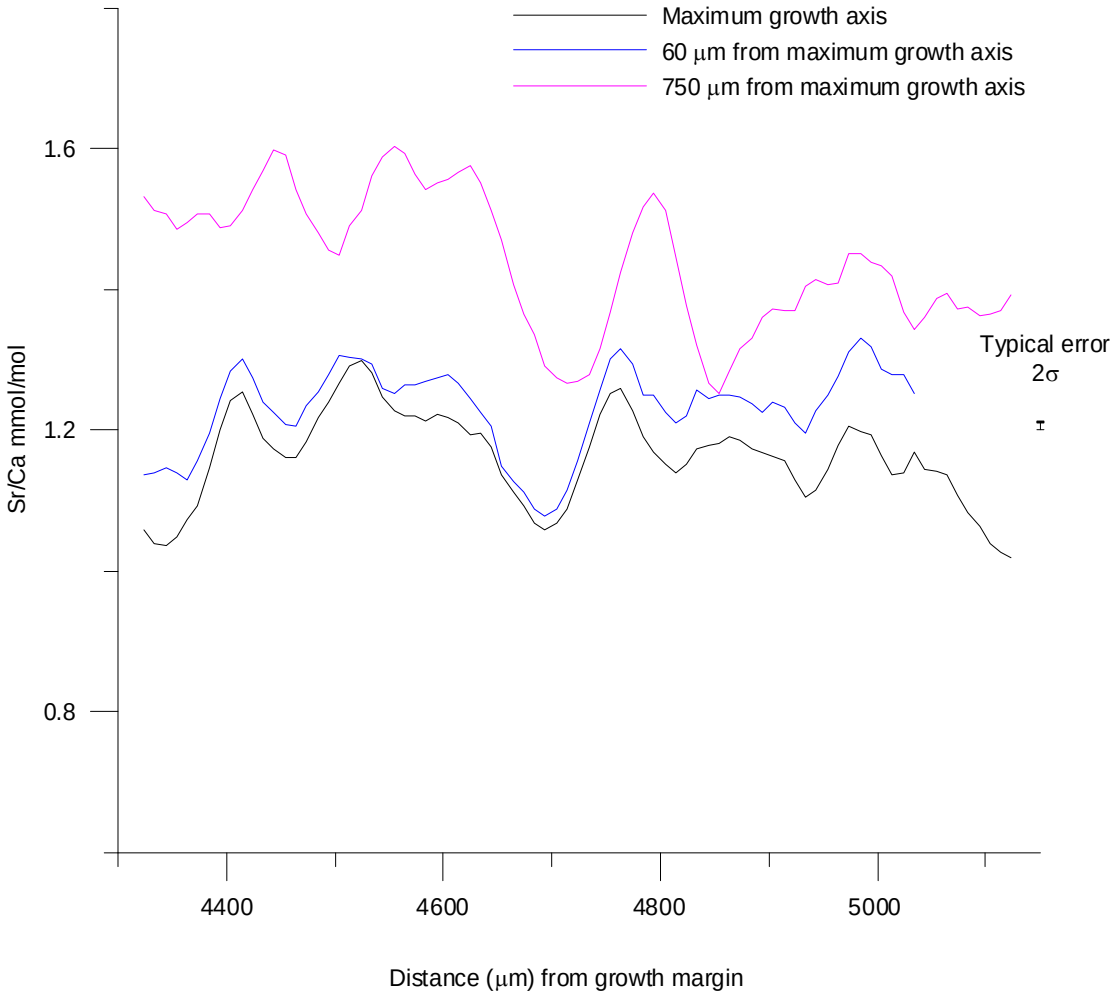

Figure 3.15a: Parallel Sr/Ca transects from the prismatic layer of the umbo of *A. islandica* specimen 248 using five point running average (during 1988-1989). The slight offset of the peaks is due to curvature of the shell.

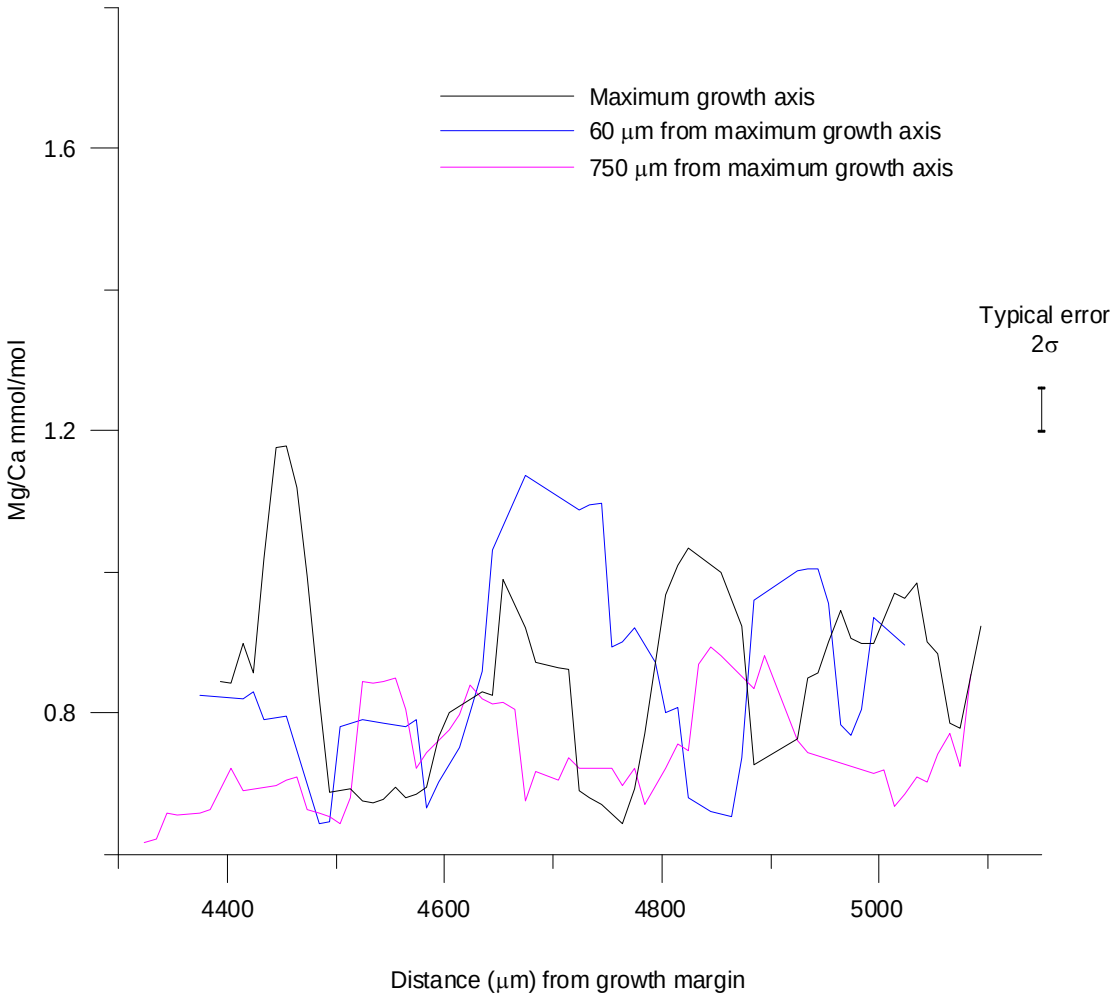

Figure 3.15b: Parallel Mg/Ca transects from the prismatic layer of the umbo of *A. islandica* specimen 248 using five point running average (during 1988-1989). Slight offset of the peaks would be expected due to curvature (see Figure 3.15a) but no consistent profile is visible. Mg/Ca concentrations measured by spot analyses to the maximum concentration measured of 1.0 mmol/mol showed no evidence of superficial contamination, but higher concentrations may be affected by superficial contamination with Mg/Ca linescan data correlating significantly with Si/Ca.

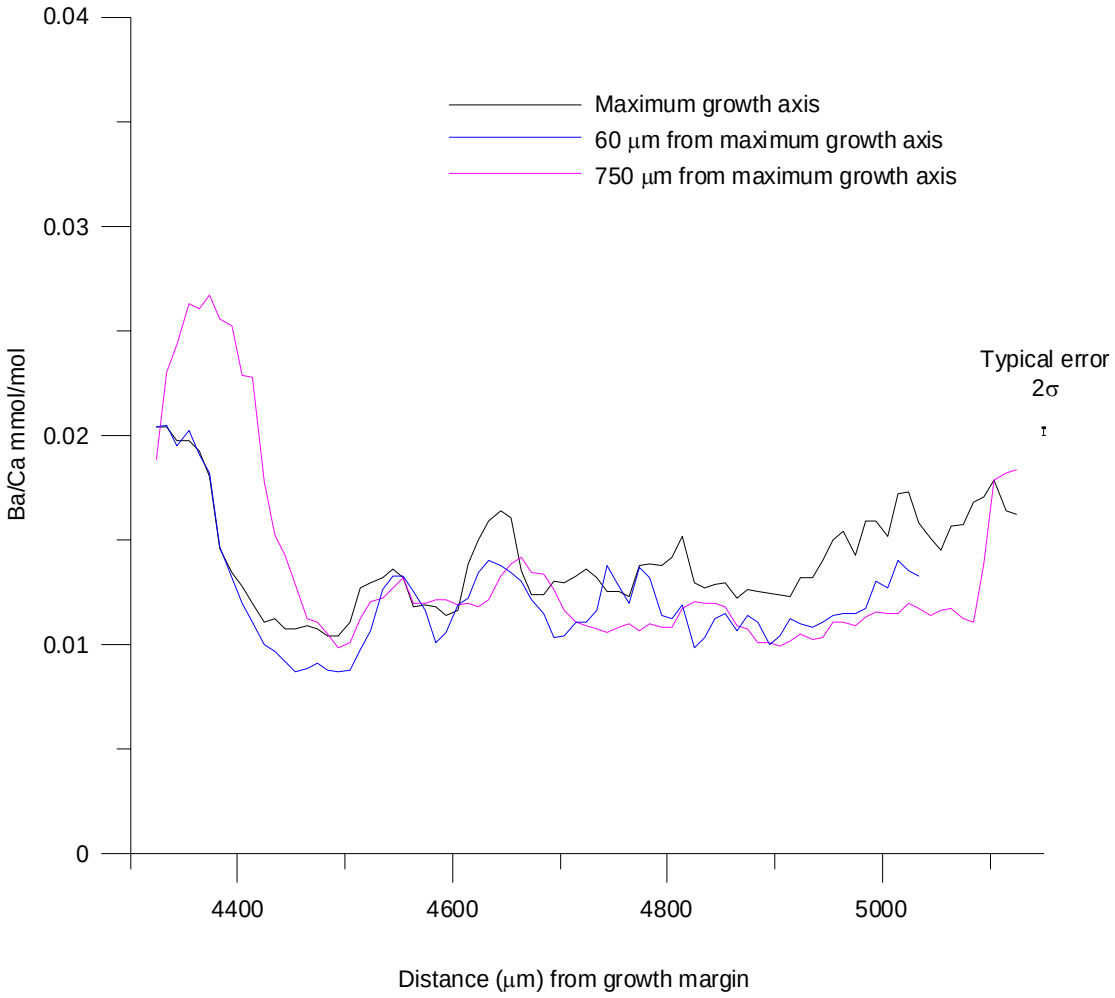

Figure 3.15c: Parallel transects of Ba/Ca the prismatic layer of the umbo of *A. islandica* specimen 248 using five point running (during 1988-1989 growth band). A slight offset of the peaks is due to curvature of the shell. Low Ba/Ca concentrations (<0.01 mmol/mol) are sensitive to contamination, showing significant correlation with Si/Ca (see Figure 3.7).

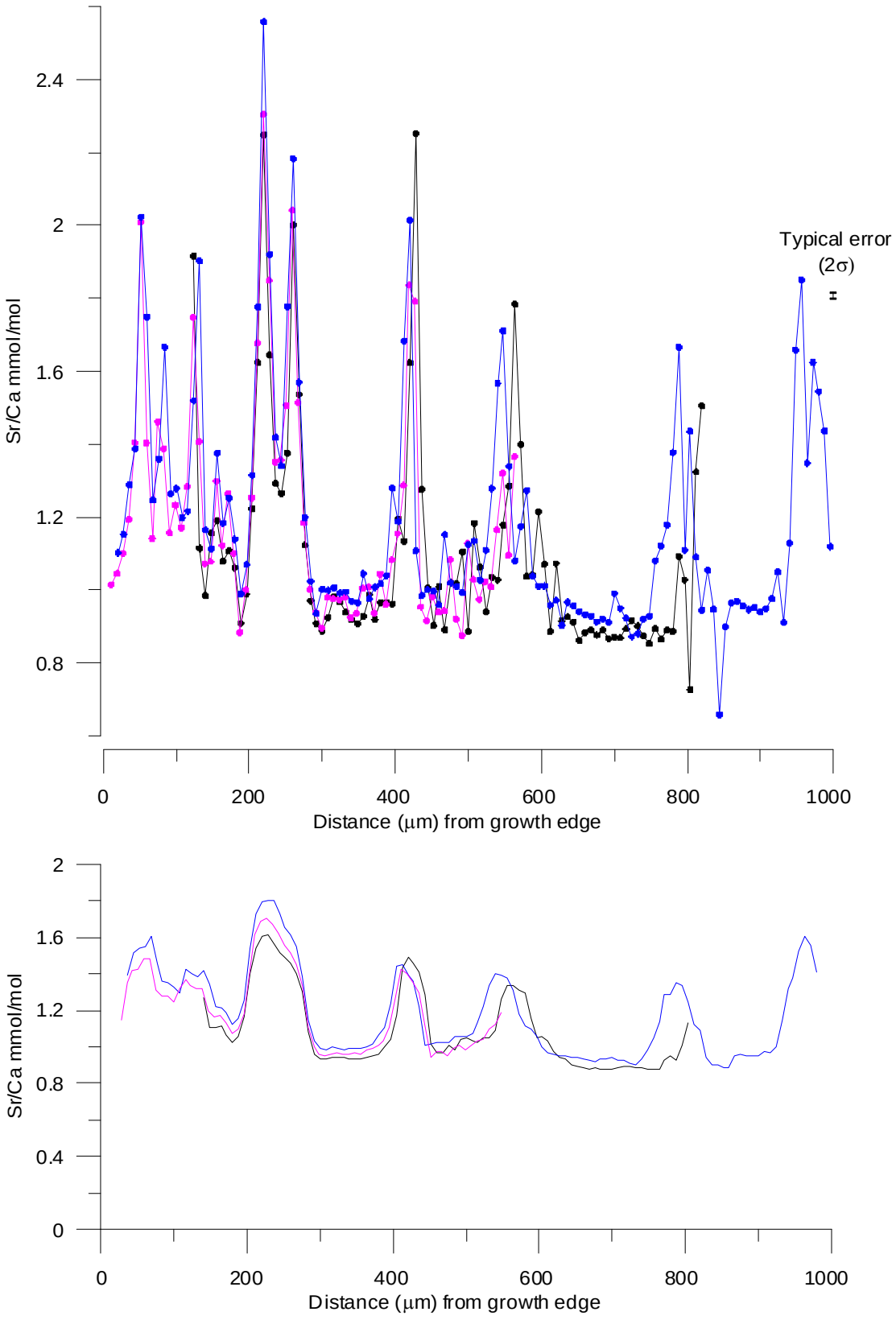

Figure 3.16a: Parallel transects of Sr/Ca taken <25 μm apart around maximum growth axis. Upper figure shows raw data, lower figure shows (5 point running) average values.

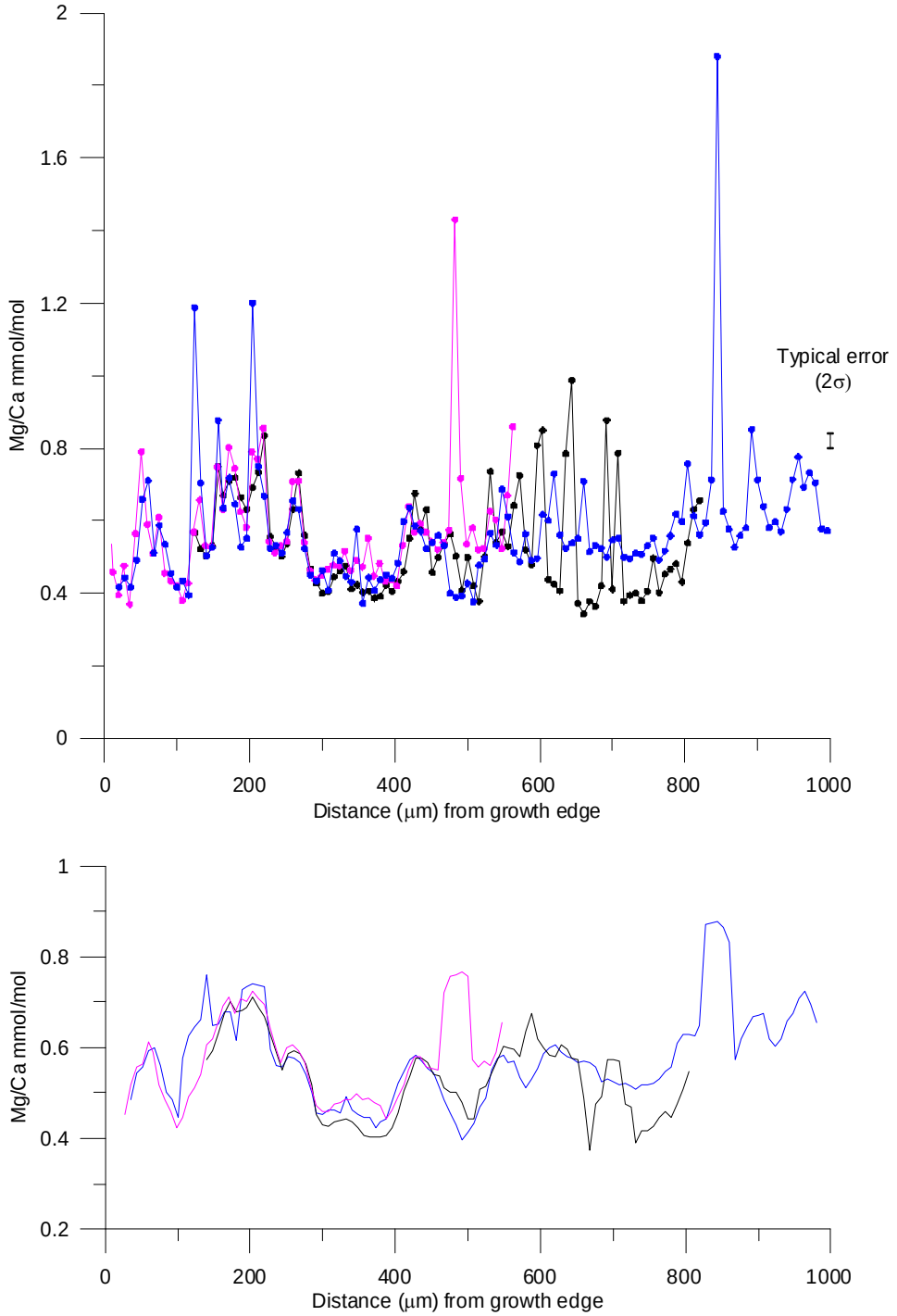

Figure 3.16b: Parallel transects of Mg/Ca taken <25 μm apart around maximum growth axis. Upper figure shows raw data, lower figure shows (5 point running) average values. Data is shown unfiltered. Mg/Ca concentrations measured by spot analyses to the maximum concentration measured of 1.0 mmol/mol showed no evidence of superficial contamination, but higher concentrations may be affected (see Figure 3.6 and text for further details).

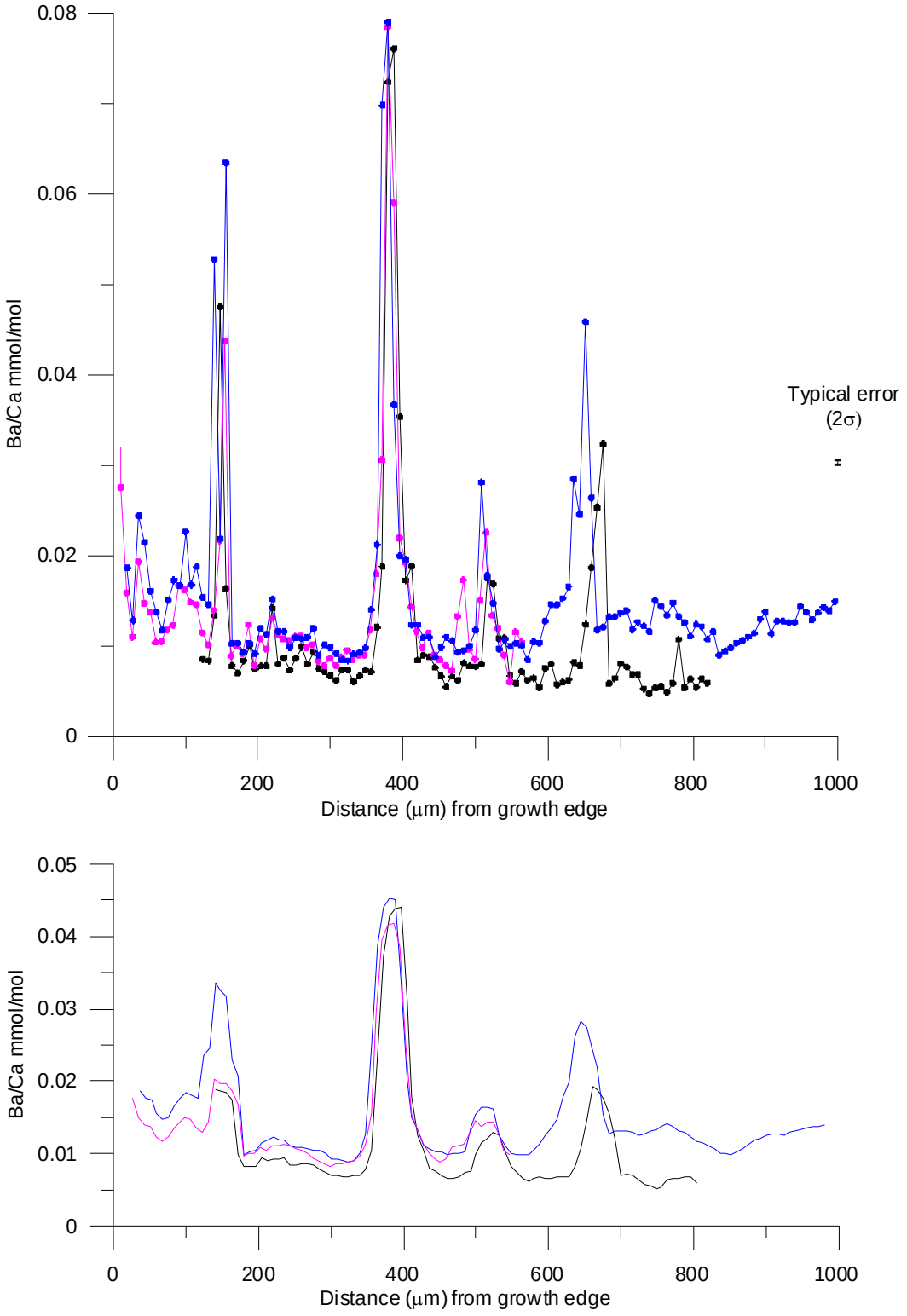

Figure 3.16c: Parallel transects of Ba/Ca taken <25 μm apart around maximum growth axis. Upper figure shows raw data, lower figure shows (5 point running) average values. Ba/Ca <0.01 mmol/mol is sensitive to contamination (see text for further details).

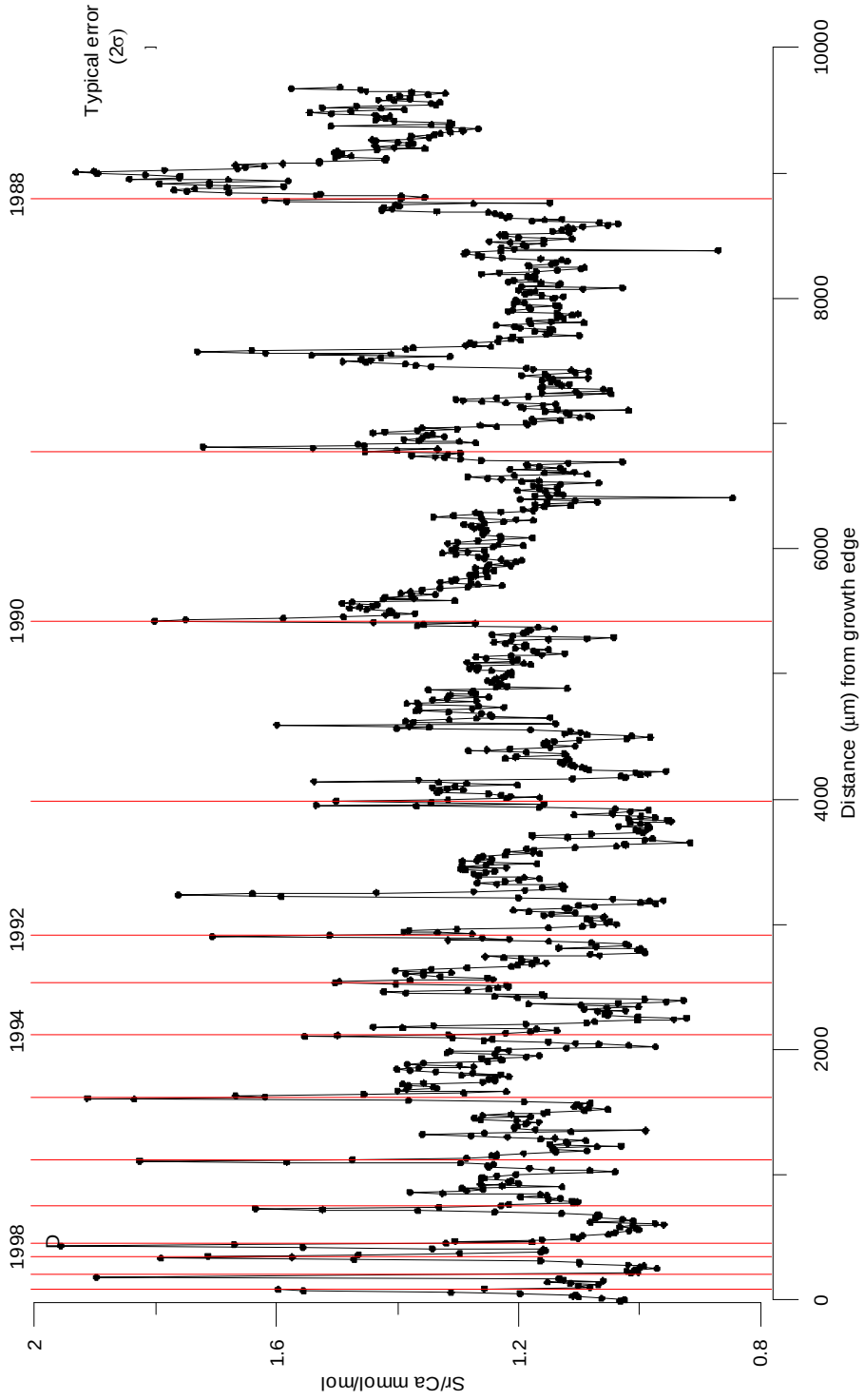

Figure 3.17: Sr/Ca fluctuations in the prismatic layer of the umbo region of *A. islandica* shell 228. The red lines mark the position of the growth checks determined visually for each year (see section 1.2.2). D signifies the presence of a doublet just prior to the main annual growth check.

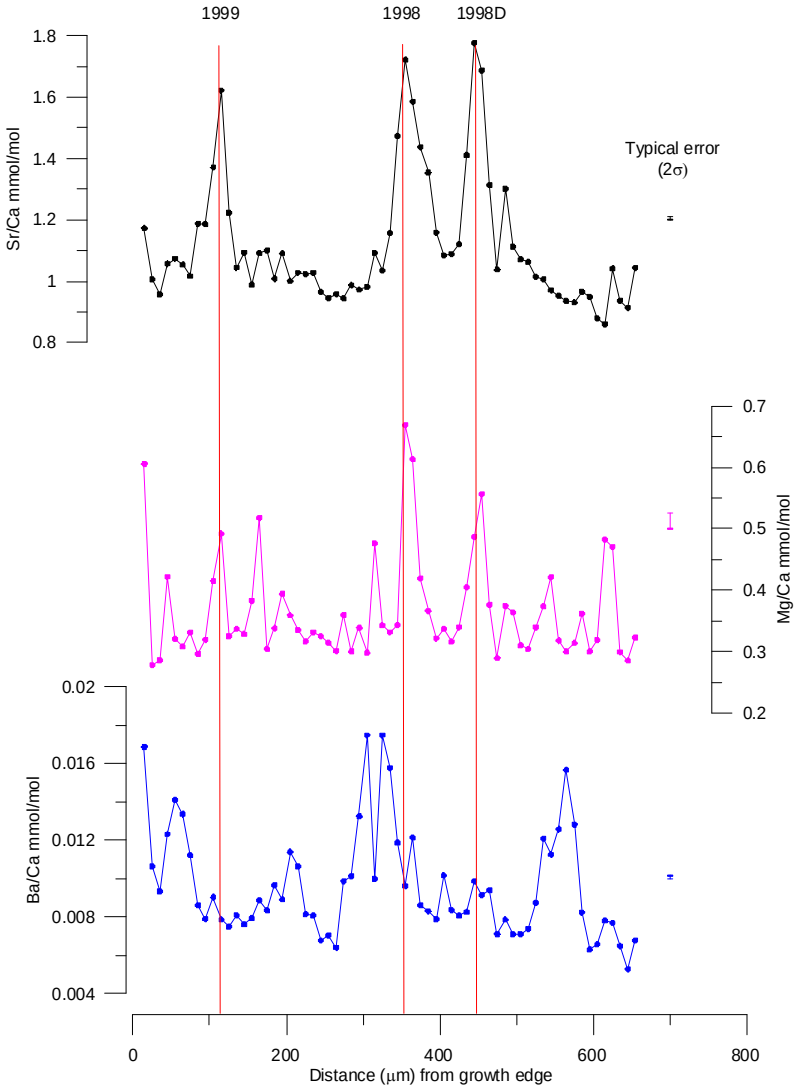

Figure 3.18: Sr/Ca, Mg/Ca and Ba/Ca fluctuations from short transect analysis of prismatic layer of the umbo of *A. islandica* shell 228 taken using a 10 μm beam. The red lines mark the position of the growth checks determined visually for each year (see section 1.2.2). D signifies the presence of a doublet just prior to the main annual growth check. Note that like U248, U228 shows increase at doublet of Sr/Ca and Mg/Ca. Ba/Ca shows very little variation with no sporadic peaks present. Ba/Ca <0.01 mmol/mol are sensitive to contamination (see text for further details).

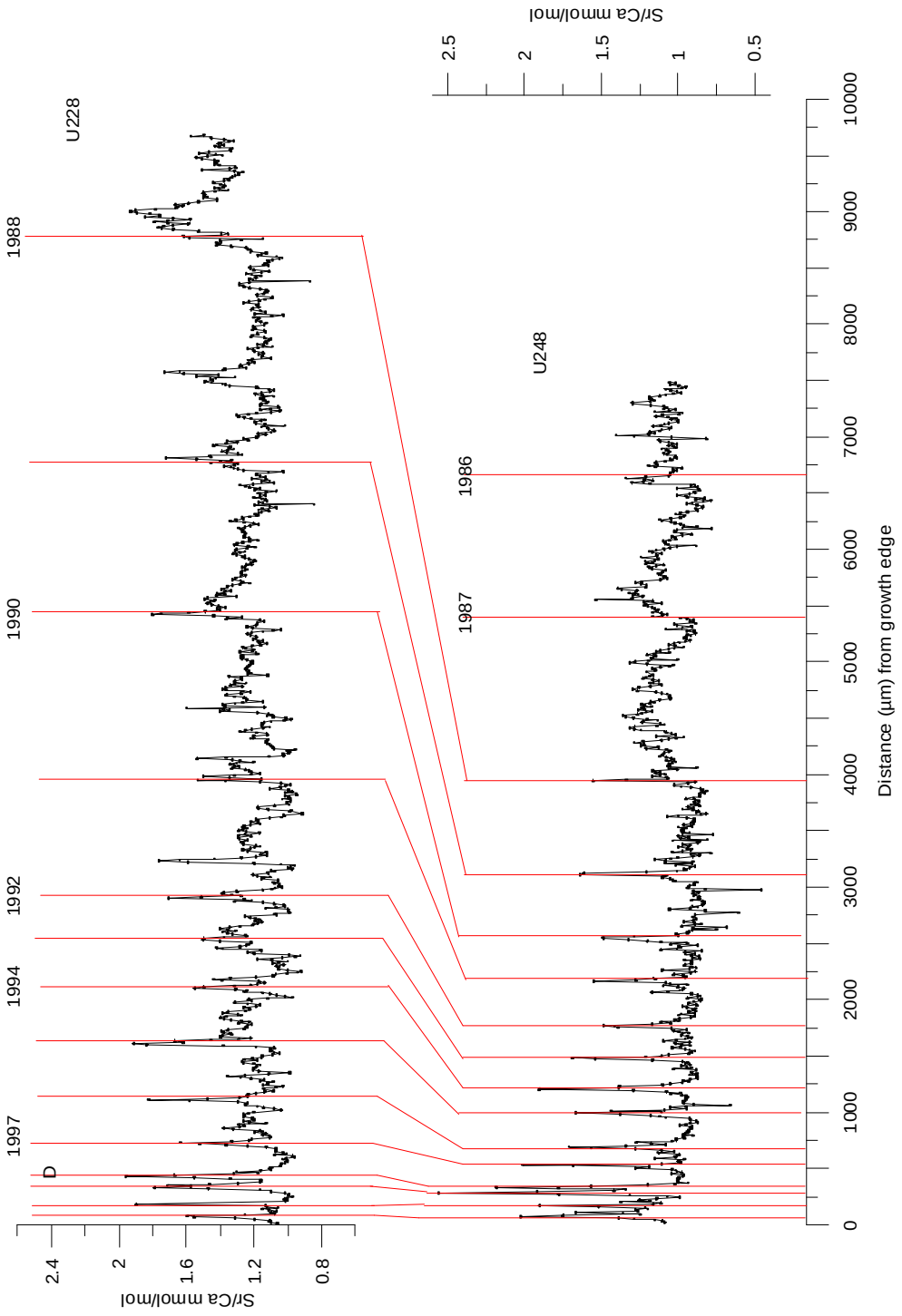

Figure 3.19a: Comparison of Sr/Ca measurement from the prismatic layer of the umbos of shell 228 (upper figure) compared to shell 248 (lower figure). The red lines mark the position of the growth checks determined visually for each year (see section 1.2.2). D signifies the presence of a doublet just prior to the main annual growth check. 2σ was too small to be shown (0.9%).

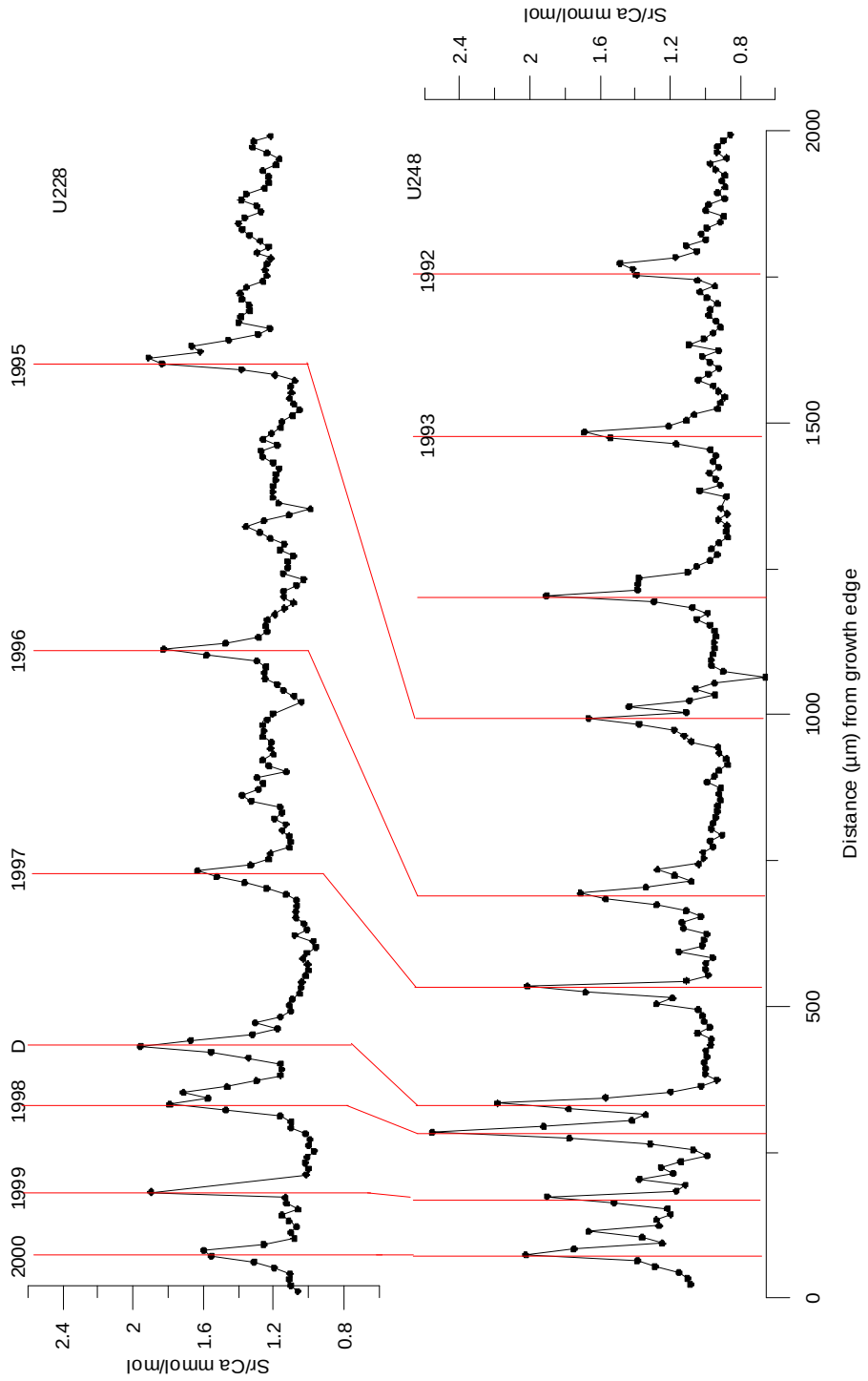

Figure 3.19b: Comparison of the Sr/Ca fluctuations in the prismatic layer of the umbos of shell 228 (upper diagram) compared to shell 248 (lower diagram) insert of 0-2000 µm. The red lines mark the position of the growth checks determined visually for each year (see section 1.2.2). D signifies the presence of a doublet just prior to the main annual growth check. 2σ error bars were too small to be shown (0.9%).

3.5 Discussion

Understanding the controls on trace elements will provide insights into the potential of *A. islandica* to provide palaeoenvironmental reconstructions. In particular, whether the trace element profiles are dominated by environmental factors or mainly affected by internal changes such as changes in the shell architecture, shell growth rate or by vital effects. Comparison of the two shells allows discussion on the similarities and differences between their profiles (especially Sr/Ca where long profiles were taken in both shells) and what may cause such differences.

3.5.1 Possible controls on Sr variation within A. islandica

Both U228 and U248 show Sr/Ca peaks at the annual growth check during the latter years of growth. The magnitude of these peaks differs between the shells, but as discussed earlier, there is a lateral variation within shells making direct comparisons between shells difficult. The difference in magnitude of the Sr/Ca peaks is typically <0.5 mmol/mol, but significantly this difference is not constant. If the maximum growth line were not analysed in both cases, this could account for the offset between the shells. In addition, it is possible that the trace elements could have heterogeneity in the third dimension i.e. the site of cutting and polishing could result in trace element offsets with depth (see Figure 1.2).

Both shells show Sr/Ca increases at the same doublet (identified by visual inspection). The presence of Sr/Ca peaks at doublets provides a strong indication that Sr incorporation is not temperature controlled, as this would require a significant temperature excursion just prior to the growth check, something that is not seen in the SST from Millport. The doublets are more likely to be a biological response. Schöne *et al. (*2005b) reported cessation in growth from mid-September to mid-November

due to spawning (or pseudo-spawning in immature specimens), with growing recommencing for one month prior to the annual growth check i.e. this would fit the profile of the doublet with a short second growing season. Sr/Ca increases at the doublets are therefore likely to relate to changes associated with biological changes or relate to the formation of the growth checks.

Two studies of the partitioning of Sr/Ca between abiogenic aragonite and seawater show the temperature dependence is ~0.039 mmol/mol/ºC (Kinsman and Holland, 1969; Gaetani and Cohen, 2006). Although Kinsman and Holland (1969) presented Sr/º C aragonite calibration between 16-90 º C, they found mixed phases of $CaCO_3$ below 30 ºC. *A. islandica* lives in waters <16 ºC but deposits single phase aragonite, suggesting that conditions present in inorganic experiments of Kinsman and Holland (1969) may not be representative of those found within the bivalve. This could include differences in physical conditions e.g. pH, but also biological effects e.g. organic matrix which is known to control the phase deposited (Belcher *et al.*, 1996; Falini *et al.*, 1996; Marin and Luquet, 2004). Closer analysis of the experiments of Kinsman and Holland (1969) reveals that only two samples were taken in the temperature range 16-30 ºC, with no significant difference between Sr/Ca uptake of the two (t test, P>0.4) (Kalish, 1989). The range of temperatures that are applicable to ecological studies may not be significant enough to affect trace element conditions (Kalish, 1989; Toole and Nielsen, 1992) with Sr/Ca varying ~0.039 mmol/mol/ºC (Kinsman and Holland, 1969; Gaetani and Cohen, 2006).

Irvine Bay has a maximum temperature variation of 8 ºC, which would equate to ~0.31 mmol/mol Sr/Ca, less than a third of the observed fluctuations. Research in corals of the temperature dependency of Sr/Ca uptake has however shown it to be approximately double that reported in abiogenic aragonite (Sinclair *et al.*, 1998 and

references therein) but this would still not account for the extent of the fluctuations recorded with *A. islandica*.

Strong Sr/Ca peaks are present only in the latter years of growth, when the growth rate is considerably decreased. In U248, when the growth rate is >1000 μm/yr the Sr/Ca peaks are no longer present, but the pattern in U228 is less clear. In these younger phases of life, the annual termination bands are much wider and are composed of a series of multiple laminations. Sr/Ca increases within the growth band are almost symmetrical in U248 ranging from 0.9-1.3 mmol/mol and 1.0-1.2 mmol/mol in U248 and U228 respectively. The positive relationship of Sr/Ca with the warmer months (the exact months of deposition are unknown) is at variance with inorganic models for Sr/Ca substitution that indicate that Sr/Ca is *inversely* related to temperature (Kinsman and Holland, 1969; Gaetani and Cohen, 2006).

Thus, changes in Sr/Ca behaviour with ontogeny could be understood in terms of shell growth rate. However a paradox exists, if Sr/Ca variation is simply dependent on shell growth rate as the highest Sr/Ca concentrations are present both at the annual terminations during latter years of growth when shell growth rate is slowest, and within the growth bands during the earlier years of growth when shell growth rate is fast. Hence, if shell growth rate is an important factor, then it must operate via two separate mechanisms. These two periods of growth are discussed independently below.

Sr during the latter years of growth

While high Sr/Ca in the latter years of growth could coincide with colder seawater temperatures, abiogenic precipitation experiments of Kinsman and Holland (1969) show that variation in Sr/Ca is too large to be accounted for by temperature-

controlled substitution. The presence of Sr/Ca in the doublets also indicates this is not exclusively temperature controlled (with doublets believed to be caused by either spawning or changes in growth rate). Epplé *et al. (*2006) hypothesised that Sr/Ca peaks at the growth checks represented winter temperatures. Qualitative comparison of the Sr/Ca during the four warmest winters (1989, 1998, 1999, 2000) and the four coldest (1993, 1994, 1996, 2001) shows that Sr/Ca could not be used to predict which of the winters was warmer or colder. Therefore Sr/Ca, even indirectly does not provide an indication of temperature at the growth checks.

Sr/Ca peak at the growth check could result from increased anaerobiosis and dissolution of the shell with preferential deposition of Sr/Ca in low energy (and low temperature) environment. Dissolution of the bivalve shell occurs within minutes of the commencement of anaerobic respiration (Dugal, 1939; Crenshaw and Neff, 1969; Wada and Fujinuki, 1976) as the carbonate buffers against acidosis of the tissue. In other words, the lack of oxygen causes the production of acid (H^+), which is then buffered by the dissolution of the $CaCO_3$ shell. *A. islandica* undergoes voluntary anaerobiosis as glycogen stores last much longer under anaerobic conditions, termed "energy-induced anaerobiosis", as well as submersion in the sediment providing protection from predators (Oeschger, 1990). The storage rather than excretion of energy-rich fatty acids is an adaptation to limit the loss of valuable energy resources, which can be re-oxidised during aerobic conditions (Oeschger, 1990). Lutz and Rhoads (1980) summarised that the dissolution occurred not only within the pallial line (as stated by Crenshaw, 1980) but also at the growing edge. The pallial line is the line where the mantle muscles are attached, and therefore the extent of the soft tissue. In fact, in a laboratory experiment lasting 50 days (July-August), *A. islandica* typically spent 1-7 days in anaerobic respiration with one specimen spending up to 24

days (Taylor, 1976). Lutz and Rhoads (1977) hypothesised that the presence of increased concentration of organics at growth checks could result from anaerobiosis-related dissolution. Therefore, dissolution effects would be strongest at the growth checks, when the highest concentration of organics occurs.

Such a mechanism could also explain why the margins of the shell (i.e. the furthest away from the maximum growth line) show elevated Sr/Ca. Areas such as the margins, where the shell deposition is much less, would be susceptible to more dissolution events as there would be less material deposited prior to the next anaerobic event. However, an increase in Sr/Ca would only occur with acidosis if low Sr/Ca areas were preferentially dissolved. Finch and Allison (2003) plotted the solvus for aragonite-strontianite system based on the data of Plummer and Busenberg (1987). The composition of the shell of *A. islandica* lies on the Sr poor-side of the solvus and hence dissolution of material with a range of Sr compositions will preferentially start with Sr-poor aragonite. This process will however only increase Sr/Ca if low Sr/Ca aragonite is not redeposited (i.e. the proportion of high Sr/Ca increases), and cannot exceed the maximum initial Sr/Ca incorporation. To determine the maximum incorporation, Sr/Ca concentration deposited within the growth bands when the specimen was younger, were examined, as this area is unlikely to be affected by dissolution. The maximum found in this area in U248 was 1.5 mmol/mol, less than the recorded maximum Sr fluxes during the latter years, at the annual growth check (>2.0 mmol/mol). Therefore, dissolution cannot be the main controlling factor.

Analysis of the outer shell prismatic layer should provide further indication of whether dissolution could influence Sr/Ca. The accumulation rate of shell is much faster in the outer shell prismatic layer than in the prismatic layer of the umbo and hence the impacts of dissolution would be less, as new material would be deposited

faster. The prismatic layer of the umbo was examined by SEM (Scanning Electron Microscopy), with the sample etched prior to analysis, in order to determine the positions of the growth checks and hence the effects of any possible dissolution could not be examined.

Sr/Ca could be linked to the organic content. The EXAFS (see Chapter 2) results however suggest that Sr is ideally substituted in aragonite (i.e. randomly substituted for Ca), thus providing independent verification that Sr is not hosted by organics. However, Sr/Ca increases at the growth checks could result from changes in the growth of the crystal due to the presence of organics. Organic material exerts control over the nucleation of the crystal with the matrix acting as nucleation surface and predefined mould, determining size and orientation of the crystals (Watabe and Wilbur, 1960; Belcher *et al.*, 1996; Mann and Ozin, 2003; De Yoreo and Dove, 2004; Heinemann *et al.*, 2006). It has been noted in calcite that different faces having different affinities for trace elements, resulting in a zoning within the crystal (Reeder and Grams, 1987; Paquette and Reeder, 1995; Reeder *et al.*, 2001). This partitioning may be more marked in aragonite as it has a lower symmetry than calcite and therefore potentially a greater number of crystallographically distinct crystal faces (Allison and Finch, 2004).

During SIMS the whole crystal is analysed since the spot size is larger than the individual crystal size. The size of the crystals in the prismatic layer of umbo could not be determined but those in the outer shell prismatic layer were <5 μm, and therefore it is extremely unlikely that the crystal size in the umbo would exceed this i.e. be >10 μm given its slower growth rate. Therefore, any intracrystal zoning would not influence the SIMS analysis. If however organics modify the crystal shape (habit), it may preferentially favour crystal growth on certain faces, which could modify the

effective bulk partition coefficients. Paquette and Reeder (1995) found the offset in Sr between the different faces of the same calcite crystal "is nearly always less than a factor of two and more commonly just a factor of 1.2-1.4." For example, one crystal showed an increase of ~1000 ppm (from 1200 to 2200 ppm) between the two faces i.e. 1.14 mmol/mol. It can be inferred from Finch *et al.* (2003b) that the lateral variation across a non-biogenic aragonite crystal was about 50 ppm (from varying from 100 to 150 ppm) i.e. increase of ~50%. Sr/Ca increases at the growth checks by >100% and thus it suggests that it is unlikely to be the main contributory factor. However, it should be noted that the change inferred from Finch *et al.* (2003b) data, is for inorganic aragonite, whereas the partitioning for biogenic crystals may differ as the matrix has a significant control on the crystal e.g. controlling the polymorph, the size, shape and texture (Herman *et al.*, 1988; Falini *et al.*, 1996; Dietzel *et al.*, 2004; Sato *et al.*, 2006).

Another possible mechanism is that the crystal growth rate impacts upon Sr/Ca incorporation. Although there are a number of published papers relating increased Sr/Ca with higher crystal growth rates (Stecher *et al.*, 1996; Gillikin *et al.*, 2005a; Carré *et al.*, 2006), none has reported low crystal growth rates associated with high Sr/Ca and hence it seems unlikely that this is a mechanism in the present system. It is more probable that high Sr/Ca peaks are controlled by biological or vital effects, including changes in metabolic rate (e.g. Rosenberg and Hughes, 1991; Klein *et al.*, 1996a).

The control of vital effects is discussed further in the following (ICPMS) chapter, but in summary, Sr/Ca uptake into the EPF could be controlled by the activity of two enzymes Ca^{2+}-ATPase and carbonic anhydrase (CA). The former pumps Ca^{2+} to the EPF while removing protons and the CA catalyses the reaction of bicarbonate

to CO_2. This can then diffuse through the membrane (Crenshaw, 1980; Cohen and McConnaughey, 2003). Therefore, when Ca^{2+}-ATPase activity increases, so does the calcification rate (Gillikin *et al.*, 2005a). As Ca^{2+}-ATPase has a higher affinity for Ca^{2+} than Sr^{2+} but uses similar pathways; Sr uptake should be inverse to growth rate (Yu and Inesi, 1995; Ferrier-Pagès *et al.*, 2002). Such a biological pathway or vital effect could influence Sr/Ca.

A number of researchers (measuring in the outer shell prismatic layer) have found that the annual growth check is marked by a decline in Sr/Ca (e.g. Stecher *et al.*, 1996; Ambrose *et al.*, 2006) including in *A. islandica* (Toland *et al.*, 2000). Toland *et al.* (2000) took samples in the outer shell prismatic layer but close to the umbo, where the growth rate was fast suggesting that a slow growth rate might be integral in forming strong Sr/Ca peaks. However, it should be reiterated that all the aforementioned research analysed the outer shell prismatic layer and not the prismatic layer of the umbo.

Mya arenaria is also reported to have a sharp increase at the annual growth check, (again measurements in the outer shell prismatic layer) (Palacios *et al.*, 1994). This is also an aragonite bivalve, with a long lifespan (typically 10-12 years and up to 28 years), which can also withstand long periods of anaerobiosis (Brousseau, 1978; MacDonald and Thomas, 1980). In addition, Swan (1956) commented that shells *Mya arenaria* with lower masses had lower Sr/Ca than heavier shells, with the latter being characteristic of slower growing individuals. The bivalve *Mercenaria mercenaria* also has a long lifespan (>50 years) but at the growth check (which occurred during the summer month) there is no distinct changes at the organic rich regions of the shell (Gillikin *et al.*, 2005a). This indicates that Sr/Ca peaks at the growth check are not the

result of a simple relationship with age. Further research is required to determine if high Sr/Ca peak at the growth check could relate to a biological adaptation.

A number of controls including temperature, growth rate, dissolution at the growth checks and modification of the crystal shape as well as vital effects have been discussed as potentially influencing Sr/Ca at the growth checks. Changes in the crystal shape caused by the organics can influence the partitioning of Sr in the aragonite, thus could increase Sr/Ca at the growth check. Vital effects may also play an important role in the uptake of Sr/Ca.

Sr within the growth band

As discussed earlier, Sr/Ca increases within the growth band, typically to 1.5 mmol/mol during the more juvenile section of the prismatic layer of the umbo. Five possible mechanisms for controls on Sr/Ca at the annual growth check; 1) temperature 2) selective dissolution 3) changes in the crystal shape 4) growth rate 5) vital effects.

Sr/Ca substitution cannot be modelled successfully using thermodynamics with the Sr/Ca variation exceeding that explicable by inorganic experiments (Kinsman and Holland, 1969; Dietzel *et al.*, 2004; Gaetani and Cohen, 2004). However, as discussed earlier Sr/Ca temperature reconstructions from coral use a temperature dependency that is much greater than expected by inorganic experiments (see Sinclair *et al.*, 1998 and references therein). While it could not explain all the variation within *A. islandica*, Sr/Ca fluctuations in the growth bands may still provide some indication of temperature changes.

The first issue to address in using Sr/Ca for a temperature reconstruction is the lateral variation found within *A. islandica*. Increasing the lateral distance from the

maximum growth axis by 750 μm resulted in a change in Sr/Ca of up to 25%. Assuming measurements were within 60 μm of the maximum growth line the offset is ~ 5% equating to an offset of ±0.5 ºC (the average temperature being ~10 ºC). Sr/Ca in two of the coolest years (1987, 1993) was compared to two warmer years (1989, 1999) in U248 to examine if there is any temperature influence. The average temperature difference between these years was 1.5 ºC. Using the equation of Hart and Blusztajn (1998) (where T (ºC) = 20.752[Sr/Ca mmol/mol)]-16.0) this would equate to a Sr/Ca offset of ~0.8 mmol/mol. However the average Sr/Ca concentrations of 1987 and 1989 overlap within error and 1999 Sr/Ca being slighted higher (0.2 mmol/mol). As discussed earlier, Sr/Ca in the latter years generally, show elevated concentrations particularly at the growth check and this may influence Sr/Ca during the growth band. Therefore, comparison of two consecutive years such as 1989 and 1988 is more meaningful. Sr/Ca variation was 0.8-1.0 mmol/mol in 1989 compared to 0.8-1.3 mmol/mol in 1988. During the former the temperature variation was 7.0 ºC (with a warmer average) compared to 8.1 ºC in the latter. Therefore, greater variation in Sr/Ca in 1988 in U248 could be related to larger changes in temperature. However, both shells show years with little or no variation within the growth bands (Figure 3.19b) thus supporting the view that Sr/Ca variation within the growth bands is not strongly temperature controlled. Changes in temperature, for example, may influence the shell growth rate, which may in turn influence Sr/Ca uptake.

The growth rate is much faster during the growth band than the growth check, and therefore the impact of dissolution is likely to be minimal. No changes in organics or crystal habit were observed in SEM analysis of the growth band. Therefore, these

two mechanisms are unlikely to have a significant control on Sr/Ca during the growth band.

Sr^{2+} incorporation into non-biogenic aragonite is independent of precipitation rates over a range of 10-500 μmol/m^2/h (Kinsman and Holland, 1969; Mucci *et al.*, 1989; Zhong and Mucci, 1989). Growth rate in the prismatic layer of the umbo of *A. islandica* is 400-5000 μmol/m^2/h (calculated from yearly growth rate in the prismatic layer of the umbo, assuming 300 days a year growth, 24 hours a day, and that the maximum growth axis has been selected and the crystals grew parallel to this axis). Therefore, the faster growth rates are outside the ranges studies in the experiments of Kinsman and Holland (1969). A number of researchers have suggested that growth rate (including crystal growth rate) is an important control within bivalves e.g. *Mercenaria mercenaria* and *Spisula solidissima* (Stecher *et al.*, 1996), *Mytilus edulis* (Putten *et al.*, 2000), *Protothaca staminea* (Takesue and van Geen, 2004) and *Mesodesma donacium* and *Chione subrugosa* (Carré *et al.*, 2006).

Work by Watson (1996, 2004) showed that in inorganic calcite, the concentration of Sr was much higher near the growth edge of the crystal and if the growth rate exceeded the ability of the material to expel "impurities" from the structure, they became incorporated into the material. Watson (2004) found where growth rate was faster than 0.01 nm/s (equivalent to 1060 μmol/m^2/h), growth entrapment of Sr occurs in calcite (i.e. kinetically controlled uptake would not be accurately modelled by thermodynamics). Gaetani and Cohen (2004, 2006) showed the same process was also applicable for aragonite crystals with the crystals being enriched with trace components relative to the crystal-fluid equilibrium.

This implies that if the crystal growth in an organism exceeds the rate at which impurities can be expelled, they will be incorporated at elevated concentrations. The

growth rate of *A. islandica* in the early years of growth reaches a maximum of 0.04 nm/s. The growth rate was calculated using 1000 μm of growth per year, assuming 24 hour growth, 300 days per year, thus the growth speed is probably much higher as growth is probably not continuous over 24 hours. In the latter years of growth, the growth rate is <150 μm/yr, this would fall considerably below the minimum threshold (<0.006 nm/s) of the growth rate at which growth entrapment occurs according to Watson (2004). There is currently no estimate for the growth rate required for entrapment in aragonite to occur, but the figures suggest that the application of the growth enrichment model can provide a plausible explanation why Sr/Ca are elevated during periods of faster growth, i.e. during the growth bands within the more juvenile parts of the shell. However, this assumes that the crystal growth rate and shell growth rate are directly linked. It could however be that increased growth rate is achieved by increased nucleation, thereby increasing the rate of extension of the shell.

In *A. islandica*, 65% of variance in shell growth rate can be explained by variation in temperature and food supply (Schöne *et al.*, 2005a) i.e. variation in growth entrapment of Sr/Ca could be dependable on these factors. However, the interaction of temperature and food supply is complex, with maximum temperature expected to be during September, with maximum food supply usually associated with spring and autumn blooms. Measurement of $\delta^{18}O$ in Chapter 6 should provide some indications of changes in shell growth rate, and comparison of Sr/Ca and $\delta^{18}O$ record will be further compared in the conclusion chapter.

Carré *et al.* (2006) reported that crystal growth rate could explain up to 74% of Sr/Ca variance seen in the bivalves *Mesodesma donacium* and *Chione subrugosa*. They also noted however, that for the same growth rate Sr/Ca were higher in the more

curved sections, which concurs with our findings, that Sr/Ca is higher at the more curved lateral margins. A possible explanation for this could be that the curvature of the shell is related to the crystal size and/or shape. As discussed earlier, it was inferred from Finch *et al*. (2001) that Sr/Ca concentrations in different faces of the non-biogenic aragonite crystals can vary by ~50%, and a more curved section of the shell may change the habit of the crystals.

Comparison of U228 and U248 Sr/Ca ratios show that the average values of faster growing U228 are slightly higher than those in U248. This together with Sr/Ca increases during the growth bands would further support that incorporation of Sr/Ca is influenced by growth enrichment. The highest Sr/Ca peaks are found at the growth checks of U248, which would agree with the hypothesis that high Sr/Ca ratios result from biological effects in conjunction with increased concentration of the organics, which modify the crystal growth and hence Sr partitioning.

In order to determine better these relative effects, analysis of the outer shell prismatic layer is presented in the following chapter. In particular, the question of whether faster shell extension rate results in significantly higher Sr/Ca, as would be expected if shell growth rate were an important control. In addition the $\delta^{18}O$ profile (see Chapter 6) provides an indication of the growth of *A. islandica* i.e. whether trace element cyclic pattern represent the growth curve of *A. islandica*.

3.5.2 Mg fluctuations

$MgCO_3$ possesses a trigonal (calcite) structure (coordinating with 6 oxygen); hence, the incorporation of Mg^{2+} into the 9-fold metal site in orthorhombic aragonite is not favoured (Dietzel *et al.*, 2004). Its ionic radius differs from Ca by >15% and thus direct ionic substitution would not commonly occur (Goldschmidt, 1954). Mg

behaviour is not well characterised in aragonite but it is occluded or trapped within lattice defects (Amiel *et al.*, 1973; Cross and Cross, 1983; Oomori *et al.*, 1987; Stecher *et al.*, 1996). Dietzel *et al*. (2004) found although Mg^{2+} incorporation in their experiments was almost within theoretical range predicted by thermodynamics, the Mg^{2+} content was highly divergent and did not depend on temperature, Sr^{2+} or Ba^{2+} incorporation. They concluded Mg^{2+} might be affected by complex adsorption onto the aragonite crystal surface during precipitation rather than by well-regulated substitution into the crystal lattice. This agreed with the findings of Oomori *et al*. (1987) who found the temperature effect on the coprecipitation of Mg^{2+} ions in aragonite to be very small. In the previous chapter the results of XANES modelling was consistent with Mg in *A. islandica* being hosted by organics.

Mg/Ca ratios show an increasing number of high single points further from the growth edge associated with high Si/Ca. This is likely to be due to increased superficial contamination. It may be that the faster growing part of the shell is less dense (and perhaps more porous) and thus more prone to the accumulation of contamination. It is notable that between 4300-6700 μm from the growth edge (T8), both Mg/Ca and Si/Ca show an increase in average concentration as well as Ba/Ca (also susceptible to contamination) (see Figure 3.12, 3.14).

Comparison of transects analysed only 25 μm apart (Figure 3.16b), close to the growth edge; shows that some Mg/Ca peaks are reproducible while others are not. The reproducibility may suggest the features are true compositional variation within the shell but may also arise if contamination is attracted to particular laminae. At the moment, there is no sure way to determine which data are dominated by contamination and which reflect actual Mg/Ca fluctuations within *A. islandica*.

Figure 3.13 shows in the latter years of growth, that there is some covariance between Sr/Ca and Mg/Ca. In particular, U248 shows that the Mg/Ca peaks associated with the annual termination bands occur at the latter part of the termination band. This covariance between Sr/Ca and Mg/Ca is only present in the last five years in U248 (although the relative magnitude of the peaks varies). Even during this period, however Mg/Ca peaks are present during the growth bands and concentrations can exceed those present at the growth check. This suggests that the formation of annual termination band exerts some influence on the behaviour of Mg/Ca. However, the slight delay seen (Figure 3.13), suggests that mechanisms controlling increases in Sr/Ca and Mg/Ca at the growth check are different. However, conclusions must remain tentative as the material density may affect the level of contamination (which in turn affects Mg/Ca). In other words, Mg/Ca increases at the annual termination band may be solely the result of increased Mg/Ca contamination at these softer parts of the shell.

3.5.3 Ba fluctuations

Ba/Ca is affected by contamination at low concentration but as discussed earlier if low Ba/Ca <0.01 mmol/mol were excluded the correlation became insignificant. Spot analyses indicate that Ba/Ca at low concentration contributes about typically 3 x 10^{-5} Ba/Ca counts for low Ba/Ca. Sporadic increases in Ba/Ca from baseline concentrations of 0.002-0.003 mmol/mol to values >5 times greater are not related to contamination. These Ba/Ca peaks are not related to the annual bands.

Very little is known about the substitution of Ba^{2+} into the lattice. Dietzel *et al*. (2004) found, like Sr^{2+}, its incorporation into inorganic precipitation is temperature driven with Ba^{2+} with its sensitivity to temperature an order of magnitude higher than

Sr^{2+}. The radius of Ba^{2+} is considerably larger than Ca^{2+} and it could be that such a large ion has difficulty substituting into the lattice. Results from *A. islandica* show no correlation between Ba/Ca and other trace elements or any of available environmental data. However, this pattern of low Ba/Ca concentrations with sharp increases has been noted not only in bivalves (Stecher *et al.*, 1996; Putten *et al.*, 2000; Lazareth *et al.*, 2003; Gillikin *et al.*, 2006) but also within corals (such as *Porites lutea*) suggesting a common cause independent of the taxon studied (Sinclair, 2005). Experiments by Gillikin *et al*. (2006) discounted the theory that Ba/Ca peaks could be used as a proxy of Ba/Ca concentrations in the water or phytoplankton, but they tentatively concluded the increase in Ba could relate to barite ingestion.

3.6 Conclusion

The trace elements in the shell of *A. islandica* vary considerably during the lifespan of the organism. Sr/Ca increases laterally by up to 25% from an average value of 1.2 mmol/mol measured at the maximum growth axis. In the latter years of growth, Sr/Ca shows sharp increases at the annual growth check with increases present within the growth bands in the younger part of the shell. A combination of factors could contribute to Sr/Ca fluctuations. In latter years, changes in crystal growth caused by organics and vital effects may affect Sr/Ca incorporation at the growth checks. During years of faster growth, crystal growth rate could be an important control as well as vital effects. The relative importance of these factors could vary through the shell. Thus, Sr/Ca in the prismatic layer of the umbo is unlikely to provide an accurate temperature reconstruction.

Mg/Ca data are influenced by contamination but many of the most strongly influenced points can be identified by reference to Si counts. The Mg/Ca profile in the

latter year is higher at the growth check (as seen with Sr/Ca) although this is often offset by ~10 μm from the Sr/Ca peaks. It is not clear if this is related to increased contamination in these areas, (which are softer and hence more prone to contamination), or due to an increased organic content which host Mg/Ca.

Ba/Ca is also affected by contamination at low Ba/Ca (<0.01 mmol/mol) but sporadic increases (>5 times) exceed this. These increases show no correlation with shell architecture, Sr/Ca or Mg/Ca, but concur with findings of other researchers (Stecher *et al*., 1996; Putten *et al*., 2000; Lazareth *et al*., 2003; Gillikin *et al*., 2006). At present, it is unclear as to the cause of these increases.

Analyses of the outer shell prismatic layer, presented in the following chapter, will provide further insights to understand the controls on trace elements, particularly the behaviour at the growth checks.

Acknowledgements

This work was supported by NERC ion microprobe grant (no. IMP223/0504), with additional support from QRA new Researcher's Award. Personal thanks are given to Richard Hinton and John Craven whom provided invaluable assistance and guidance.

CHAPTER 4: ICPMS ANALYSIS: QUANTIFYING TRACE ELEMENT FLUCTUATIONS WITHIN THE OUTER SHELL PRISMATIC LAYER.

Abstract

The variation of three trace elements Sr, Mg and Ba in the prismatic region of the outer shell layer of two live collected *Arctica islandica* shells (228 and 248) are examined here using Laser Ablation-Inductively Coupled Plasma Mass Spectrometry (LA-ICPMS) and solution-ICPMS. All three elements show a lateral decrease in concentration from the periostracum e.g. Sr/Ca decreases by ~45% with a lateral change in distance of 750 μm.

Sr/Ca increases by >0.6 mmol/mol at the growth checks in the latter (last 3-4) years as well as at doublets, but at higher shell growth rates, these increases are not present. Sr/Ca incorporation may be influenced by changes in the crystal habit during formation caused by increased organics at the growth check, crystal growth rate as well as vital effects. However any effect of seawater temperature on Sr/Ca incorporation was obscured by these other factors.

Mg behaviour is related to the organics, which is consistent with the conclusions from XANES discussed in Chapter 2, which suggest that Mg is bound to organic molecules in the shell. However, fluctuations in Mg/Ca may not be linear to the concentration of organics, but could also be influenced by vital effects. Further work is required to determine if this is the case. Ba/Ca fluctuations show sporadic large increase in concentration (greater than five times the norm) but the timing of these did not correlate between specimens. It remains unclear which environmental factors, if any, are encoded by the sporadic increases of Ba.

4.1 Introduction

The behaviour of trace elements in the outer shell prismatic layer of *Arctica islandica* is examined in this chapter. As discussed in the previous chapters, *A. islandica* has annual termination bands that allow the timing of changes in the geochemistry of the shell to be calculated. If the geochemical signatures in the shell relate to environmental factors, *A. islandica* has great potential to provide an *in situ* record of climate changes. Fluctuations in the geochemistry of two live-collected specimens (228 and 248) from Irvine Bay, UK, can be compared to each other as well to sea surface temperature (SST) data collected for >50 years at the nearby Millport marine station to help determine the controls on trace element uptake.

Measurements in the outer shell prismatic layer (PL) were taken using Laser Ablation- Inductively Coupled Plasma Mass Spectrometry (LA-ICPMS) and solution-ICPMS. ICPMS is a more widely available technique than SIMS, which was used in analyses of the prismatic layer of the umbo. LA-ICPMS has a larger spot size (in this study 40 μm and 60 μm were used during LA-ICPMS compared to 10 μm in SIMS) and is therefore more suited to the higher growth rate in the outer shell prismatic layer. This chapter tackles a number of issues on the behaviour of trace elements within the outer shell prismatic layer, in particular:

- Whether the concentrations are heterogeneous across a growth band i.e. consistent between material deposited at the same time;
- If there is a relationship between shell architecture and the trace element incorporation;
- The role external environmental factors e.g. temperature, have on trace element incorporation.

Comparisons of the trace element profiles from two shells and their timing of geochemical fluctuations can provide insight into the behaviour of trace elements. Ultimately, measurements of the prismatic layer in the outer shell and the umbo of the same shell will allow comparison of the trace element fluctuations and a more detailed understanding of their controls in Chapter 8.

4.2 Introduction to ICPMS

Inductively Coupled Plasma Mass Spectrometry (ICPMS) is an analytical technique for determining minor and trace element concentrations. The mass spectrometer (MS) measures isotopic ratios of the ions generated by the inductively coupled plasma (ICP) from which elemental compositions are determined using tables of natural isotopic abundances. The technique is used for a range of different analysis types from biological, geological to environmental.

A schematic of an Induced Coupled Mass Spectrometer ICPMS (Thermo ELEMENT2) is shown on Figure 4.1. The plasma torch generates an ion source using radio frequency magnetic fields induced by a copper coil with temperatures exceeding 7000 K. As the sample aerosol is injected into the plasma, it collides with free electrons, argon cations and neutral argon atoms causing the aerosol to be broken down into charged atoms. The hot argon and sample ions accelerate through the sample cone to produce a supersonic jet in the expansion chamber. The skimmer cone extracts small proportion of the plasma, which is then focused into the mass spectrometer using ion lenses. The electromagnet then deflects the ions, with the angle of the deflection dependent on the mass to ion energy ratio. ELEMENT2 allows simultaneous registration of analog and counting signals (depending on the signal

intensity). The counting mode for ELEMENT2 typically <5x10^6 counts per second (cps) and the analog mode between 10^4 and 10^{10} cps (Figure 4.2).

Since the samples are rarely in a form suitable for direct introduction to ICPMS, it must be introduced by either laser ablation or solution nebulisation (Jarvis and Jarvis, 1992; Longerich *et al.*, 1996).

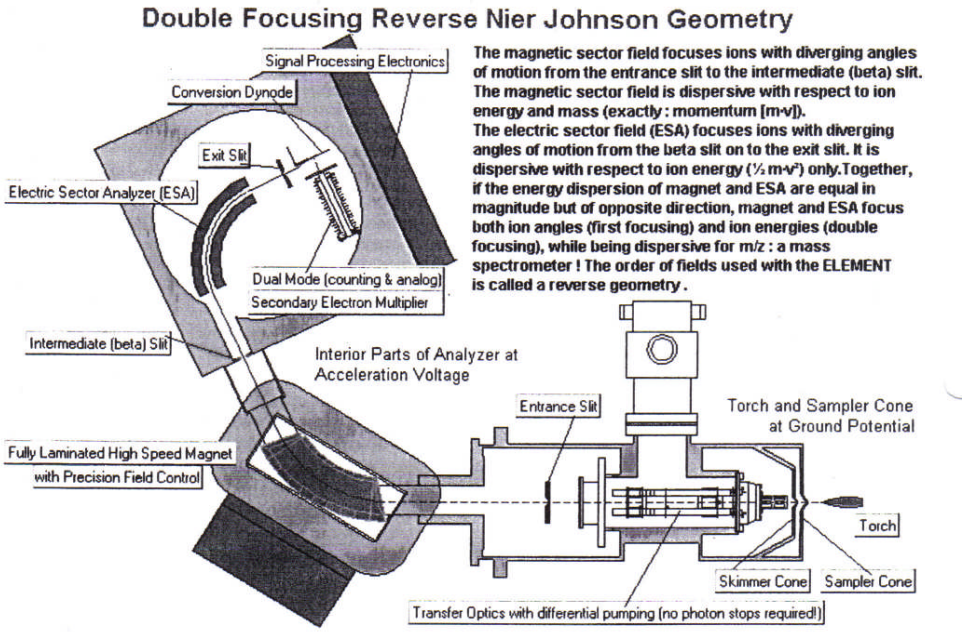

Figure 4.1: Schematic diagram of analyser and detector ELEMENT2 ICPMS (ThermoFinnigan, 2001).

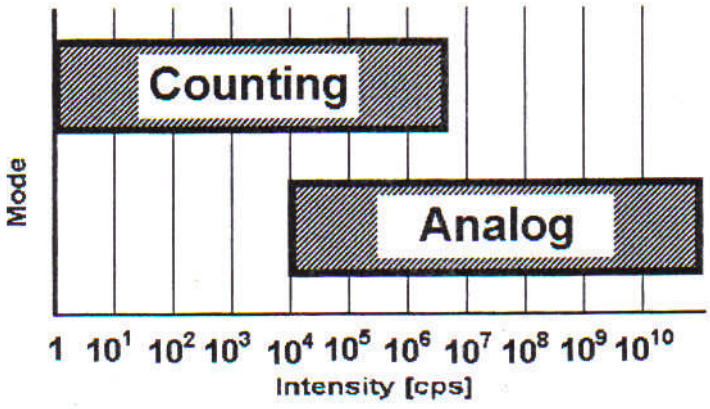

Figure 4.2: Dynamic range of the counting devices in the ELEMENT2 ICP-MS (ThermoFinnigan, 2001).

4.2.1 Sample introduction by solution

In this method of introduction, the sample is aspired by a nebuliser using a peristaltic pump, which enters a spray chamber (for aerosol filtering). The spray droplets (<10 μm) are carried into the ICP using an Ar carrier gas. Only about 1% of the original sample aerosol has the correct droplet size for efficient ionisation within the plasma, with the remaining 99% drained from the base of the spray chamber using the peristaltic pump (ThermoFinnigan, 2001). A diagram of a standard inlet system is shown on Figure 4.3.

Solution methods are often preferred as a means of introducing samples since the aerosol is more consistent in the manner in which material is delivered to the ICP and typically has a better precision.

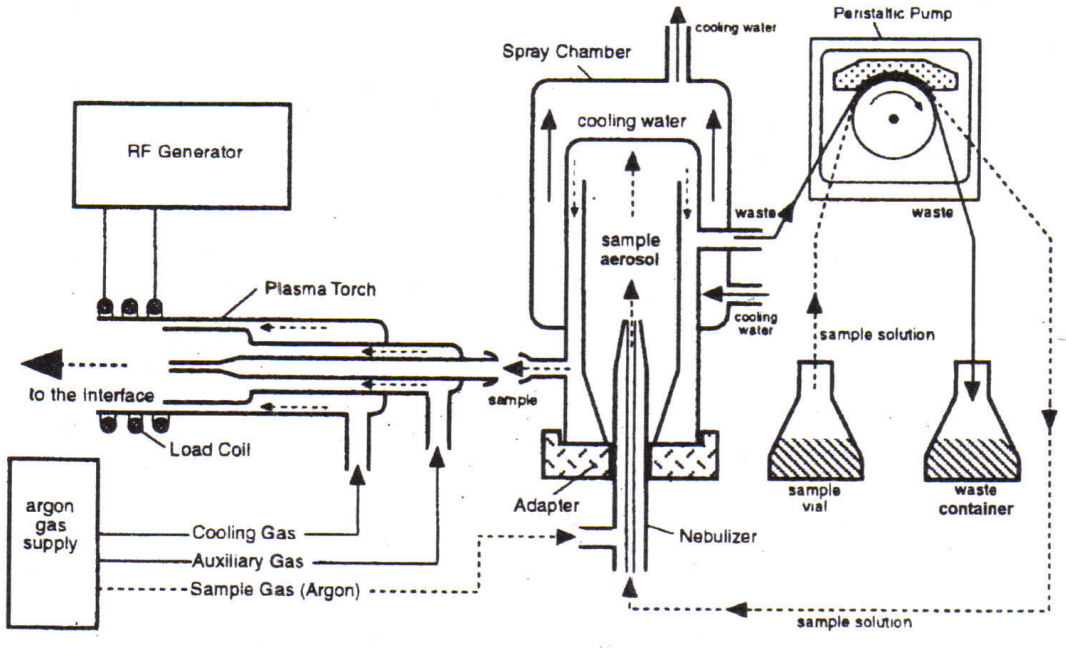

Figure 4.3: Diagram of standard inlet system for solution-ICPMS (ThermoFinnigan, 2001).

4.2.2 Sample introduction by laser ablation

The laser produces an intense beam of radiation, in which the high energy photons are absorbed by the sample surface and are thereby converted to thermal energy, vaporising most of the exposed solid surface. This ablated material is carried by an argon stream into an ICPMS (Figure 4.4). The laser provides a much simpler method for the user of introducing solid samples into the ICPMS, with a shorter preparation time (the sample has only to be polished), and allows *in situ* analysis (e.g. the trace element fluctuations measured by LA-ICPMS could be compared *in situ* to the shell architecture). It also provides a more dynamic sampling system, with changes in sampling positions possible throughout the analysis session. The stability of the laser is however, an issue for the precision of the LA-ICPMS measurements, and different matrices respond very differently to the laser pulse. These can be circumvented by matrix matching to standards but finding appropriate standards with precisely the same matrix is often impossible. Hence, the accuracy of some LA-ICPMS measurements is difficult to quantify. It also has a poorer precision than solution-ICPMS, with the loss of precision directly attributable to instability of the laser and the vagaries of the response of the sample to the laser.

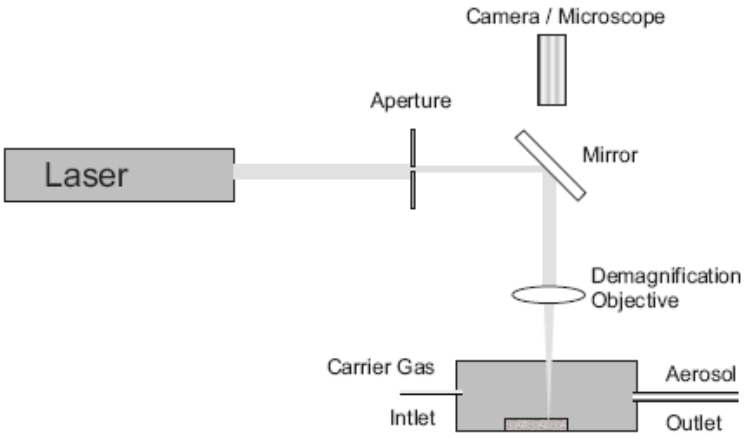

Figure 4.4: Diagram of laser ablation system (Guillong, 2004)

4.3 Method

4.3.1 Sample preparation

The same *A. islandica* shells used for SIMS were also used for ICPMS analyses. The shells were sectioned along the axis of maximal growth from which a small subsample at the ventral margin, last ~1.5 cm of growth was taken. This was set in Buehler Epo-thin epoxy and polished to 1 μm using diamond paste. The sample width is limited by the size of the laser ablation chamber. The age was determined from the other half of the section, which was etched in 0.1 N HCl and then a peel taken for analysis of growth bands. The sections analysed by LA-ICPMS covered the last 6 and 8 years of growth in outer shell prismatic layer from 228 (PL228) and 248 (PL248) respectively.

For solution-ICPMS, the section of PL228 used for the peel was repolished and aliquots using a New Wave™ micromill were taken (see Chapter 6 for further details on the micromill).

4.3.2 LA-ICPMS set-up

LA-ICPMS analyses were carried out at the University of Bergen, Norway using a New Wave UP213 laser ablation system coupled to an ELEMENT2 ICPMS. The Nd: YAG laser emits at 1064 nm in the IR range but the fourth harmonic of emission is taken providing a UV pulse with a wavelength of 267 nm. For each spot analysis, the laser warm-up time was 40 s, pulsed at 10 Hz with 110 s dwell time per sample, with washout delay of 40 s. During the warm-up time, the laser is firing into the shutter (not at the sample); with the dwell time referring to the time the laser was firing and the sample being delivered into the ICPMS. The washout delay is the time delay prior

to the next sample being taken, which allows the previous sample to be flushed from both the sample chamber as well as the ICPMS. The pulse energy was ~0.3 mJ (60% energy).

The sample was ablated in a flow of He, which was then mixed with Ar to provide optimal conditions for successful introduction to the ICP (Gunther and Heinrich, 1999). He reduces the amount of ablated material condensed back onto the sample surface and thus improves signal intensity (Rege *et al.*, 2005). The ratio is He: Ar is approximately 5:1, with Ar flow rate ~1.0 dm^3/min.

Standards were analysed every 20 samples and consisted of two consecutive analyses of a selection of the following: NIST610, NIST612, BCR (US National Institute of Standard and Technology Standard Reference Material) (Pearce *et al.*, 1997) and MACS1 (a calcite powdered sample under development) with the exception of analyses on 28th July 2006. Then NIST610 and BCR were analysed, together with a new otolith standard NIES (due to concerns about poor reproducibility of NIST612). The location of each analysis within the standard was randomised to lessen any effects of heterogeneity.

4.3.3 Analysis of A. islandica by LA-ICPMS

A spot size of ~60 μm was used for PL228 and 40 μm in PL248 with spot analysis taken every 100 μm. The spot size was reduced, as an improvement to the technique with the 60 μm spot showing that the area affected by the laser extended beyond a 50 μm radius, but with a smaller spot, the area this effected was smaller (<50 μm) (see Secondary Electron (SE) image Figure 4.10). The depth of the laser crater was typically 200-250 μm (determined by Scanning Electron Microscopy (SEM)).

Table 4.3 outlines all the analyses carried out on PL228 and PL248. Three transects were taken in each sample taken parallel to the periostracum- T1 250 μm from the periostracum, T2 500 μm and T3 1000 μm (see Figure 4.5a). Only T0 PL228 was taken non-parallel, it started ~200 μm from the periostracum increasing to ~800 μm, (it was the initial characterisation transect). Transect T0 highlighted the need to analyse parallel to the periostracum. Temporal resolution increased from <7 analyses yr^{-1} in the latter years of growth (where growth rate is slowest), to >15 yr^{-1} by 1996 in PL228.

PL248 was analysed 1^{st}-3^{rd} May 2006. The sample was then repolished to remove ~125 μm, approximately half of the estimated pit depth, prior to analysis on the 28^{th} July 2006 i.e. a vertical change (see Figure 4.5b for schematic) to determine the impact of changes vertically on the sample heterogeneity. T3 was extended to provide more analyses closer to the growth edge, as well as an additional transect (T2) analysed. The nomenclature used reflects that used for PL228 i.e. T1 is 250 μm from the periostracum, T2 500 μm and T3 1000 μm.

A chip of OKA standard was analysed in two separate LA-ICPMS sessions. These data were then compared to that from analyses of the same OKA chip analysed by SIMS. Thus, enabling a better comparison between the outer shell prismatic layer measured by LA-ICPMS and the umbo prismatic layer measured by SIMS. As the OKA matrix has a matrix closer to that of *A. islandica*, the reproducibility of the OKA (2σ) over these two sessions was used to calculate the typical error for measurements on *A. islandica*. As Table 4.6 shows the two analysis sessions OKA were representative of the typical variation seen during other sessions.

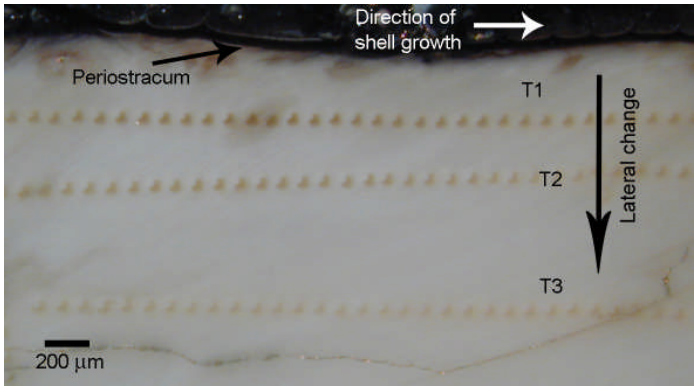

Figure 4.5a: Reflected light micrograph showing transects 1, 2 and 3 (T1, T2, T3), 250 µm, 500 µm and 1000 µm respectively from the periostracum (unetched sample) for the outer shell prismatic layer of *A. islandica* shell 228.

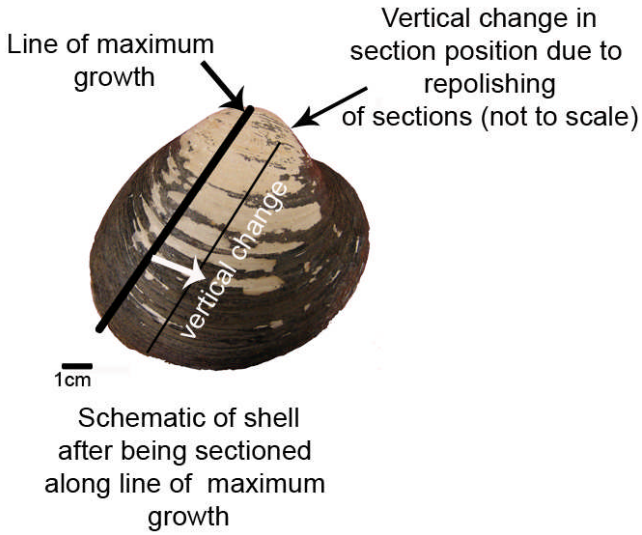

Figure 4.5b: Schematic showing vertical change away from the maximum growth axis due to repolishing on the vertical distance from the line of maximum growth.

4.3.4 SEM analysis

The number of the bands and position of the bands was determined by acetate peels (see section 1.2.2). However, to understand better how the organics changes in the shell, and to compare the position of each laser spot to the shell architecture at that particular point, Secondary Electron (SE) images were taken. The samples were

etched for 60 s using 0.1 N HCl. These samples were then thoroughly rinsed. Without etching, it was impossible to determine the growth checks from the growth bands.

The samples were carbon coated (as this provides a finer film than gold and thus a better resolution). It should be noted that by etching the samples, it caused the supporting calcium carbonate structure to dissolve, with the surface tension causing a crushing effect due to drying in air (Clark, 1980). Figure 4.6 shows images from *Mytilus californianus* polished, etched, and air-dried compared to polished and etched section prepared by critical-point etching taken from Clark (1980). It can be clearly seen that Critical Point Drying helps to maintain the dimensional stability of the sample. Unfortunately, it could not be used with the LA-ICPMS as the size of the sample prohibited it. Future work using smaller samples would be extremely interesting to further study the structure of *A. islandica*.

SE images allow the growth check to be clearly distinguished (see Figure 4.7). The concentration or nature of the organics changed both laterally as well as between different growth checks. This is important when examining whether trace elements are affected by the presence of organics, either directly (e.g. they are hosted by it) or indirectly (e.g. it effects trace element partitioning through modification of the crystal nucleation and propagation).

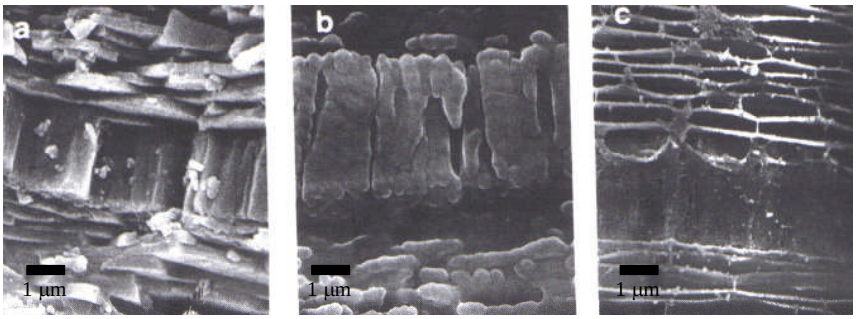

Figure 4.6: Secondary Electron images from *Mytilus californianus* of the pallial myostracum (thick layer in middle of images) a) fractured section: organic matrix present but cannot be readily distinguished from the aragonite crystals b) polished and etched and air-dried c) polished and etched section prepared by critical-point drying. Images and captions taken from Clark (1980).

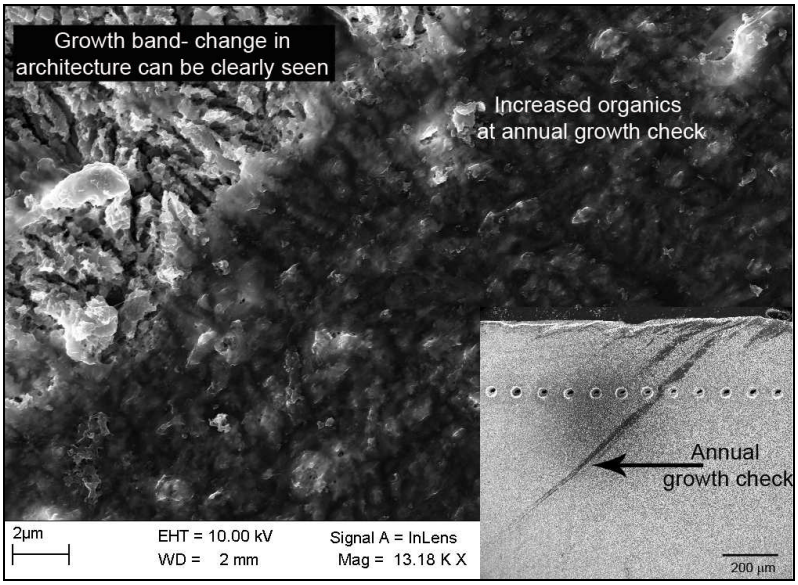

Figure 4.7: Secondary electron images of the growth check (1999) from the outer shell prismatic layer of shell 248. The main image highlights the distinct changes between the growth band (left) and the increase in organics indicating the growth check (right). The insert highlights position of spots compared to the growth checks. This *in situ* comparison is important particularly in this example, as it highlights that the spot missed the narrow growth check of 1999. Direction of growth is from left to right.

4.3.5 Data processing

The start position of each transect has been standardised relative to Transect 1 (T1) 250 μm from the periostracum. This is in order that the start position of each transect is comparable, as the width of the growth band decreases laterally away from the periostracum. Note that the distance axis was not otherwise altered; with the position of the annual growth, checks marked on the trace element fluctuations of the plots.

Data where the Li/Ca ratio exceeded 0.05 were removed. Li is a relatively constant measure of background and large changes in Li/Ca indicate changes in the raw Ca counts. Apparent decreases in Ca concentration result from cracks or imperfections within the shell. ^{27}Al was used to provide a check on contamination since Al is present in the polishing media. Mass-27 counts also include a component from $^{54}Fe^{2+}$, which is also a surface contaminant. No high Al/Ca ratios were observed in PL248. Calibration was carried out using GLITTER© software under license by New Wave™, developed by van Achterbergh *et al.* (2001). The software uses a linear fit of the count ratio of the internal normalising isotope, (in this case ^{43}Ca) to the element of a standard to calculate the concentrations of the unknowns based on an estimate of the weight percent CaO (Table 4.1b) i.e. the trace element concentration in GLITTER© is calculated by:

$Conc_{ni} = (cps_{ni}/abundance_j)/yield_{ni}$

Where:

$Conc_{ni}$ = Concentration of element i in analysis n.

cps_{nij} = mean count rate (background subtracted) of isotope j of i in analysis n.

$abundance_j$ = natural abundance of isotope j.

$yield_n$ = cps per ppm of element i in analysis n.

Yield of element i in analysis n is determined by:

$yield_{ni} = yield_{ns} \times Int(yield_{ni} / yield_{ns})^{std}$

Where:

$yield_{ns}$= cps per ppm of internal standard s in analysis n.

$Int(yield_{ni} / yield_{ns})^{std}$ = ratio of the yield of the internal standard s in analysis n, interpolated over standard analyses.

The software selects a background and signal window for these calculations, which can then be reviewed by the user, to confirm that the most stable part of the signal has been selected. The review window (see Figure 4.8) indicates to the user where the signal is most intense for each element (by the colour scheme in the upper panel), the signal window chosen will be applied to all elements measured.

The review of the stability of the signal is important. If the signal is unstable, the results will be strongly influenced by the positioning of the sample window, with the calculated concentrations changing significantly. During one analysis session (data not shown), the signal decayed significantly due to the decay of detector sensitivity. This resulted in a change in concentration of the element concentration depending on the position of the signal window e.g. Sr/Ca changed by ~30%, whereas typical variation was ~1%.

The concentrations of the standards (plus typical concentrations in the samples) are shown on Table 4.1b.

The precision and accuracy are both estimated at 95% confidence (2σ). The Mean Detection Limit (MDL) is calculated at 99% confidence (i.e. 3σ) determined by Poisson counting statistics:

$$MDL = 2.3\sqrt{2B}$$

Where B= total counts in background interval

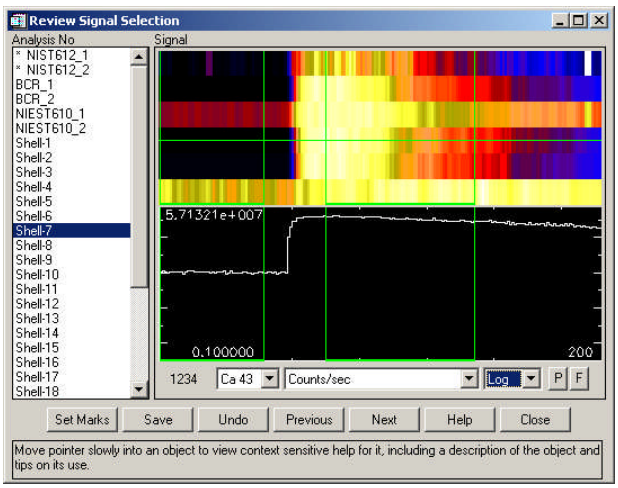

Figure 4.8: Typical signal selection window within GLITTER© showing signal from analysis of outer shell prismatic layer of *A. islandica* (shell 248 spot 7). The background signal selection is delimited by the first (green) box, with the sample signal denoted by the second (green) box. The colour scheme for the LA-ICPMS represents the count rates.

Isotope	Mass Window	Settling time (s)	Sample time (s)	Samples per peak	Segment duration (s)	Integration window (%)	Detection mode	Typical Limits of detection (ppm)
^{7}Li	10	0.3	0.01	10	0.01	10	Both	
^{24}Mg	10	0.046	0.01	10	0.01	10	Both	2-5
^{43}Ca	40	0.029	0.01	10	0.04	10	Both	40-80
^{44}Ca	10	0.001	0.01	10	0.01	10	Both	50-75
^{55}Mn	40	0.014	0.01	10	0.04	10	Both	0.2-0.6
^{88}Sr	40	0.03	0.01	10	0.04	10	Both	0.03-0.05
^{137}Ba	40	0.033	0.01	10	0.04	10	Both	0.1-0.3

Table 4.1a: Experimental set-up for LA-ICPMS measurements (used for both standards and unknowns). 250 runs, with one pass were used each analysis. When both analog and counting are used to record signals at the same time, this is called "both" mode. Samples per peak refer to the measurement of slightly different masses for the same mass window.

Standard	NIST610	NIST612	BCR	MACS1	NIES	OKA	Samples
CaO (%)	11.45	11.9298	7.12	56.0	54.3	56.0	56.0

Table 4.1b: CaO weight programmed into GLITTER© to calculate absolute concentration.

Element	NBS610		NBS612		BCR		MACS1	
	ppm	mmol/mol	ppm	mmol/mol	ppm	mmol/mol	ppm	mmol/mol
Sr	497.40	0.57	76.15	0.09	337.00	0.38	200-240	0.23-0.27
Mg*	482.4	1.99	60.31	0.248	20986	86.38		
Ba	424.1	0.31	37.74	0.027	684.00	0.50	100-150	0.073-0.11

Table 4.2: Certified concentrations within the standards. Where values are not available, cell is left blank. *Where values were quoted as oxides, they have been converted to ppm.

Specimen	Month of analysis	Date of analysis	Transects covered	Distance from perisotracum	Distance from growth edge (μm)	Total length of analysis (μm)	Years covered	Comments
PL228	Sep-05	06/09/2005	T0		200- 4000	3800	2001 - 1998	
		07/09/2005	T1	250	2100-15100	13000	1998 - 1993	
		08/09/2005	T2	500	1800-14900	13200	1998 - 1994	
		08/09/2005	T3	1000	4500-13200	8800	1997 - 1995	
PL248	May-06	01/05/2006	T1	1000	10700-12200	1500	1993 - 1992	
		02/05/2006	T3	500	4500-6500	12100	1997 - 1995	
		03/05/2006	T1 cont	1000	100-10600	2000	2001- 1993	
	Jul-06	28/07/2006	T3 cont	250	2000-4400	25000	1998 - 1995	Section was repolished 125 μm to remove debris from previous sampling
		28/07/2006	T2	250	100-4000	2000	2001 - 1997	
OKA	Apr-06	12/04/2006	-	-	-	-	-	
	May-06	18/05/2006	-	-	-	-	-	

Table 4.3: Details of analyses sessions with a log of transects, distances and years covered. Analysis of T3 was continued (cont) for PL248 on 3rd May 2006. Nomenclature for PL248 is same as that used for PL228, i.e. T1 is 250 μm from the periostracum, T2 500 μm and T3 1000 μm.

4.3.6 Solution-ICPMS analysis

Each aliquot was milled from PL228 from an area 500 μm wide (parallel to the periostracum), 2000 μm long (parallel to the annual bands) and 500 μm deep using a New Wave™ Micromill. The aliquot was sub-sampled for stable isotopes ($\delta^{18}O$ and $\delta^{13}C$), with the remaining material used for solution-ICPMS. The last 7 years of growth of the shell was analysed.

Each aliquot was weighed prior to 55 μl HNO_3 + 1.75 ml distilled water (from Purelab Ultra Elga) being added. The aliquot was then reweighed. A 0.2 ml of 50 ppb ^{115}In spike was added to 0.8 ml of this solution, together with 4 ml HNO_3 (2%) to make a 5 ml solution. Nitric acid was used as a solvent since other mineral acids can cause spectral interference (ThermoFinnigan, 2001). The ^{115}In spike provides internal mass calibration.

The concentration calibration standards were made up from multi-element standard Std1105800, with NIEST standard used as the matrix (Table 4.4 outlines the calibration standards) to make a total of 5 ml solution. The calibration standards were analysed a number of times until the machine was optimised and calibration lines showed correlation coefficient >0.95. The matrix is added to mimic the interaction of the ions found within the sample. A procedural blank was analysed at the beginning of analysis, with one sample (acid only) as a final analysis (to check out for "memory effect" i.e. cross contamination), which occurs when the washout is not sufficient to remove elements between analyses. The memory effect was found to be <0.1% for all the elements (see Table 4.4), and thus the error is minimal compared to the precision, which was typically >5% (2σ). The coefficient of variation is calculated using 2σ of the mean concentration. The typical percentage is given on Table 4.4.

	Sampling matrix (ml)	Std 1105800 100 ppb (ml)	50ppb In (ml)	2% HNO_3 (ml)	Total volume (ml)
B1	0	0	0.2	4.8	5
ST0	0.1	0	0.2	4.7	5
ST1	0.1	0.025	0.2	4.675	5
ST2	0.1	0.05	0.2	4.65	5
ST3	0.1	0.25	0.2	4.45	5
B2	0	0	0.2	4.8	5

Table 4.4: Composition of calibration standards for solution-ICPMS.

Isotope	Mass window	Settling time (s)	Sample time (s)	Samples per peak	Segment duration (s)	Integration window (%)	Detection mode	Washout memory* ppm (2s.f.)	Typical coefficient of variation (2σ)
^{7}Li	200	0.03	0.01	10	0.20	80	Both	<LoD	<30%
^{24}Mg	170	0.001	0.01	10	0.17	80	Both	0.25	<4%
^{43}Ca	170	0.056	0.01	10	0.17	80	Analog	260	<4%
^{55}Mn	170	0.039	0.01	10	0.17	80	Both	0.093	<5%
^{88}Sr	170	0.001	0.01	10	0.17	80	Both	4.6	<4%
^{137}Ba	170	0.001	0.01	10	0.17	80	Both	0.0060	<10%

Table 4.5: Instrumental set-up for solution-ICPMS. *Note the washout memory is calculated from a blank sample analysed at the end of the sample set. Three runs (i.e. three measurements of the ICPMS-solution) and five passes were used (i.e. change over time). Samples per peak refer to the measurement of slightly different masses for the same mass window. Typical coefficient of variation calculated from the multiple runs (2σ).

Total running time per aliquot was 42 s plus a washout time of 180 s giving a total of 222 s per aliquot. The set-up for solution-ICPMS analysis is shown on Table 4.5.

4.4 Standards

4.4.1 LA-ICPMS analysis of the standards

Standards were normally analysed every 20 samples (apart from OKA where it was carried out after six analyses). Two analyses of the same standard were analysed consecutively to examine the heterogeneity of the standard but minimise the potential effects of any machine drift. The difference in the "sample pairs" for both NIST610 and NIST612 was very similar (calculated from all analyses) e.g. both showed a precision (2σ) of 5.8% for Sr/Ca, 3.5% for Mg/Ca and NIST610 was slightly better for Ba/Ca showing a precision of 2.3% compared to 3.8% for NIST612. This shows the standards were relatively homogeneous and there is little difference in their reproducibility (i.e. one standard is not more homogeneous than the other is). Since the concentrations in NIST610 than NIST610 were closer to that of the unknown (i.e. *A. islandica* shell), it was used in GLITTER© for the calculation of the absolute compositions of the unknowns (using the values of Pearce *et al*. (1997)). BCR, a basalt standard, was used to provide an independent measure of the stability of the machine.

The precision of the standards (calculated as 2σ given as a percentage from average of that day's analysis) is shown on Table 4.6 for Sr/Ca, Mg/Ca and Ba/Ca. The difference to the published value is calculated by taking the average value calculated for that day for each element, which is then compared to the published value. This provides an indication of the direction of the error i.e. the calculated

values from a day were typically either under or overestimating. Wherever possible, a single transect was completed with one day's analysis, to reduce effects of machine instability. In addition, it was important to determine whether the lateral variation seen in the data could be due to machine drift. Therefore, T2 and T3 were analysed on the same day for PL228. For PL248 analyses, although each transect was done on a different day, this showed a similar pattern and the extent of the offset could be not explained by the changes in the standards (this is discussed later in the chapter).

The precision of the standards for this laboratory is usually quoted as ±10% (2σ). The CaO value put into GLITTER© for the calculation of the concentration of the elements affects their accuracy. An inaccurate value of CaO would produce a consistent offset. The standard pairs show good agreement (5.8% 2σ) suggesting that the machine stability was the main contributory factor to the errors.

It would be expected that the sample of another matrix would differ in behaviour. MACS1, a powdered calcite standard, may provide a matrix closer to *A. islandica* than rhyolite glass. The pressed sample behaved differently to the solid sample of *A. islandica* during laser ablation with the laser pit in the pressed sample almost invisible, perhaps suggesting that the powder is explosively mobilised (Sinclair *et al.*, 1998). The effect of a laser on a powder also appears to be inconsistent, with an inconsistent output signal, which adversely affects the calculated values. Thus, MACS1 standard produces significantly different values, making it a very poor calibration standard. In addition, there are no published Mg values for MACS1. As the rhyolite glass has a significantly different matrix, the 2σ precision calculated from repeat measurements of the OKA over two sessions was used to indicate the typical error, which would be expected during analyses of *A. islandica*.

		Calculated Sr/Ca (mmol/mol) using NIST610 as internal standard					
		612		BCR		MACS1	
		Precision of standards (per day) %	Difference to published value %	Precision of standards (per day) %	Difference to published value %	Precision of standards (per day) %	Difference to published value %
Sep-05	06-Sep	5.6	9.2	6.6	-3.2	10.2	-77.9
	07-Sep	14.8	3.8	9.8	-8.2	24	-77.9
	08-Sep	9.2	-1.1	3.6	-7.7	20	-78.2
Apr-06	11-Apr	3.4	-11.0	12.4	-1.6	3.8	0.9
May-06	01-May	1.8	-12.6	11.8	-6.2	11.2	-6.1
	02-May	6.8	-5.4	7	-3.4	13.6	-1.5
	03-May	5.4	-3.9	5	-3	6.8	-0.9
	18-May	15	-9.2	25.2	-14.5	12	8.9
Jul-06	28-Jul			3.5	-5.3	-	-

		Calculated Mg/Ca (mmol/mol) using NIST610 as internal standard					
		612		BCR		MACS1	
		Precision of standards (per day) %	Difference to published value %	Precision of standards (per day) %	Difference to published value %	Precision of standards (per day) %	Difference to published value %
Sep-05	06-Sep	12.4	33.5	Mg values were recorded as being at limits of detection.		23.2	No Mg value provided by USGS
	07-Sep	7.8	27.3			25	
	08-Sep	7.4	27.6			36	
Apr-06	11-Apr	9	16.6	4.2	-2	6.4	
May-06	01-May	2.6	35.4	10.2	9.4	7.4	
	02-May	9	33.4	11.8	4.4	20.6	
	03-May	4.8	39.7	6	5.9	9.8	
	18-May	15.6	10.5	19	-15.3	47	
Jul-06	28-Jul			2.8	-4.2	-	-

		Calculated Ba/Ca (mmol/mol) using NIST610 as internal standard					
		612		BCR		MACS1	
		Precision of standards (per day) %	Difference to published value %	Precision of standards (per day) %	Difference to published value %	Precision of standards (per day) %	Difference to published value %
Sep-05	06-Sep	7.8	6.7	2.6	-6.1	39.2	-98.8
	07-Sep	12.8	4.3	12	-9.5	45.4	-98.8
	08-Sep	10.2	5.1	4.8	-8.4	49.8	-98.8
Apr-06	11-Apr	8.2	4.9	4.6	0.3	10.4	7.1
May-06	01-May	7.2	0.9	16.2	5.1	15.2	-6.6
	02-May	6.6	8	13.2	1.5	26	5.6
	03-May	6.4	5	6	-0.6	26.6	1.3
	18-May	12	1.2	5.8	7.1	24	11.6

Table 4.6: Sr/Ca, Mg/Ca and Ba/Ca in the standards calculated with NIST612 (values quoted as 2σ). Precision of the standards is calculated as 2σ given as a percentage from average of that day's analysis. The difference to the published value is calculated by taking the average value calculated for that day for each element, which is then compared to the published value. It is unknown why Mg was not detected in BCR during September 2005 as MgO is quoted as 3.48% and is recorded in later analyses of BCR. Mg was detected in all other standards. NIST612 was unavailable for use in July 2006. Ba/Ca could not be detected by the ICPMS in July 2006 (reason unknown).

Comparison to OKA standard

A chip of OKA was analysed as a standard during two analysis sessions, 11th April 2006 and 18th May 2006 with an average of the two taken. An OKA grain is used as a calcite standard by the SIMS facility in Edinburgh and is considered the most homogeneous calcite standard used by that group (Finch, Pers. Comm., 2007). The grain mounted here was part of the same batch of OKA used in Edinburgh, but was not the same grain. During the burn time of each spot, a number of cracks formed and instead of a regular pit, small pieces around the laser site cleaved (Figure 4.9). These led to concerns about the stability of the signal, but the behaviour of the OKA signal was akin to that of *A. islandica*. Two different spot sizes (40 μm and 60 μm) were taken to determine whether this influenced the concentrations measured (as different spot sizes were used in analysis of *A. islandica*). OKA provides a better comparison, as homogeneity is likely to be good and the matrix is closer to the shell material than the glass standards. Therefore, the error for the measurements on *A. islandica* is calculated from the OKA variation of these two sessions. The calcite, as discussed earlier having a closer matrix match than the glass, and therefore errors from the OKA are more likely to represent errors on the concentrations calculated for *A. islandica*.

The same chip was analysed using SIMS at the Edinburgh ion probe facility, UK by Dr. N. Allison in June 2006 and normalised to the OKA used in that laboratory (Table 4.7). Hence, analysis of OKA allows direct comparison of SIMS and LA-ICPMS results. The ion probe technique has an order of magnitude better (2σ) precision for e.g. Sr/Ca 0.5% (SIMS) vs. 4.1% (LA-ICPMS). Analyses of OKA indicate that LA-ICPMS, normalised to the rhyolite glass, underestimates Mg/Ca by >15%, Sr/Ca by >24% and overestimates Ba/Ca by >20%. It is likely that these offsets result from differing matrix effects between the glass and the OKA standards.

These findings are important for direct quantitative comparison of the SIMS data from the umbo region with the LA-ICPMS data from the outer shell and will be discussed further in Chapter 8.

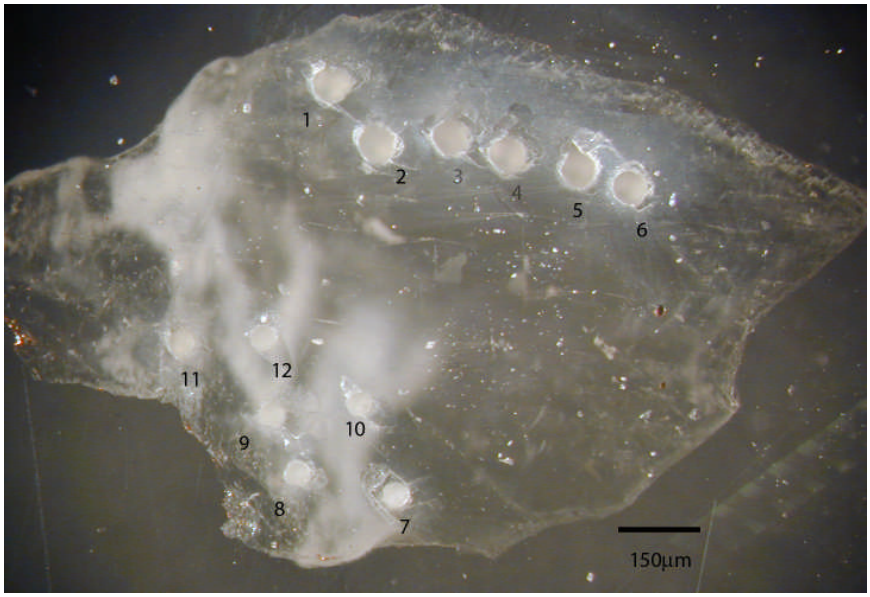

Figure 4.9: Reflected light micrograph of the 12 laser pits sampled on the OKA chip. The numbers refer to the sampling order. Spots 1-6 were sampled using 60 μm spot size, compared to 40 μm for spots 7-12.

Analysis of laser pits

Depth profiles by Scanning Electron Microscopy (SEM) show that the depth of the crater generated by the laser was typically 200-250 μm. However, the images show that the shape at the bottom of the pit is not uniform (Figure 4.10). In addition, the material affected by the laser extends beyond the surface (shown by a darker area even after etching).

Ion probe

	mmol/mol	Mg/Ca	Sr/Ca	Ba/Ca
	OKAAF1	3.40E+00	1.29E+01	6.57E-01
	OKAAF2	3.37E+00	1.30E+01	6.69E-01
	OKAAF3	3.41E+00	1.29E+01	6.01E-01
	OKAAF4	3.42E+00	1.29E+01	5.87E-01
	Mean	3.40E+00	1.29E+01	6.28E-01
	Stdev (2σ)	4.59E-02	6.48E-02	8.15E-02
	CV (2σ)	1.35%	0.50%	12.96%

LA-ICPMS

	mmol/mol	Mg/Ca	Sr/Ca	Ba/Ca
12th April	OKA_1	2.82E+00	1.01E+01	7.86E-01
12th April	OKA_2	2.78E+00	9.54E+00	7.38E-01
12th April	OKA_3	2.85E+00	9.57E+00	7.23E-01
12th April	OKA_4	2.93E+00	9.70E+00	6.76E-01
12th April	OKA_5	2.95E+00	9.52E+00	7.33E-01
12th April	OKA_6	2.82E+00	9.35E+00	7.39E-01
	Mean	2.86E+00	9.63E+00	7.32E-01
	Stdev (2σ)	1.36E-01	5.11E-01	7.05E-02
	CV (2σ)	4.78%	5.31%	9.62%

LA-ICPMS

	mmol/mol	Mg/Ca	Sr/Ca	Ba/Ca
18th May	OKA_7	2.89E+00	1.02E+01	8.14E-01
18th May	OKA_8	2.81E+00	9.81E+00	7.88E-01
18th May	OKA_9	2.78E+00	9.94E+00	8.29E-01
18th May	OKA_10	3.02E+00	9.94E+00	7.78E-01
18th May	OKA_11	3.00E+00	9.94E+00	7.21E-01
18th May	OKA_12	2.96E+00	1.03E+01	8.34E-01
	Mean	2.91E+00	1.00E+01	7.94E-01
	Stdev (2σ)	2.00E-01	3.39E-01	8.38E-02
	CV (2σ)	6.88%	3.38%	10.56%

	OKA analysis (same chip) (mmol/mol)					
	Mg/Ca		Sr/Ca		Ba/Ca	
	mean	stdev (2σ)	mean	stdev (2σ)	mean	stdev (2σ)
Ion probe	3.40E+00	4.59E-02	1.29E+01	6.48E-02	6.28E-01	8.15E-02
LA-ICPMS	2.88E+00	1.72E-01	9.82E+00	5.73E-01	7.63E-01	9.78E-02

Table 4.7: OKA concentrations calculated under typical conditions by (a) ion probe data (b) LA-ICPMS 11th April (c) LA-ICPMS 18th May d) summary of data (a)(b)(c). Note that the laser pit is deeper than that of the ion probe 250 μm vs. <20 μm. CV (coefficient of variation) is calculated at standard deviation as percentage of the mean.

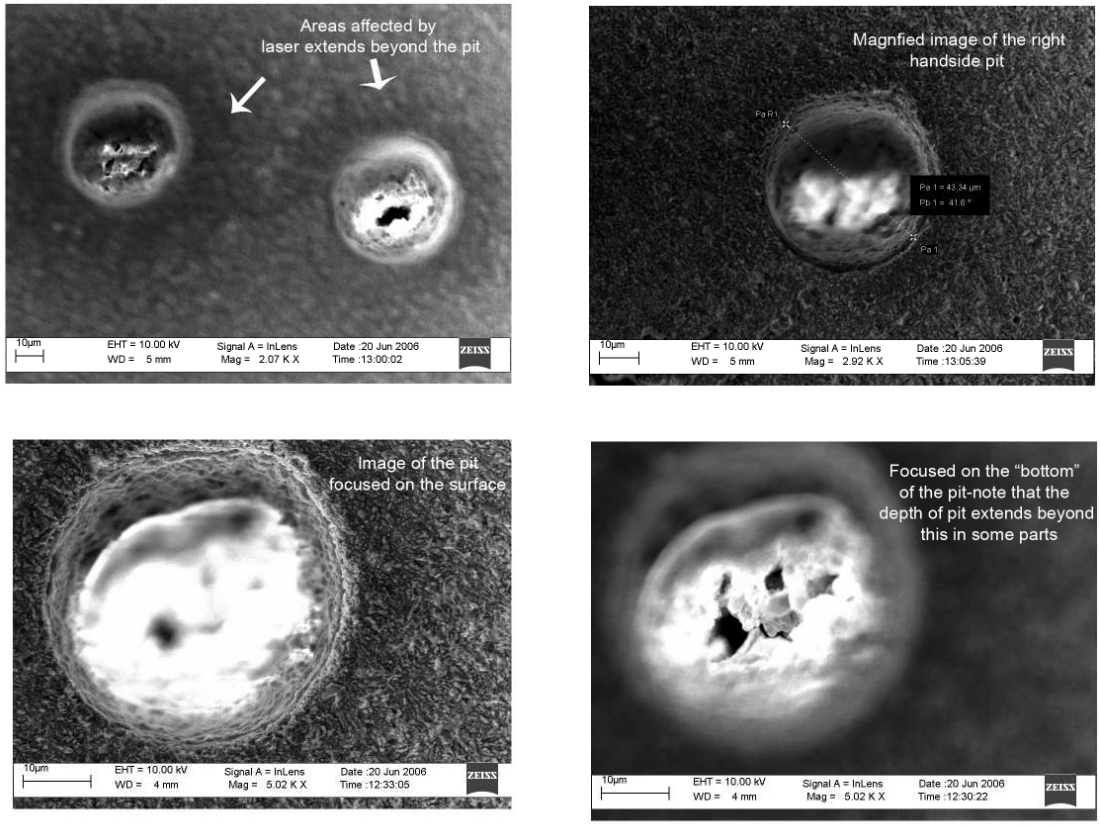

Figure 4.10: SE (Secondary Electron) images of laser pits taken post-etching in outer shell prismatic layer of *A. islandica* shell 248. It is possible to see that the effects of the laser extend beyond the laser crater.

4.4.2 Solution-ICPMS

Solution-ICPMS was performed on powder samples digested using the process described above. The calibration lines produced by the aqueous standards have a R-factor of >0.95, with a precision (2σ) of Sr/Ca 2.6%, Mg/Ca 3.0%, and Ba/Ca 4.4%. Details of reproducibility are found on Table 4.5, together with measurements of the memory effect (i.e. cross-contamination), measured from a blank.

4.5 Results

4.5.1 PL228 T1 Results

Transect 1 (T1) 250 μm from the periostracum is the longest transect analysed (15000 μm) and covers 1993-1998. Geochemistry variations between analyses are significant (Figure 4.11). Sr/Ca, Mg/Ca and Ba/Ca concentration ranges are shown in Table 4.8 (together with the T2 and T3). The dating of transects is made by reference to the visual banding in the acetate peels and confirmed through SEM analysis. Sampling of $\delta^{18}O$ reconfirmed the assignment of the growth checks.

Sr/Ca shows maximum concentration at the annual growth checks of 1997-1998. Prior to this, Sr/Ca peak occurs at the growth check but they are not the highest concentrations found during a single year, with variation within the growth bands exceeding it. Sr/Ca variation in the growth bands between 1994 and 1997 is ~0.4 mmol/mol.

Mg/Ca shows variation between 0.5-1.4 mmol/mol with the highest values in the latter years of growth. High Mg/Ca is found at all the growth checks with the exception of 1994, which shows very little increase. Within the growth bands, Mg/Ca variation is within error in T1. As described within the previous chapters, sharp increase and decreases deposited over short distances (<2000 μm) are defined as peaks for the remainder of the discussion. This is in keeping with previously published work (e.g. Lazerth *et al*., 2003; Gillikin *et al*., 2006) and with the annotation used in the previous chapter.

Sr/Ca and Mg/Ca co-vary at the annual termination bands 1996-1998 but the relative magnitude of each varies. Mg/Ca maximum occur at the beginning of the annual termination band whereas Sr/Ca increases in the latter part (Figure 4.12). At the 1996 termination band, Sr/Ca and Mg/Ca peaks occur concurrently but the Sr/Ca

peak is very small. Prior to 1996, Sr/Ca does not show strong annual peaks whereas Mg/Ca increases to >150% of the concentration measured within the growth band.

Ba/Ca shows average data are <0.005 mmol/mol, with sporadic peaks increases to a maximum of 0.07 mmol/mol (covering more than one measurement). Increases in Ba/Ca do not correlate to Sr/Ca or Mg, or with the position within a band (i.e. time/season).

	Sr/Ca mmol/mol	Mg mmol/mol	Ba mmol/mol
T1	1.0-2.4	0.5-1.0	0.0008-0.07
T2	0.6-1.8	0.5-1.2	0.0005-0.065
T3	0.8-1.2	0.4-0.7	0.0005-0.051

Table 4.8: Range in the data between three parallel transects. Mean Detection limit (MDL) (3σ) is typically 1 $x10^{-4}$, 4 $x10^{-3}$ and 7 $x10^{-5}$ mmol/mol for Sr/Ca, Mg/Ca and Ba/Ca respectively.

4.5.2 Comparison of results across all three transects

Transect 2 (T2) (500 μm from the periostracum) and transect 3 (T3) (1000 μm from the periostracum) are shown on Figures 4.13 and 4.14 respectively. These show a similar pattern of variation as described above, but the amplitude of the variations is suppressed (also see Table 4.8). Figure 4.15a-c plot a five point running average of the Sr/Ca, Mg/Ca and Ba/Ca values respectively for each transect, including T0 (which was analysed non-parallel to the periostracum). A five point running average is used to compensate for slight differences in the relative sampling positions. The slight offset in position of the peaks is due to the narrowing of the band width laterally away from the periostracum.

This shows that Sr/Ca decreases with increasing distance from the periostracum but the offset between each transect varies throughout the analyses. Mg/Ca values in T1 and T2, lie within error, but are significantly higher than that found in T3. Ba/Ca values show a decrease away from the periostracum between T1 and T3 at the highest Ba/Ca values with the lower values being within error of each other. Ba/Ca values of T1 and T2 are within error.

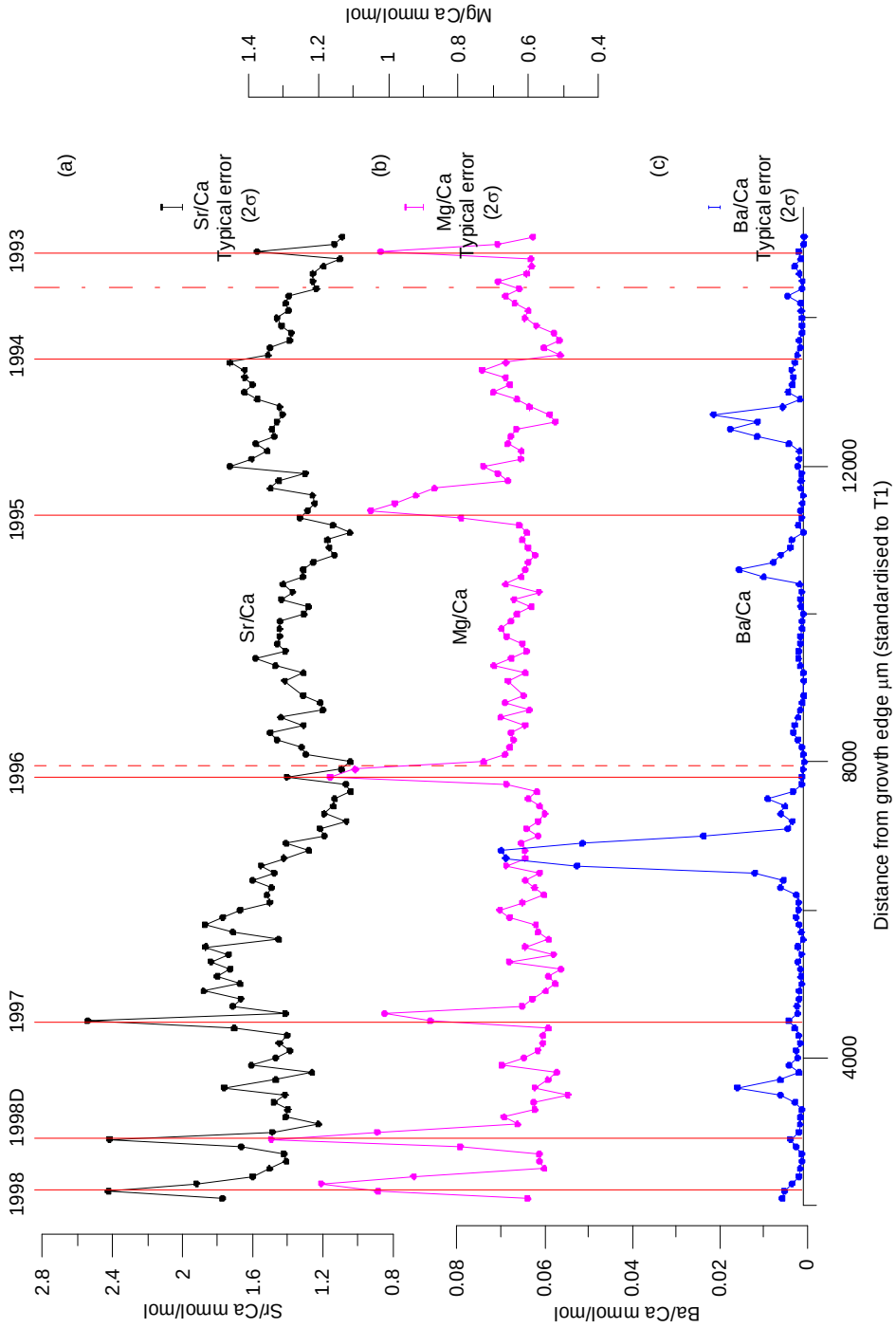

Figure 4.11: T1 profile taken parallel to the periostracum (at a distance of 250 µm) in outer shell prismatic layer of *A. islandica* shell 228 of (a) Sr/Ca, (b) Mg/Ca and (c) Ba/Ca. The typical error (2σ) is calculated from the reproducibility of the OKA. The solid red line marks the end of the termination band; the dashed line marks the start of the termination band (where it covers more than one analysis), with the dot-dash line marking intra-annual bands. D identifies a doublet.

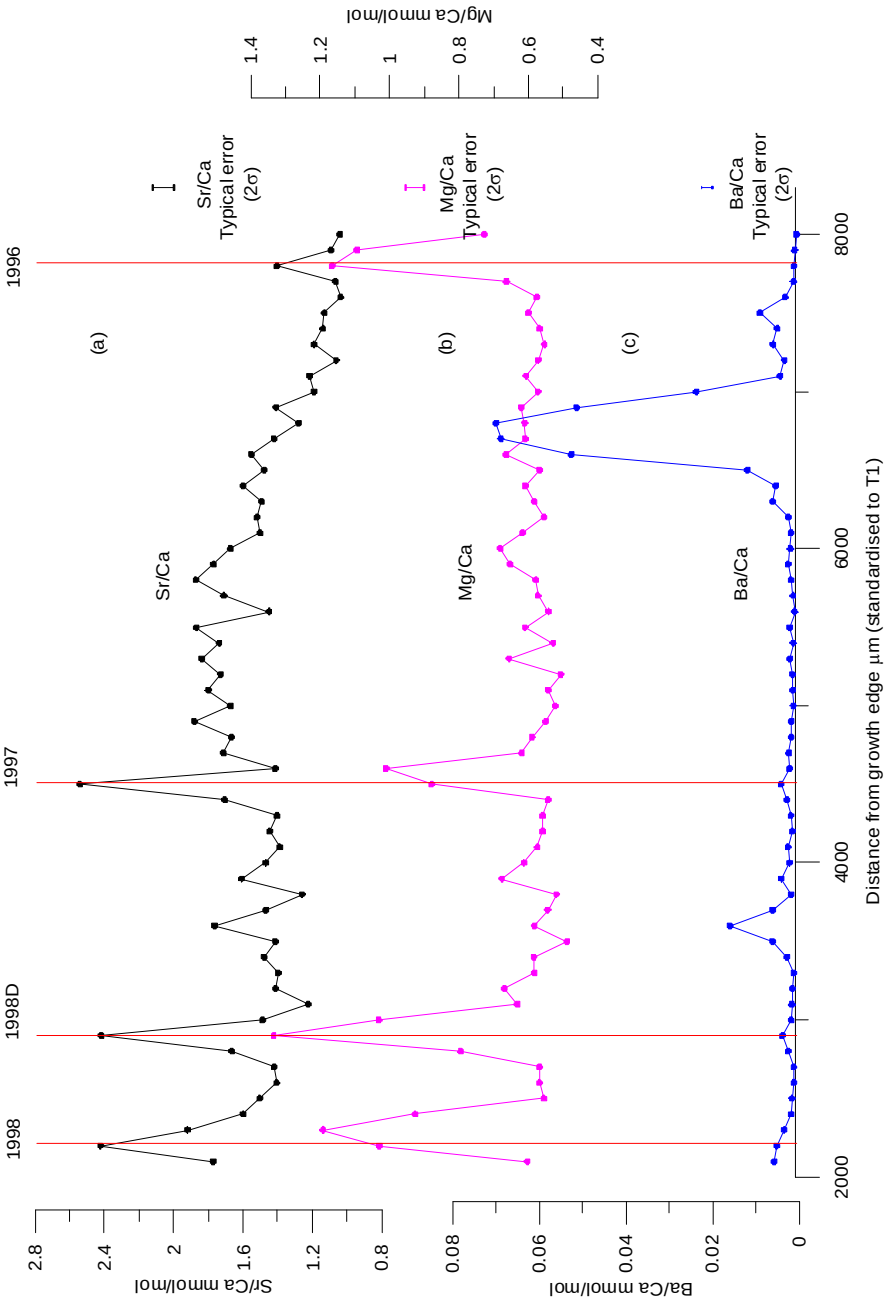

Figure 4.12: Magnified section of the PL228 T1 analyses shown in Figure 4.11 of (a) Sr/Ca, (b) Mg/Ca (c) Ba/Ca. The typical error (2σ) is calculated from the reproducibility of the OKA. The Mg/Ca increase can be clearly seen to precede the increase in Sr/Ca associated with the annual termination band, although not at the doublet. The solid red line marks the end of the termination band; the dashed line marks the start of the termination band (where it covers more than one analysis), with the dot-dash line marking intra-annual bands. D identifies a doublet.

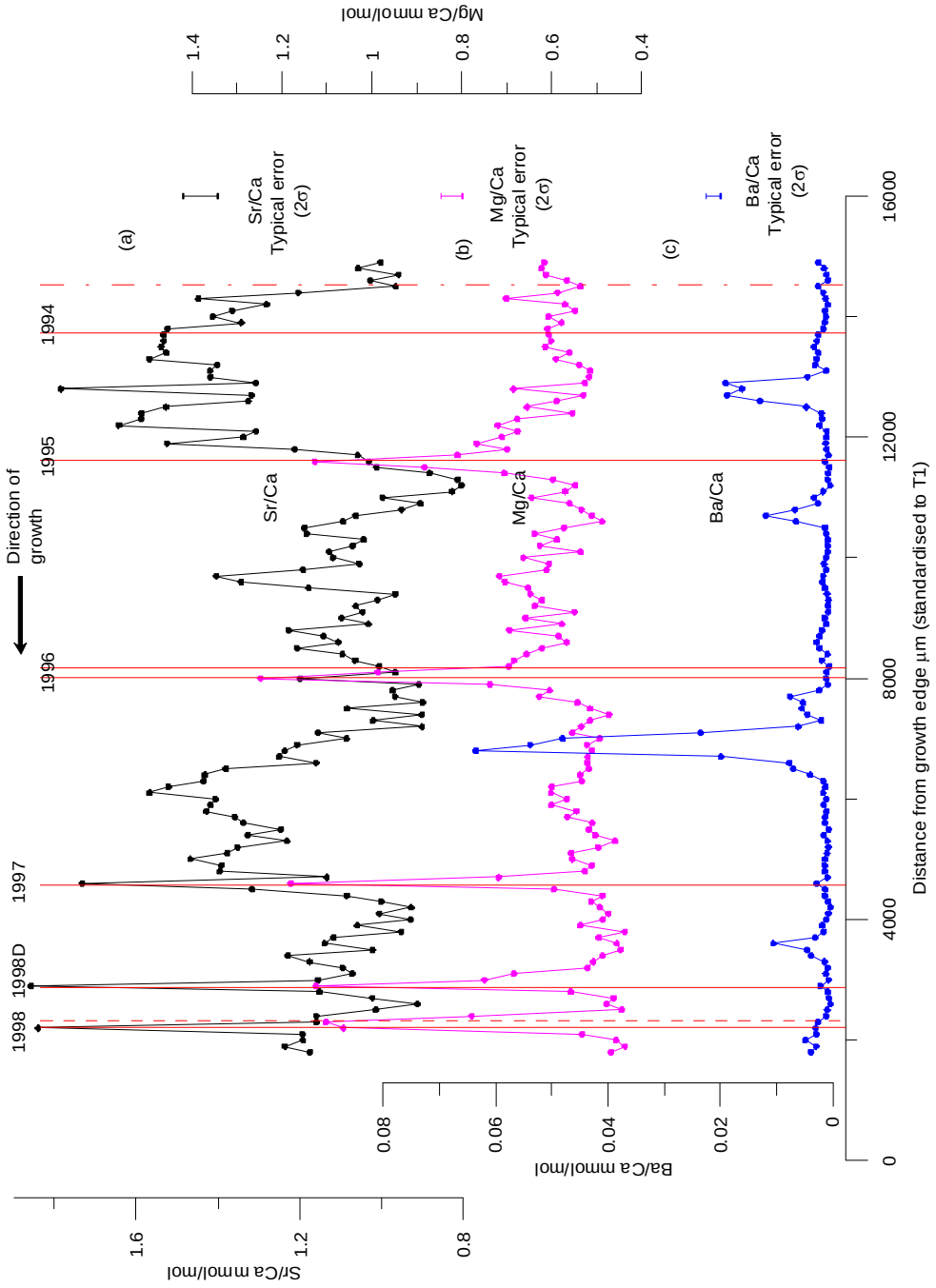

Figure 4.13: T2 profile taken parallel to the periostracum (at a distance of 500 µm) in prismatic layer of *A. islandica* shell 228 of fluctuations of (a) Sr/Ca, (b) Mg/Ca and (c) Ba/Ca. The typical error (2σ) is calculated from the reproducibility of the OKA. The solid red line marks the end of the termination band; the dashed line marks the start of the termination band (where it covers more than one analysis), with the dot-dash line marking intra-annual bands. D identifies a doublet.

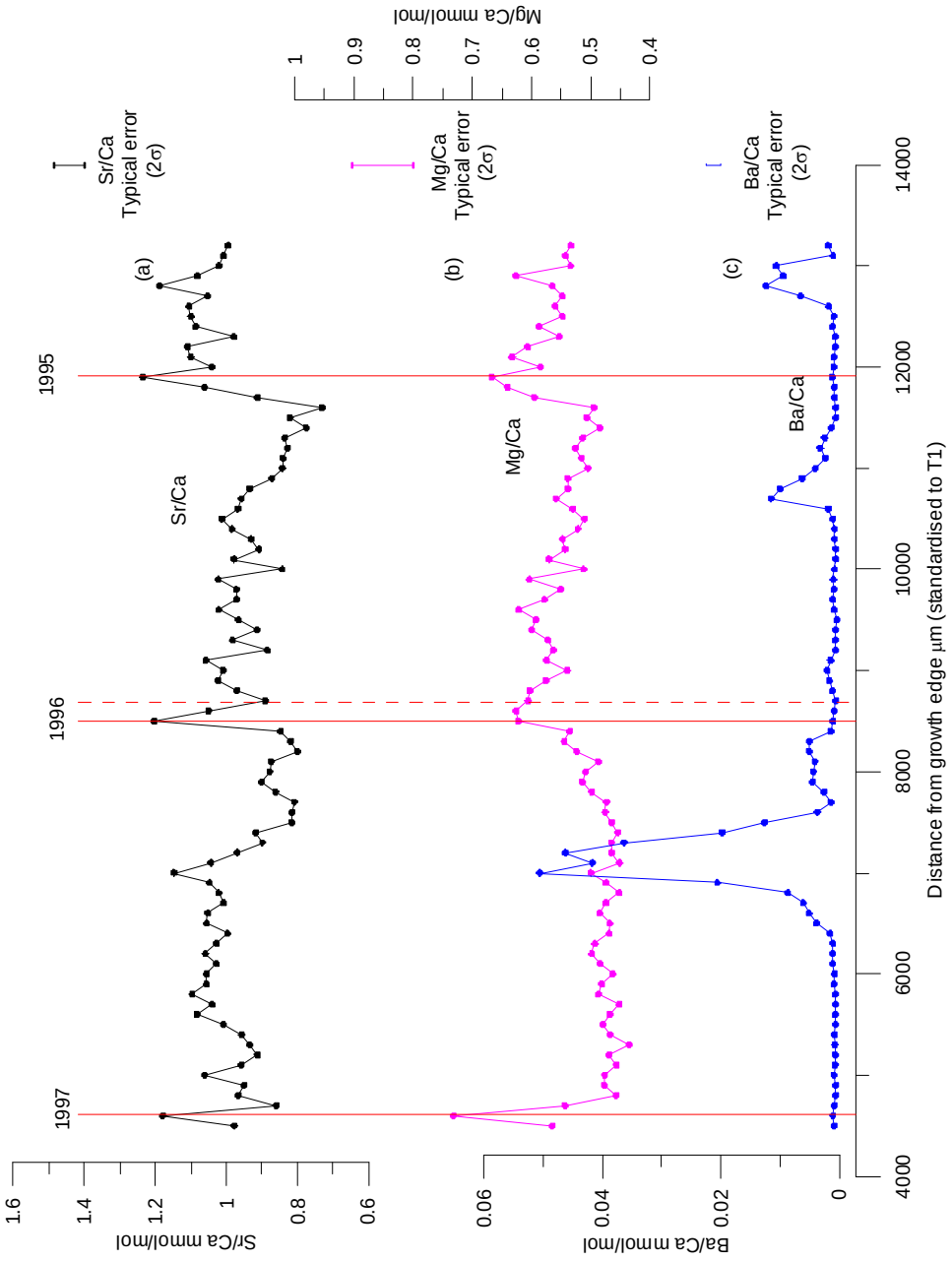

Figure 4.14: T3 profile taken parallel to the periostracum (at a distance of 1000 µm) in outer shell prismatic layer of *A. islandica* shell 228 of fluctuations of (a) Sr/Ca, (b) Mg/Ca and (c) Ba/Ca. The typical error (2σ) is calculated from the reproducibility of the OKA. The solid red line marks the end of the termination band; the dashed line marks the start of the termination band (where it covers more than one analysis), with the dot-dash line marking intra-annual bands. D identifies a doublet.

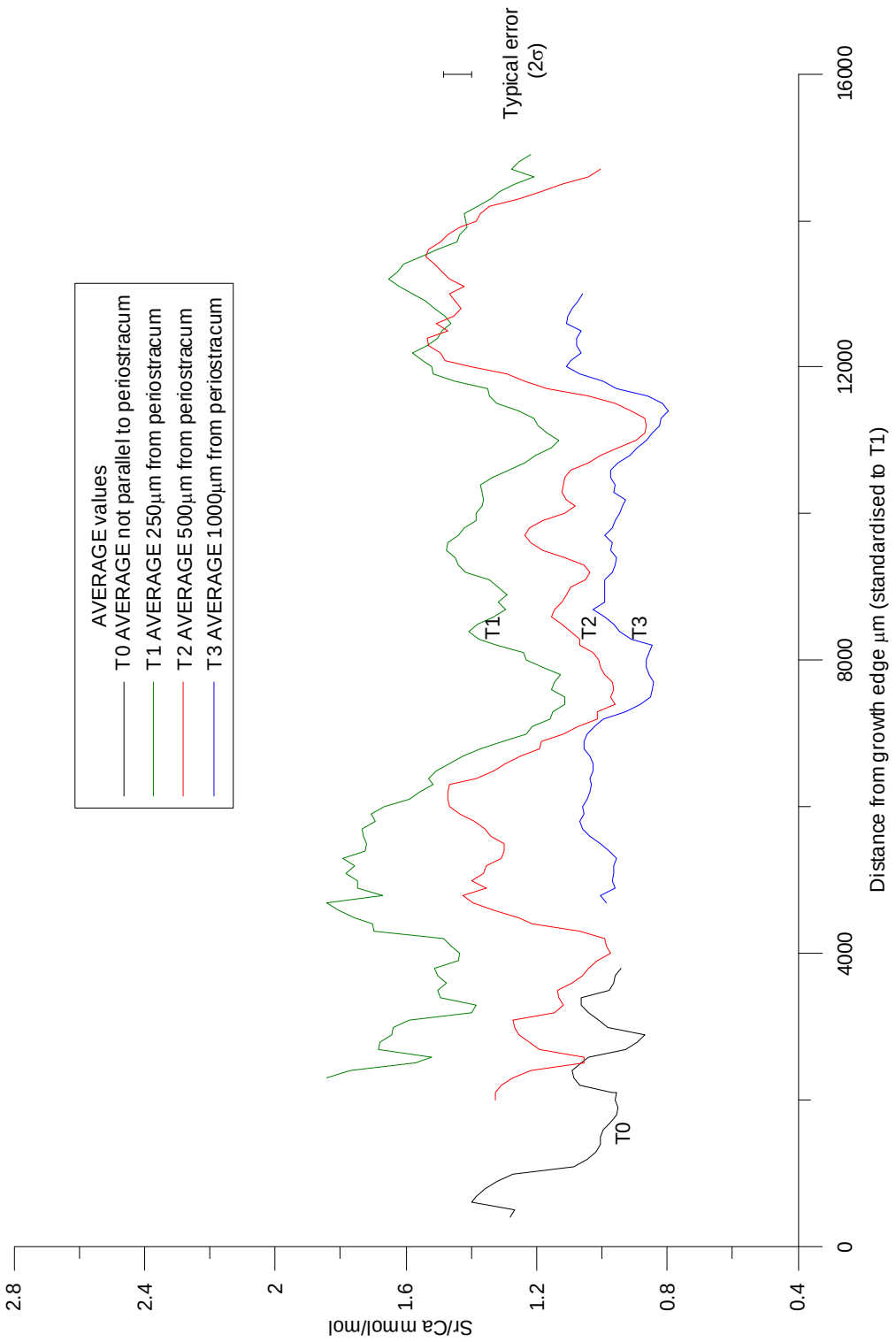

Figure 4.15a: Sr/Ca results of three transects (T1-T3) measured in the outer shell prismatic layer of *A. islandica* shell 228 with increasing distance from the periostracum. Results are averaged (five point) for each transect. The typical error (2σ) is calculated from the reproducibility of the OKA.

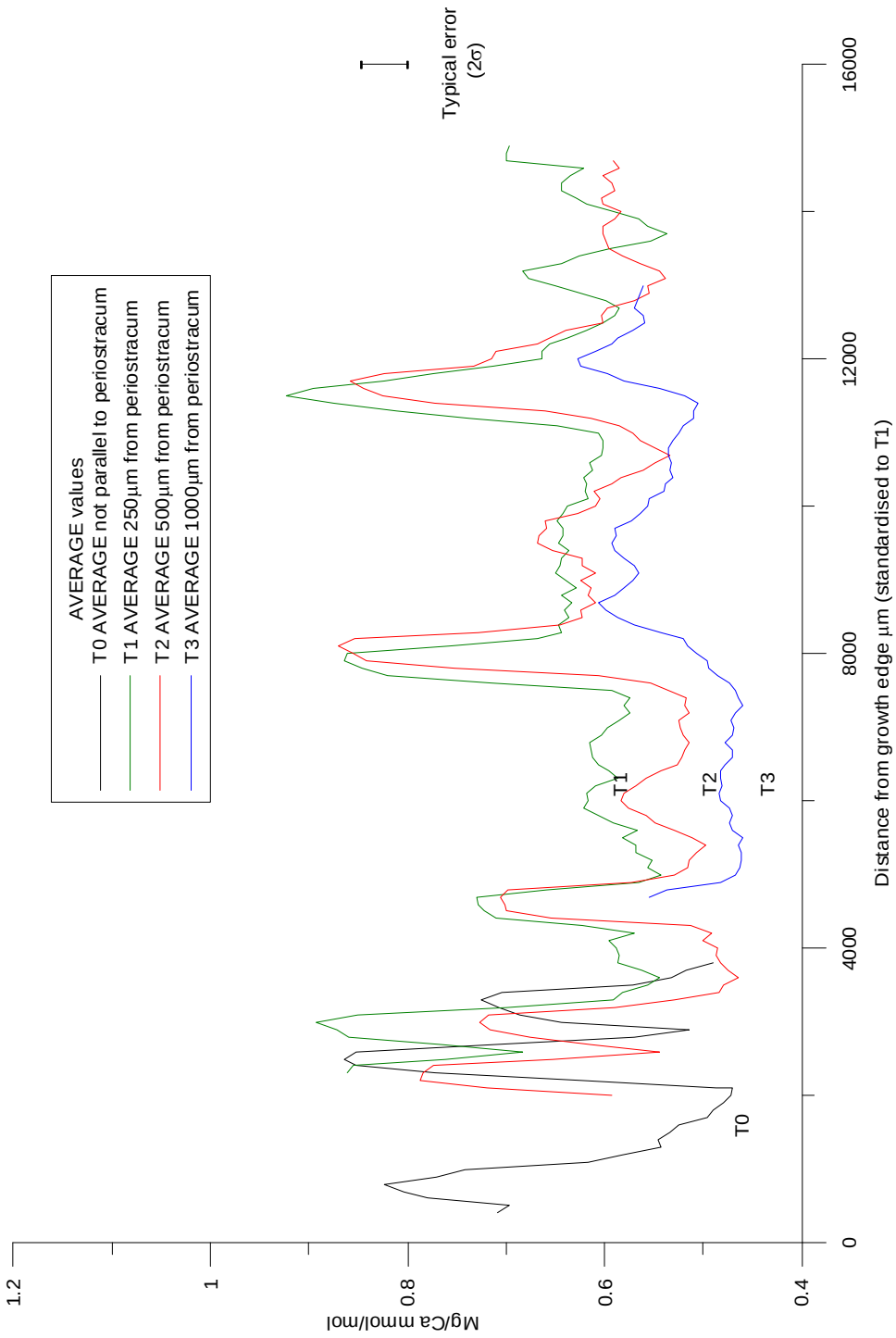

Figure 4.15b: Mg/Ca results of three transects (T1-T3) measured in the outer shell prismatic layer of *A. islandica* shell 228 with increasing distance from the periostracum. Mg/Ca results of three transects (T1-T3) with increasing distance from the periostracum. Results are averaged (five point) for each transect. The typical error (2σ) is calculated from the reproducibility of the OKA.

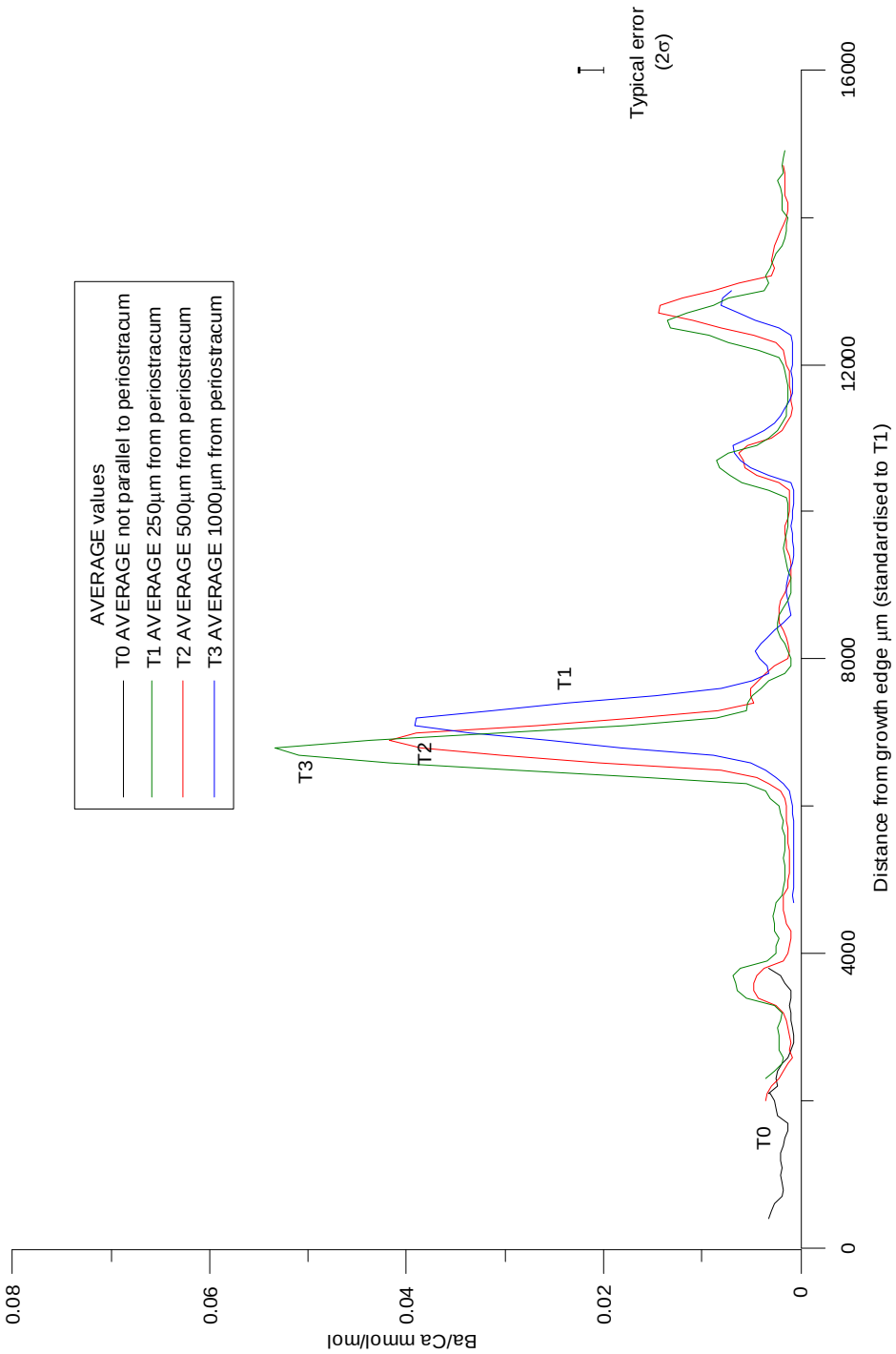

Figure 4.15c: Ba/Ca results of three transects (T1-T3) measured in the outer shell prismatic layer of *A. islandica* shell 228 with increasing distance from the periostracum. T1 to T3 are with increasing distance from the periostracum. Results are averaged (five point) for each transect. The typical error (2σ) is calculated from the reproducibility of the OKA.

4.5.3 PL248 Results

PL248 was measured in two separate analyses sessions - T1 and some of T3 (4500-6500 μm from growth edge standardised to T1) were measured in May 2006. T2 was measured in July 2006 with T3 extended by 1400 μm after the sample was repolished to remove the surface 125 μm. It provided a preliminary investigation into vertical variation of the elements, (as the original positions of the laser pits could be seen) (see Figure 4.5b for schematic). The nomenclature used is the same as that used for PL228, i.e. T1 is 250 μm from the periostracum, T2 is 500 μm from the periostracum, and T3 is 1000 μm from the periostracum.

PL248 analyses 1992-2001, and shows generally a similar pattern for the trace elements as PL228 (Figure 4.16). Sr/Ca increases are found during the growth checks in the latter years with increases >2.0 mmol/mol for T1. Spot analysis in T1 missed the (thin) termination band of 1999 (see Figure 4.7). Sr/Ca increases for the 1999 growth check were very small (and were much higher in T2). Increases in Sr/Ca are also seen in PL248 during some earlier growth checks compared to PL228 e.g. 1995.

Mg/Ca shows variation of typically 0.8-1.2 mmol/mol in T1. Generally, elevated Mg/Ca is found at the growth checks with the highest in the latter years (1997-2000). Damage to the shell during 1998 was noted, during visual examination of the shell (see Figure 4.20). This can be seen by cessation of shell growth and evidence of an external scar (in which regrowth of the shell occurs lower than the original shell height). The internal growth bands also showed evidence of infilling- in which the material is more porous with a different texture and behaved differently during laser ablation (see Figure 4.20). This damage was accompanied by a gradual increase in Sr/Ca, but Mg/Ca only shows an increase covering one analysis spot (<100 μm).

Ba/Ca shows a similar pattern to PL228, with consistently low values <0.005 mol/mol interspersed with sporadic increases of >0.04 mmol/mol. These peaks occur at the same part of the growth band laterally, i.e. they are high reproducible across a band (though there is a lateral decrease).

Lateral variation is also found in PL248 with a decrease of ~25% in Sr/Ca and >60% in Mg. The limited data of Ba/Ca between T1 and T3 (no T2 was measured) also showed a lateral offset.

Comparison of analyses collected in May 2006 and those from July 2006 (after the sample had been repolished to remove the top ~125 μm) shows that there is an offset of 0.4 mmol/mol for Mg/Ca (Figure 4.18) whereas Sr/Ca shows no discernible offset between the two sets of analyses (Figure 4.17).

As NIST612 was not analysed (with NIST610 used for calibration), the only other common standard was BCR. In BCR, Sr/Ca values are within error for the two sessions being (3% and 5.3% below the published values in May 2006 and July respectively). For Mg/Ca, they were +5.9% and -4.2% respectively, but this is within the precision of the standards. The offset in the sample was >40% with the caveat that the matrix effect was not the overriding factor. The maximum difference in the accuracy of the standards during analyses (for NIST612 vs. BCR) was 30% indicating that the difference in Mg is unlikely to relate to problems with the precision of the standards.

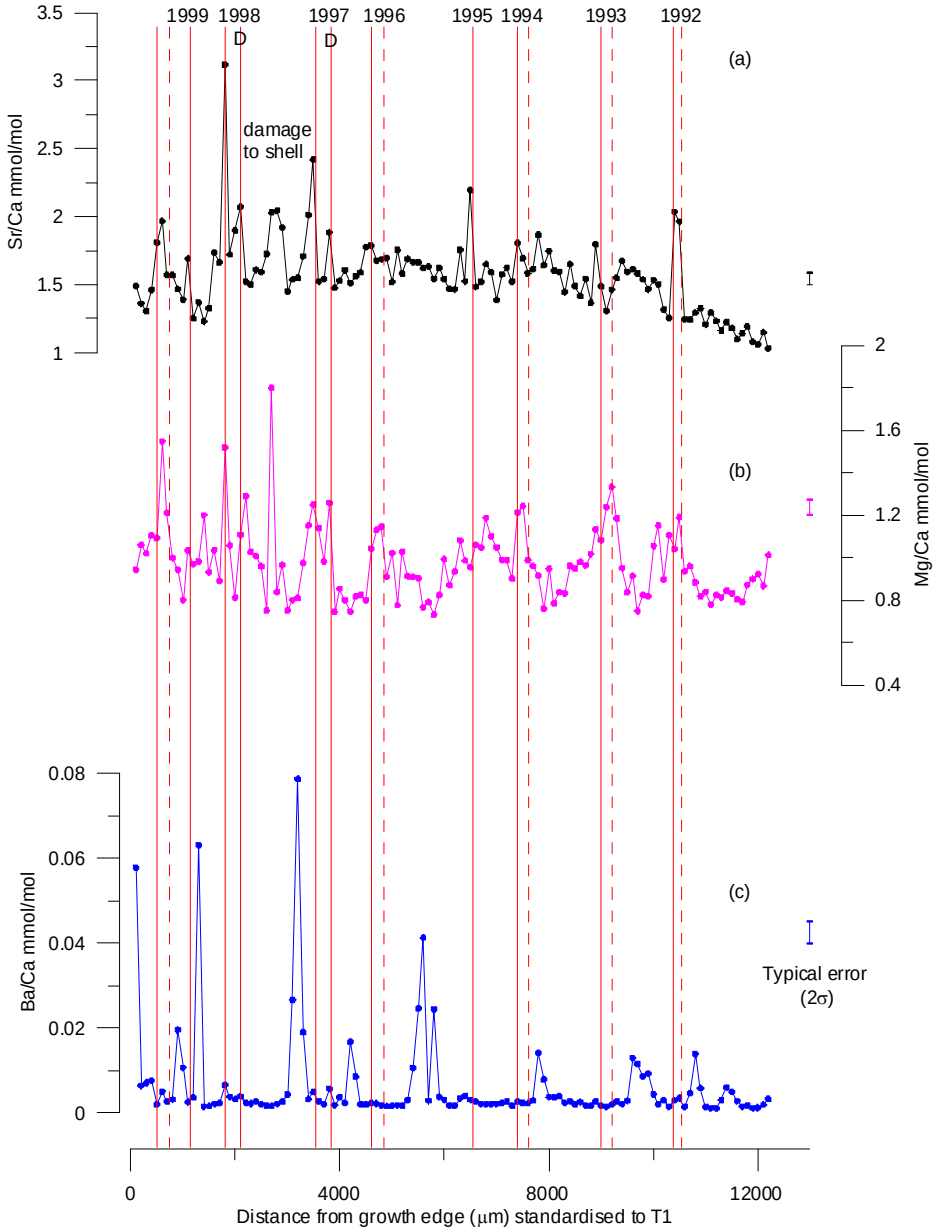

Figure 4.16: T1 analysed parallel to the periostracum (at a distance of 250 μm) in the outer shell prismatic layer of *A. islandica* shell 248 showing (a) Sr/Ca, (b) Mg/Ca and (c) Ba/Ca fluctuations (May 2006 analysis). The typical error (2σ) is calculated from the reproducibility of the OKA. The solid red line marks the end of the termination band; the dashed line marks the start of the termination band (where it covers more than one analysis), with the dot-dash line marking intra-annual bands. D identifies a doublet. Note damage to the shell during 1998 resulted in infilling of material (see Figure 4.20).

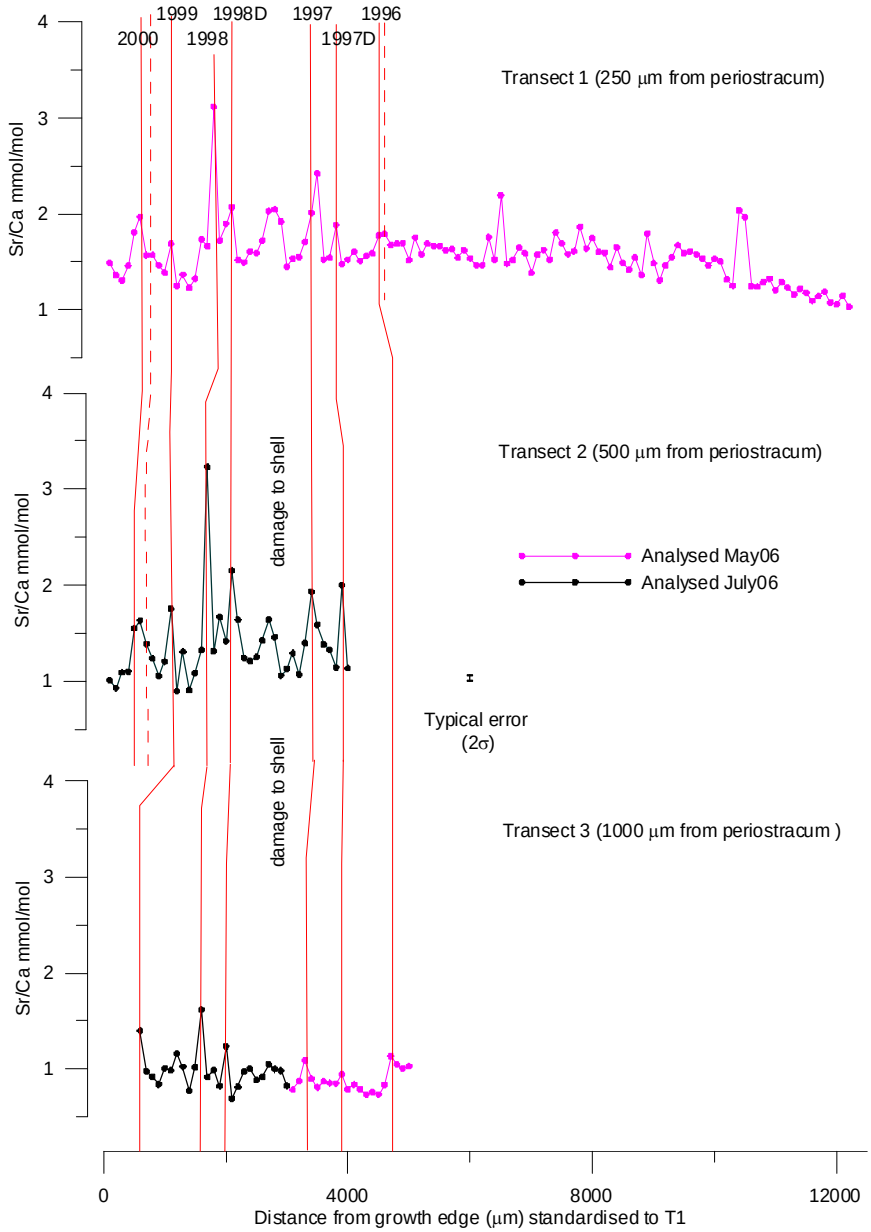

Figure 4.17: Sr/Ca results from the outer shell prismatic layer of *A. islandica* shell 248 using analyses from May 2006 (pink line) and July 2006 after ~125 μm repolish (black line). Note that the doublet for 1997 was visually difficult to locate in T3. The typical error (2σ) is calculated from the reproducibility of the OKA. The solid red line marks the end of the termination band; the dashed line marks the start of the termination band (where it covers more than one analysis), with the dot-dash line marking intra-annual bands. D identifies a doublet. Note damage to the shell during 1998 resulted in infilling of material (see Figure 4.20).

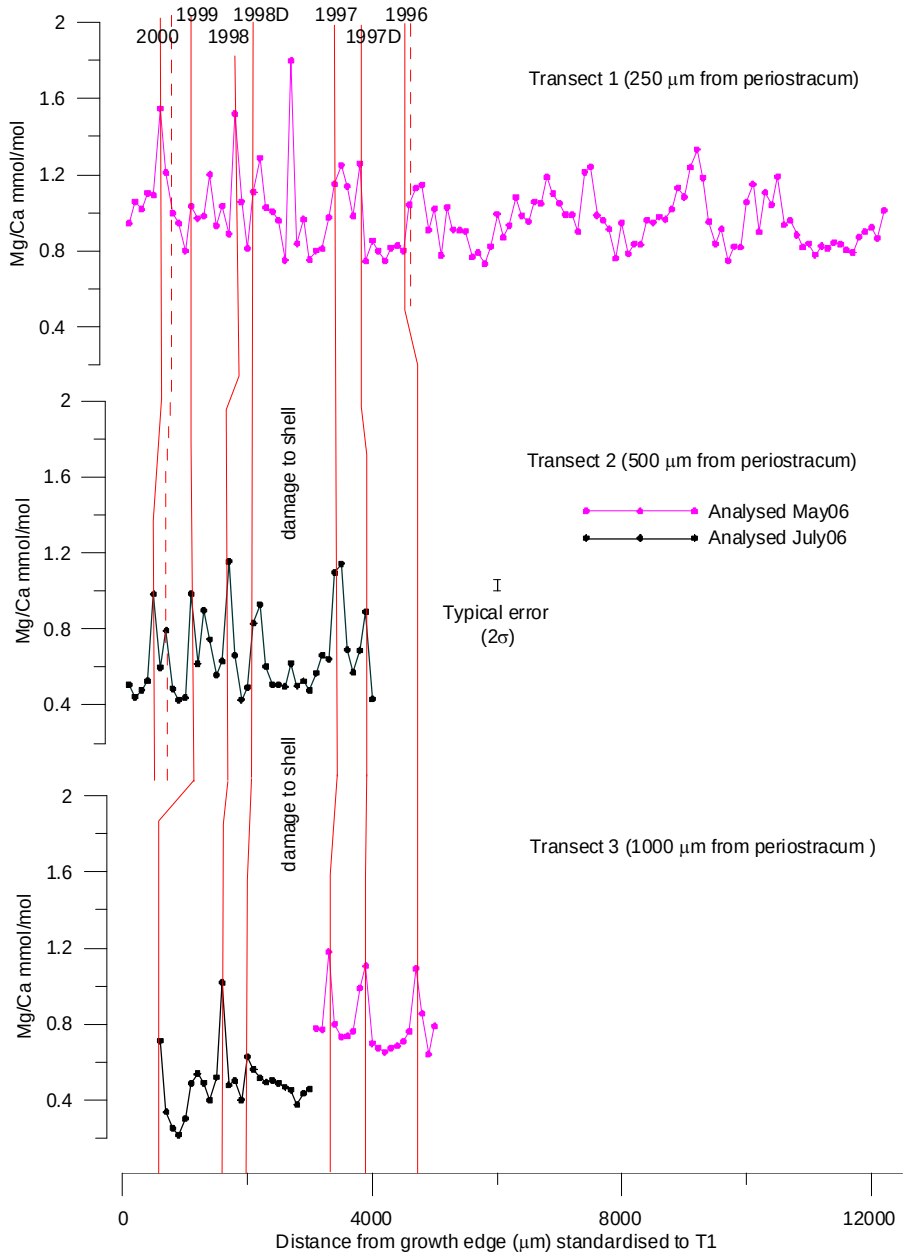

Figure 4.18: Mg/Ca results from the outer shell prismatic layer in *A. islandica* shell 248 using analyses from May 2006 (pink line), and July 2006 after 125 μm polish (black line). The typical error (2σ) is calculated from the reproducibility of the OKA. The solid red line marks the end of the termination band; the dashed line marks the start of the termination band (where it covers more than one analysis), with the dot-dash line marking intra-annual bands. D identifies a doublet. Note damage to the shell during 1998 resulted in infilling of material (see Figure 4.20).

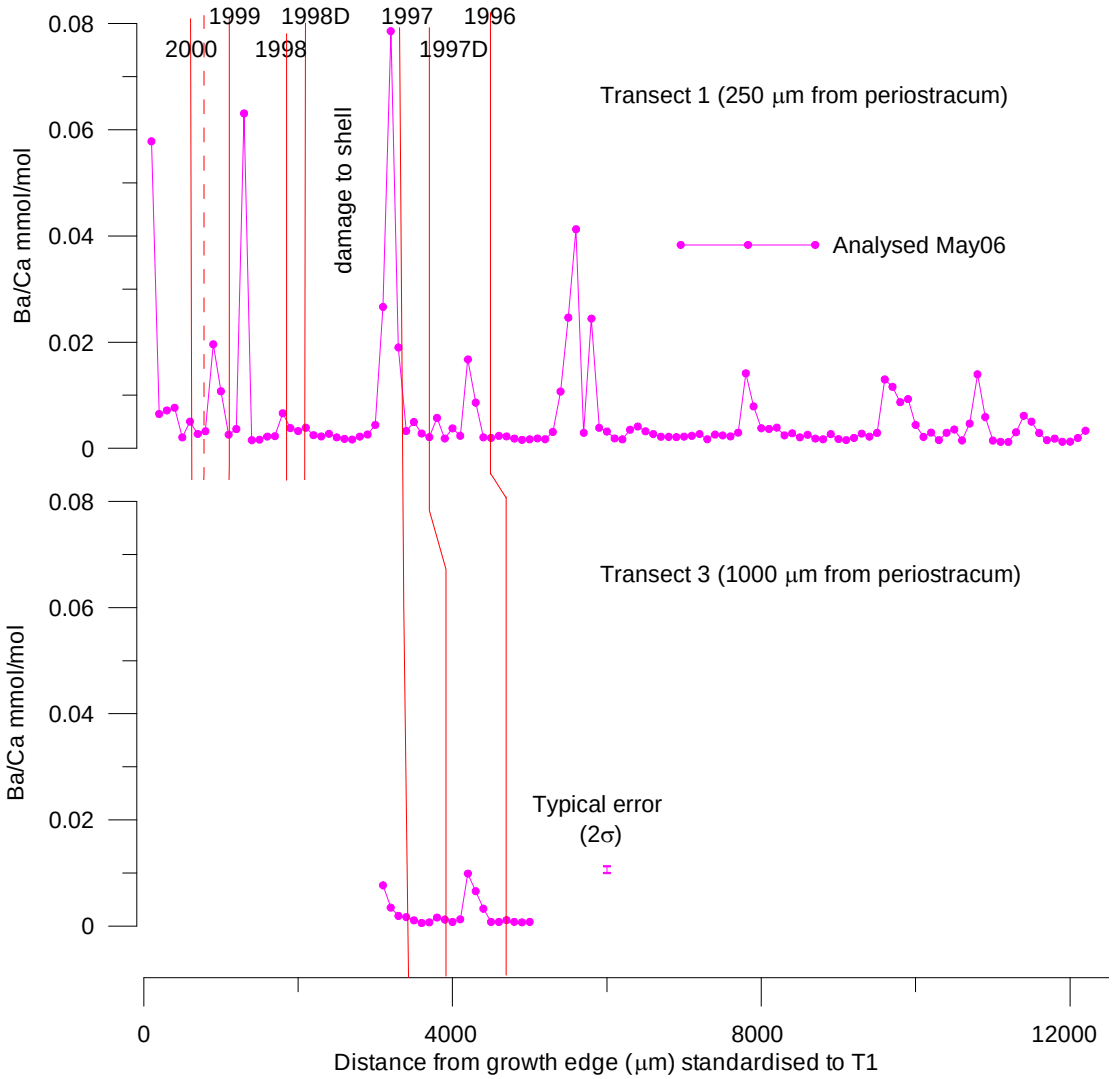

Figure 4.19: Ba/Ca results from the outer shell prismatic layer of *A. islandica* shell 248 using analyses from May 2006. The typical error (2σ) is calculated from the reproducibility of the OKA. The solid red line marks the end of the termination band; the dashed line marks the start of the termination band (where it covers more than one analysis), with the dot-dash line marking intra-annual bands. D identifies a doublet. Note damage to the shell during 1998 resulted in infilling of material (see Figure 4.20).

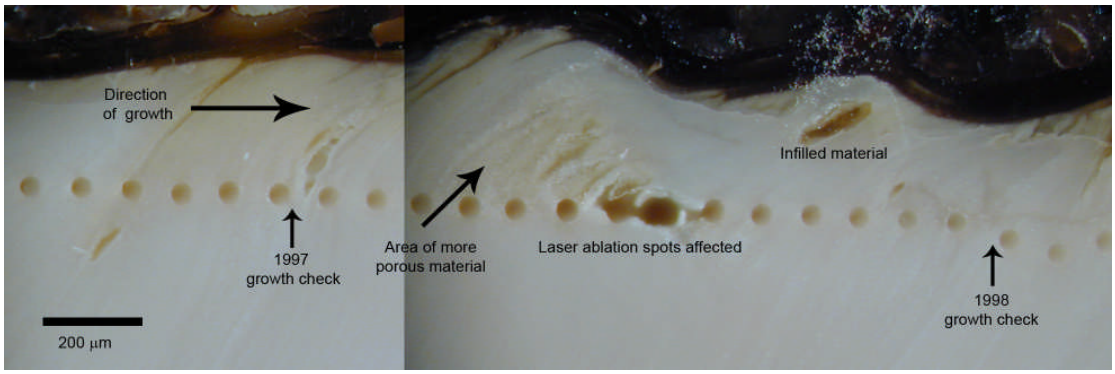

Figure 4.20: Reflected light micrograph of damaged section of outer shell prismatic layer of *A. islandica* shell 248. The shell is affected by infilled material, and the material in 1998 behaves differently to the laser.

4.5.4 Results of Solution-ICPMS (PL228)

The results of solution ICPMS on the milled aliquots also show fluctuations in trace element values (Figure 4.21). Comparison of measurements by solution-ICPMS and those by LA-ICPMS shows the former has a much more subdued variation. This was as expected given the lateral decrease found by LA-ICPMS away from the periostracum. The aliquots for solution-ICPMS were 500 μm wide (parallel to the periostracum) measuring a total lateral distance of 2000 μm from the periostracum (LA-ICPMS spots were taken a maximum distance of 1000 μm from the periostracum).

Solution-ICPMS show Sr/Ca varies 0.95-1.6 mmol/mol, and interestingly, the highest increase in Sr/Ca is found at 1992 growth check. This may be in response to changes in temporal resolution, (with increasing temporal resolution as the growth rate is higher in the younger parts of the shell). Thus, Sr/Ca at the growth check is less affected by material incorporated around the growth check, which is of lower concentration.

Mg/Ca varies between 0.2-0.5 mmol/mol and in the latter years, Mg/Ca correlates well with the annual growth checks and intra-annual bands.

The timing of Ba/Ca sporadic increases is the same as those found by LA-ICPMS. However, the magnitude is ~60% less than that found in T3. This is a larger decrease than seen laterally in the LA-ICPMS data over 750 μm (of ~25%) between T1 and T3.

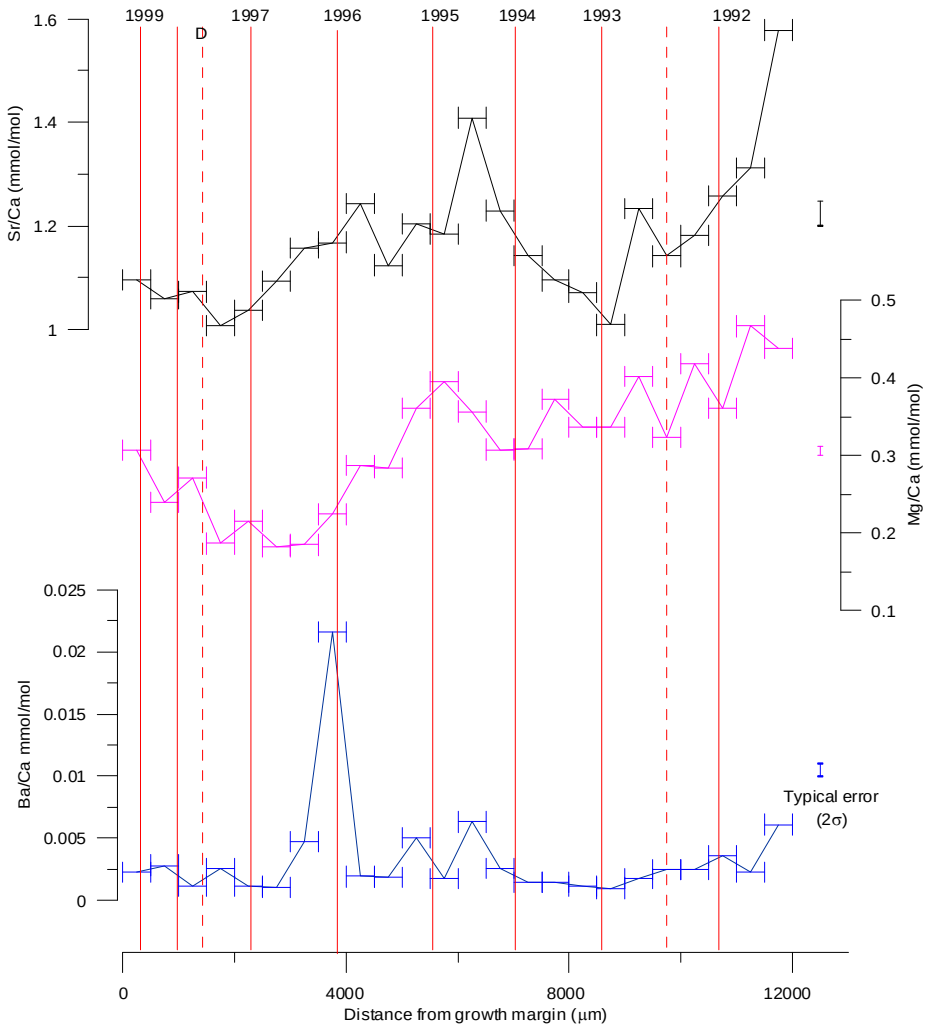

Figure 4.21: Trace element variation measured by solution-ICPMS from the outer shell prismatic layer of shell 228. The typical error (2σ) is calculated from multiple cycles of the aliquot. The horizontal error bar represents the width of the milled samples (500 μm). The red lines mark the annual termination bands.

4.6 Discussion

Results of LA-ICPMS show variation in all the trace elements beyond the 95% confidence intervals. The possible controls on behaviour are discussed below, starting with an examination of the cause of lateral variation present in all the trace elements. Results from the two Irvine Bay specimens are then compared to determine whether the fluctuations are replicated between shells. Sr/Ca behaviour is discussed first, in particular its covariation in the latter years to the growth checks, and variation within the growth bands. Mg and its relationship with the annual growth checks is then considered. Finally, the timing of the Ba/Ca sporadic increases (which are more than five times the usual concentration) from the two shells is compared and possible controls discussed.

4.6.1 Lateral variation

PL228 and PL248 show the concentration of Sr/Ca decreases significantly away from the periostracum. For example, the same annual growth band (~5000 μm from the growth edge in PL228) shows 45% Sr/Ca decrease between transect 1 and transect 3 (see Figure 4.15a and 4.17). Mg/Ca showing a significant decrease between T1 and T3 of >25%, but T2 and T3 are within error (Figure 4.15b and 4.18). The maxima in Ba/Ca show a lateral decrease between T1 and T2 with the offset being ~25%, but lower Ba/Ca values being within error (when increase in Ba/Ca is <100%) (see Figure 4.15c and 4.19). T2 and T3 lateral offset in Ba/Ca is within error.

The lateral offset between transects is not consistent. It is however important to consider that the lateral temporal resolution changes, with the resolution closest to the periostracum being the highest. Averaging the aliquots compensates for slight differences in positions in sampling and may compensate for slight differences in

temporal resolution (which is <100 μm between T1 and T3). The effects of reducing temporal resolution have been explored in $\delta^{18}O$ in bivalves (within this thesis and Goodwin *et al.,* 2003), with reduced temporal resolution reducing the magnitude of $\delta^{18}O$ variation. However, lateral variation for Sr/Ca and Mg/Ca shows a decrease in all values (i.e. not a reduction in magnitude of variation), indicating that this does not result from changes in temporal sampling.

Preliminary results from PL248 show there is vertical heterogeneity in Mg/Ca (i.e. the sample shows variation with depth) (see Figure 4.5b for schematic), with Mg/Ca increasing by >40% after repolishing by 125 μm. Further sampling would be required to investigate this.

Thus, lateral variation is an important control on the absolute trace element concentrations and has implications for palaeoenvironmental reconstructions. As the change in trace element concentration is very high, e.g. Sr/Ca shows that for a change in lateral distance of 750 μm a change of up to 45%, the potential for environmental reconstructions are likely to be severely restricted. However if a control can be attributed and can be independently measured it may be possible to reconstruct data despite the lateral variation. For example, Goodkin *et al.,* 2007 constructed a temperature profile using Sr/Ca corrected for a crystal growth effect in coral. Therefore, it is important to understand the control on lateral variation.

In this section, three mechanisms are discussed which may control lateral variation; 1) growth rate, 2) changes in the shell architecture and 3) changes in the EPF (Extrapallial Fluid) composition as the band is formed.

1) Growth rate

The effect of growth rate was discussed extensively in the Chapter 3. Work by Watson (1996, 2004) highlighted in calcite, that if the growth rate of a crystal exceeded the rate at which impurities could be expelled, these would become incorporated into the crystals. Work by Gaetani and Cohen (2006) extended these findings to biogenic aragonite, examining the uptake of trace elements into corals. They found that both compatible and incompatible elements were enriched in aragonite at higher growth rates e.g. Mg^{2+}, Sr^{2+}, Ba^{2+} predicted of the equilibrium-seawater partitioning coefficient ranges from 65-137 for Sr^{2+} (compatible) to 2.0×10^{-5} for Ba^{2+} (strongly incompatible within aragonite) (Gaetani and Cohen, 2006). Results from XAS (see Chapter 2) suggest that Sr and Mg are hosted differently, the former being ideally hosted (i.e. randomly in the aragonite structure), the latter by organics. While it is therefore logical to suggest Sr may be affected by the crystal growth rate, the impact it has on the organics and thus Mg is a less clear. Organics are not simply found between the crystals but that the crystals themselves are composed of densely packed grains, tens of nanometres in diameter, embedded in a thin layer of organic material (see Stolarski and Mazur, 2005 and references therein).

In *A. islandica*, crystals closest to the periostracum where the shell bands are widest, must by inference, either grow faster or have increased nucleation than those further away from the periostracum in which the band is narrower. The difference however in shell growth rate over a year between T1 and T3 was very small <100 μm in the sections measured, equating to a change of ~0.3 μm/day (about 10% of the estimated daily growth rate). Thus, growth entrapment would have to be a strong control for an offset of ~45% in Sr/Ca to occur. The growth rate in the shell sections for PL228 and PL248 shows that the former has approximately double the growth

rate. Therefore, it would be expected that PL228 would show a higher baseline Sr/Ca value if growth rate has a strong control. However, PL248 shows higher Sr/Ca values, by ~20%.

Lateral decrease within the outer shell prismatic layer is the reverse of that found in the prismatic layer of the umbo, where Sr/Ca and Ba/Ca were found to *increase* significantly away from the maximum growth axis. Therefore, shell growth rate cannot be a main contributory factor if both areas of the shell are affected by (and to the same extent) the same controls. It is therefore likely that if crystal growth rate and shell growth rate are linked, any effect of crystal growth rate is obscured by other factors.

2) Changes in the shell architecture

Changes in the aragonite architecture, such as variation in the nature or amount of the organic material within aragonite crystals in the shell may directly result in changes in organics which host the trace element (e.g. Mg) or indirectly through changes in partitioning factors within the aragonite crystals (e.g. Sr). SE images from PL248 on Figure 4.23 shows the 1998 growth check ~250 μm from the periostracum compared to ~1000 μm from the periostracum. This shows that there is a strong lateral change in the architecture of the crystals away from the periostracum. The amount of organics at the growth checks appears to decrease (or the nature of organics) as the growth check becomes less well defined further away from the periostracum.

Organic material exerts control over the nucleation of the crystal, with the insoluble matrix acting as nucleation surface and predefined mould, determining the size and orientation of crystals (Watabe and Wilbur, 1960; Belcher *et al.*, 1996; Mann and Ozin, 2003; De Yoreo and Dove, 2004; Heinemann *et al.*, 2006). The manner in

which biominerals grow affects the uptake of the trace elements as different faces of the crystals having different affinities for trace elements (Reeder and Grams, 1987; Paquette and Reeder, 1995; Reeder *et al.*, 2001).

Changes in Sr concentration can occur within a single aragonite crystal, with Sr changes of ~50% inferred from data presented by Finch *et al*., (2003b). While changes in organic content can be clearly inferred at the annual growth checks (and doublets) (see Figure 4.23), the lateral change in trace element concentration also occurs during the growth bands. It would therefore be expected that if the offset in trace element concentration were solely due to organics, changes in concentration would be significantly greater within the growth checks than within the growth bands, as the latter shows no visible change in organics. For Sr and Mg this is the case, with changes in concentrations with the increasing from the periostracum more pronounced at the growth checks. However, for Ba/Ca, which increases independently of the growth checks, decreases of ~ 25% laterally, are seen. The crystal shapes however change laterally across the band (see SE images, Figure 4.23). Therefore, changes in how the crystal grows may exert some control.

3) Changes in the EPF composition

The third possible mechanism is that the lateral variation is caused by a vital effect, i.e. that the concentration of elements in the EPF is controlled by biochemical pathways mediated by the organism. Many organisms actively transport metals using specific enzymes and the relative efficiencies of these transport processes can influence the Metal (Me)/Ca ratio in the EPF (Gillikin *et al.*, 2005a; Lorrain *et al.*, 2005; Carré *et al.*, 2006). Trace element rich material may be deposited first close to the periostracum, with the EPF becoming increasingly trace element-depleted (as

trace elements are transported to the EPF less efficiently than Ca^{2+}), thus resulting in a lateral decrease in Me^{2+}/Ca^{2+}, i.e. it is relative transport of metal compared to Ca. This could be a significant control.

Two pathways have been generally considered for Ca^{2+} transport through calcifying mantle: passive non-selective intercellular pathway (direct exchange with seawater) or active (energy consuming) selective intracellular pathway involving Ca^{2+}-ATPase enzymes (Ca^{2+}-pump) (Klein *et al.*, 1996a; Gillikin *et al.*, 2005a). The active pathway is thought to dominate during shell formation (Crenshaw, 1980). An additional third pathway has been proposed in which Ca^{2+} is transported through calcium channels (Carré *et al*., 2006).

In the active selective pathway, the two enzymes Ca^{2+}-ATPase and carbonic anhydrase (CA) are important, the former pumps Ca^{2+} to the EPF while removing protons and the CA catalyses the reaction of bicarbonate to CO_2. This can then diffuse through the membrane (Crenshaw, 1980; Cohen and McConnaughey, 2003). When Ca^{2+}-ATPase activity increases, so does the calcification rate (Gillikin *et al.*, 2005a). As Ca^{2+}-ATPase has a higher affinity for Ca^{2+} than Sr^{2+}, but both use similar pathways, Sr/Ca should be inverse to growth rate (Yu and Inesi, 1995; Ferrier-Pagès *et al.*, 2002). This is not the case with lateral variation, so the third model is examined.

Carré *et al*. (2006) proposed that since neither of these two pathways could accommodate the Ca^{2+} flux necessary for biomineralisation in an aragonitic bivalve with a growth rate of 20 μm/day, a new calcification model involving calcium channels was required. A calcium channel is an aqueous pore facilitating Ca^{2+} diffusion (Carré *et al.*, 2006) that can support very high ionic fluxes (Sather and McCleskey, 2003). The gradient in Ca^{2+} caused by mineralisation, drives the ion flux,

and thus the higher the mineralisation rate, the easier Sr^{2+} ions cross the pores (Carré *et al.*, 2006). Thus, lateral variation could be caused by changes in the rate of mineralisation. They suggest however, that the model would not be applicable to very slow growing specimens ("very slow" is not defined), as they may not involve Ca^{2+}-channels in ionic transport. Growth rates of *A. islandica* in the outer shell prismatic layer can >~11 μm/day and therefore such a model may be applicable to the outer shell prismatic layer. It is not however know whether the uptake of Mg/Ca and Ba/Ca would also be influenced by such controls. It also unclear, whether such heterogeneity would be present within the EPF during growth, i.e. if the EPF is relatively homogeneous it would not be expected to cause such a strong lateral variation.

Further work is required to develop a fuller understanding on the controls of pathways for the uptake of trace elements. However, the model presented by Carré *et al*. (2006) can provide a possible hypothesis to the cause of lateral variation.

Therefore, in conclusion lateral variation could be due to factors such as vital effects, or through modification of the crystal nucleation and propagation due to the organic matrix.

Although the discussion to the cause of the lateral variation is inconclusive, the lateral variation prohibits the use of the trace elements to reconstruct palaeoclimate using a universal calibration equation with concentrations highly dependable on sampling location within the shell. There is no simple means to calibrate the composition as a function of architecture. Significantly the decrease in concentrations is not constant but appears to effect extreme variations more e.g. in 1997 in U248 the Sr/Ca peak at the growth check found in T1 is significantly greater than the error (2σ) with increase by >50% whereas in T3 the slight Sr/Ca increase is within error. Reducing the temporal resolution is known to dampen the extremes in

oxygen isotopes (see Chapter 6) and it would be expected that a similar process would occur with the trace elements. However, the temporal resolution of sampling changes laterally as the bands narrows further away from the periostracum, though this effect is relatively small (typically 100 μm for a year between T1 and T3 for the years measured).

Comparison therefore of the published work on trace element fluctuations in *A. islandica* (e.g. Toland *et al.*, 2000; Epplé, 2004) is difficult, since the data recorded depend on the distance from the periostracum that the analyses were made. In addition, there may be a vertical heterogeneity, which modifies the trace element concentration as a function of depth (i.e. depending on the amount on the cut of the shell and the amount of polishing). Klein *et al*. (1996a) found lateral Sr/Ca variation in *Mytilus trossulus* across the shell, which they attributed to changes in the rates of mantle metabolic activity. Changes in metabolic activity laterally across the bands will be explored through measurement of $\delta^{13}C$ in Chapter 6, and the implications for trace element incorporation discussed.

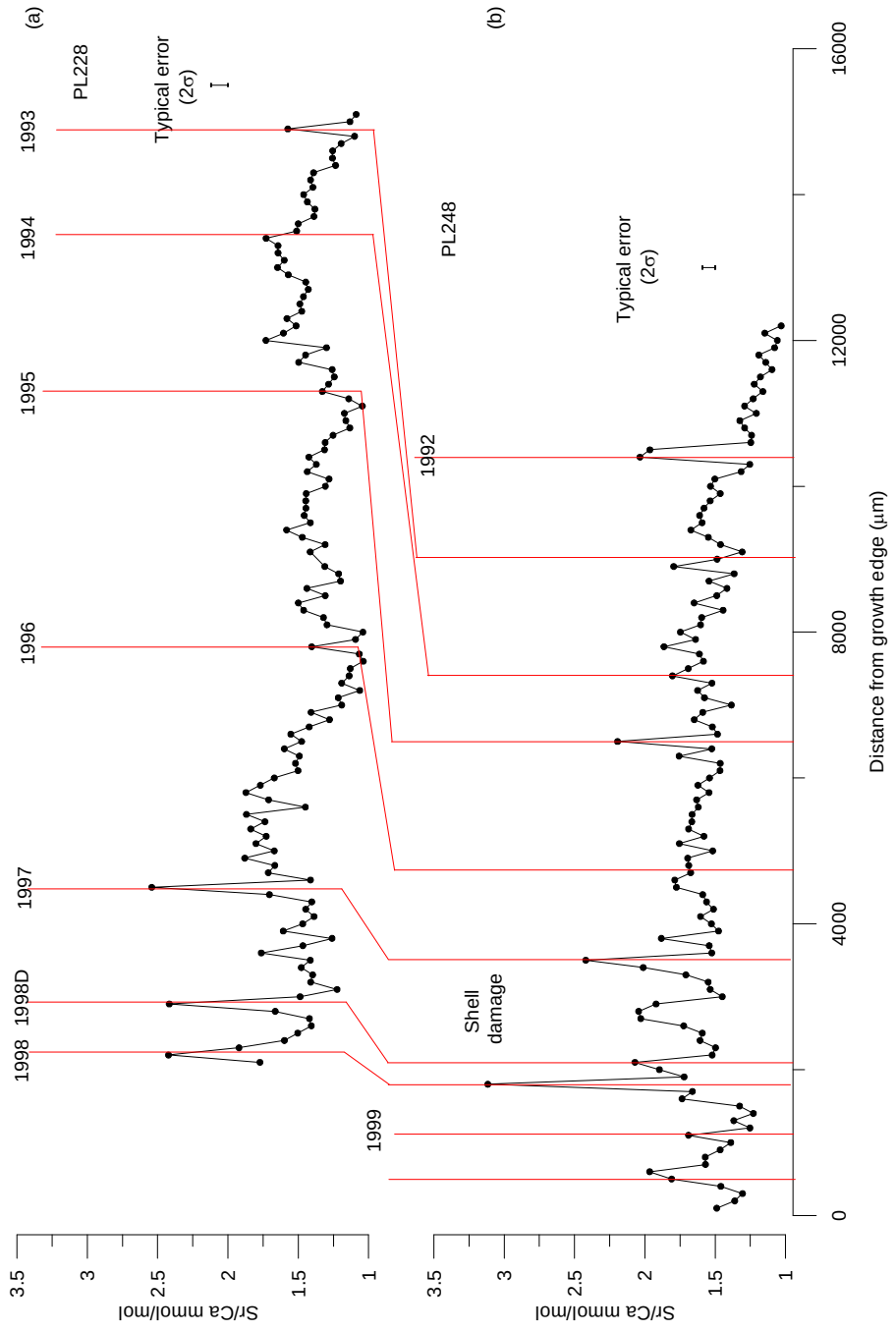

Figure 4.22a: Sr/Ca measurements from Transect 1 (analysed parallel to the periostracum at a distance of 250 μm) taken in the outer shell prismatic layer of (a) shell 228 (upper diagram) compared to (b) shell 248 (lower diagram). The typical error (2σ) is calculated from the reproducibility of the OKA. The solid red line marks the end of the termination band (year shown), with D marking a doublet. Note shell 248 was damaged in 1998, which resulted in infill of material.

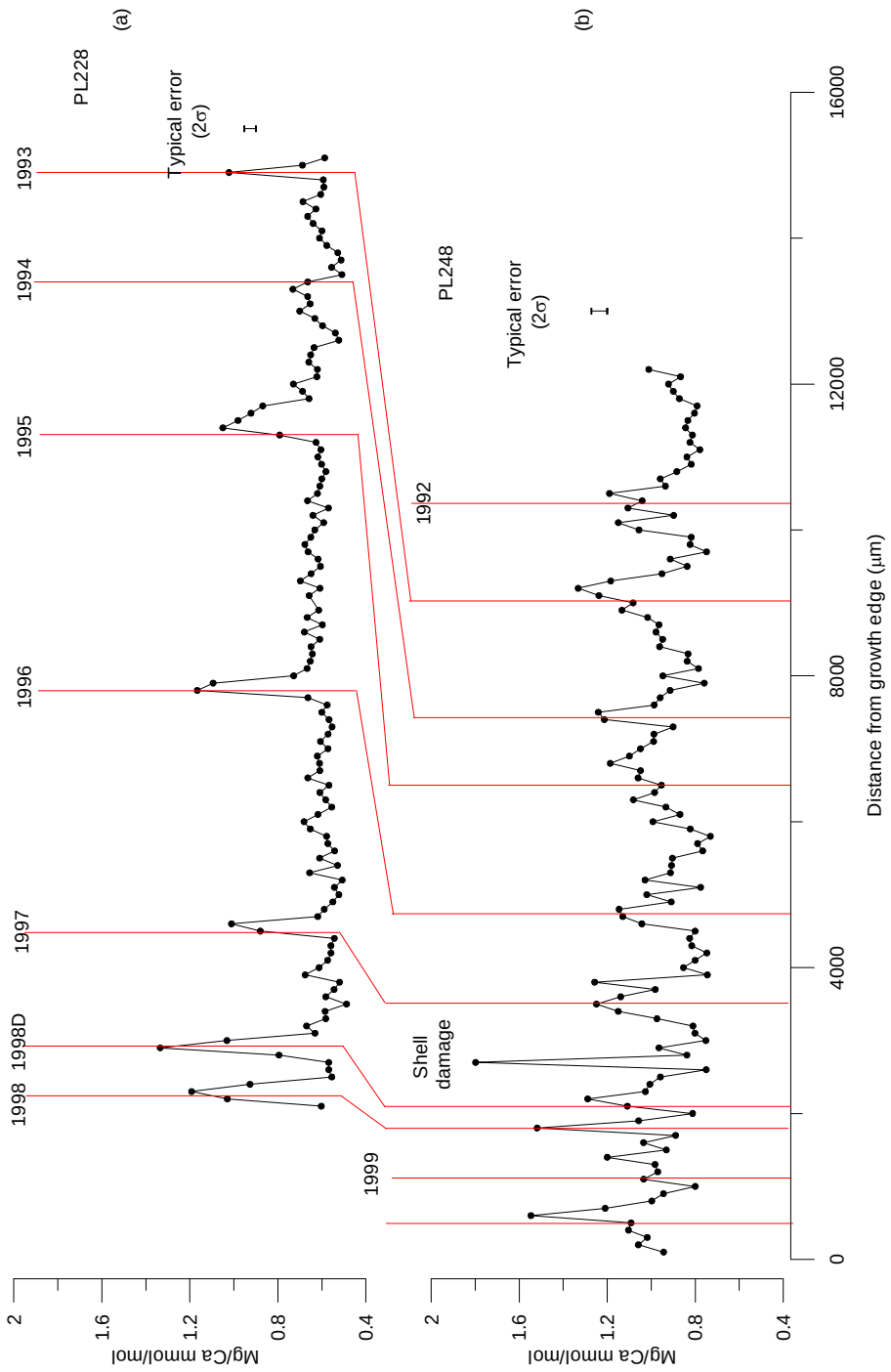

Figure 4.22b: Mg/Ca measurements from Transect 1 (analysed parallel to the periostracum at a distance of 250 μm) in the outer shell prismatic layer of (a) shell 228 (upper diagram) compared to (b) shell 248 (lower diagram). The typical error (2σ) is calculated from the reproducibility of the OKA. The solid red line marks the end of the termination band (year shown), with D marking a doublet. Note the increase of Mg/Ca in 1998 when damage to the shell occurred.

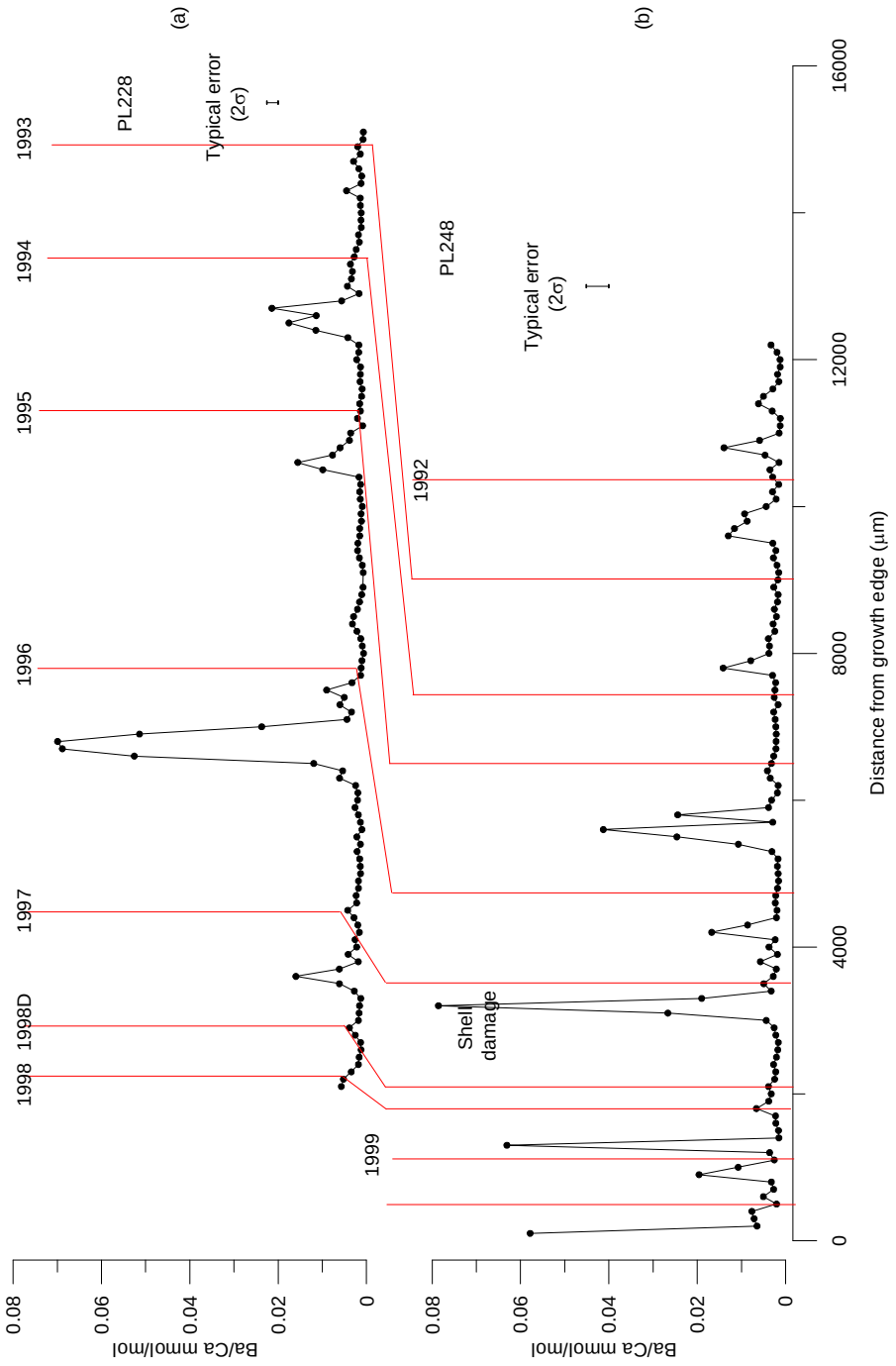

Figure 4.22c: Ba/Ca measurements from Transect 1 (analysed parallel to the periostracum at a distance of 250 μm) taken in the outer shell prismatic layer of (a) shell 228 (upper diagram) compared to (b) shell 248 (lower diagram). The typical error (2σ) is calculated from the reproducibility of the OKA. The solid red line marks the end of the termination band (year shown), with D marking a doublet.

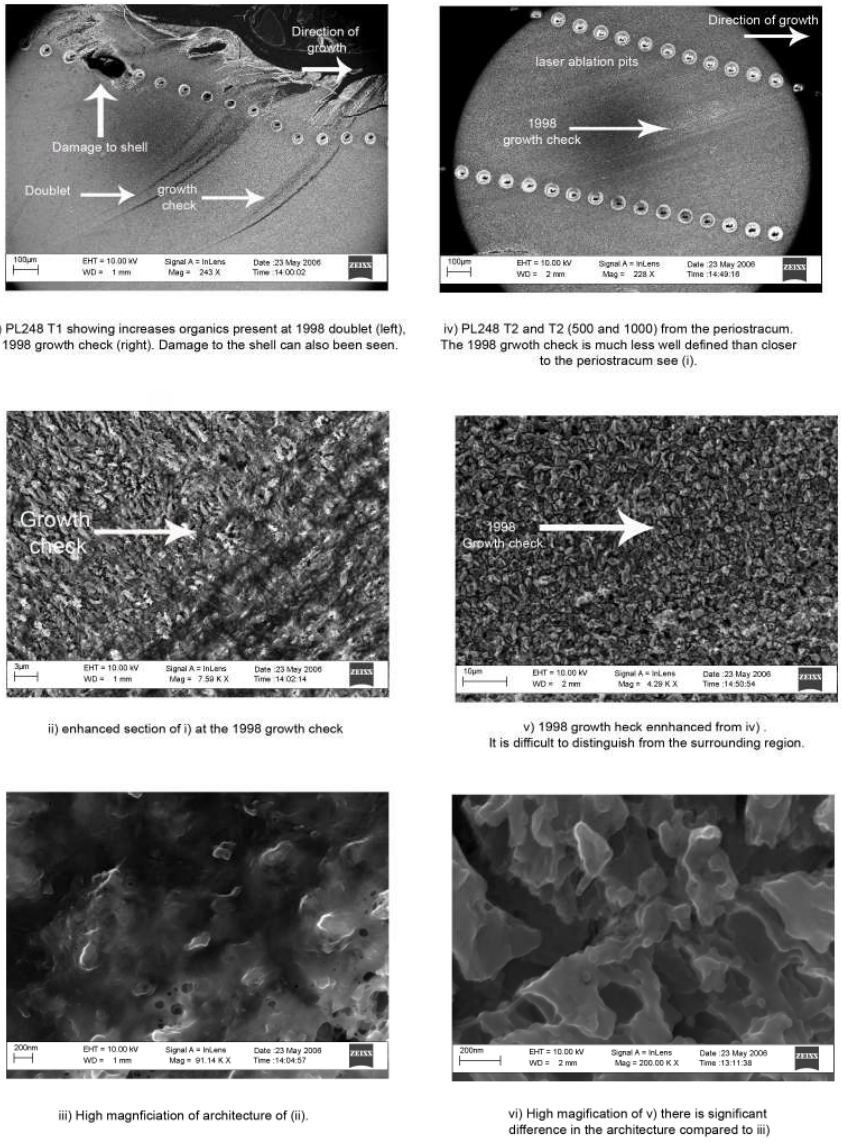

Figure 4.23: Secondary Electron (SE) image taken after etching, 250 μm (i-iii) and 1000 μm (iv-vi) from periostracum, in shell 248 of the same growth band. SE images show an increasingly magnified image of the crystals at the growth checks. The organics at the growth checks intersect the crystal growth, which results in new crystals being less well aligned. (i-iii) the crystals are in general alignment to growth direction with interlocking crystals, with the organics can be differentiated from the surrounding crystals. (iv-vi) The crystals further from the periostracum show much poorer alignment with the organics much harder to discern. This highlights the change in architecture across the shell.

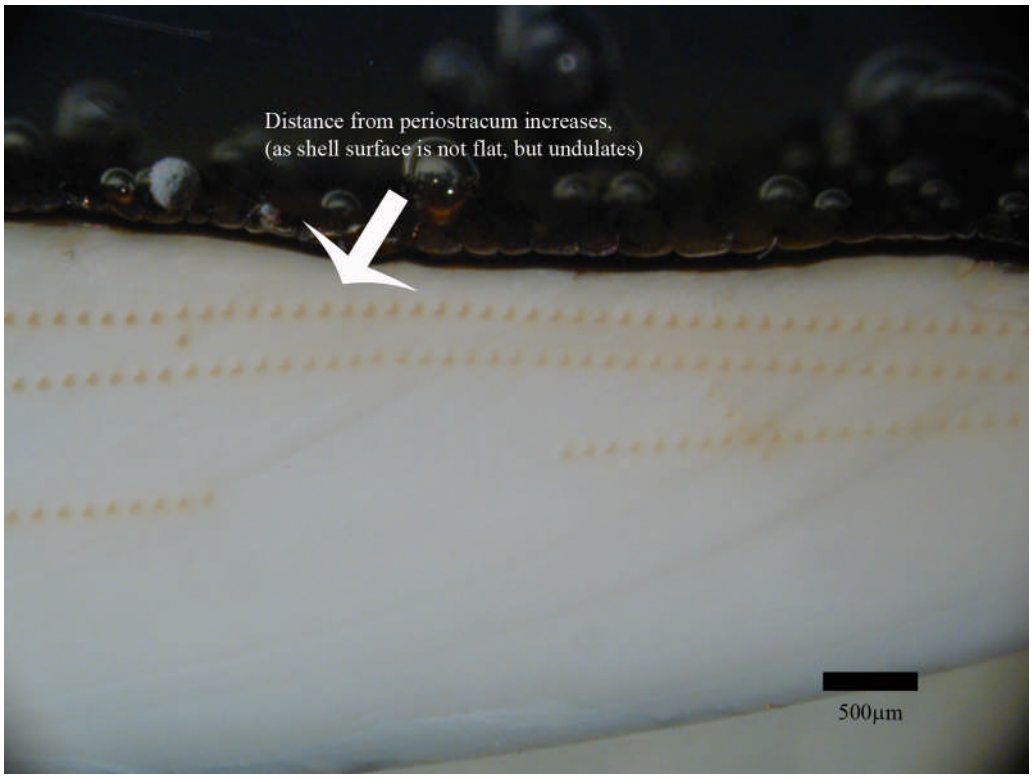

Figure 4.24: Reflected light micrograph in the outer shell prismatic layer of shell 228 showing that the sampling distance from the periostracum show variation due to undulations in the shell edge.

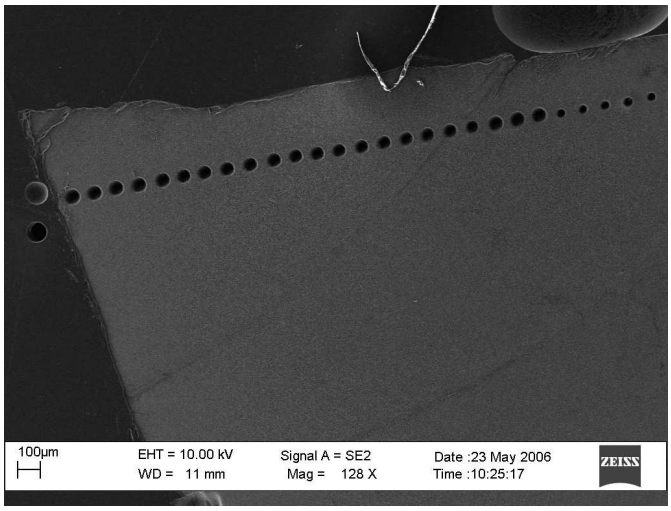

Figure 4.25: Secondary Electron image showing that the size of the laser spot size increased during the first 22 spots of the analysis of the outer shell prismatic layer of shell 248 due to poor focusing on the laser. The possible impacts of this are discussed in the text.

4.6.2 Comparison of the two Irvine Bay specimens

Comparison of the two specimens collected from Irvine Bay allows a better understanding of the controls on the trace elements. As discussed in the previous section, lateral variation is found within both shells and therefore T1 traverses of PL228 and PL248 (both 250 μm from the periostracum) are used to examine the similarities and differences in each of the three element profiles (Figure 4.22a-c). By comparing the results from T1, the controlling factors on the behaviour of trace elements within *A. islandica* are discussed.

4.6.3 Sr behaviour at the growth checks

Both PL228 and PL248 show an increase in Sr/Ca at the termination band after 1996 e.g. in PL228 Sr/Ca increases by >50% at the growth check. Prior to this, the Sr/Ca peaks become increasingly less well defined. Comparison of the Sr/Ca profiles in Figure 4.22a shows that increases at the growth checks are not similar and can differ by >20%. The difference in concentrations at the doublets is ~30%. This lack of covariation suggests that Sr/Ca is not dominated by an external, environmental factor e.g. temperature. This is further supported by the lateral offset which shows the Sr/Ca peaks at the growth checks becoming increasingly less well defined (and become within the range of Sr/Ca concentrations seen during the rest of the year in T3).

In the previous chapter, a number of hypotheses were proposed on the controls on Sr/Ca within the growth check:

1) Preferential dissolution of Sr-poor material resulting in enrichment of Sr at the growth check,
2) Changes in crystal nucleation and propagation influencing Sr partitioning

3) Biological (vital) effects.

These are discussed below and in particular, the extent to which they are likely to control trace element incorporation.

1) Preferential dissolution

Lutz and Rhoads (1977) hypothesised that daily growth checks originate from increased concentration of the organic matrix, caused by anaerobiosis-related dissolution of previously deposited calcium carbonate, which may in fact act as a buffer (Dugal, 1939; Crenshaw and Neff, 1969; Taylor and Brand, 1975; Wada and Fujinuki, 1976; Gordon and Carriker, 1978; Richardson, 2001). In other words, the lack of oxygen causes the production of acid (H^+), which is then buffered by the dissolution of the $CaCO_3$ shell (which produces CO_3^{2-}). An alternative hypothesis is that the increased organics at the growth check results from an increase in the secreted organic matrix or cessation of calcium carbonate deposition (Lutz and Rhoads, 1980) i.e. the shell deposited during this time has a lower organic content.

Using unetched material, evidence of dissolution was looked for using the SEM, but the presence of the organics made it difficult to discern any changes. It is unclear from examinations using the SEM whether dissolution occurs at the growth edge.

If preferential dissolution takes place i.e. not all material will be dissolved at the same rate, with the solvus dependent on Sr-concentration (see Finch and Allison, 2003), this could affect the elemental concentrations. The composition of the shell of *A. islandica* lies on the Sr poor-side of the solvus and hence dissolution of material with a range of Sr compositions will preferentially start with Sr-poor aragonite. However, preferential dissolution will only increase Sr concentrations if redeposition

of Sr-poor material did not occur and then only to the maximum level at which it was originally incorporated i.e. it does not increase the amount of Sr in the Sr-rich material but rather changes the ratio of Sr-rich to Sr-poor material. Within the prismatic layer of the umbo, this was found not to be a major control as Sr/Ca increases at the growth check exceeded those found in the earlier part of the umbo i.e. the concentration at the growth check exceeded the maximum incorporated. The same is also true for the outer shell indicating that any impact of dissolution is relatively minimal. In addition, Sr/Ca peaks of the outer shell would be expected to be smaller than those measured in the umbo as the slower growth rate in the umbo would make material more susceptible to the effects of the dissolution (i.e. new material is not deposited as quickly). The reverse however is found, with Sr/Ca peaks in the outer shell prismatic layer being higher (especially taking into account the offset of the values measured by LA-ICPMS compared to SIMS). Therefore, dissolution is unlikely to be a significant mechanism.

2) Changes in crystal nucleation and propagation

As discussed earlier, in reference to lateral changes, organics influence the growth of aragonite crystals (e.g. Belcher *et al.*, 1996; De Yoreo and Vekilov, 2003; De Yoreo and Dove, 2004) and this may in turn influence Sr uptake. As discussed in Chapter 3, it can be inferred from Finch *et al.* (2003b) that different aragonite crystal faces incorporate different Sr/Ca concentrations, with a change in Sr concentration of ~50% across the crystals from a speleothem. Changes at the growth check can be >100%, and thus the data from Finch *et al.* (2003b) would indicate that changes in Sr/Ca induced by changes in crystal propagation would be too small. However, it is not known the effect an organic matrix would have on the formation of the crystals

compared to an inorganic precipitation within speleothems. Changes in crystal nucleation and propagation could contribute to changes in Sr/Ca uptake.

3) Vital effects

Vital effects such as changes in biochemical pumping of Ca and trace elements may also be important in the uptake of Sr/Ca. By changing the proportion of Sr to Ca pumped to the site of deposition, changes in Sr/Ca would occur. High Sr/Ca peaks were found throughout the shell of an *A. islandica* shell from the German Bight, not just within the latter years of growth (Epplé, 2004). Here the specimens grow more slowly but live longer than those from Irvine Bay. In contrast, Toland *et al*. (2000) who studied only the more juvenile section of an *A. islandica* shell found no Sr/Ca peaks at the growth checks. This indicates that changes in Sr/Ca behaviour could be affected by the growth rate of the organism, which could result from changes in biochemical pumping of Sr/Ca.

As discussed earlier, Ca^{2+}-ATPase supplies Ca^{2+} to the site of calcification and concentrates CO_3^{2-} (Crenshaw, 1980; Cohen and McConnaughey, 2003). Thus, increased activity of enzyme Ca^{2+}-ATPase increases the calcification rate and as Ca^{2+}-ATPase has a higher affinity for Ca^{2+}, the proportion of Sr^{2+} decreases; conversely, at lower calcification rates, the proportion of Sr^{2+} must increase (Gillikin *et al.*, 2005a). Such a mechanism could explain how a biological control may influence Sr/Ca at the growth check. It would also provide a hypothesis to suggest why Sr/Ca peaks at the growth checks are only seen when the growth rate is <~2000 μm. It would also not preclude other biological models such as that of Carré *et al*. (2006) that could be applicable to faster growing parts of *A. islandica*.

4.6.4 Sr behaviour within the growth bands

PL228 shows variation during the growth band between 1995 and 1996 with gradual increase to the approximate centre of the band and decrease of ~0.5 mmol/mol but in 1997, this curve is truncated against the termination band (Figure 4.22a). In 1998, variation in Sr/Ca during the growth band is within error. In PL248, Sr/Ca variation during the growth band is within error during 1995-1996. However, in other years, such as 1993 and 1994, there is a general change in Sr/Ca during the year of ~ 0.4 mmmol/mol, with a similar positive curve as that seen during 1996 in PL228.

The data also appear to show an ontogenetic trend in the Sr/Ca values in PL2248 and PL248. However, decrease in PL248 occurs after 10,000 μm during the last 22 analyses of T1. These were analysed on 1st May 2006 (in reverse order - i.e. from 12,200 μm to 10,000 μm) with analysis stopped due to concerns about the poor laser focusing. This may have affected the Sr/Ca ratios (Figure 4.25 shows a SE image of the spots). PL228 shows no ontogenetic changes.

In the previous chapter, it was proposed that Sr/Ca within the growth band could be controlled by crystal growth entrapment (Watson, 1996, 2004; Gaetani and Cohen, 2006). Watson (1996, 2004) found that where the growth rate was 0.01 nm/s or faster, growth entrapment of Sr occurs in calcite. This process has also been observed in aragonite (Gaetani and Cohen, 2006) though no threshold for entrapment within aragonite has been published. Growth entrapment may therefore be an important consideration with shell growth rates in *A. islandica* are ~0.13 nm/s in the outer shell prismatic layer (assuming 300 days growth a year, 24 hours per day). Schöne *et al*. (2004c) showed that the daily growth rate in *A. islandica* shells from the North Sea was average of 31.9 μm/day with a maximum of 55 μm/day, equivalent to

0.35 nm/s and a maximum of 0.63 nm/s respectively (assuming 24 hours growth per day). However, shell extension rates may not accurately reflect crystal growth rate, as the shell extension rate is dependent on the angle between the shell growth direction and the crystal growth direction (see Carré *et al*., 2006). In addition, increased shell extension rate could also be achieved by increased nucleation of the crystals.

Sr/Ca shows a sharp increase of ~0.6 mmol/mol during the early part of 1997 in PL228. An image of the transect shows that the distance from the periostracum decreases (Figure 4.24). The transect although measuring an average of 250 μm from the periostracum, due to natural changes in the shell height during the growth season, some variation in the lateral distance occurs. Sr/Ca variation due to lateral changes in shell height in 1997 is greater than the variation seen within the growth bands in PL228 (of <0.6 mmol/mol). Therefore, Sr/Ca fluctuations within the growth bands can be explained by changes in the distance from the periostracum.

Further evaluation on whether the growth rate influences the Sr/Ca profile can be provided by examining the $\delta^{18}O$ profile of *A. islandica*. The $\delta^{18}O$ sampling and modelling (Chapter 6) can show when the shell grows and changes in growth rate during the year. This however presumes crystal growth rate is strongly related to the shell growth rate (increased shell growth rate could be achieved by increased nucleation). Thus, changes in growth rate derived from the $\delta^{18}O$ record can then be compared to changes in trace element uptake, to determine whether shell growth rate has a significant impact on Sr/Ca uptake.

4.6.5 Potential of Sr for palaeoenvironmental reconstructions

Sr/Ca data are unlikely to provide an accurate temperature reconstruction using *A. islandica*. Comparison to the temperature data at Millport shows no common

features, either with maximum or minimum temperatures for Sr behaviour at the growth checks or in the growth bands. This implies that temperature exerts relatively little control on Sr/Ca uptake in *A. islandica*. Hence, growth corrected-Sr/Ca data such as those of Goodkin *et al*. (2007) are unlikely to provide successful temperature reconstruction. Sr/Ca can change laterally by as much as 45% with an inconsistent offset. Comparison of the two shells shows that there are some positive increases during the year, but these can be explained by the lateral offset due to undulations of the shell through the growth season.

High Sr/Ca peaks at the growth checks appear to be associated with slower growth rates. Within our results, slow growth rates only occur within the latter years of growth but in specimens from the German Bight, which are much slower growing specimens, high Sr/Ca peaks at the growth check are found throughout the lifetime of the organism (Epplé *et al.*, 2006). This suggests Sr/Ca behaviour is influenced by slow growth rates.

4.6.6 Mg behaviour

Mg/Ca analysis within the umbo was susceptible to contamination. There was no burn-time used with the laser to remove surface contamination. However, analysis of ^{27}Al counts (indicative of contamination) in the outer shell prismatic layer failed to show any evidence of increased values at the growth checks. There is also good replication of the patterns of the fluctuations laterally across the bands.

Figure 4.22b shows that in PL228 Mg/Ca increases at the growth checks are well defined with increases >0.4 mmol/mol, with the exception of 1994, in which the increase was much smaller (~0.2 mmol/mol). The 1994 growth check was not well-defined suggesting lower concentrations of organics, being identified by the notch in

the shell and later confirmed by $\delta^{18}O$ analysis. This implies that the presence of organics is linked to Mg variation.

PL248 also shows Mg/Ca increases at the growth checks, but unlike PL228, it shows variation within the growth bands, which are beyond the confidence limits. PL248 is the slower growing specimen- showing a growth rate of approximately half that of PL228. Thus, it would be expected if increased organics relates to a slowdown in growth rate (similar to growth checks); PL248 would have a higher organic content during the same years. While fluctuations in the organic concentrations are not quantifiable, visual inspection of the shells indicated the presence of more organics in PL248 during the year. Figure 4.26 shows a micrograph image of PL248 in which organics can be seen, similar microscope analysis of PL228 did not show such variation visually. Schöne *et al*. (2005b) stated that *A. islandica* deposits daily growth bands, so changes in organics during the growth band are to be expected. However, it appears that the intensity of intra-annual bands may differ between shells.

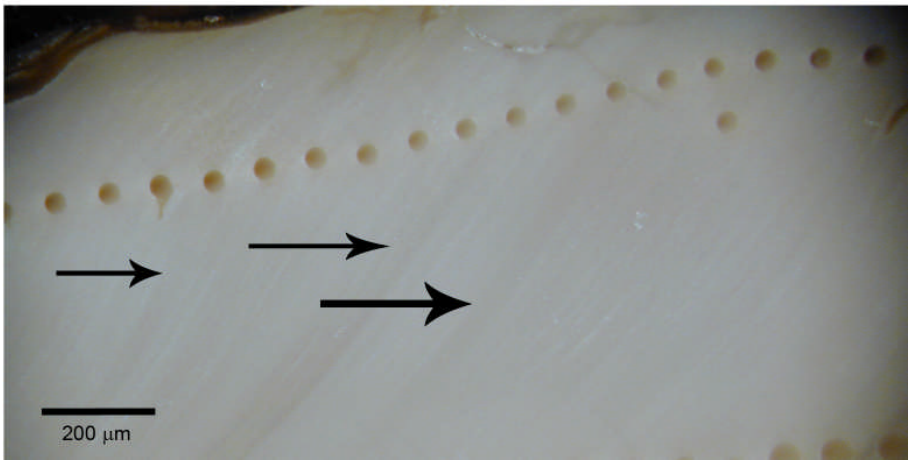

Figure 4.26: Reflected light micrograph showing the outer shell prismatic layer of *A. islandica* shell 248. PL248 sub-annual growth bands can be seen indicating the presence of organics intra-annually (examples highlighted by the arrows).

Mg/Ca showed a strong lateral change between T1 and T3 (though T1 and T2 were within error), with a decrease of >100% at the Mg/Ca peaks and >25% between these peaks i.e. the lateral change is not constant. Figure 4.18 shows a vertical heterogeneity in the sample with increase >40% after removal of top 125 μm, indicating that the change may be vertical as well as laterally across the bands.

Rosenberg and Hughes (1991) measured the changes in S/Ca in *Mytilus edulis* in the outer calcitic layer bivalve. They found that S/Ca values along the slow-growing sections were 1.25 higher than along rapidly growing axes of low curvature. S/Ca were interpreted as an index of matrix content, as S is primarily concentrated in various acid mucopolysaccharides and amino acids within the shell (Rosenberg and Hughes, 1991). Therefore, higher S/Ca ratios are indicative of higher Mg/Ca concentrations. This suggests that the organic concentration within a bivalve shell can vary significantly.

These findings concur with those of Chapter 2 in which XANES modelling was consistent with Mg hosted by the organics. It would be expected that if the measured Mg/Ca variation resulted from changes in the absolute concentration of organics, Mg/Ca would always be significantly higher at the growth checks. However, since this is not the case (though it was not possible to measure absolute organic concentration), it indicates that Mg/Ca uptake is not a linear response to organic concentration. Epplé (2004) found Mg/Ca increases not associated with the growth checks, and thus may provide further support that this is the case. Further work on this is required to measure organic fluxes, and to separate out different organic complexes within the shell of *A. islandica*. Mg/Ca is however unlikely to provide a temperature reconstruction. If however, the controls on Mg within the organics are better understood, fluctuations in Mg may provide some qualitative understanding of

environmental factors or biological factor that controls organic composition or quantity.

4.6.7 Ba behaviour

Ba/Ca generally shows low concentrations with sporadic sharp increases, which are seen in all transects. This indicates that Ba/Ca is not the result of direct incorporation of detrital Ba. This pattern of sporadic increases was also evident in the prismatic layer of the umbo of shell 248 and has been reported both in other *A. islandica* specimens (e.g. Toland *et al.*, 2000; Epplé, 2004) as well as in other bivalves (e.g. Stecher *et al.*, 1996; Putten *et al.*, 2000; Lazareth *et al.*, 2003; Gillikin *et al.*, 2006). The timing of these Ba/Ca increases in *A. islandica* do not occur at the same position in the growth year, nor does the timing of the Ba/Ca peaks between the PL228 and PL248 coincide (Figure 4.22c). This suggests that the Ba/Ca peaks do not relate to an environment forcing such as productivity. Therefore, Ba/Ca peaks are unlikely to provide an indication of the timing of an environmental forcing.

Very little is known about the substitution of Ba^{2+} into the lattice, although Dietzel *et al.* (2004) found its incorporation into inorganically precipitated aragonite is dependent on temperature. Rosenthal and Katz (1989) suggest that Ba is bound to the crystal in molluscs.

Experiments by Gillikin *et al.* (2006) discounted the theory that Ba/Ca peaks could be used as a direct proxy of Ba/Ca concentrations in the water or phytoplankton. They found a relationship between $\delta^{13}C$ and Ba/Ca in the shells, but discounted spawning as a control as Ba/Ca peaks in *Pecten maximus* did not correlate with spawning breaks. Comparison of the $\delta^{13}C$ profile and Ba/Ca peaks will be discussed in Chapter 8. Gillikin *et al.* (2006) tentatively concluded the peaks could be

related to ingestion of barite crystals. The mechanism by which barite crystals precipitates is however unclear (e.g. González-Muñoz *et al.*, 2003). It is uncertain how barite crystals would be incorporated into the shell, but as Ba/Ca peaks can be seen laterally across the shell, it indicates that is it is not incorporated directly, but is taken up through the EPF.

Gillikin *et al*. (2006) determined that the low Ba/Ca concentrations showed a linear relationship to Ba concentration within the seawater using both laboratory and field experiments. However, these two experiments showed differing results:

For laboratory experiments:

background $[Ba/Ca]_{shell} = 0.10 (\pm 0.02) \times [Ba/Ca]_{water} \pm 1.00 (\pm 0.68)$ giving $R^2 = 0.84$

For field experiments:

background $[Ba/Ca]_{shell} = 0.071 (\pm 0.01) \times [Ba/Ca]_{water}$ giving $R^2 = 0.96$

Gillikin *et al*. (2006) suggested the difference in the equations related to inaccuracies in the field measurements or stress induced by handling in the laboratory experiments. In *A. islandica* low $[Ba/Ca]_{shell}$ are <0.003 mmol/mol, similar to the concentration incorporated into the calcite bivalve *Mytilus edulis* from the North Sea (Gillikin *et al.*, 2006). This suggests that the low Ba/Ca found within the *A. islandica* shells could relate linearly to Ba concentrations within the seawater. The lateral change in Ba/Ca for the low values is within the error of the precision of the instrument. Measurement of Ba/Ca on an instrumental capable of higher precision would be required to determine whether there is a lateral decrease in the low Ba/Ca as well. If no lateral change occurs, it indicates that low Ba/Ca may provide a proxy for the Ba/Ca concentration of seawater.

Further work would be required to analyse *in-situ* Ba/Ca of seawater and compare it to the concentrations found within the shell. The cause of the sporadic increases is unknown but the timing does not correlate between shells, or at a specific time of year. Ba/Ca increases in *A. islandica* higher than that observed within *Mytilus edulis* (0.020-0.025 mmol/mol) (Gillikin *et al.*, 2006). The highest Ba/Ca in *A. islandica* occurs at the beginning of 1998 in shell 248, though this may have been affected by damage to the shell. It would be interesting to investigate further how such infilling may have influenced Ba/Ca incorporation.

Investigation is required into whether the lateral decrease found at higher Ba/Ca ratios, also occurs at lower Ba/Ca concentrations. This together with *in situ* Ba/Ca seawater measurements would determine whether low Ba/Ca could be a proxy for Ba/Ca concentrations within seawater.

4.7 Conclusion

Analyses from both specimens shows heterogeneity in the trace elements within material deposited at the same time within the outer shell prismatic layer. Sr, Mg and Ba decrease in concentration away from the periostracum. Sr/Ca behaviour in general shows a sharp increase in the latter years of growth (which can be >100%), while in the more juvenile sections, this increase becoming less evident. Sr/Ca incorporation may be influenced by changes in the crystal habit during formation caused by increased organics at the growth check, crystal growth rate as well as vital effects. Sr/Ca changes within the growth band reflect changes in the lateral distance from the periostracum, with the shell height varying intra-annually.

Mg shows a close correlation with the presence of organics providing further support for the organic XANES model proposed in Chapter 2. Mg/Ca concentration

appears not to be linearly related to uptake, with initial evidence indicating that vital effects play a role.

Finally, low Ba/Ca may be proportional to Ba/Ca concentrations within the seawater, being similar to the concentrations found in *Mytilus edulis* from the North Sea (Gillikin *et al.*, 2006). Further work, particularly *in situ* measurements would be required to confirm this. The sporadic increases in Ba/Ca, often greater than five times the average, are found in both shells. However, the timing of these increases is not correlated between the two shells, nor does it reflect a specific timing within a band. Further work is required to understand the controls on Ba/Ca incorporation.

Acknowledgements

This work was supported by a Marie Curie Training Fellowship (EVK2-GH-00-57123-10) with additional support from QRA New Researcher's Award. Special thanks are given to Ole Tumyr, Claudia Kruber, Hildegunn Almelid and Jan Kosler for their invaluable assistance in the laboratory.

CHAPTER 5: EFFECTS OF DRILLING AND MICROMILLING ON ARAGONITE.

Abstract

The shell of *Arctica islandica* is composed of aragonite, a metastable polymorph of calcium carbonate, which will potentially undergo transformation to the more stable calcite upon heating and/or stress. Conversion from aragonite to calcite during drilling has been noted by a number of researchers (e.g. Aharon, 1991; Gill *et al.*, 1995). The impact of this on the isotopic composition is, however, unclear.

Two different sampling techniques, drilling and micromilling were used to extract aliquots from *Arctica islandica*, and the subsequent percentage of calcite in the aliquots was measured using XRD. Typical conversion was >5% with the highest in the drilled aliquots. Using the micromill, aliquots were taken from aragonitic otoliths, which were from cod grown in laboratory tanks under stable temperatures. Although XRD analysis showed the conversion to calcite to be 6%, $\delta^{18}O$ results suggest that there is no significant effect on $\delta^{18}O$.

5.1 Introduction

Extraction of small aliquots (μg-mg) from *Arctica islandica* without modification or contamination is imperative for accurate climate reconstruction. Researchers such as Aharon (1991) and Gill *et al*. (1995) however noted that drilling caused conversion of aragonite to calcite, and modification of $\delta^{18}O$. However, the direction and magnitude of the shift in $\delta^{18}O$ was inconsistent. This chapter examines whether aragonitic material such as *A. islandica* and cod otoliths undergo such a transformation. The otoliths from cod grown in a temperature-controlled tank enabled the impact on isotopic composition to be examined.

5.1.1 Rationale for study

In sclerochronological records such as corals, bivalves and speleothems, greater sampling resolution provides better temporal resolution. Although *in situ* microanalytical methods (e.g. SIMS, LA-ICPMS) are increasingly available, precise microsampling remains the most widely used means of producing high resolution climate reconstruction.

Extraction of aliquots is usually carried out by a drill (usually on a stable platform) or a micromill. The former is a much cruder sampling method with positioning of the aliquots to be taken, carried out manually. The latter is computer controlled and allows positioning of sampling to 1 μm spatial resolution, controlled sampling depth and volume as well as the capacity for 3D sampling (Dettman and Lohmann, 1995). For example, using the micromill, aliquots of a particular volume (and hence mass) can be repeatedly taken such that systematic weighing of aliquots for $\delta^{18}O$ (and $\delta^{13}C$) prior by mass spectrometry is not required. This is a significant advantage as powdered aliquots are difficult to weigh, and there is a high risk of

contamination with small volumes. Thus, this sampling technique is rapidly becoming the norm for sampling material for high resolution climate proxies.

During sampling, considerable shear stress is applied to the sample, which heats up the drill bit. Aragonite, a metastable polymorph of calcium carbonate undergoes rapid transition to calcite following heating for 30 mins at 470 °C (Epstein and Mayeda, 1953; Land *et al.*, 1975). However, shear stress may contribute directly to the transformation, with conversion within a ball mill occurring within 30 mins (Dachille and Roy, 1960). In addition, biogenic aragonite (with a high organic content) may invert at a significantly lower conversion temperature or at a smaller shear stress (Gaffey *et al.*, 1991). Hence, during drilling, modification of the polymorph is a real concern.

The inversion to calcite can affect the data in two ways. Firstly, calcite and aragonite have slightly different fractionation factors in the mass spectrometer (1.01025 and 1.01034 respectively) (Sharma and Clayton, 1965). This could be corrected for, if the percent calcite formed during the drilling were known. However, an aliquot of 25% calcite and 75% aragonite would provide negligible depletion (<0.0003 ‰) compared to the precision of the instrument.

Secondly, exchange of O between the sample and atmospheric O_2, H_2O or CO_2 may take place. Such exchange would modify the oxygen (and potentially C) composition of the aliquot. Such modification would be difficult to correct for if the amount of exchange were inconsistent from aliquot to aliquot.

The potential of these processes to influence climate reconstruction has already been established by researchers. Aharon (1991) found during drilling of a giant clam (*Tridacna gigas*), conversion from aragonite to calcite (percentage not specified), and noted depletion in $\delta^{18}O$ of up to 8 ‰ compared to non-milled material.

This offset was greater than could be explained by any discrepancies in sampling position, with non-drilled showing a maximum variation of 2 ‰ (Aharon, 1991). However, work by Gill *et al*. (1995), found the opposite in corals (*Montastrea annularis*) in which the aliquots were $\delta^{18}O$ enriched by drilling. Gill *et al*. (1995) found a poor negative correlation between the isotopic shift and the quantity of calcite produced by drilling. Moreover, such isotopic shifts could occur even when the amount of calcite were below the XRD (X-ray Diffraction) limit of detection (typically 0.5 wt %). Although the polymorphic transition may allow exchange with ambient CO_2, this would result in a negative shift in the oxygen isotopic composition, not the positive shift Gill *et al*. (1995) reported. Even when Gill *et al*. (1995) drilled the sample under Ar, an isotopic shift was still observed suggesting that isotopic fractionation is not solely via atmospheric exchange. This makes a consistent correction very difficult to apply, as the controls on the shift are unclear, and may depend on factors such as drill type, drill bit, and operator (e.g. time to taken to drill sample, pressure applied). Furthermore, a change in skeletal density through the shell may affect the results (Gill *et al.*, 1995).

Gill *et al*. (1995) commented that the maximum isotopic deviation of ~0.75 ‰ in dry-drilling (of aragonite coral) corresponds to an apparent temperature error of -3.0 ºC, with the average error due to isotopic shift being –1.1 ºC. However, Swart and Leder (1996) argued that the changes in $\delta^{18}O$ seen by Gill *et al*. (1995) were due to differences in sampling positions (i.e. $\delta^{18}O$ variation within the original sample) and not due to the drilling of the aliquots. Therefore, the impact of drilling on the isotopic composition is unclear. Clearly, such effects have the potential to provide wholly erroneous estimates of $\delta^{18}O$ from drilled or milled aliquots.

To explore this issue further, five *A. islandica* shells were used to examine whether sample preparation could induce structural changes in the samples. Unfortunately, the isotopic composition of *A. islandica* varies through time due to changes in temperature (and to a much lesser extent salinity). Therefore, as Swart and Leder (1996) argued in their interpretation of Gill *et al*. (1995) any recorded isotopic shift could be due to changes in $\delta^{18}O$ incorporation rather than an artefact of drilling.

In order to determine whether sampling does modify $\delta^{18}O$ of the aliquot, otoliths from cod grown in a temperature-controlled laboratory were examined. The $\delta^{18}O$ composition of this material is only influenced by changes in temperature and salinity (see Campana, 1999). The salinity is however often assumed constant for $\delta^{18}O$ reconstructions. However, the controls on $\delta^{13}C$ in otoliths are not fully understood, though it is thought it deposits under non-equilibrium conditions (e.g. Kalish, 1991; Gauldie, 1996). Therefore, the possible effects of drilling on $\delta^{13}C$ are not discussed.

5.2 Samples

A range of different *A. islandica* shells were studied in order to examine the impact of milling on different areas of the shell, using both live and dead collected specimens. Table 5.1 shows the details of the specimens: two shells from Irvine Bay (313 and Dead Arctica 1), two from the Viking Bank (V0017 and V05-257-3) and one from Fladen Ground (400260).

The otoliths were provided by Hans Høie, University of Bergen, Norway (reference 05.03.99 No15 TJ; 05.03.99 No18TJ). The cod were hatched in April 1997, and were reared at a constant 10 ºC until May 1998 (during the juvenile stage). They were then reared at 15 ºC for another 10 months at the fisheries laboratory at the

University of Bergen, Norway. The seawater in the laboratory tank is pumped from just outside Bergen from a depth of 70 m and is affected thus by natural salinity variability during the year. The salinity variation for 2002-2003 is shown on Figure 5.3. It is assumed that the salinity variation during these years was similar to that of 1998-1999 when the cod were grown. Salinity variation in the laboratory tank was ~1.6 equivalent to a change in seawater $\delta^{18}O$ ~0.4 ‰ (based on the isotope mixing line for the North Sea (Israelson and Buchardt, 1991). Thus, the study of otoliths allows the separation of natural $\delta^{18}O$ fluctuations from the effects of milling.

	Location	Latitude	Longitude	Water depth (m)	Specimens studied	Live or dead collected?
Artica islandica	Irvine Bay	55° 45'N	4° 54'W	6	313	Live
				From beach	Dead1	Dead
	Viking Bank	60° 24'N	2° 20'E	98.3	VO5-257-3	Dead
					V0017	Live
	Fladen Ground	59° 23'N	0° 30'E	129	400260	Live
Otolith	HIB marine laboratory, Bergen				05.03.99No15TJ	Live
					05.03.99No18TJ	Live

Table 5.1: Location details of *A. islandica* and otolith samples for drilling and milling experiments.

5.3 Method

5.3.1 A. islandica sampling

Aliquots from *A. islandica* were taken prior to sectioning to provide a pristine sample for XRD analysis to confirm no calcite was present in the original sample. This was done by removing a small chip with a scalpel, and very gently crushing it into a powder. The shell was then sectioned using a geological saw (thickness 2 mm) (Irvine

Bay shell 313 only), or a Buehler Isomet low speed saw (at speed 7 with no additional weights attached, saw thickness of 0.4 mm). This was to examine whether differences in preparation have an influence. Some samples were milled after sectioning only, while others after polishing i.e. to examine if there was any particular step in sample preparation that affected the sample structure. The samples were polished using the standard preparation for stable isotopes, i.e. progressing down to 5 μm diamond polish. An additional aliquot was taken to confirm that no changes took place when the sample was mounted onto the drilling plate using QuickStick™ 135 Mounting Wax crystal bond (with temperatures of 100-200 °C required for bonding).

Shell 313 (Irvine Bay) was sampled using a coarse drill with a drill bit of 1 mm diameter, with the position set manually. This much coarser sampling technique is increasingly being replaced by more precise micromill technology. Thus, other shells were sampled using a New Wave™ micromill to examine whether variations in calcite/ aragonite were more consistent when variations due to the operator were removed (e.g. pressure).

The aliquots were extracted by micromill with a length of 100 μm and depth of 1000 μm. Typically, a milling speed of 40% was used, but a couple of aliquots were taken at milling speed of 100% to examine whether the milling speed affected the conversion to calcite. The total length of shell analysed for each aliquot was typically 5 cm. On shells 313 and V0017, two different areas of the shell were sampled, one area covering the latter years of the growth, the second covering the youngest years of growth near the umbo. This examined the possibility of differences occurring due to age. For shells V05-2573 and 400260, thick sections across the shell were prepared (see Figure 5.1 for schematic). The same bands were sampled throughout the shell i.e. the same temporal resolution was sampled (these are labelled

as “same” in the Table 5.2). The different types of tests are outlined in further detail with XRD results in Table 5.2.

Figure 5.1: Schematic of *A. islandica* sectioning for XRD analysis (not actual sample used). Typical sectioning is show by the lines.

5.3.2 Sampling of Otoliths

Two pairs of fish otoliths from cod were used for sampling (Figure 5.2). The otoliths are present in cod as pairs. Due to the limited size, the whole otolith was required for XRD to provide the minimum 40 mg required. Therefore, one pair was used (05.03.99 No18 TJ) solely for XRD analysis, with another otolith taken from a second cod was used for isotopic analysis (05.03.99 No15 TJ).

For XRD, one otolith of the pair was left as a pristine sample; the other (from the same cod) was sectioned. Using the micromill, an aliquot for XRD was collected using 10 passes, each cutting a depth of 300 μm into the sample, with a 40% scan speed, 200 μm plunge speed and 100 μm interpolation.

A single otolith taken from a second pair (05.03.99 No15 TJ) was used for isotope analysis. It was set in epoxy and then sawed into 500 μm thick sections. From one of these sections, aliquots were taken at three different speeds (45, 80, 100% of maximum speed equivalent to 16680, 20700, 21720 rpm (revolutions per minute) respectively), and an unmilled aliquot was extracted using a scalpel. Aliquots were

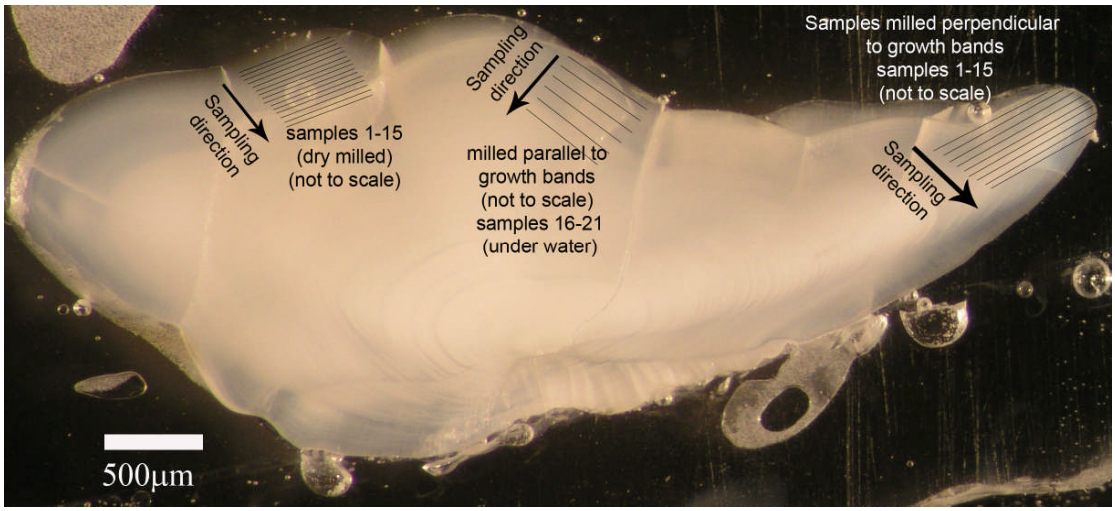

Figure 5.2: Transmitted light micrograph of 500 µm thick section of a laboratory reared cod otolith, with schematic of sampling. Note that the otolith bands from laboratory-reared cod are less well defined than otoliths taken from wild specimens.

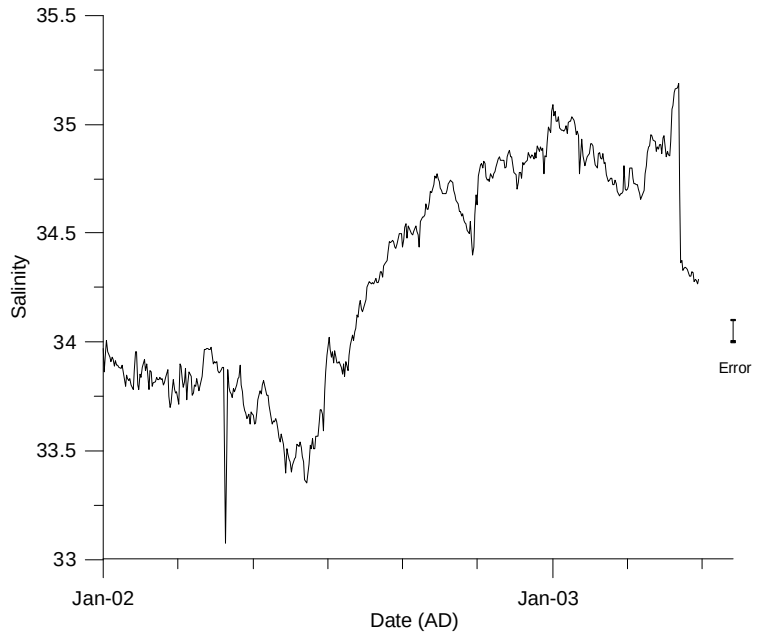

Figure 5.3: Variations in salinity of laboratory tanks at University of Bergen in 2002 and parts of 2003. Data supplied by Dr H. Høie (Department of Biology, University of Bergen). Error on the salinity measurements is ±0.1.

only taken from the part of the otolith deposited during adulthood to ensure that the growth bands formed in water at 15 ºC. The aliquots were taken parallel to the growth bands with 38 μm interpolation comprising an aliquot volume ~0.02 mm^3 (equivalent to 20-35 μg). In addition, aliquots were milled under distilled water. These aliquots were taken adjacent to the dry-milled aliquots. The aliquots milled under water were spaced further apart than the dry-milled aliquots (~ 100 μm apart), as parafilm (a self-sealing, mouldable and flexible film) requires a smooth, flat surface to allow adhesion. The sampling method, used for milling under water, was that developed and described by Charlier *et al*. (2006). Parafilm is first punctured and then heated before being placed on the sample and then gently heated again to form an airtight bond with the sample surface. A water droplet is placed on the sample (in the parafilm hole) just prior to milling. The parafilm keeps hypertension on the water droplet, and thus the aliquot as it is milled is suspended within the water droplet. Without the parafilm, the water would drain away from the sample, and the milled aliquot could not be recovered. The aliquot (including water) is then removed with a variable pipette - size 0.5-10 μl. Additional water droplets were added as required to collect any remaining material for the aliquot. The aliquots were then left to dry in the oven at 40 ˚C overnight before analysis.

The aliquots taken parallel to the growth bands would however, experience changes in the salinity over time. Therefore, to provide an independent check whether salinity could account for any changes in the samples, an additional set of aliquots was taken perpendicular to growth. The same number of bands was sampled (regardless of the total widths of the bands), i.e. the same temporal resolution was sampled (see Figure 5.2).

5.3.3 XRD analysis

XRD was carried out on automated Philips PW1050 X-ray diffractometer with Philips WinXRD V2 software at the University of St. Andrews, UK. The percentage of calcite was calculated using Rietveld Refinement procedures with Siroquant™ software http://www.sietronics.com.au/siroqnt/siroqnt.htm. The limits of detection of other calcium carbonate (particularly calcite) in an aragonite matrix by XRD are <1% (Finch, unpublished data).

5.3.4 Mass spectrometer analysis

The aliquots were analysed on a Finnigan MAT253 mass spectrometer at Bergen University, Norway. The order the aliquots were analysed was randomised to offset for machine drift with standards every 20 aliquots. The aliquots were analysed in two sessions, with the aliquots from the same sampling direction analysed together (i.e. all aliquots from Table 5.3 were analysed in one batch, and all those in Table 5.4 in another). CO_2 is produced by reaction of carbonate in the aliquots with orthophosphoric acid at 70 °C in an automated on-line system. Results are reported with respect to the VPDB through calibration with NBS-18 and NBS-19 standards. The external precision of the instrument is ±0.06 ‰ $\delta^{13}C$ and ±0.15 ‰ $\delta^{18}O$ (1σ) based on replicate measurements of an internal carbonate standard. Further details on the mass spectrometer (and method) are given in Chapter 6 (Section 6.3.4).

5.4 Results

5.4.1 A. islandica XRD

The XRD results are shown on Table 5.2. All unmilled aliquots regardless of sample preparation (including those heated, sawed, polished) show a single phase aragonite complying with the standard pattern of aragonite (International Centre on Diffraction Data card 41-1475). All milled and drilled aliquots however include calcite in varying amounts from 2-15% ±2% for milled aliquots and 15-24 ±2% for drilled aliquots (limit of detection <1% (Finch, Unpublished data)). Aliquots from shell 313 generally show a higher conversion to calcite (11%), as well as the best reproducibility (0.8% (2σ)) calculated from all the milled aliquots of 313). The dead collected specimen from Irvine Bay (Dead Arctica 1) shows the widest range of calcite percentages. Milling of 400260 and VO5-2573 showed that even when drilling the same bands in each section (i.e. the same temporal resolution) the percentage conversion to calcite is not the same. From the limited aliquots taken at a higher milling speed, it appears that the milling speed does not have a significant control (though more aliquots would be required to confirm this). The XRD spectra of two aliquots taken from the same Fladen Ground specimen are plotted in Figure 5.4, an unmilled aliquot showing a single phase aragonite, and a milled aliquot showing the presence of calcite.

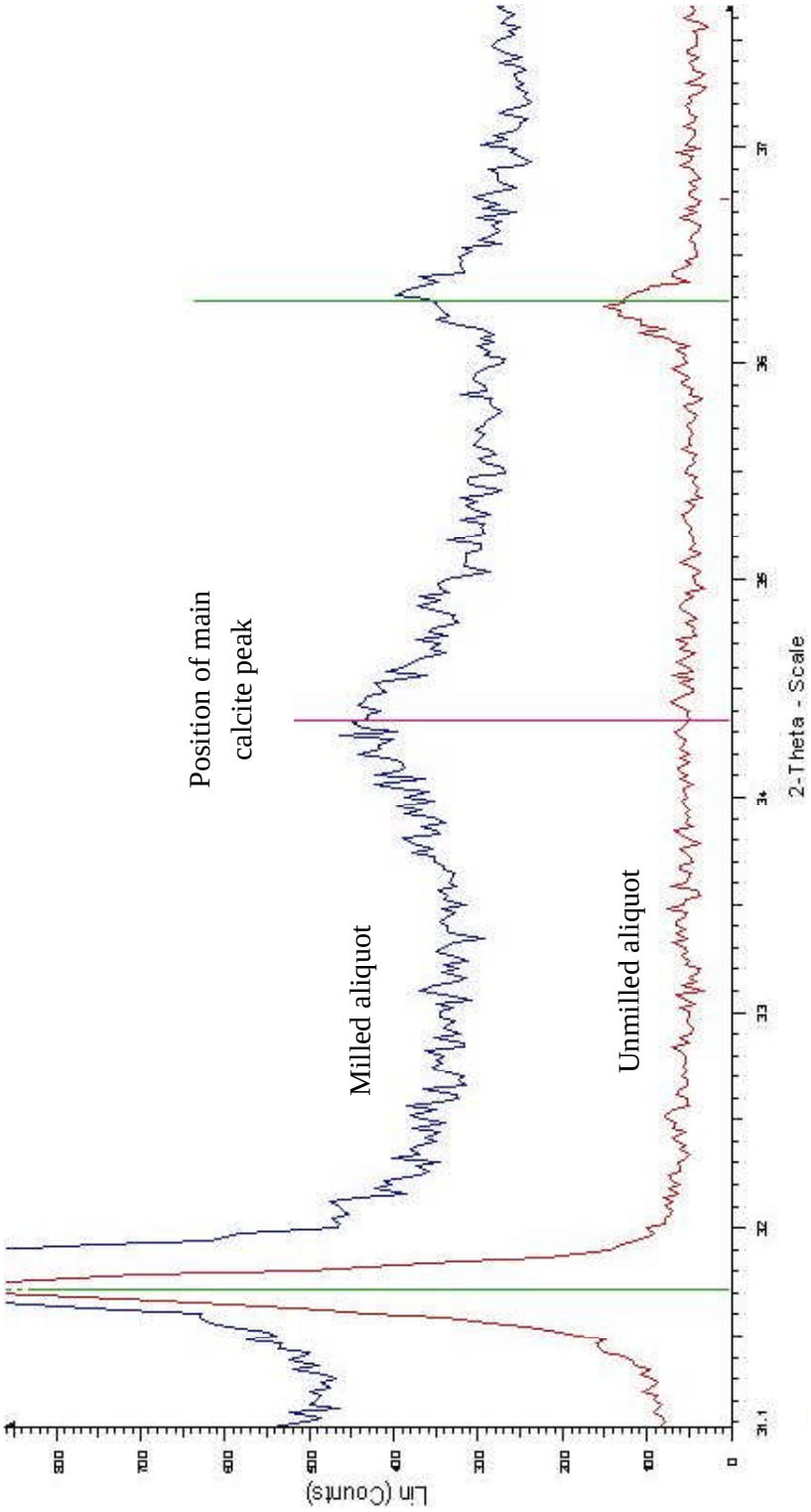

Figure 5.4: Plot of XRD results (background removed) from same Fladen Ground *A. islandica* specimen, unmilled sample FGL3V (upper blue line), and milled sample R1FGUP (lower red line).

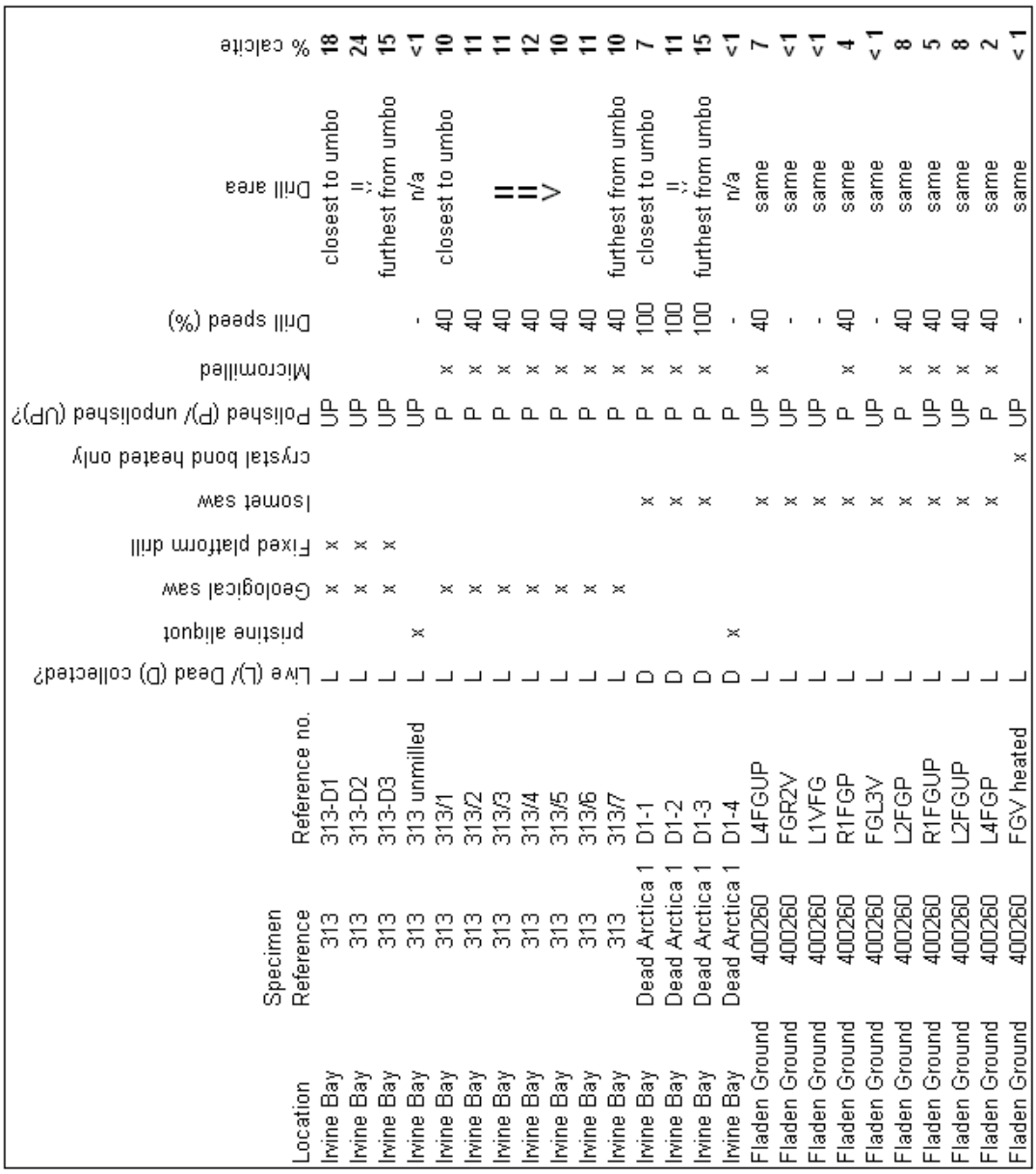

Location	Specimen Reference	Reference no.	Live (L)/ Dead (D) collected?	pristine aliquot	Geological saw	Fixed platform drill	Isomet saw	crystal bond heated only	Polished (P)/ unpolished (UP)?	Micromilled	Drill speed (%)	Drill area	% calcite
Irvine Bay	313	313-D1	L		x	x			UP		-	closest to umbo	**18**
Irvine Bay	313	313-D2	L		x	x			UP			=	**24**
Irvine Bay	313	313-D3	L		x	x			UP			furthest from umbo	**15**
Irvine Bay	313	313 unmilled	L	x					UP		-	n/a	**<1**
Irvine Bay	313	313/1	L		x				P	x	40	closest to umbo	**10**
Irvine Bay	313	313/2	L		x	x			P	x	40		**11**
Irvine Bay	313	313/3	L		x	x			P	x	40	=	**11**
Irvine Bay	313	313/4	L		x	x			P	x	40	=	**12**
Irvine Bay	313	313/5	L		x	x			P	x	40	>	**10**
Irvine Bay	313	313/6	L		x	x			P	x	40		**11**
Irvine Bay	313	313/7	L		x	x			P	x	40	furthest from umbo	**10**
Irvine Bay	Dead Arctica 1	D1-1	D				x		P	x	100	closest to umbo	**7**
Irvine Bay	Dead Arctica 1	D1-2	D				x		P	x	100	=	**11**
Irvine Bay	Dead Arctica 1	D1-3	D				x		P	x	100	furthest from umbo	**15**
Irvine Bay	Dead Arctica 1	D1-4	D	x					P		-	n/a	**<1**
Fladen Ground	400260	L4FGUP	L				x		UP	x	40	same	**7**
Fladen Ground	400260	FGR2V	L				x		UP		-	same	**<1**
Fladen Ground	400260	L1VFG	L				x		UP		-	same	**<1**
Fladen Ground	400260	R1FGP	L				x		P	x	40	same	**4**
Fladen Ground	400260	FGL3V	L				x		UP		-	same	**< 1**
Fladen Ground	400260	L2FGP	L				x		P	x	40	same	**8**
Fladen Ground	400260	R1FGUP	L				x		UP	x	40	same	**5**
Fladen Ground	400260	L2FGUP	L				x		UP	x	40	same	**8**
Fladen Ground	400260	L4FGP	L				x		P	x	40	same	**2**
Fladen Ground	400260	FGV heated	L					x	UP		-	same	**< 1**

Table 5.2: XRD results with percentage conversion with different preparation, sampled by drilling or micromilling showing the percentage of calcite in each aliquot. For sample areas, listed at "same" this refers to the same bands being sampled using sections taken across the shell, i.e. same temporal resolution. "Closest to the umbo" to "furthest from the umbo" refers to sampling in the outer shell prismatic layer, with the position of the transect becomingly increasing further away from the umbo, with the last aliquot taken at the growth edge of the outer shell prismatic layer.

Location	Specimen Reference	Reference no.	Live (L)/ Dead (D) collected?	pristine aliquot	Geological saw	Fixed platform drill	Isomet saw	crystal bond heated only	Polished (P)/ unpolished (UP)?	Micromilled	Drill speed (%)	Drill area	% calcite
Viking Bank	VO5-2573	L1CUP	D						UP	x	40	same	5
Viking Bank	VO5-2573	R2C1UP	D	x					UP	x	40	same	3
Viking Bank	VO5-2573	R2C2UP	D						UP	x	40	same	5
Viking Bank	VO5-2573	VO5-2573	D				x		UP		100	same	6
Viking Bank	VO5-2573	Carin R1V (CR'	D				x		UP		-	same	<1
Viking Bank	VO5-2573	CL2V	D				x		UP		-	same	<1
Viking Bank	VO5-2573	CV	D	x					UP		-	n/a	<1
Viking Bank	VO5-2573	R2C1P	D						P	x	40	same	5
Viking Bank	VO5-2573	L3C2UP	D						UP	x	40	same	2
Viking Bank	VO5-2573	L3C1UP	D						UP	x	40	same	5
Viking Bank	VO5-2573	L1CP	D						P	x	40	same	2
Viking Bank	VO5-2573	R2C2P	D						P	x	40	same	5
Viking Bank	V0017	V0017-SP1	L				x		P		-	n/a	<1
Viking Bank	V0017	V0017P	L						P		-	n/a	<1
Viking Bank	V0017	V0017SU1	L				x		UP		-	n/a	<1
Viking Bank	V0017	Voo17-1	L				x		UP	x	40	losest to periostracur	4
Viking Bank	V0017	voo17-2	L				x		UP	x	40	closest to nacre	3
Viking Bank	V0017	voo17-4	L				x		UP	x	40	umbo section	6
HIB Marine Lab, Bergen	Otolith	cod 05 03 99 no18 LS	L	x					UP		-	n/a	< 1
HIB Marine Lab, Bergen	Otolith	cod 05 03 99 no18 LS	L						P	x	40	All of otolith	6
Tjörnes Bed	Arctica 3.7 Ma	Arctica 3.7 Ma	D	x					UP		-	n/a	2

Table 5.2 (cont.): XRD results with percentage conversion with different preparation, sampled by drilling or micromilling showing the percentage of calcite in each sample. For sample areas, listed at "same" this refers to the same bands being sampled using sections taken across the shell, i.e. same temporal resolution. "Closest to the umbo" to "furthest from the umbo" refers to sampling in the outer shell prismatic layer, with the position of the transect becomingly increasing further away from the umbo, with the last aliquot taken at the growth edge of the outer shell prismatic layer.

5.4.2 Otolith analysis

Otolith XRD analysis shows 6% conversion to calcite, with the pristine aliquot showing no calcite (within limits of detection) (Table 5.2). The $\delta^{18}O$ and $\delta^{13}C$ results for aliquots taken parallel to the growth edge and perpendicular to the growth edge are shown in Table 5.3 and Table 5.4. Figure 5.5 shows a plot of $\delta^{18}O$, when sampling was parallel to the growth edge. The aliquots show a gradual increase from 0.7 ‰ to a maximum of 1.5 ‰. The aliquots milled under water again show an increase in $\delta^{18}O$ values, but with a faster increase in values than those of the non-water aliquots. The unmilled aliquots are within the range of 1-1.3 ‰. Aliquots taken perpendicular to the growth edge (Figure 5.6) show a high degree of scatter but the $\delta^{18}O$ of the milled aliquots typically between 1.0-1.5 ‰, with unmilled aliquots 1.1-1.3 ‰.

Sample order	Identifier 1	Line	water?	micromill speed (%)	$\delta^{13}C$ (‰)$_{VPDB}$	$\delta^{18}O$ (‰)$_{VPDB}$	$\delta^{18}O$ per sample group with 2σ
1	LF06-2	Line 1.01	No	45	-2.66	0.97	
4	LF06-14	Line 1.04	No	45	-2.78	1.00	
7	LF06-6	Line 1.07	No	45	-2.90	1.01	
10	LF06-7	Line 1.10	No	45	-2.51	1.18	
14	LF06-8	Line 1.14a	No	45	-2.19	1.52	
15	LF06-19	Line 1.14b	No	45	-2.10	1.42	1.18±0.47
2	LF06-5	Line 1.02	No	80	-2.68	0.74	
5	LF06-11	Line 1.05	No	80	-2.91	0.91	
8	LF06-15	Line 1.08	No	80	-2.88	1.08	
11	LF06-12	Line 1.11	No	80	-2.19	1.43	
13	LF06-17	Line 1.13	No	80	-2.36	1.29	1.09±0.56
3	LF06-9	Line 1.03	No	100	-2.72	1.06	
6	LF06-3	Line 1.06	No	100	-2.93	0.93	
9	LF06-10	Line 1.09	No	100	-2.46	1.14	
12	LF06-16	Line 1.12	No	100	-2.13	1.49	1.15±0.48
16	LF06-20	water 1	Yes	45	-2.73	0.93	
17	LF06-4	water 2	Yes	45	-2.76	1.22	
18	LF06-21	water 3	Yes	45	-2.47	1.49	1.21±0.56
19	LF06-24	water 4	Yes	100	-2.18	1.48	
20	LF06-22	water 5	Yes	100	-2.11	1.41	
21	LF06-23	water 6	Yes	100	-1.94	1.51	1.47±0.10
n/a	LF06-1	Unmilled	n/a	n/a	-2.37	1.31	
n/a	LF06-18	Unmilled	n/a	n/a	-2.51	1.09	
n/a	LF06-13	Unmilled	n/a	n/a	-2.52	1.15	
n/a	LF06-25	Unmilled	n/a	n/a	-2.48	1.11	1.17±0.20

Table 5.3: $\delta^{18}O$ and $\delta^{13}C$ results from otoliths taken parallel to growth bands at varying speeds, including aliquots milled under water. Mean of values shown with standard deviation of samples taken at under same conditions (drill speed, with/without water).

Sample order	Identifier	Line	water?	micromill speed (%)	$\delta^{13}C$ (‰)$_{VPDB}$	$\delta^{18}O$ (‰)$_{VPDB}$	Mean of $\delta^{18}O$ per sample group with 2σ
1	LF06-27	1	No	45	-2.44	1.13	
2	LF06-26	2	No	45	-1.97	1.03	
6	LF06-32	6	No	45	-2.19	1.45	
7	LF06-45	7	No	45	-2.25	1.47	
15	LF06-42	16	No	45	-1.85	1.35	
11	LF06-38	12	No	45	-1.98	1.41	1.31±0.37
5	LF06-43	5	No	80	-2.37	1.19	
8	LF06-34	9	No	80	-2.34	1.20	
12	LF06-35	13	No	80	-1.82	1.34	
13	LF06-40	14	No	80	-2.18	1.22	
14	LF06-41	15	No	80	-2.08	1.39	1.27±0.18
3	LF06-37	3	No	100	-2.13	1.44	
4	LF06-36	4	No	100	-2.43	1.12	
9	LF06-28	10	No	100	-2.05	1.18	
10	LF06-31	11	No	100	-2.00	1.42	1.29±0.33
n/a	LF06-29	Unmilled	No	n/a	-2.53	1.32	
n/a	LF06-33	Unmilled	No	n/a	-2.60	1.07	
n/a	LF06-39	Unmilled	No	n/a	-2.67	1.08	
n/a	LF06-44	Unmilled	No	n/a	-2.60	1.15	1.16±0.23

Table 5.4: $\delta^{18}O$ and $\delta^{13}C$ results from otoliths sampled perpendicular to growth bands.

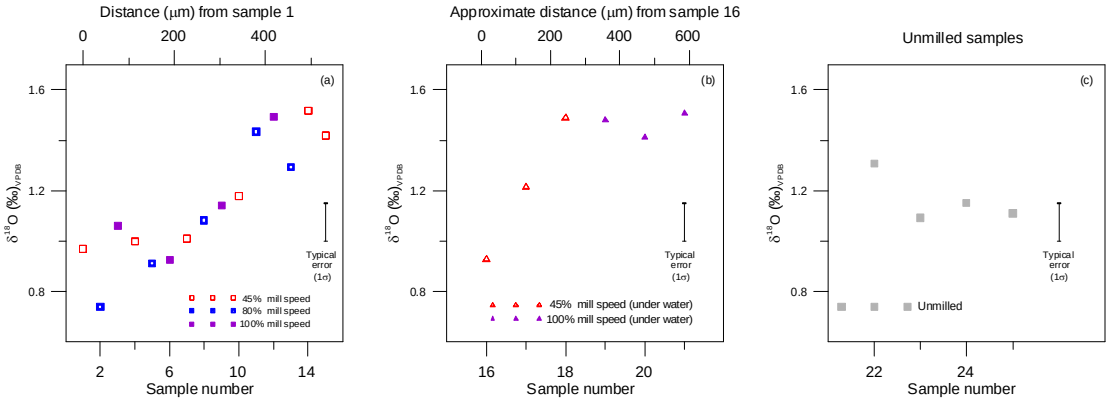

Figure 5.5: Plots of $\delta^{18}O$ results from an otolith, aliquots sampled parallel to growth axis; (a) dry milled (b) milled under water (c) ummilled aliquots. The sample number 1-18 indicates the order in which they were sampled (see Figure 5.2 for schematic). Note that the samples milled under water were taken further apart (see text for details). The sampling number for the unmilled samples is for reference purposes only. Typical error (1σ) is calculated from the reproducibility of the carbonate standard.

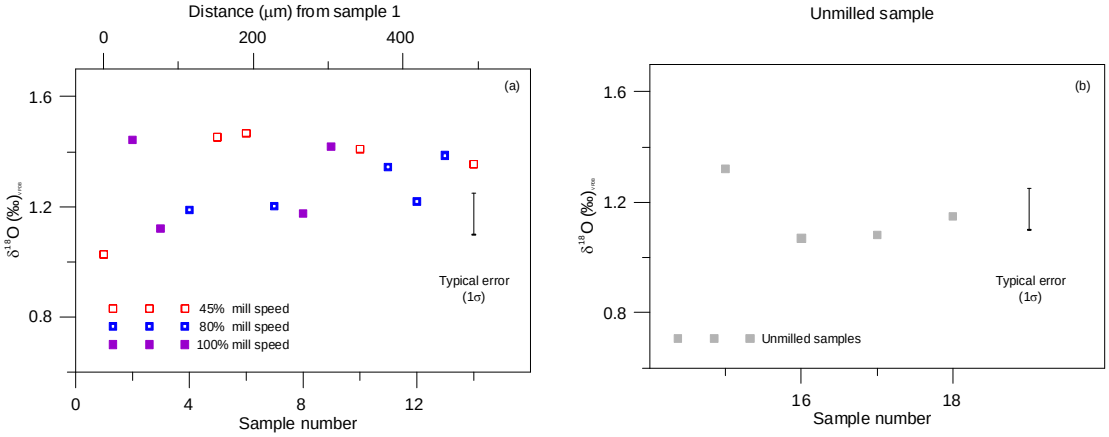

Figure 5.6: Plots of $\delta^{18}O$ results from an otolith, aliquots sampled perpendicular to growth axis (a) dry milled (b) not milled. The sample number 1-14 indicates the order in which they were sampled (sampling numbers for the unmilled samples are for reference purposes only) (see Figure 5.2 for schematic of sampling). Typical error (1σ) is calculated from the reproducibility of the carbonate standard.

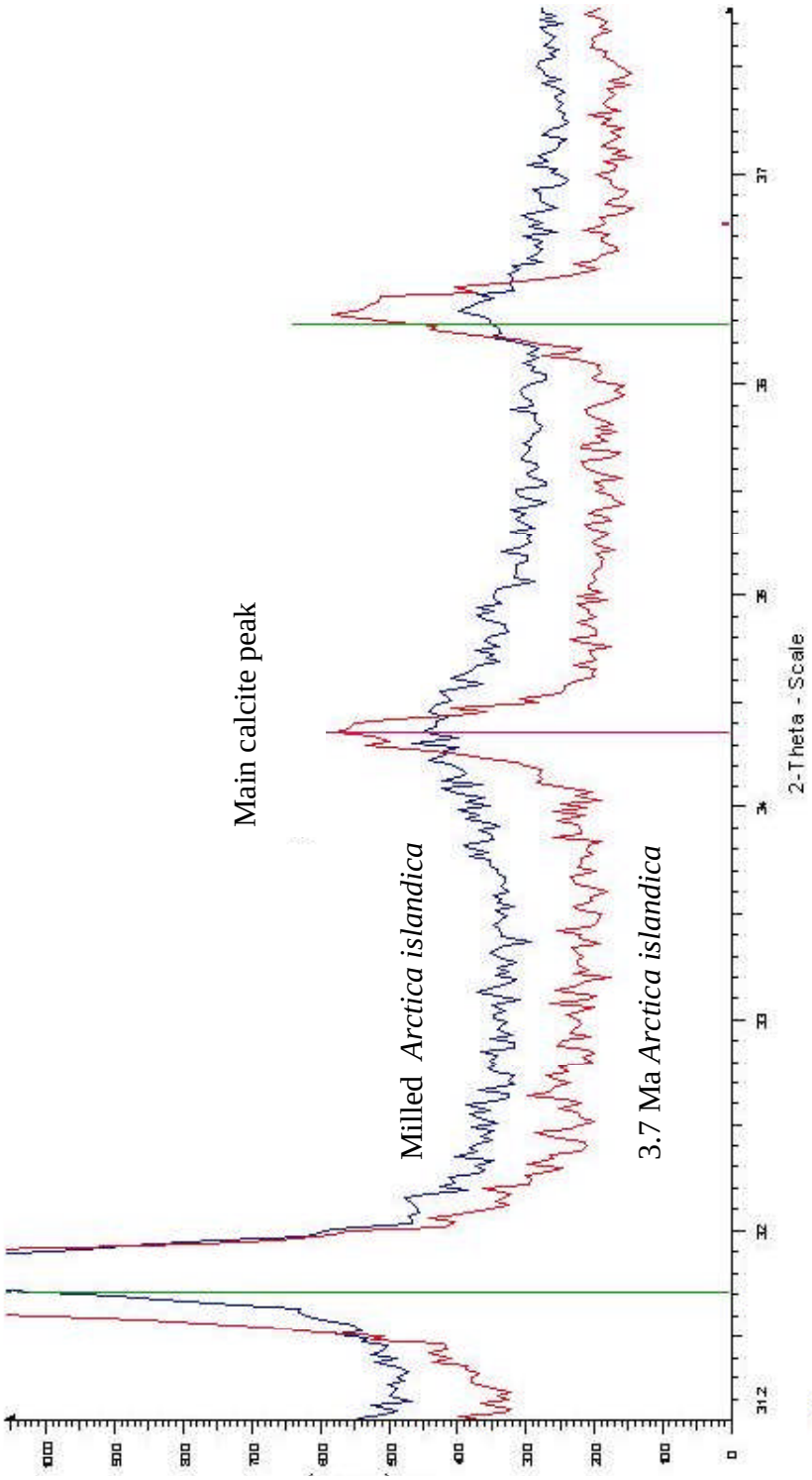

Figure 5.7: XRD results (background removed) of milled *A. islandica* specimen R1FGUP (upper blue line) compared to an *A. islandica* specimen (lower red line) aged 3.7 Ma. The characteristics of the XRD peak are different, with a wider main calcite peak for the milled specimen compared to diagenetically altered material.

5.5 Discussion

The XRD results from *A. islandica* show that milling and drilling produces calcite in all aliquots. No calcite was produced by any of the preparation stages prior to milling or drilling. The percentage conversion is not consistent. The faster drill speed did not appear to show a significantly different percentage of calcite to those drilled at lower speeds, though different milling speeds on the same sample would be required to confirm this. Drilling however produced considerably more calcite producing an average of 19% compared to 11% by micromilling of the same sample (313), with minimum by drilling 15%, and the maximum by micromilling being 12%.

XRD spectra show that the broadness of the peak is much wider than that in diagenetically formed calcite (Figure 5.7). This broadening of peaks in XRD, so-called "diffuse scattering," explores the state of crystallinity in a material (see Welberry, 2004). The width of an XRD peak is related to the degree of long- and short-range order in structures and the wider peak indicates that the calcite is ordered relatively poorly. Iguchi and Senna (1985) hypothesised that during the aragonite-calcite transformation, samples may go through an intermediate disordered state that would contribute to the broadening of the peak.

The otolith shows a 6% conversion to calcite, with no calcite, within the limits of detection, found in the unmilled sample. The percentage conversion is therefore similar to that seen in *A. islandica*. Therefore, it would be expected any impact due to conversion would be similar in *A. islandica*. As discussed earlier, the uptake of $\delta^{18}O$ by otoliths appears to be independent of vital effects, i.e. solely dependent on temperature and salinity (see Campana, 1999 and references therein).

The otolith aliquots taken parallel to the growth bands show a broad increase in $\delta^{18}O$. The unmilled aliquots taken parallel to the growth bands show a mean of

1.12 ‰ ± 0.20 (2σ), not statistically different for the unmilled aliquots (1.20 ‰ ± 0.49 (2σ)). Examining the changes with different milling speeds, as well as under water, shows that there is no statistical difference between the samples (i.e. within 2σ of each other). For example, at a mill speed of 45% (dry drilled) the mean was 1.18 ‰ ± 0.247 (2σ), compared to 1.16 ‰ ± 0.48 (2σ) at 100%.

The aliquots taken perpendicular to the growth band show a smaller range of values than those milled parallel (Figure 5.6). Comparison of the otoliths taken perpendicular to the growth bands shows that there is no difference between the milled 1.29 ‰ ± 0.28 (2σ) and unmilled 1.21 ‰ ± 0.23 (2σ). There is no correlation with milling speeds (e.g. samples drilled at 45% show a mean of 1.31 ‰ ± 0.37 (2σ), compared to 1.31 ‰ ± 0.33 (2σ) at 100%).

Salinity typically varies by ~ 1.6 (see Figure 5.2), which corresponds to a variation in $\delta^{18}O$ of about 0.4 ‰, based on the isotope mixing line for the North Sea (Israelson and Buchardt, 1991). This is in good agreement with the magnitude of variation observed (Figure 5.5). Thus, the change in salinity over the months sampled account for changes in $\delta^{18}O$.

It is also necessary to comment upon the extended time required to get a sufficiently large aliquot for XRD using milling (sampling time was 3-4 hours), compared to 2 minutes for stable isotopes. Hence heating and shear stress may be considerably less for the smaller aliquots required for isotopic analysis and this may be reflected in the results. Aharon (unpublished data) quoted in Aharon (1991) noted the percentage calcite reflected the drilling time. It would explain why no calcite is seen when a geological saw is used, despite this causing stress on the shell. Drilled aliquots however take <5 mins to sample had the highest conversion rates to calcite (up to 24%). The aliquot with 24% calcite also contained significant amounts of

nickel (noted on the XRD plot, and not seen in other aliquots), with examination of the drill bit showed what appeared to be melting, indicating the extremely high temperatures are reached.

5.6 Conclusion

Drilling and micromilling produce a variable amount of calcite in aliquots of *A. islandica*. There is no obvious trend in the data with the conversion controlled by a combination of duration of milling, drill stress and density of the material.

Any $\delta^{18}O$ offset seen between samples could be accounted for by changes in salinity. There was no difference between the $\delta^{18}O$ at different milling speeds. Micromilling does not significantly affect the $\delta^{18}O$ of the aliquots, with any modification of $\delta^{18}O$ being within the error of the mass spectrometer,

Acknowledgements

Special thanks are given to Hans Høie, University of Bergen, who provided both the otolith samples and extensive advice on sampling, and to Angus Calder, University of St. Andrews, who ran numerous XRD samples. Analysis was supported as part of Marie Curie Training Fellowship (EVK2-GH-00-57123-10).

CHAPTER 6: STABLE ISOTOPE GEOCHEMISTRY.

Abstract

The annual growth banding of *Arctica islandica* provides an ideal opportunity to reconstruct intra-annual resolution climate records. Stable isotope analyses (carbon and oxygen) of the outer shell prismatic layer of three specimens collected at 6 m from Irvine Bay, UK 228, 248 and 405 are evaluated here. Specimen 405 was sampled using a drill, while specimens 228 and 248 were sampled using a micromill. Shell 248 was sampled at higher resolution (75 μm) than 228 (500 μm). The larger aliquots from specimen 228 were subsampled for analysis of $\delta^{18}O$ (and $\delta^{13}C$) with the remaining aliquot used for solution-ICPMS trace element composition analysis. Data from 248 show that $\delta^{18}O$ fluctuates between 0.6 and 2.6 ‰; which, using a constant salinity, indicates growth temperatures of ~+5 to +13 ºC. This temperature range differs by ~2.1 ˚C from sea surface temperatures measured at the nearby Millport marine station. A simple model replicated suggested that changes in growth rate impact significantly on the temporal resolution of $\delta^{18}O$ sampling, and thus change the appearance of the $\delta^{18}O$ profile. The model also suggested that salinity had little impact on the $\delta^{18}O$. A strong ontogenetic effect is seen in $\delta^{13}C$ of all three specimens, but no lateral variation was found suggesting that the EPF is relatively homogeneous.

6.1 Introduction

The partitioning of oxygen isotopes during the secretion of carbonate by marine organisms is dependent on both the $\delta^{18}O$ of seawater ($\delta^{18}O_{seawater}$) and the ambient temperature at the time of formation (e.g. Urey, 1947; Epstein and Mayeda, 1953; Killingley and Berger, 1979; Bice *et al.*, 1996).

In this study, three live-collected specimens of *Arctica islandica* (228, 248 and 405) dredged from 6 m in Irvine Bay, UK were selected for measurement of $\delta^{18}O$ and $\delta^{13}C$ along the outer shell prismatic layer. Fluctuations in $\delta^{18}O$ in the shell ($\delta^{18}O_{shell}$) are compared to instrumental sea surface temperature (SST) measurements made at the nearby Millport Marine station. This allows the relationship between $\delta^{18}O_{shell}$ and instrumental data to be examined. Modelling allows the relative impact of changes in temperature and salinity as well as the effect changes in temporal resolution of the sampling, resulting from changes in shell growth rate, has on the $\delta^{18}O_{shell}$ profile to be explored. The results of $\delta^{18}O$ and $\delta^{13}C$ will facilitate discussions in the cause of fluctuations in the incorporation of trace elements, which will be discussed in Chapter 8.

6.1.1 Existing A. islandica data

A. islandica provides, in principle, an excellent material from which to reconstruct temperature from a time series of oxygen isotope composition along the growth axis. The species is long lived with specimens over 350 years in age reported (Schöne *et al.*, 2005a). Longer multi-shell records can be produced through sclerochronology, making it ideal for high resolution palaeotemperature reconstructions. As the chronology within *A. islandica* is unaffected by bioturbation and the organism is

immobile once the spat has been deposited from the water column, the location and chronology are well defined (excluding movement due to storm surges, turbidity flows etc). Weidman *et al*. (1994) used a 38 year old *A. islandica*, which was live-collected near to the former position of the Nantucket Shoals Lightship (41ºN, 69ºW) off the coast of North America, to assess the reproducibility of $\delta^{18}O$ measurements. $\delta^{18}O$ measurements from the shell were compared to the ambient bottom temperature and salinity measured from the lightship. They found that the empirically derived equation (from aragonite molluscs) of $\delta^{18}O$ incorporation of Grossman and Ku (1986) could reproduce the temperature to within an average of 0.38 ºC. This site is particularly important as usually *in situ* salinity measurements are not available, which increases the error on the temperature reconstruction. Weidman *et al*. (1994) calculated for the same samples, the reconstructed temperature using a constant value of $\delta^{18}O_{water}$ (–0.88 ‰), which replicates the typical situation in which the $\delta^{18}O_{water}$ is unknown. An accuracy of ~1.2 ºC was obtained, indicating that the impact of changes in salinity is relatively small. This is important, as there are few *in situ* salinity measurements, particularly for benthic waters.

Further work has been done on the use of *A. islandica* as a proxy for water temperature e.g. Schöne *et al*. (2005a) who examined a 374- year old specimen to reconstruct temperature off the North-east coast of Iceland from 1496-1533 (i.e. from the ontogenetic years 2 to 40). They found evidence of the North Atlantic Oscillation (NAO) type periods in the $\delta^{18}O$ record as well as the presence of 12-14 year cycles, which may represent teleconnections to cycles in the tropical Atlantic.

Witbaard *et al*. (1994) used live collected shells from the North Sea to examine when annual bands were deposited. They concluded that the growth check (i.e. reduced period of growth) was not a product of low temperatures as suggested by

Weidman *et al*. (1994) but rather of food availability. Further research in the North Sea has been since carried out by Schöne *et al*. (2004c) which constructed a 99-year record from *A. islandica* in which they reported the growing season to be February to September. This was later modified during further work, to mid-February to mid-December, with a hiatus due to spawning between early September and mid-November (Schöne *et al.*, 2005b). This is important as it determines which months *A. islandica* can provide a record of $\delta^{18}O$ incorporation.

The magnitude of seasonal $\delta^{18}O_{shell}$ variations declines with increasing size and age of molluscs (Jones *et al.*, 1986; Krantz *et al.*, 1987; Weidman *et al.*, 1994). This can be attributed to the loss of finer scale signals in the thin growth bands characteristic of the latter years of growth compared to the higher temporal resolution attainable in the earlier, wider bands. Adaptive sampling has been used by authors such as Schöne *et al*. (2005a) where the sampling width for each year is changed according to band width, with finer sampling possible in the slower growing, older shell portions.

6.1.2 Oxygen isotopes

The oxygen isotopic composition of marine carbonate shell material is generally assumed to be a product of two main factors: $\delta^{18}O_{seawater}$ and the ambient temperature at the time of formation (e.g. Urey, 1947; Epstein and Mayeda, 1953; Killingley and Berger, 1979; Bice *et al.*, 1996). This chapter will employ the equation published by Grossman and Ku (1986), which is based solely on aragonitic molluscs and therefore appropriate for *A. islandica.*

$$T(^{o}C) = 20.19\text{-}4.56(\delta^{18}O_{aragonite} - \delta^{18}O_{w}) + 0.19(\delta^{18}O_{aragonite} - \delta^{18}O_{w})^{2}$$

Where:

$T(^oC)$ = temperature of ambient water during shell formation

$\delta^{18}O_{aragonite}$ = $\delta^{18}O$ of aragonite from the shell compared to VPDB

$\delta^{18}O_w$ = $\delta^{18}O$ value of the seawater with respect to VPDB

This equation is derived from empirical measurements of $\delta^{18}O$ values. From the above equation, it can be seen that it is necessary to know the $\delta^{18}O$ value of the water when the material was incorporated into the shell in order to calculate the temperature. The $\delta^{18}O$ of water is usually expressed as against the international Standard Mean Ocean Water (SMOW) scale and thus it is necessary to standardise to the carbonate VPDB scale using the equation:

$$\delta^{18}O\ (SMOW) = 1.03092 * \delta^{18}O\ (VPDB) + 30.92$$

Coplen *et al*. (1983)

As seawater $\delta^{18}O$ measurements are often unavailable, salinity measurements are used to estimate the water $\delta^{18}O$ value using empirical relationships derived for a particular region:

E.g. $\delta^{18}O\ (SMOW) = 0.412 * S - 14.66$ for the Gulf of Maine (Fairbanks, 1982)

compared to:

$\delta^{18}O\ (SMOW) = 0.417 * salinity - 14.555$ for the North Atlantic

Ganssen unpublished, cited in Witbaard *et al*. (1994).

This latter equation will be applied during this study, as it is the location closest to Irvine Bay (no other calibration data was found closer to the sample site, see http://data.giss.nasa.gov/o18data/). In addition, its robustness has been demonstrated in a number of published papers on *A. islandica* from the North Sea (e.g. Witbaard *et al.*, 1994; Schöne *et al.*, 2004a).

Over relatively short timescales (decadal), the $\delta^{18}O_{seawater}$ may fluctuate, reflecting changes in freshwater input, evaporation rates (especially in shallow environments) and changes in the source waters of the region. Over longer time scales (10^4-10^5 years), the $\delta^{18}O$ values may also be influenced by the global $\delta^{18}O$ balance, which is mainly dependent on the volume of glacial and polar ice.

The use of the equation of Grossman and Ku (1986) has been demonstrated for both *A. islandica* (e.g. Weidman *et al.*, 1994; Schöne *et al.*, 2004a; Schöne *et al.*, 2005c) and other aragonitic molluscs (e.g. Elliot *et al.*, 2003). Wefer and Berger (1991) showed that bivalves generally (but not always) produce calcium carbonate in oxygen isotope equilibrium with the $\delta^{18}O$ of seawater. Carré *et al.* (2005a, 2005b) highlighted the differences in $\delta^{18}O$ fractionation equations for aragonitic material of inorganic experiments (Zhou and Zheng, 2003), compared to biogenic material such as otoliths (Patterson *et al.*, 1993), benethic foraminifera (Dunbar and Wefer, 1984), and sponges (Bohm *et al.*, 2000), as well as, crucially for this study, differences between aragonite bivalves, (Grossman and Ku, 1986; Carré *et al.*, 2005a) (Figure 6.1). Deviations from the predicted equilibrium have been explained by the kinetic effect during the calcification at the CO_2 hydroxylation/hydration steps that results in depletion with respect to the equilibrium (McConnaughey, 1989; McConnaughey *et al.*, 1997). The CO_2 hydroxylation/hydration step is particularly sensitive to pH (Owen *et al*., 2002).

The good agreement between $\delta^{18}O_{shell}$ with salinity and temperature measurements (e.g. Weidman *et al.*, 1994) however suggests that the application of the Grossman and Ku (1986) equation for *A. islandica* is appropriate. However, the use of such an equation means that the non-equilibrium controls on $\delta^{18}O$ must be constant throughout the whole of the shell. Comparison to the $\delta^{13}C$ record is important to determine if any correlation can be found between the two.

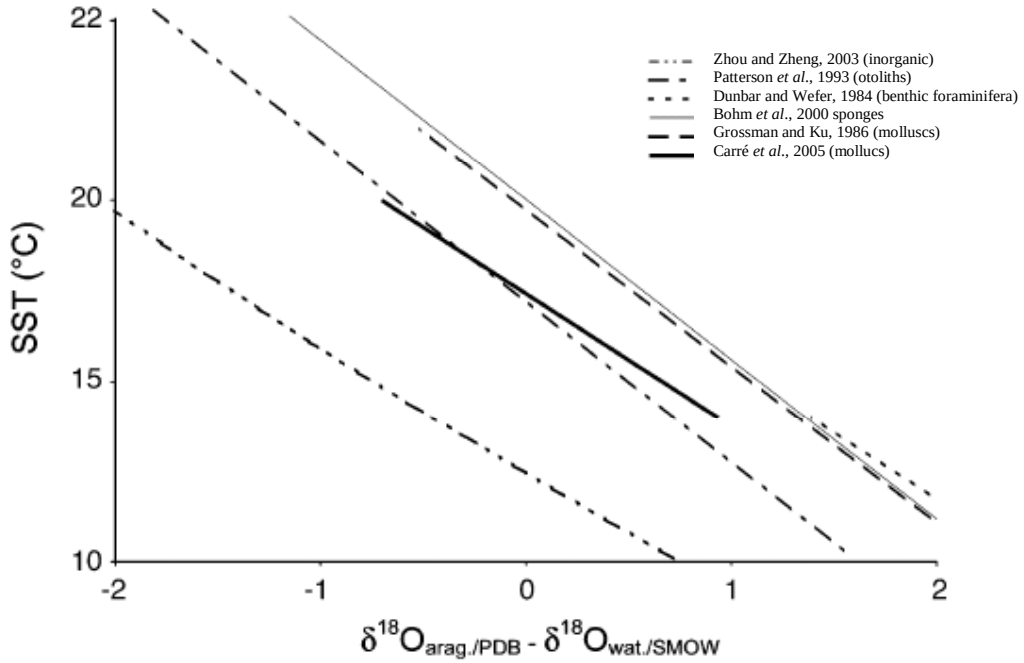

Figure 6.1: Comparison of temperature $\delta^{18}O$ fractionation equations for aragonite from various studies (taken from Carré *et al.*, 2005a)

6.1.3 Carbon isotopes

The incorporation of carbon isotopes into molluscs is less well understood, but temperature dependence is very small (Grossman and Ku, 1986). A number of hypotheses have been proposed to explain the variations observed across growth bands in molluscs. Generally, $\delta^{13}C$ is thought to be derived from either metabolic

sources with ^{12}C enrichment derived from respiration CO_2 (e.g. Borchardt, 1985; Tanaka *et al.*, 1986; McConnaughey, 1989; Klein *et al.*, 1996a; McConnaughey *et al.*, 1997; Lorrain *et al.*, 2005) and/ or marine dissolved inorganic carbon (DIC) in the water column (e.g. Mook and Vogel, 1968; Fritz and Poplawski, 1974). Variations in DIC $\delta^{13}C$ are influenced by variations in primary productivity, upwelling and mixing (Killingley and Berger, 1979; Purton and Brasier, 1997). McConnaughey *et al*. (1997) estimated that molluscs typically incorporate ~10% of carbon from metabolic CO_2, with changes of this magnitude having been found in the bivalves, *Saxidomus giganteus* and *Pecten maximus* (Owen *et al.*, 2002; Gillikin *et al.*, 2005b).

6.2 Instrumental measurements

A. islandica samples were collected live from Irvine Bay in May 2001 (see section 1.3 for more details). Millport Marine station is ~22 km north of Irvine Bay. Sea surface temperature records (SST) extend beyond the last 50 years at Millport. Therefore, the calibration of the temperature $\delta^{18}O$ relationship in the shell against instrumental data can be explored. SST at Millport was collected daily until 1983 when financial cutbacks reduced data collection to working days only (P. Barnett, Pers. Comm., 2007). Figure 6.2 shows a monthly average of SST (as supplied by Millport Marine station). Ongoing research (since 2003) at Millport in association with Aberdeen Fisheries laboratory has compared temperature measurements collected by the "traditional" bucket method with automated loggers. The maximum difference is ~2 ºC and is attributable to factors such as the temperature of bucket and how the bucket lands e.g. if the water fills over the bucket lip the top 1-2 cm will be measured whereas other times it may fill from the top 10-20 cm (P. Barnett, Pers. Comm. 2007). *In situ* temperature and salinity measurements for Irvine Bay ((Figure 6.3) are also

available as limited time snapshots for Irvine Bay itself (1990-1996, with typically 4 measurements per year). These are taken at 7 m in a water depth of >30 m, whereas *A. islandica* grows at a depth of 6 m, i.e. the temperature was not logged in the same water depth. However, it provides the closest approximation to temperature where *A. islandica* was collected. Measurements from Irvine Bay at 7 m show good agreement with SST measurements from Millport marine station, typically within 1.2 °C (2σ), with maximum temperature range of 6.3 °C to 15.6 °C (1990-1996).

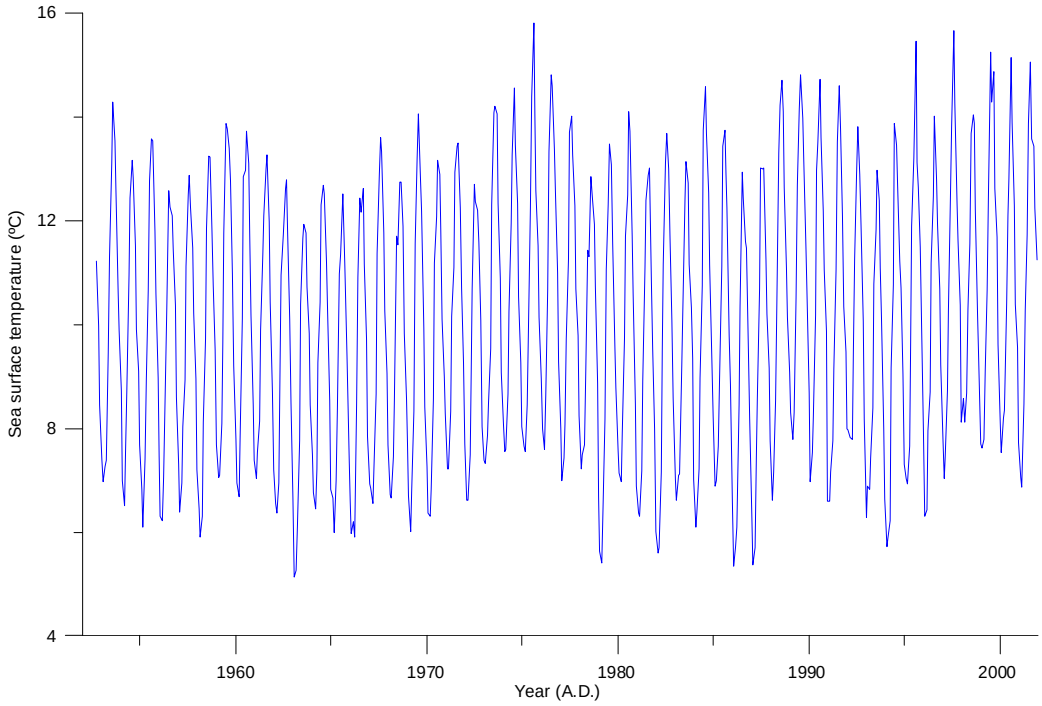

Figure 6.2: Sea surface temperature (using monthly averaged values) at marine sampling station Millport, Isle of Cumbrae, NW Coast of Scotland from 1953-2001 (Millport Marine station data). See text for details on data collection method and possible errors.

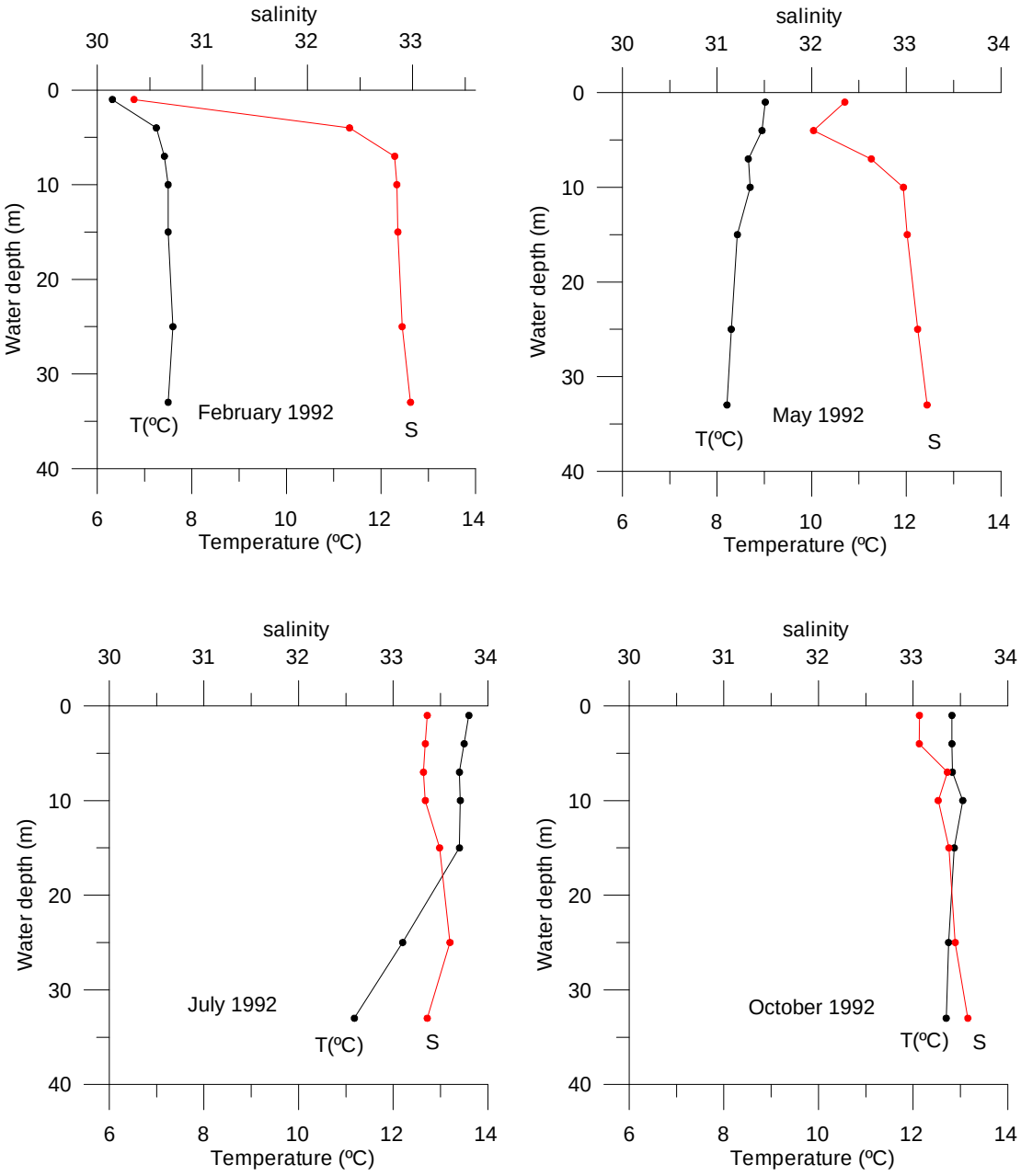

Figure 6.3: Depth profile of temperature (T/ºC) (black) and salinity (S) (red) from Irvine Bay in 1992. Data provided by SEPA (Pers. Comm. 2007). Instrumental measurement errors are <0.005 ºC and <0.005 for temperature and salinity respectively (B. Miller, Pers. Comm. 2007).

6.3 Method

Three samples, shell 405, 228 and 248 were sampled using different methods (Table 6.1). Results of analyses of the effects of milling/drilling on aragonite taken from otoliths (see Chapter 4) showed that although aragonite undergoes transformation into calcite, within the limits of precision of the instrument, $\delta^{18}O$ is unaffected. Therefore, these methods are appropriate for sample extraction.

6.3.1 Drilled aliquots

The outer shell prismatic layer (PL) of shell 405 (subsequently referred to as PL405) was sampled using a fixed drill platform, over a spot (drill bit 1 mm wide). Aliquots were analysed on Finnigan DeltaplusXP at the University of St. Andrews, UK. The instrument required a sample size of 0.2-0.3 mg. The shell was sampled between 1975 until 2001 (date of collection), with the specimen 32 years old. The earliest 7 years were not sampled due to the narrow width of the growth band.

				Dimensions of each aliquot (μm)			
Sample	Sampling platform	Resolution	Continuous sampling?	Width	Length	Depth	Additional analysis taken
405	Fixed drill platform	Coarse	No	1000*	1000*	6000*	n/a
248	New Wave Micromill™	Fine	Yes	75	1000	350	Aliquots taken to examine lateral changes in $\delta^{13}C$
228	New Wave Micromill™	Coarse	Yes	500	2000	500	n/a

Table 6.1: Sampling details of the three *A. islandica* specimens used in stable isotope analysis. * Estimate

6.3.2 Milled aliquots

A New Wave™ micromill was used to sample the outer shell prismatic layer (PL) of shell 228 and 248 (subsequently referred to as PL228 and PL248). Aliquots were analysed on the Finnigan MAT253 mass spectrometer at the University of Bergen, Norway. Both PL228 and PL248 were sampled from 1992-2001, with the years comparable to those sampled by LA-ICPMS (see Chapter 4).

The New Wave™ micromill can calculate the area and volume of a selected line and can interpolate between two selected lines to produce sample lines of a specific dimension and volume. Figure 6.4 shows photographs of the system, plus a screen capture taken during the set-up of the milling of PL248 showing the interpolated sample lines (to give a volume of ~0.02 mm^3).

For PL228, a total volume of ~0.3 mm^3 per aliquot was extracted. Two aliquots for $\delta^{18}O$ analysis was then taken from the sample while on the milling plate, (20-35 µg per aliquot with sample size determined visually and placed directly into the vial). The remaining sample (~ 1 mg) was collected for solution-ICPMS.

For PL248, aliquots were only for analysis of stable isotopes, so an aliquot volume of ~0.02 mm^3 was sampled using the micromill. The slightly larger sample size than required for the mass spectrometer is to compensate for loss during transfer from the milling plate to the vial. The specimen remains on the milling plate until all the sampling has been completed.

The sampling resolution was significantly different between the shells, resulting in a significantly different temporal resolution. PL405 has a maximum of ~ 9 aliquots per year, with an aliquot covering >2 years at the slowest growth rate. PL228 decreased from 5 aliquots/yr to 1 aliquot/yr. PL248 was sampled at the highest resolution, with a minimum of 8 aliquots/yr and a maximum of >20 aliquots/yr.

In addition, shell 228 was sampled laterally in the outer shell prismatic layer across the bands to examine whether any changes in $\delta^{13}C$ occurred. Three sets of samples (6-7 aliquots in each) were taken at 250 µm and 1000 µm from the periostracum with each set constrained within the same growth bands. Klein *et al*. (1996a) suggested that $\delta^{13}C$ (and Sr/Ca) within calcite layer of *Mytilus trossulus* were primarily controlled by rate of mantle metabolic activity and variation in seawater salinity. Thus, changes in $\delta^{13}C$ laterally across a band may indicate variations in metabolic activity, which could assist in the interpretation of lateral variation in the trace elements.

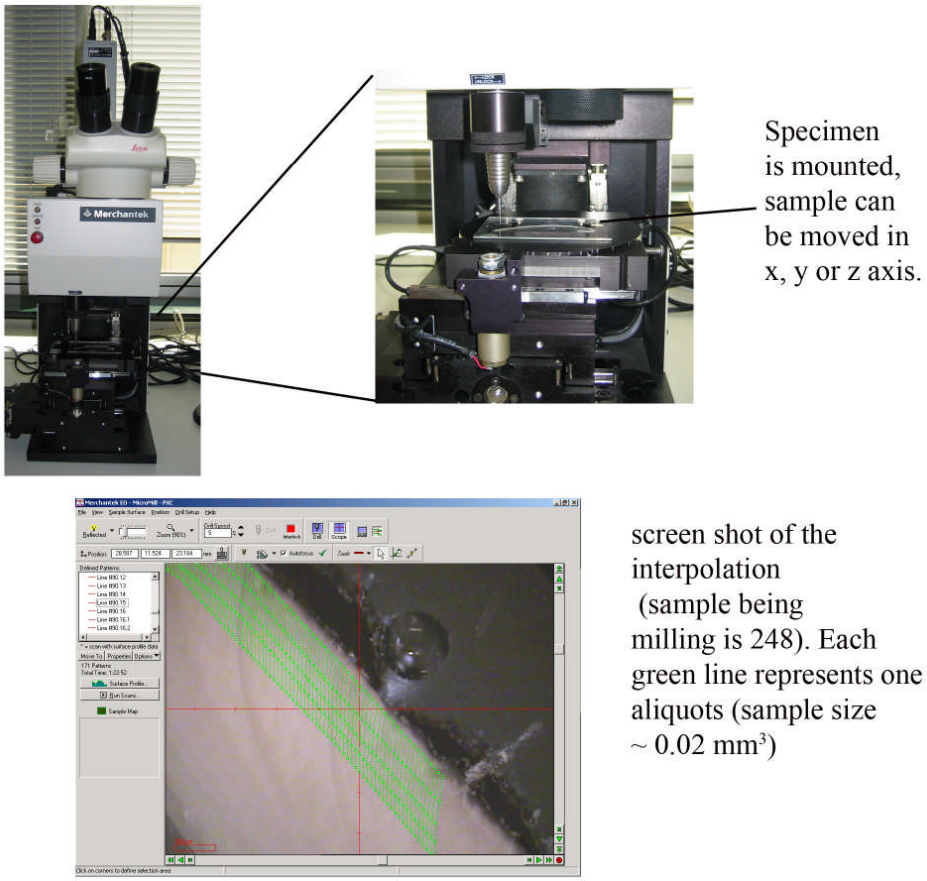

Figure 6.4: Images of the New Wave™ Micromill system showing milling of the outer shell prismatic layer of *A. islandica* shell 248.

http://www.new-wave.com/1nwrProducts/MicroMill.htm

6.3.3 Analysis using Finnigan DeltaplusXP mass spectrometer

Carbonate aliquots from PL405 were analysed using a gasbench microcarbonate device coupled to a Finnigan DeltaplusXP gas source mass spectrometer operated in continuous mode at the University of St. Andrews, UK. The samples were calibrated to the Vienna Peedee belemnite (VPDB) via NBS-18. Samples were weighed prior to analyses with aliquots between 0.2-0.3 mg. The sample order was randomised to offset any machine drift.

The samples were left a minimum of 24 hours in the autosampler tray at a constant 25 ºC. The samples were then flush-filled with He (i.e. the air was removed and replaced with He) after which excess 100% pure phosphoric acid was added manually to produce CO_2 for analysis in a mass spectrometer. Samples were left a minimum of 24 hours before the CO_2 was analysed in the mass spectrometer.

The sample gas was introduced into the mass spectrometer using a continuous He gas flow method. This has the advantage over the dual inlet of allowing pulse injections of the sample gas to be analysed; thus reducing volume constraints and sample size. A check on linearity was performed at the beginning of the analysis, with replicate analysis taken every five aliquots.

The sample is carried in a flow of helium into an ionisation chamber where it is bombarded with electrons. These ionised gases are then accelerated and focused before passing through a magnetic field (mass analyser), which separates the ions according to their mass/charge ratios. These are then detected in Faraday cups with the total amount of charge collected providing a measure of isotope ratios. The ion beams are measured simultaneously in Faraday cups with the strength of the ion currents of each mass relating to the isotopic ratios, i.e. for CO_2, there are three principal peaks at mass 44 ($^{12}C^{16}O_2$), mass 45 ($^{13}C^{16}O_2$ and $^{12}C^{17}O^{16}O$) and mass 46

($^{12}C^{16}O^{18}O$). These provide information on the isotopic composition of the material, which are, theoretically, independent of sample size. In practice, however the change in sample size does influence isotopic measurement so linearity standards are measured at the beginning (or at regular intervals for larger batches) to correct for this effect. In addition, standards are measured at regular intervals to check for instrument drift. The raw isotopic data are corrected for linearity effects during post-processing, with generally the second peak (of the ten gas pulses) taken. These samples were analysed after the initial installation of the instrument. The reproducibility for the carbonate standards was typically ±0.05 ‰ (1σ) and ±0.15 ‰ (1σ) for $\delta^{13}C$ and $\delta^{18}O$ respectively.

6.3.4 Analysis using Finnigan MAT253 with Kiel device

The Finnigan MAT253 works principally the same way as the Finnigan DeltaXplus, although there are a number of crucial differences that reduce the sample size. The most important is the absence of a carrier gas, which means that the sample CO_2 is the only gas within the mass spectrometer during the analysis, significantly reducing the background and thus the sample size. The sample gas pulses are directly compared to reference gas pulses, using a dual inlet system. In addition, the detector of this instrument is more sensitive than that of the Finnigan DeltaplusXP. Figure 6.5 shows a schematic of such a system.

The MAT253 has two parallel CO_2 extraction lines (1 and 2) with samples loaded into a revolving sampling carousel into the Kiel Device, which is an automated online system (Figure 6.6). The vials are pushed up to the extraction line and pumped out to form a vacuum. Orthophosphoric acid at 70 °C is then added through an acid drip valve (one for each line) to the individual vials. During the acid reaction, all the

gases are collected in the first cold finger (cooled with liquid nitrogen to a temperature –170 ºC). The non-condensable gases are pumped away at the end of the reaction time (480 s), and then trap 1 is warmed to –115 ºC to keep H_2O frozen but allow CO_2 to become a gas. The second trap is then cooled to –170 ºC to trap CO_2 before being isolated from trap 1. Trap 2 is then warmed to 30 ºC to liberate CO_2 and this travels through capillary tubes to the mass spectrometer. The traps are baked at 150 ºC and opened to vacuum to remove any water. Details of the machine set-up are outlined in Table 6.2.

Sample sizes required are between 20-35 µg, but samples as small as 10 µg are possible. Smaller samples have an increased number of measurement cycles (bergen2 method). Standards used were CM03 (carrera standard) together with AII (a deep sea coral standard) (see Ostermann and Curry, 2000). Long-term replicate measurements of daily carbonate standards with a mass >40µg is better than ±0.04‰ $\delta^{13}C$ and ±0.08‰ $\delta^{18}O$ (1σ). However, many of the samples run in this study were <40µg and long term replication of standards in the mass range between 7-40µg during this period was ±0.06‰ $\delta^{13}C$ and ±0.12‰ $\delta^{18}O$ (1σ). The values are calibrated to the VPDB scale using NBS-19 and NBS-18 as a control.

Acid Temperature	70 ºC
Reaction Time 1 (s)	480
Reaction Time 2 (s)	60
Transfer Time (s)	90
Traps cooled to:	-170 ºC
Traps baked to:	150 ºC
No. of acid drops	3
No. of cycles of analysis	8 (bergencarb); 13 (bergen12)
Predelay before analysis (s)	5
Reference	Right
Sample	Left
Reference refill	Every 5th sample

Table 6.2: Set-up details of the mass spectrometer. Bergen12 is used for smaller samples with increased number of cycles to improve the precision.

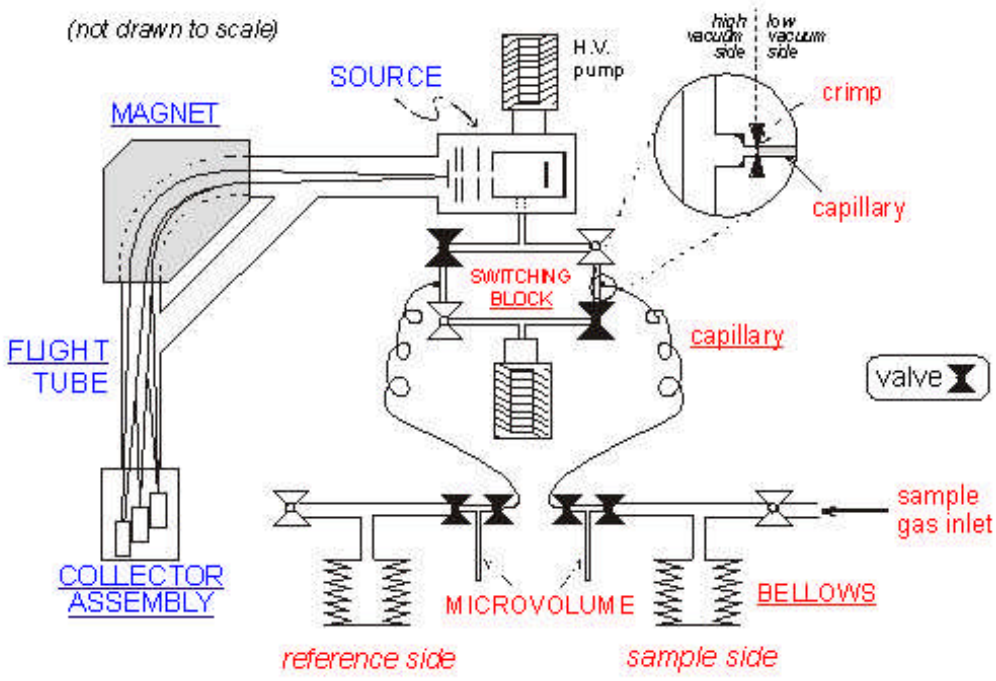

Figure 6.5: Schematic of a typical mass spectrometer (Sharp, 2004).

Figure 6.6: Photograph of the Kiel Device.

6.4 Results

Results from PL405 are shown on Figure 6.7. $\delta^{18}O$ varies +1.3 and +3.0 ‰ while $\delta^{13}C$ varies between +0.4 and +3.2 ‰. $\delta^{13}C$ shows a general decline through the shell of >2 ‰. The positions of the annual bands are marked, but it should be noted that the samples taken by drill typically covered >2 years during (at least) the last 10 years of shell growth, due to the shape of the drill bit resulting in overlaps in the sampling. It is also difficult to estimating the true temporal resolution covered due to the depth of the drilling.

Two aliquots were sub-sampled for each milled aliquot of PL228 to gain an average (with the rest of the milling sample used for solution-ICPMS analysis). There is a high degree of heterogeneity within the sample pairs, which is not accounted for

by instrumental precision. Closer analysis shows that when an offset in $\delta^{18}O$ values is present, a smaller offset in $\delta^{13}C$ is also observed which are typically within error (Figure 6.8). $\delta^{13}C$ decreases from ~+2.2 to <+1.6 ‰.

The results of $\delta^{18}O$ and $\delta^{13}C$ from PL248 are shown on Figure 6.9a. The $\delta^{18}O$ values are highly variable with no ontogenetic trend. The minimum value is +0.6 ‰ and the maximum is +2.5 ‰. The $\delta^{13}C$ values decrease through the life of the shell with a maximum of +2 ‰ in 1993, with a minimum of 0 ‰ in 1998.

The $\delta^{18}O$ record shows a saw-tooth pattern (Figure 6.9a). The lowest values found just prior to the growth check are typically <1.0 ‰ with the largest increase after the growth check, with the highest $\delta^{18}O$ just after the growth check (typically >2.5 ‰). $\delta^{18}O$ then increases rapidly before reaching steady values of ~ 1.8 ‰, and then there is a final increase prior to the growth check of ~ >0.5 ‰. The lowest $\delta^{18}O$ values are recorded in 1996 and 1995, with the highest $\delta^{18}O$ in 1993-1995, a reflection of the maximum and minimum temperatures recorded within a year respectively.

The shell damage which occurred after the 1997 resulted in the infilling of material, and this can be seen in a significant change in $\delta^{13}C$ value of >0.5 ‰. In addition, at ~5200 μm from the growth edge, the shell appears to be more porous perhaps suggesting evidence of infilled material and there is associated increase of $\delta^{18}O$ and $\delta^{13}C$ (~ 0.3 ‰ and >0.5 ‰ respectively).

Results from PL228 (Table 6.3) show that the values of $\delta^{13}C$ taken at varying distances from the periostracum do not vary for two sets of analysis (those taken 3,000 and 10,000 μm from the growth edge). The mean with the standard deviation e.g. at 3,000 μm from the growth edge, $\delta^{13}C$ 250 μm from the periostracum is 1.83 ±

0.21 (2σ) compared to 1.84 ± 0.09 500 μm from the periostracum being within 2 σ. However, the $\delta^{13}C$ of the aliquots differ when the sample was taken 500 μm from the edge (the reason for this is discussed below). In addition, a decline in $\delta^{13}C$ through ontogeny can be clearly seen.

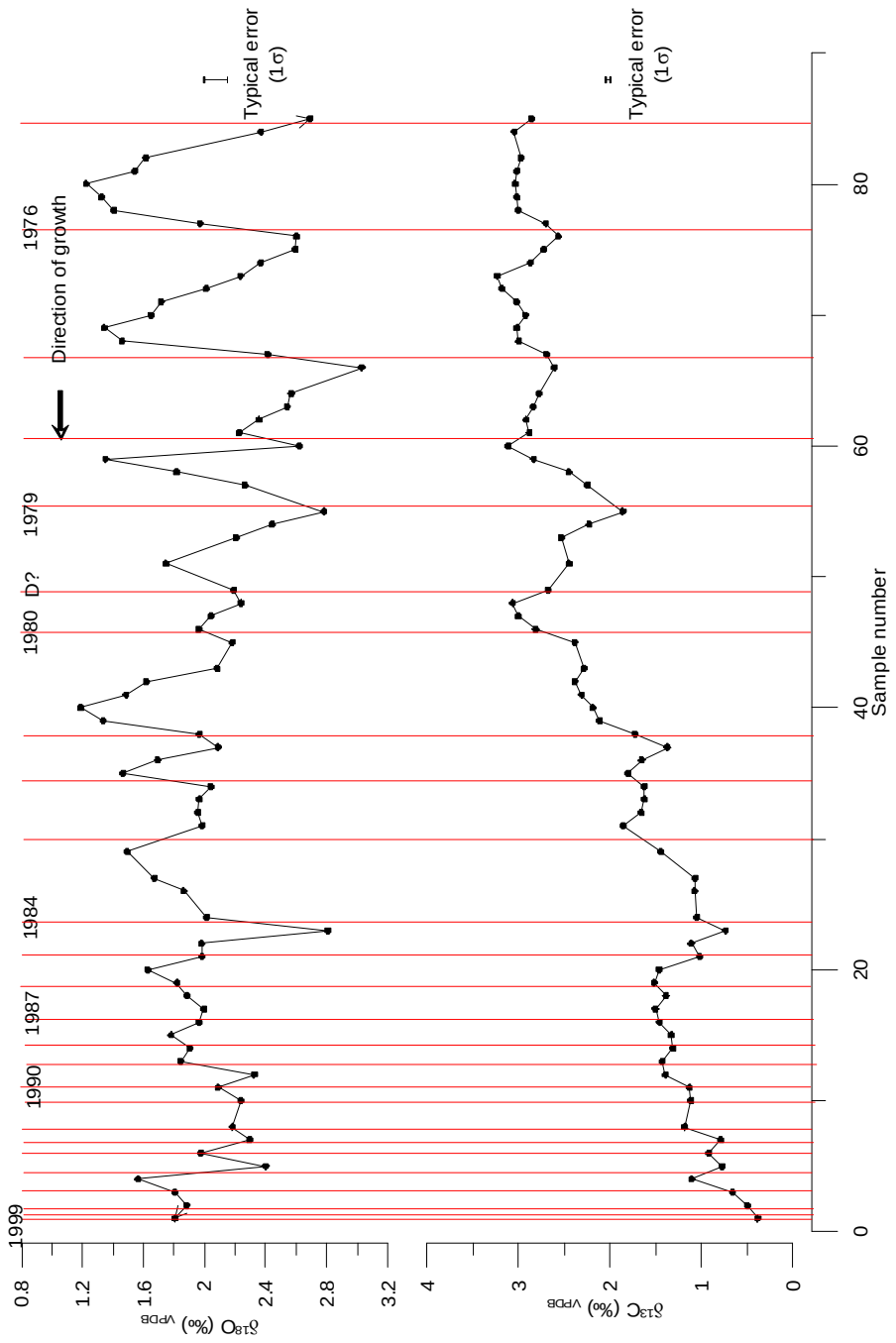

Figure 6.7: Plot of results from the outer shell prismatic layer of *A. islandica* specimen 405 for (a) $\delta^{18}O$ (b) $\delta^{13}C$. The red lines correspond to the position of the annual termination band. Note that during the most recent 12 years sampled (i.e. 1999-1987) each sample typically covers >2 years, as sampling of aliquots overlapped (see text for more details). The typical error (1σ) is calculated from reproducibility of carbonate standards (carrera).

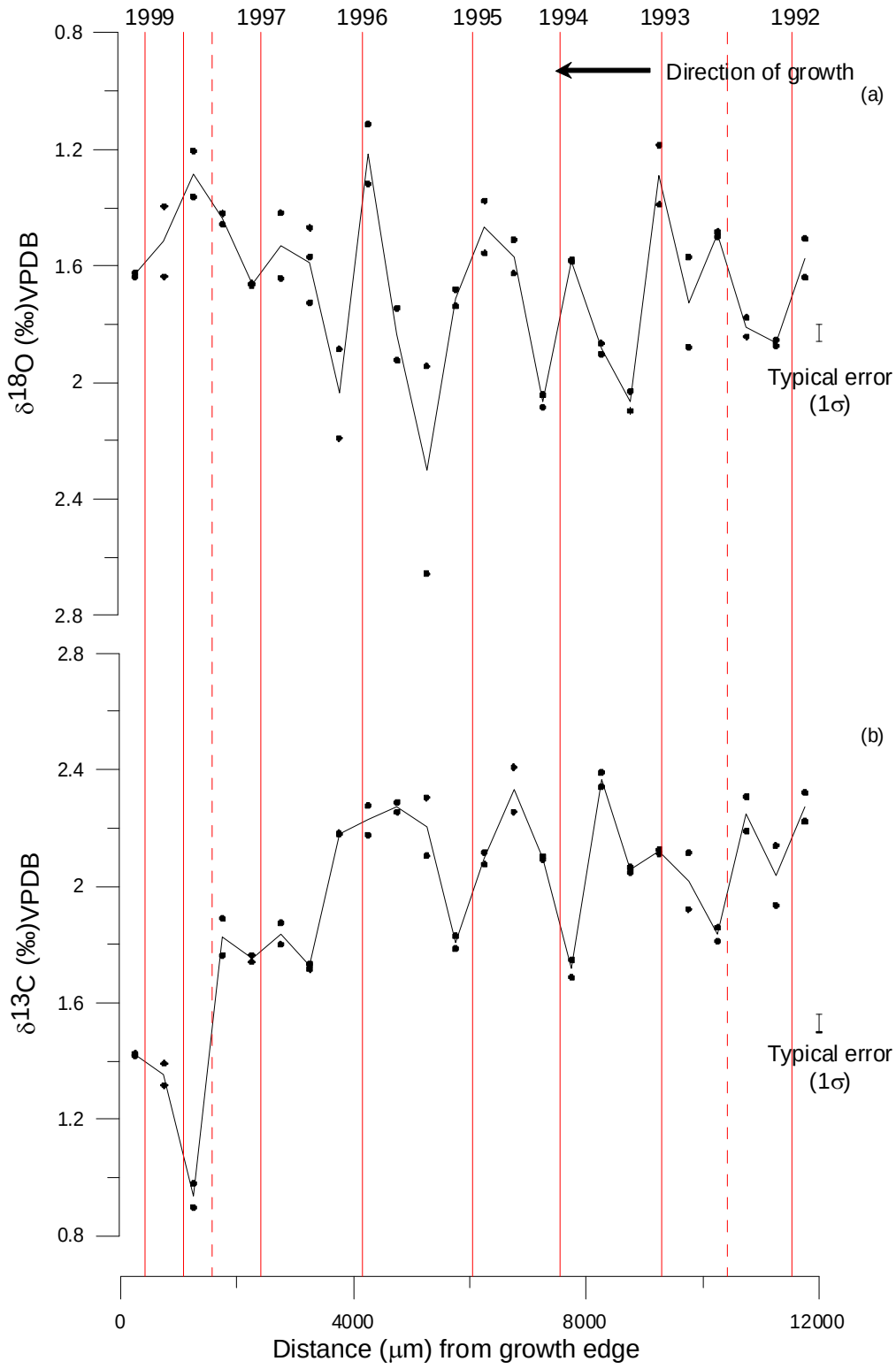

Figure 6.8: Results of (a) $\delta^{18}O$ and (b) $\delta^{13}C$ from the outer shell prismatic layer of *A. islandica* specimen 228, the rest of the aliquot was used for solution-ICPMS. The typical error (1σ) is calculated from the reproducibility of the carrera standard. The dark lines join the averages of the two analyses per aliquot.

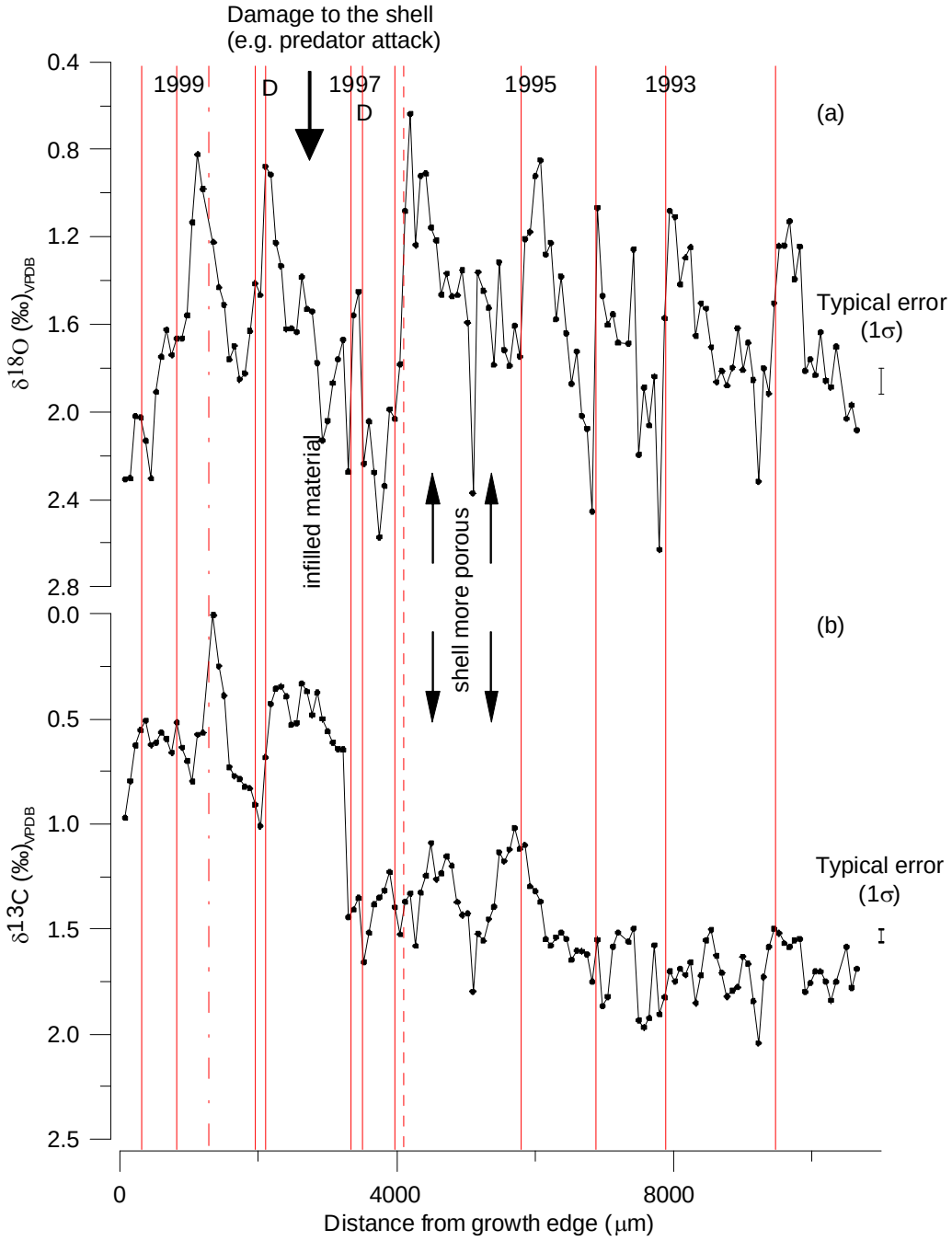

Figure 6.9a: Fluctuations in the outer shell prismatic layer of *A. islandica* shell 248 for (a) $\delta^{18}O$ and (b) $\delta^{13}C$. The dashed line indicates the start of the annual growth check. The dot-dash lines indicate the position of intra-annual bands, i.e. increased organics. D represents a doublet. Note the $\delta^{18}O$ axis is reversed. The typical error (1σ) is calculated from the reproducibility of the carrera standard. The damage to the shell could be seen visually (see Figure 4.20).

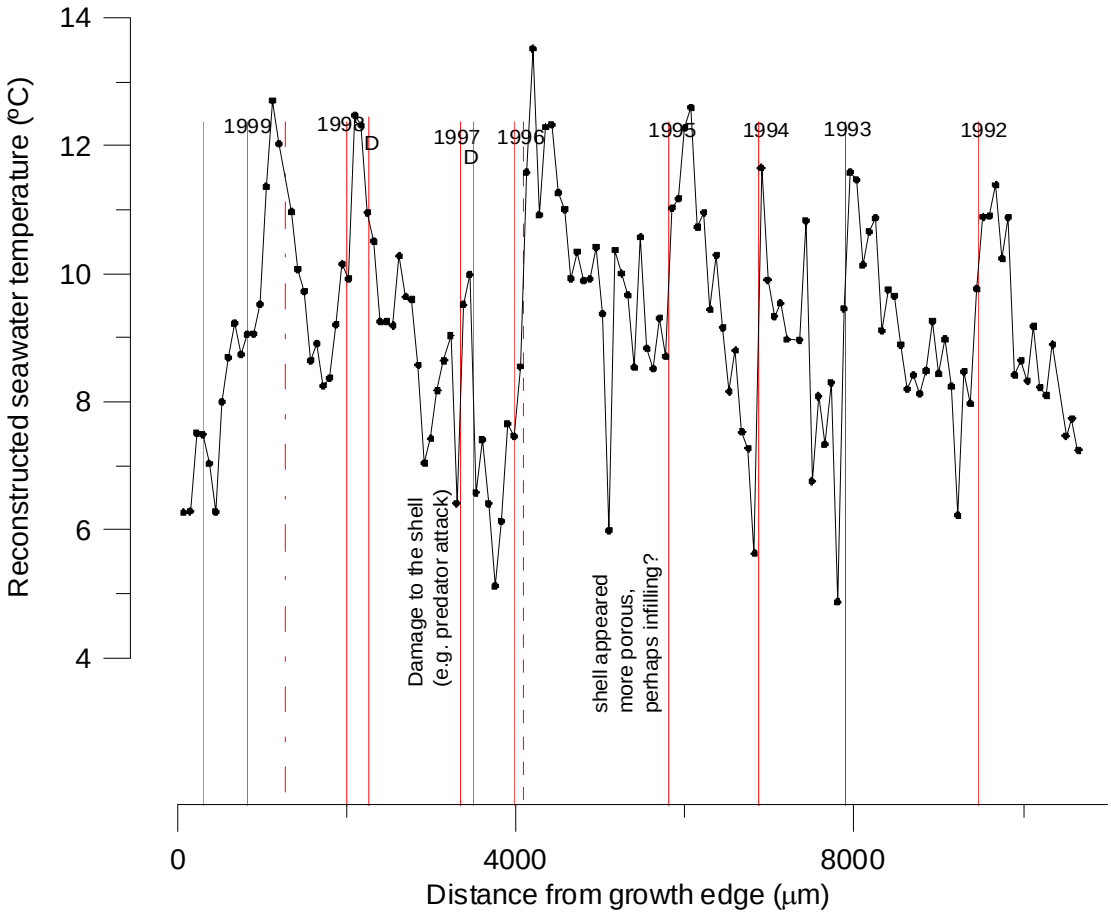

Figure 6.9b: Reconstructed temperature from $\delta^{18}O$ measured from outer shell prismatic layer of shell 248. The dashed line indicates the start of the annual growth check. The dot-dash lines indicate intra-annual bands, i.e. increased organics. Note the temperature calculation assumes a constant salinity. The maximum fluctuation of the salinity during the year is 1.2 (equating to ~2.1 ˚C) taken from measurements in Irvine Bay) at 7 m with the average salinity taken for calculating the constant used (see text for more details) i.e. the error on the temperature calculation due to an assumed constant salinity should be <1.1 ˚C. The damage to the shell could be seen visually (see Figure 4.20).

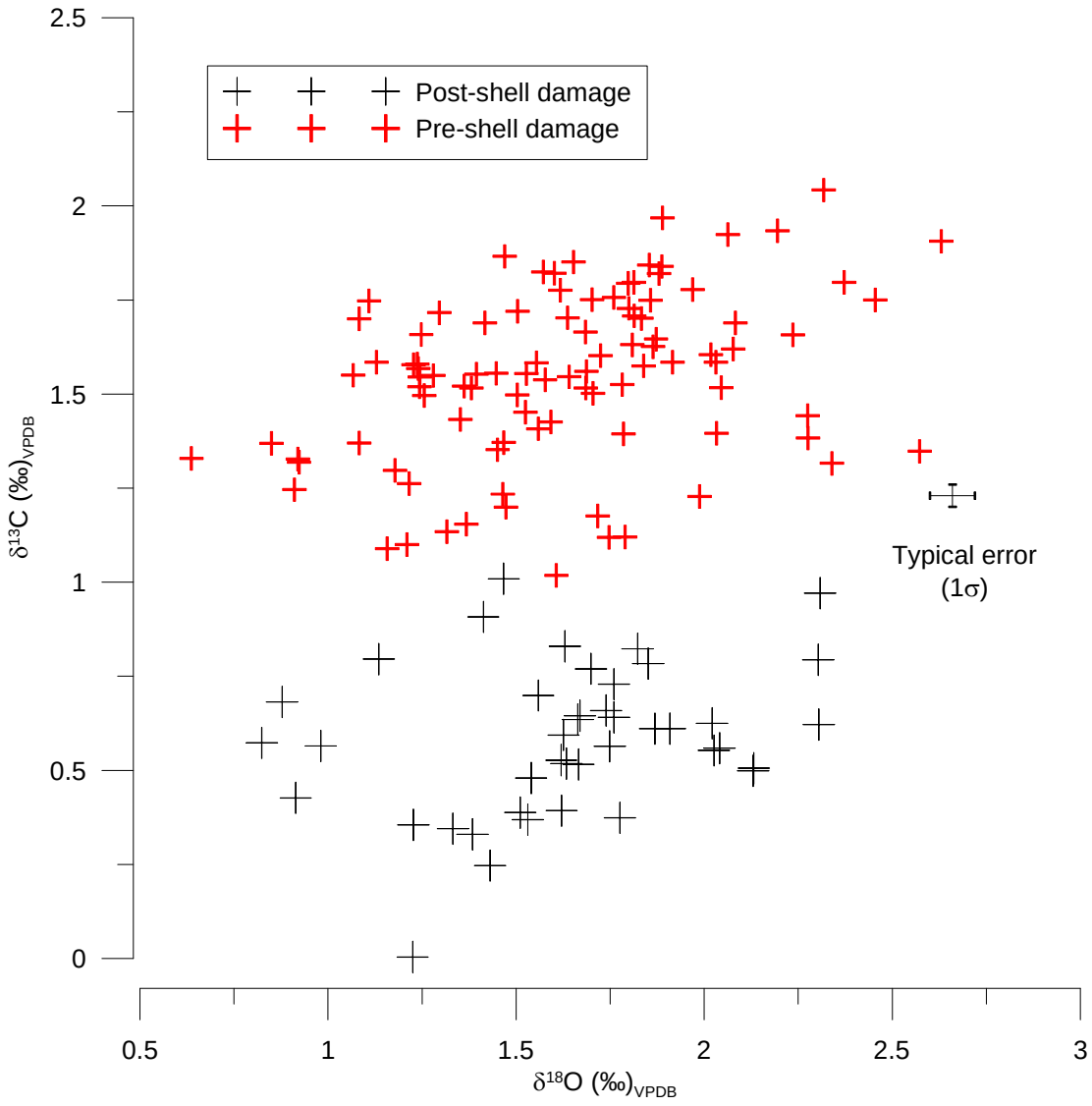

Figure 6.10: Plot of $\delta^{18}O$ versus $\delta^{13}C$ results from the outer shell prismatic layer of shell 248. The typical error (1σ) is calculated from the reproducibility of the carrera standard. After the shell is damaged, there is a significant shift (~1 ‰) in overall $\delta^{13}C$.

mass spec order number	sample reference	Sample group	Distance from periostracum (μm)	Distance from growth edge (μm)	$\delta^{13}C$ Mean $(‰)_{VPDB}$	$\delta^{18}O$ Mean $(‰)_{VPDB}$	mean $\delta^{13}C$ for each sample group, with 2σ
LF06_105	13c-1	1	250	500	1.44	1.35	
LF06_107	13c-2	1	250	500	1.55	1.74	
LF06_114	13c-3	1	250	500	1.59	1.38	1.53 ± 0.16
LF06_97	13c-4	1	1000	500	1.22	1.58	
LF06_102	13c-5	1	1000	500	0.98	1.50	
LF06_99	13c-6	1	1000	500	0.93	1.81	1.04 ± 0.31
LF06_100	13c-7	1	1000	500	Lost during mass spec analysis		
LF06_108	13c-15	3	250	3000	1.71	1.40	
LF06_109	13c-16	3	250	3000	1.90	1.33	
LF06_96	13c-17	3	250	3000	1.88	1.67	1.83 ± 0.21
LF06_111	13c-18	3	1000	3000	1.79	1.33	
LF06_104	13c-19	3	1000	3000	1.87	1.61	
LF06_115	13c-20	3	1000	3000	1.87	1.37	1.84 ± 0.09
LF06_101	13c-8	2	250	10000	1.99	1.71	
LF06_98	13c-9	2	250	10000	2.08	1.92	
LF06_112	13c-10	2	250	10000	2.15	1.66	
LF06_103	13c-11	2	250	10000	2.19	1.86	2.10 ± 0.18
LF06_106	13c-12	2	1000	10000	2.07	1.46	
LF06_110	13c-13	2	1000	10000	1.99	1.49	
LF06_113	13c-14	2	1000	10000	2.06	1.63	2.04 ± 0.17

Table 6.3: $\delta^{13}C$ results from PL228 of samples taken across bands 250 μm and 1000 μm from periostracum to look at possible variation in $\delta^{13}C$, which may be indicative of changes in metabolic pumping. The mean of each set of aliquots (i.e. taken at approx the same distance from the periostracum at the same distance from the growth edge) are given in the final column with the standard deviation (2σ) of the 3-4 aliquots. The reproducibility of the aliquots (calculated from the carrera carbonate standard) was ±0.06 ‰ and ±0.12 ‰ for $\delta^{13}C$ and $\delta^{18}O$ respectively (1σ).

6.5 Discussion

6.5.1 $\delta^{18}O$ variation in PL405

The outer shell prismatic layer of shell 405 was sampled at a coarse resolution due to the large sample size required and the drill bit thickness. It should also be noted that the drill bit results in more material sampled from the centre of the drill hole than compared to the edge (i.e. the drill hole is not flat at the bottom). Aliquots therefore covered >2 years during the last 12 years of growth, with overlaps between aliquots also occurred due to the shape of the drill pit. However, these temporal overlaps were often difficult to assess due to the depth of drill holes. This would have been particularly significant at the slower growth rate (where small shift in distances can result a significant shift in the time material was deposited). These issues, combined with the discontinuous sampling produced by the drill inhibit in-depth analysis of fluctuations, but rather provide an overview of the stable isotope record in this shell.

The $\delta^{18}O$ values typically vary from +1.2 to +3 ‰ (Figure 6.7), which using the equation of Grossman and Ku (1986) gives a reconstructed temperature range between +3.1 and +11.1 ºC using constant salinity of 33. The constant salinity is calculated from the mean of the *in situ* sporadic measurements from Irvine Bay using the salinity at 7 m (no data was available at 6 m) between 1990-1996. The instrumental measurements in Irvine Bay may differ slightly from the site where the *A. islandica* were sampled (which was at a depth of 6 m), as the salinity and temperature measurements were taken in a water depth of >30 m.

The earliest part of the shell shows the best temporal detail because of its faster growth rate. Here the oxygen isotope record typically shows a saw tooth profile (not though 1978-9). This pattern is consistent with a model whereby increasing water temperature in the spring reduces the carbonate $\delta^{18}O$ value incorporated into the shell.

This is then followed by a slowing or cessation of growth during summer (due to low food supply). The reduction in growth rate influences the temporal resolution of the sampling and hence the shape of the $\delta^{18}O$ profile. Growth rate then (recommences and) becomes faster during the early autumn, when the sea temperatures reach their maximum, followed by a decrease in temperature through the winter when growth significantly reduces or ceases. Thus, changes in the $\delta^{18}O$ profile can be induced simply by changes in growth rate, which changes the temporal resolution of the sampling. The impact of growth rate variations has been recognised as an issue when sampling at interannually frequency, and this has been addressed with adaptive sampling whereby the same temporal resolution per aliquot is achieved by changing the spatial resolution (e.g. Schöne *et al.*, 2005a).

6.5.2 $\delta^{18}O$ variation in PL228

PL228 shows high degree of variability between the two samples with differences in sample pairs seen in both $\delta^{18}O$ and $\delta^{13}C$, although the former shows a greater offset. The two aliquots were taken directly from the milling plate, and the lack of heterogeneity suggests that the mixing of the aliquot was not sufficient on the milling plate. An alternative technique such as mixing the sample within the solution-ICPMS vials and then sub-sampling would be used for future studies. Note the lack of heterogeneity reflects the large sample milled, and is not an issue for other samples, as for all other samples the whole aliquot was measured. It does however, provide some indication of the timing of deposition and will be discussed in Chapter 8 in relation to the results of solution-ICPMS analysis.

6.5.3 $\delta^{18}O$ variation in PL248

Analysis of PL248 provided the most detailed record of stable isotope variations (Figure 6.9). The oxygen isotope record shows the lowest values just prior to the winter growth check (+~1 ‰), with the highest values immediately after the annual growth check (+~2.5 ‰). The $\delta^{18}O$ variation in PL248 shows a greater fluctuation than that seen in PL405 or PL228, which probably reflects the increased resolution. Reducing temporal resolution dampens $\delta^{18}O$ variations e.g. Goodwin *et al*. (2003), and has lead to adaptive sampling e.g. Schöne *et al*. (2005a).

The salinity variation within Irvine Bay is 1.2 with a mean of 33 (1990-1996). Calculation of the temperatures using the equation of Grossman and Ku (1986), using a constant salinity of 33 gave a variation of temperature 4.9-13.5 °C with instrumental data showing that Millport SST varied 6.3-15.6 °C for the whole year (between 1992-2001). Assuming the shell has continuous linear growth throughout the year (i.e. growth rate is constant) the $\delta^{18}O_{shell}$ and the temperature profile are plotted on Figure 6.11. The plot shows that while there is some agreement between the profile, *A. islandica* does not show the same temperature pattern seen within the SST, with a sharp decrease from the maximum temperature to the minimum, indicative of a shell shutdown during the winter months.

Lower salinity would result in decrease in $\delta^{18}O_{seawater}$ and therefore an increase in temperature reconstruction of ~1.2 °C for 0.6 change in salinity, i.e. the maximum error on temperature reconstruction due to salinity reconstruction is ~1.2 °C. Assuming the minimum salinity and minimum temperature occurred simultaneously, this would result in an increase in the temperature reconstruction to +6.1 °C. Conversely, a higher salinity at the maximum seawater temperature would lead to decrease in the maximum temperature to 12.3 °C. Therefore the lower temperature are

within error of 1.2 °C (the standard deviation (2σ) found between the snapshot Irvine Bay data and that of Millport), however the maximum temperature is not. However, SST temperatures in the summer are particularly susceptible to diurnal warming, and therefore it is unsurprising that benthic waters do not see the full range of summer temperatures seen at the sea surface. Comparison to the SST measurements from Millport to *in situ* instrumental Irvine Bay measurements during the summer months, show the latter is typically cooler by >0.7 °C (there is no systematic offset in the winter).

The reconstruction also assumes that *A. islandica* grows when $\delta^{18}O$ incorporation would be at the maximum and minimum. However, researchers such as Schöne *et al*. (2005b) have found that *A. islandica* has two growth seasons, with a hiatuses during mid-September to mid-November, with a winter shut down mid-December to mid-February. Cessation in growth between mid-December to mid-February may affect the lowest temperature recorded, as Millport data shows February to have the lowest SST.

Cessation in growth during the year would also explain the saw tooth profile seen *A. islandica* from Irvine Bay as well as that seen in the results of Schöne *et al*. (2005a). Schöne *et al*. (2005b) hypothesised that the growth hiatuses from mid-September to mid-November was due to spawning, but it is not clear whether *A. islandica* reproduce annually, with Thórarinsdóttir (1990) finding recruitment occurred every 20 years.

Changes in food supply could also cause a reduction in growth rate, with Witbaard (2007, Pers. Comm) finding food supply was the main control on growth, with *A. islandica* able to grow even in water temperatures of 2 °C. During the spring and autumn months during the phytoplankton blooms growth rate would be expected

to be the fastest, with slow or cessation of growth during the summer months and winter months due to lack of food. The timing of the growth slowdown/cessation could therefore affect the maximum and minimum temperatures recorded. In addition, the minimum in $\delta^{18}O_{shell}$ occurs just prior to the growth check, closely followed by the maximum $\delta^{18}O$. This may result in a significant reduction of the reconstructed maximum and minimum temperature due to loss of temporal resolution.

Between 1992-1994, the maximum reconstructed temperature in all three years was ~11.5 °C, 11.6 °C 11.8 °C. SST measurements from Millport were ~+13.8 °C for 1992 and 1994, but for 1993, the maximum temperature was ~1 °C cooler. In other words, $\delta^{18}O$ profile is not accurately reflecting variation between years although the reconstructed range is just outside error. Comparison of the minimum temperatures 1992-1994 shows that the values of the winter growth check of 1993, is the coldest year in the SST record (<5.9 °C) as well as in *A. islandica* (5.9 °C). However, the reconstructed temperature in 1992 is higher than 1994 (by ~0.4 °C), but the opposite is found with SST (1994 is ~0.6 °C higher). While the difference between 1993 and 1994 is just within the error of the salinity variation, but no significant differences were noted between years. This indicates that the temperature reconstructions are more sensitive to lower temperatures than higher temperatures, which may be a reflection of a summer shutdown in growth or as discussed previously summer months measurements were typically cooler at 7 m in Irvine Bay by >0.7 °C. Note that there was no clear difference during the winter months.

Goodwin *et al*. (2003) modelled $\delta^{18}O$ fluctuations in the bivalve *Chione cortezi* from the Gulf of California and concluded that isotopic amplitudes and averages may reflect decreases in growth rate rather than environmental fluctuations.

Therefore understanding the interactions of changes in temporal resolution with changes in temperature and salinity is important. Therefore, by constructing a simple model the interaction and relative importance of changes in temporal sampling due to changes in growth rate, temperature and salinity can be better understood. This is important to understand if future studies are to examine the accuracy of empirical equations such as Grossman and Ku (1986).

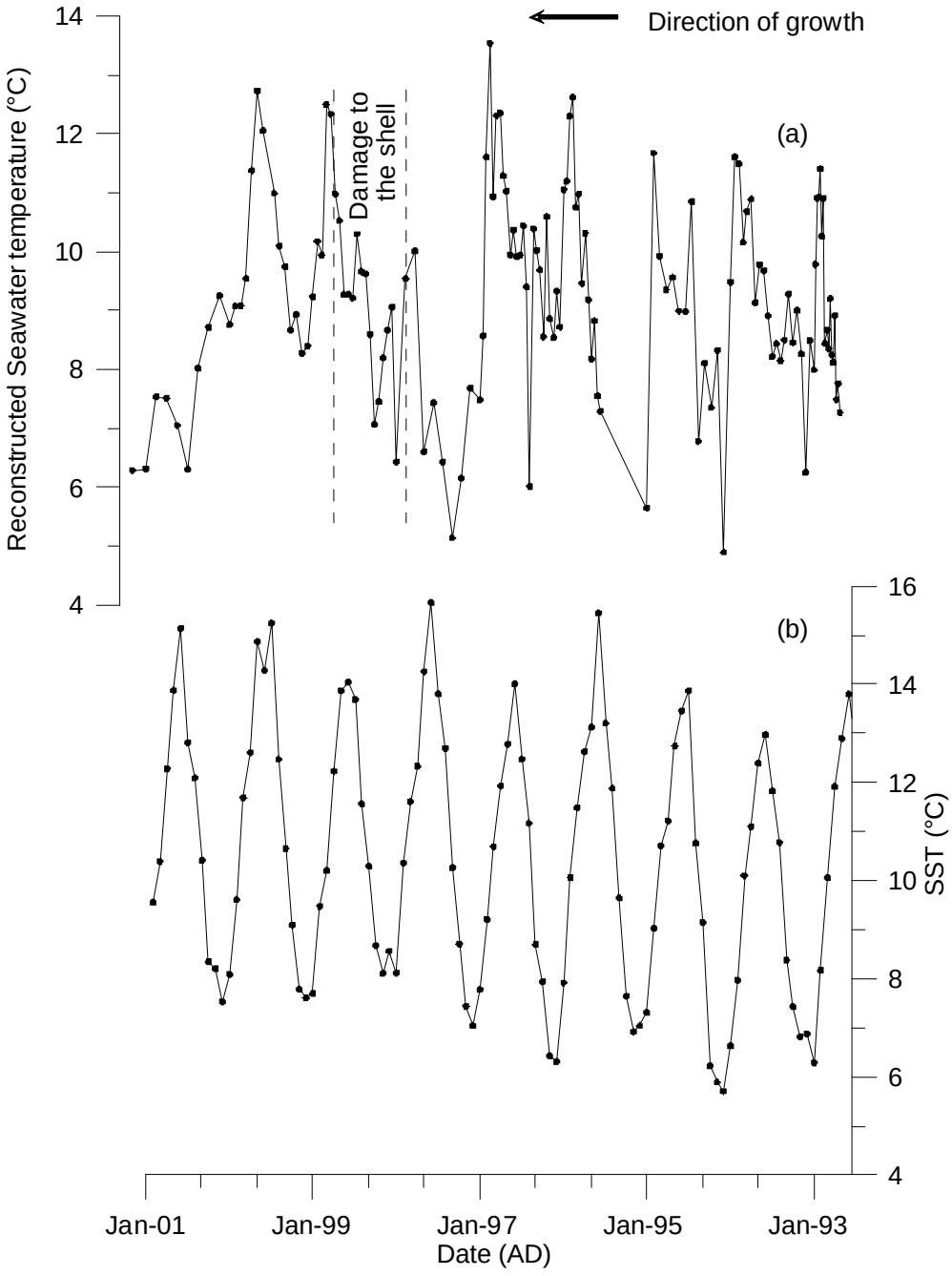

Figure 6.11: Comparison of (a) $\delta^{18}O$ measurements from the outer shell prismatic layer of shell 248 compared with (b) sea surface temperature measurements from Millport marine station. The annual timescale is determined by the growth check, which is assumed to be December with continuous growth throughout the year- i.e. no growth rate changes or shutdown. The damage to the shell could be seen visually (see Figure 4.20).

6.5.4 Modelling $\delta^{18}O$

To understand better how the $\delta^{18}O$ record within *A. islandica* may be influenced by changes in temperature, salinity, and the temporal resolution of the sampling, a simple model was constructed. Temperature and salinity control on $\delta^{18}O$ incorporation is well documented (e.g. Grossman and Ku, 1986) and adaptive sampling to compensate for ontogenetic growth rate changes in the shell is well established (Schöne *et al.*, 2005a). However, the interactions between these three variables are important in interpreting the $\delta^{18}O$ profile. Since these factors do not co-vary (i.e. temperature is typically highest in late September-October, salinity during the July-August, while the fastest shell growth rate is likely to coincide with the spring and autumn algal blooms, in approximately March-April, and September-October), modelling allows one to view how changing each component may influence the shape of the annual cycle. The timing of the maximum salinity and temperature were approximated from *in situ* salinity measurements, the timing of the increases in phytoplankton was assumed to reflect typical timing of phytoplankton blooms.

Comparison of the model to the measured $\delta^{18}O$ highlights which years differ from the "norm," e.g. warmer temperatures. Modelling can also help indicate whether the assessment of the position of the annual growth bands is correct. In addition, in the case of PL248, it can help to understand how damage to the shell may impact on the $\delta^{18}O$ record.

The $\delta^{18}O$ record of *A. islandica* can be compared with a cosine model of growth rate, water temperature and salinity. The residuals of the model can be compared to historical SST from Millport marine station and differences from the model can be examined.

The relative effects of the SST and salinity components are calculated by:

$S_{mag.}COS\ (M_{com}+2\ \pi\ (M_{model} - M_{max}))/12$

Where:

S_{mag}= magnitude of influence

M_{com}= month the model commences

M_{model}= month being modelled

M_{max}= month during which maximum magnitude is reached

For the growth rate component, a very similar equation is used except that the growth function assumes two growth seasons per year, one during March and the second in September i.e.

Growth rate = $S_{mag}.COS\ (M_{com} + 2\pi(M_{model} - M_{max}))/6$

The sum of these components was scaled to reproduce $\delta^{18}O$ fluctuations, with the model then tested against the $\delta^{18}O_{shell}$ from specimen PL248. Dates were assigned to the measured $\delta^{18}O$ data, using the position of the annual bands that had been determined visually. These provided the controls for the end of each year, with dates for the commencement of growth set as 15th February, ending 15th December as proposed by Schöne *et al*. (2005b). $\delta^{18}O$ decreases just around the growth check, then $\delta^{18}O$ rises sharply at the beginning of the year, before either levelling off or showing a slight decreasing before increasing again prior to the growth check. Apart from 1999 when increased concentration of organics were noted on sampling, (indicative of slow growth) the summer shutdown is fixed to the point just prior to where $\delta^{18}O$ values begin to rise for the second time during the year. Dates between these fixed points were then interpolated linearly. The results of the model were then compared to the observed $\delta^{18}O$ fluctuations. Iteration was used to refine the relative positions of the

maximum (i.e. month) of each of the three parameters and provide the best fit. The fit parameters are shown on Table 6.4.

The starting date of the model can be adjusted by M_{com}, and it was found that starting the model 0.18 months earlier, produced a model with a better fit to the data i.e. growth recommenced 1st February (not 15th February as set initially in the model).

A model in which *A. islandica* experiences two periods of growth mostly closely fits the observed $\delta^{18}O$ curve suggesting that there are two seasons of growth. The R^2 fit between 1992-1996 is 0.32 (to 2 sf), decreasing slightly to 0.31 (to 2 sf) when 1992-2000 are included, the decrease in fit is likely to relate to the shell damage in 1998 (see Figure 6.12) during which there was infilling of material (i.e. the material was not from a sequential deposition).

	Temperature	Growth	Salinity
Mag	0.7	0.8	0.1
Max	10.1	2.8	8.9

Table 6.4: Fit parameters for modelling seawater temperature, growth and salinity (given to 1 dp). R^2 is 0.31 using the whole data set (including area damaged) increasing to 0.32 using 1992-1996 (i.e. pre-damage). Mag refers to the relative magnitude of that component; max refers to the month in which the maximum was reached.

	Temperature	Growth	Salinity
50%	0.31	0.24	0.31
200%	0.29	0.30	0.31

Table 6.5: Effect on the R^2 values when the model parameters (temperature, growth and salinity) are changed. The magnitude of the parameters of the best fit (as given above) were decreased by 50% and increased by 200% to understand the impact it has on the R^2 values.

Magnitude of the components

The relative magnitude (i.e. the amount of influence that one component has upon the $\delta^{18}O$ profile compared to the other components) is shown on Table 6.4. To highlight how changing the magnitude of these three components can influence the shape of the $\delta^{18}O$ curve, the magnitude of each was halved and doubled while the other two components were left at their optimum values (Table 6.5). Plotting these (Figure 6.12) shows the effect that each parameter has on the overall profile.

The profile is relatively insensitive to changes in salinity, suggesting that even within shallow water sites such as Irvine Bay; the $\delta^{18}O$ is not significantly affected. Variations in the growth-rate and seawater temperature produce the most pronounced effect. Goodwin *et al*. (2003) modelled $\delta^{18}O$ fluctuations in a bivalve (*Chione cortezi*), concluding that isotopic amplitudes and averages may reflect decreases in growth rate rather than environmental fluctuations. This reduced growth rate associated with ontogenetic effects has lead to "adaptive sampling" by researchers such as Schöne *et al*. (2005a). However, this present study highlights that not only does inter-annual variability that needs to be considered, but also the intra-annual variation, i.e. changes in temporal resolution of sampling caused by changes in growth rate may occur not just through ontogenetic changes in growth rate, but also during a single year.

Temperature and food availability account for ~65% of variation in shell growth (Schöne *et al.*, 2005a). Food supply in turn may be influenced by the North Atlantic Oscillation through changes in current flow leading to resuspension of organic particles (Schöne *et al.*, 2003) or through changes in copepod abundance, with copepods reducing the amount of food available to bottom dwellers such as *A. islandica* (Witbaard *et al.*, 2003).

Conversely differences in the growth season compared to modern day specimens are an important consideration when examining $\delta^{18}O$ results from older specimens e.g. specimens from the Clyde Beds, Lochgilphead, SW Scotland, covering 14,000 and 11,500 calendar years before present (Peacock *et al.*, 1977) which grew during a time of extremely rapid climate change.

Timing of components

Our model and $\delta^{18}O$ data suggests that the growth season for *A. islandica* within these shallow water sites is modified by a growth check during the summer months (June-August) rather than mid-September to mid-November as reported by Schöne *et al*. (2005b). A shutdown timing as proposed by Schöne *et al*. (2005b) was modelled but the fit factor decreased by ~20%. Other alternative models were tried including no growth check and a growth check only during the winter, but the model presented here provided the best fit. The data of Schöne *et al*. (2005b) would imply a growth season of <1.5 months (i.e. one-eighth of the growth season) which does not appear to be the case from our modelled results. This would not be unreasonable as Irvine Bay is a shallow water site and therefore the controls on the biological productivity may differ to that found within the North Sea.

Comparison of the model to PL248

The model calculates the typical $\delta^{18}O$ seen during a year, i.e. the same magnitude and timing of changes in temperature, salinity and growth parameters are applied to each year. Therefore, discrepancies between the model and actual data, may highlight an atypical year, and thus may indicate areas for further research.

A discrepancy between the model and data occurs between 1999 and 2001. The annual growth during this period is very small (<500 μm), and the magnitude of the $\delta^{18}O$ fluctuations are dampened (as expected) but in favour of heavier $\delta^{18}O$ values. Further work on other specimens would be required to discern if this was a general effect and whether it related to changes in the biological growth season, the result of reduced sampling or inaccuracies in the modelling.

The residuals of the modelled $\delta^{18}O$ and measured $\delta^{18}O$ records (Figure 6.13) highlight three particular years, 1993, 1997 and 1998, in which the model provides a poor fit. Comparison to the temperature record from Millport shows that during May 1993, the average temperature was ~1 ºC cooler than the average which would equate to an increase in $\delta^{18}O$ of ~0.35 ‰, approximately the offset seen in the model.

Shell damage occurs at the end of 1997 would explain why the reconstructed temperature is lower than that record at Millport, with damage resulting in the loss of growth which occurred during the maximum temperature and/or caused growth cessation during the maximum seawater temperatures. Interesting the damage to the shell is associated with a decrease in $\delta^{18}O$. *A. islandica* incorporates any material available to repair the damage; including sand grains (see Witbaard, 1997). It is however unclear what $CaCO_3$ material would be incorporated. This would be extremely interesting as if $CaCO_3$ material is solely generated by the organism i.e. not from external sources, it suggests that such stress events could affect $\delta^{18}O$ uptake.

During the first part of growth in 1996, $\delta^{18}O$ differs from that predicted by the model. Although shell damage and visible infill occurs at the end of 1997, it is possible that the material deposited here is also affected by a disturbance. Review of the laboratory notes taken during the milling reported that this area appeared to have a different texture appearing “more porous” than surrounding material, although there

was no sign of infill. This, combined with comparison to the model suggests that material here may be also been affected. Further research would be required to determine if this was indeed the case.

The earlier part of 1997 also shows heavier $\delta^{18}O$ than in other years. Comparison to the SST at Millport shows that 1997 was not colder than other years. It is unclear why this is. It would initially suggest that the area damaged is greater than that noted in laboratory notes, or it could reflect that the growth season commenced earlier in the year and was therefore subject to colder temperatures. The reconstructed temperatures and measured SST is estimated to be 1 °C cooler, which would however fit with the earlier discussion that this could be due to lower salinity during winter. Therefore, in fact, it is providing a more accurate temperature reconstruction, and it is in fact earlier $\delta^{18}O$, which are overestimating the temperature.

The model provides an indication of the main controls on the $\delta^{18}O$ record. Such processes provide insights into the sensitivity of the *A. islandica* isotope record to changes within the environment, as well as effects of growth rate and shell damage. It also provides an independent assessment of the validity of the visual identification of the growth checks. It can also show that changes in the growth rate are an important consideration for future research into vital effects on $\delta^{18}O$ uptake. In faster growing *A. islandica*, daily growth bands can be identified which may help to constrain the record better temporally (Schöne *et al*., 2005b).

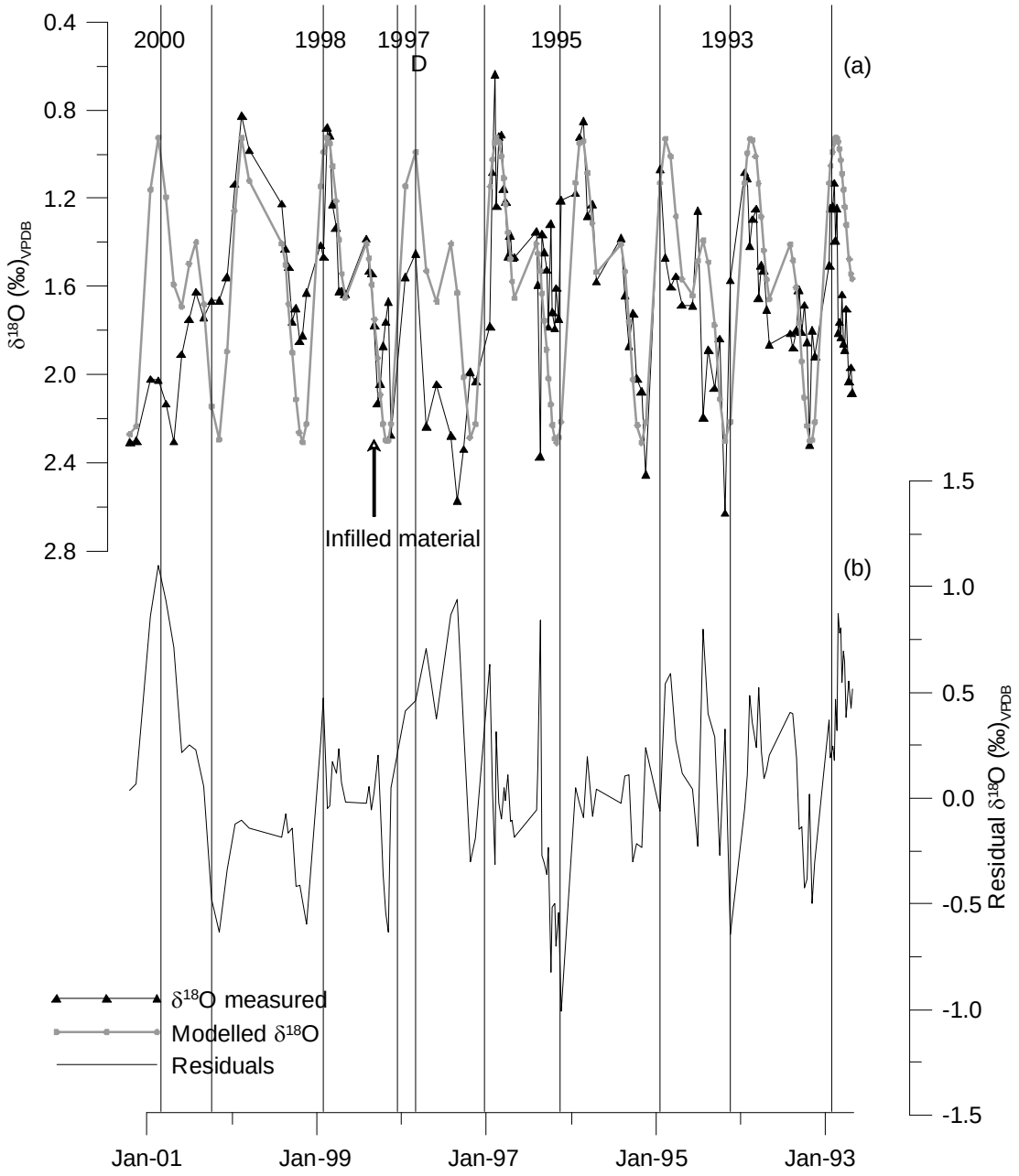

Figure 6.12: Upper figure (a) shows the plot of $\delta^{18}O$ model (pink) with the plotted $\delta^{18}O$ data (blue), with the residuals plotted on the lower figure (b). The poor fit 1997-1998 is likely to be due to shell damage, affecting the growth rate and subsequent infilled material just after the 1997 growth check.

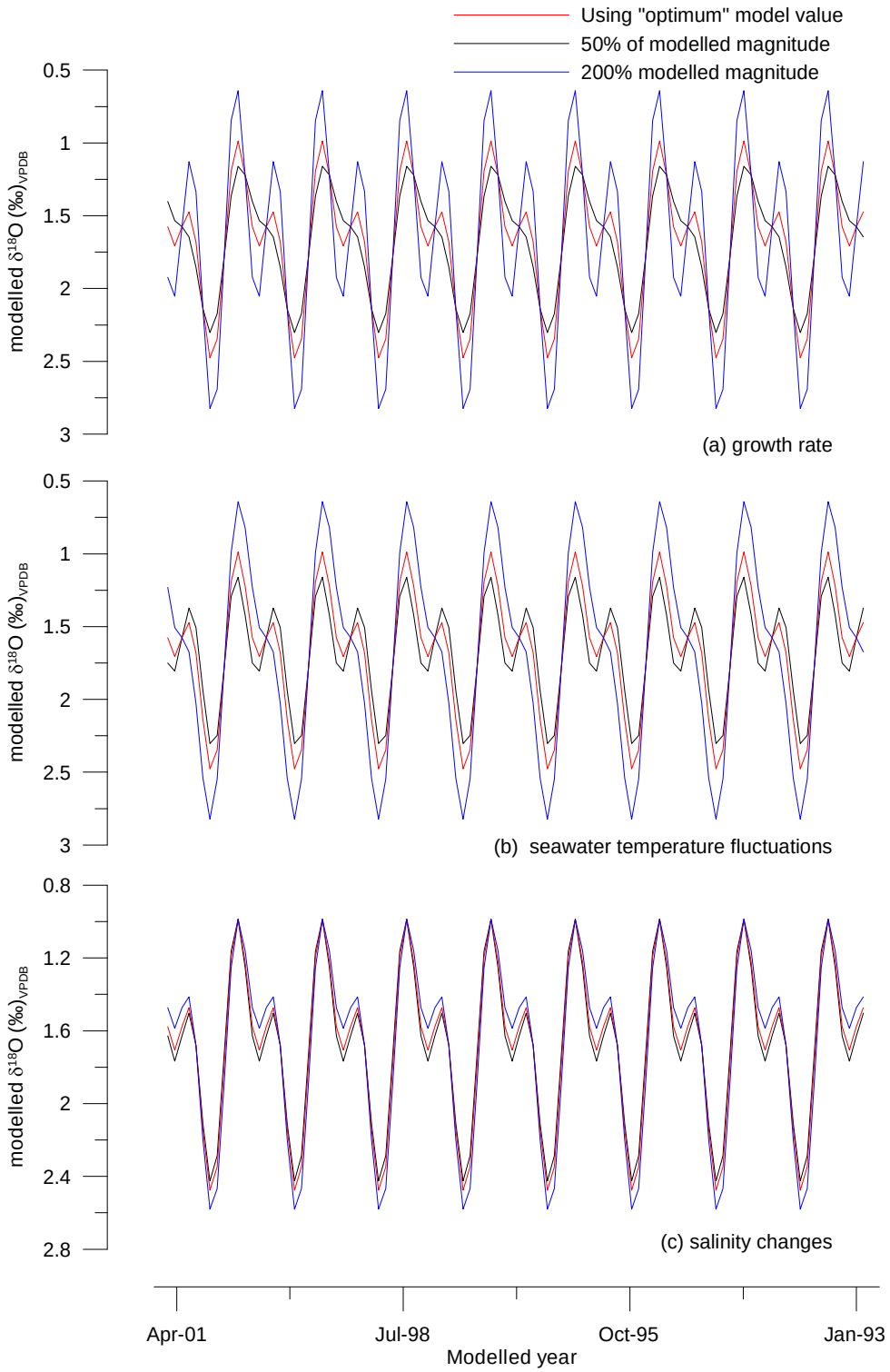

Figure 6.13: Modelling controls on $\delta^{18}O$ in PL248. The impact of halving and doubling the strength of the controls from the optimum values given in Table 6.5 of (a) growth rate (b) seawater temperature and (c) salinity. Note that variations in salinity have little effect on the final profiles.

6.5.5 $\delta^{13}C$ variation through the shell

$\delta^{13}C$ shows a decrease with age in all three specimens (Figure 6.7, 6.8, 6.9a). The whole lifespan of specimen PL405 except the first 7 years of growth (when the bands were too narrow) was analysed, and with analyses of PL228 and PL248 covering only the last 9 years of growth. PL228 and PL248 are very similar in age (23 vs. 18 years), but the former is the much faster growing (and hence larger) of the two specimens. The magnitude of the decreases in $\delta^{13}C$ of shell with age differs greatly (even when comparing the same years), e.g. specimen PL248 shows a decrease from +1.8 ‰ to <+1 ‰ 1993-2000 whereas specimen PL405 decreases from +1.4 ‰ to ~+0.5 ‰ over the same period. However, the age of these specimens differs, shell 248 was 22 years old in 2000, shell 405 was 32 years old, with *A. islandica* in Irvine Bay typically living to <40 years old. As $\delta^{13}C$ declines with age as the growth rate decreases, and PL248, with slowest growth rate shows the lowest $\delta^{13}C$ suggesting that growth rate is an important factor controlling $\delta^{13}C$ value.

Inorganic experiments of Romanek *et al*. (1992) have shown that the equilibrium fractionation of ^{13}C for aragonite relative to $HCO_{3(aragonite\text{-}bicarbonate)}$ is +2.7 ± 0.6 ‰. In order to determine how the fractionation, which occurs on uptake, it is necessary to estimate the dissolved inorganic component of $\delta^{13}C$ within the water ($\delta^{13}C_{DIC}$). No $\delta^{13}C_{DIC}$ data however was available for Irvine Bay. $\delta^{13}C$ measurements by Gillikin *et al*. (2005b) which were taken in the estuarine conditions of Puget Sound (Washington, USA) (salinity range 0-28) gave a $\delta^{13}C$ relationship of 0.57 * Salinity - 16.54. If this were extrapolated for a salinity of 33, it would give a $\delta^{13}C_{DIC}$ of 2.3 that would give an estimated incorporation of $\delta^{13}C_{DIC}$ of 4 ‰ using the inorganic fractionation of Romanek *et al*. (1992). Owen *et al*. (2002) reported a depletion of up

to 2 ‰ in *Pecten maximus* (calcitic bivalve) from the Menai strait, Irish Sea, which infers an initial $\delta^{13}C_{DIC}$ of 3.5 – 4 ‰. $\delta^{13}C$ measurements within *A. islandica* from Irvine Bay show a maximum $\delta^{13}C$ of 3 ‰ (PL405), suggesting $\delta^{13}C_{shell}$ could be depleted relative to $\delta^{13}C_{DIC}$ in the water. The ontogenetic decrease in $\delta^{13}C$ PL405, also seen in PL228 and PL248, indicates that $\delta^{13}C$ values do not simply reflect $\delta^{13}C_{DIC}$, but there is incorporation of metabolic $\delta^{13}C$ (e.g. Tanaka *et al.*, 1986; McConnaughey *et al.*, 1997; Dettman *et al.*, 1999).

These findings would be in agreement with results from *Pecten maximus* (Lorrain *et al.*, 2004), which showed a decline in $\delta^{13}C$, which was attributed to an ontogenetic increase in the contribution of metabolic CO_2 to skeletal carbonate. Schöne *et al*. (2005a) however found no ontogenetic changes in $\delta^{13}C$ in *A. islandica*, whereas Witbaard (1997) did finding an increase of >1.5 ‰ (from ~+0.8 to ~+2 ‰). Comparison of the specimens used in each study showed the latter sampled a 6 year old juvenile specimen (with faster growth rate) whereas Schöne *et al*. (2005a) sampled an older, slower growing specimen. The findings of Witbaard (1997) would agree with those of McConnaughey (1989) and Klein *et al*. (1996a) who found higher $\delta^{13}C$ at slower growth rates. The cause of the difference is unknown, but may relate to the difference in habitat or growth rate, with specimens from the North Sea growing slower than those from Irvine Bay do.

During and after damage to the outer shell prismatic layer, the $\delta^{13}C$ record in PL248 shows a sharp decrease of >0.5 ‰. This observation is a strong indication that metabolic rate has a key influence. McConnaughey *et al*. (1997) proposed that metabolic carbon can account for ~10% of the $\delta^{13}C$ signal in molluscs, and other researchers have supported this conclusion (Owen *et al*., 2002; Lorrain *et al*., 2004; Gillikin *et al*., 2005b). However, the results presented here suggest that, in times of

stress, this percentage can be considerably higher, with $\delta^{13}C$ in PL248 showing a decrease of >50% after damage to the shell occurred, and a change in $\delta^{13}C_{seawater}$ of this magnitude is unlikely and is not recorded in PL228. Comparison of $\delta^{18}O$ and $\delta^{13}C$ (Figure 6.10) show no correlation either before or after the shell damage indicating that while $\delta^{13}C$ is affected by metabolic changes, there appears to be no impact on $\delta^{18}O$.

Although respiring organisms consume $^{16}O^{16}O$ 10 to 20 ‰ more rapidly than $^{18}O^{16}O$, resulting in a pool of ^{18}O-depleted CO_2 and cell H_2O, the large cell water reservoir and large water fluxes across the membrane may cancel out this effect (McConnaughey, 1989; Bijma *et al.*, 1999). Thus, incorporation of CO_2 can lower $\delta^{13}C$ but probably does not affect $\delta^{18}O$ (Bijma *et al.*, 1999).

6.5.6 Lateral variation in $\delta^{13}C$

The results of $\delta^{13}C$ taken from PL228 laterally across three single bands initially do not categorically show whether $\delta^{13}C$ varies across a band (Table 6.3). However, analysis of samples closest to the growth edge was difficult as the shell was very fragile and sampling was not solely from the milling line (as the shell fractured during sampling). In addition, as the bands are so close it is difficult to position accurately the mill to ensure inclusion of the same growth band in each lateral sample. Therefore, this set of results should be discounted. The other datasets show that the $\delta^{13}C$ values show no relationship to distance from the periostracum, being within error (2σ) of each other e.g. aliquots taken 3000 μm from the growth edge show $\delta^{18}O$ values of 1.83±0.21 ‰ and 1.84±0.9 ‰ when 250 μm and 1000 μm from the periostracum respectively (see Table 6.3). If there are changes in the metabolic

pumping within different sections of the shell, it should be reflected within the $\delta^{13}C$ record, with a more negative $\delta^{13}C$ caused by the addition of ^{12}C enriched metabolic CO_2. These findings suggest that either $\delta^{13}C$ values are largely independent of metabolic activity, which appears not to be case (see above). Alternatively, and more likely therefore is that there is no difference in metabolic pumping rates within different areas of the same band suggesting that EPF is well mixed. This is important for interpreting the lateral change in trace elements measured in *A. islandica*.

6.6 Conclusion

$\delta^{18}O$ within shell 248 varied from +1 ‰ to +2.5 ‰ giving a reconstructed range of seawater temperatures for 1992-2001 of 5-13 ºC, with an error of <1.1 ˚C due to the use of a constant salinity (calculated from the mean of sporadic salinity measurements in Irvine Bay). Measured SST in Millport Marine station for the same period was between 6.3 and 15.6 ˚C, indicating the range is typically within 2.1 ˚C. However, it appears that *A. islandica* does not grow during the whole year, and as well as a growth check during the winter months, there may be a slowdown during the year as well which may account for the poorer reproducibility of the warmest temperatures. Particularly noticeable was that the range of temperatures intra-annually was not consistent with the variation in instrumental SST, i.e. the coldest years reconstructed from $\delta^{18}O$ were not the coldest years measured by SST, suggesting that it is relatively insensitive to intra-annual temperature variation.

The data are consistent with a model whereby $\delta^{18}O$ is relatively insensitive to changes in salinity even within shallow water sites but is sensitive to changes in temporal resolution resulting from changes in growth rate. In particular, “adaptive sampling” may need to take into account intra-annual variation in growth rate and not

just ontogenetic changes, and the impact such changes may have on recorded $\delta^{18}O$. Any changes in biogenic fractionation could not be discerned. Improvements in the sampling (e.g. use of daily bands) may be significant for understanding any possible impacts it has on $\delta^{18}O$ temperature reconstructions.

Ontogenetic changes in $\delta^{13}C$ are seen in all three specimens, but the absolute $\delta^{13}C$ and the rate of decrease varied between shells. There is no evidence of changes of $\delta^{13}C$ across a single band that might imply changes in metabolic pumping laterally across a band. The timing of the $\delta^{13}C$ increases does not seem to correlate with position in the band (i.e. the season), nor with the $\delta^{18}O$ record. PL248 shows a sharp decrease in $\delta^{13}C$ after it sustained damage to the outer shell prismatic layer, suggesting that metabolic rate can have a strong controlling influence with a decrease in $\delta^{13}C$ of 50% after damage to the shell was sustained.

Acknowledgements

Thanks are given to Marine station at Millport who provided temperature records and to SEPA (in particular Brian Miller) who provided the environmental data for Irvine Bay. Personal thanks are given to Rune Søraas, Ulysses Ninnemann and Jonathan Wynn for invaluable assistance with analysis of samples in the mass spectrometer, as well as to Michael Bird who helped to significantly improve the chapter. Analysis at the Bjerknes centre was supported by a Marie Curie Training Fellowship (EVK2-GH-00-57123-10).

CHAPTER 7: TRACING THE UPTAKE OF RADIOCARBON IN *ARCTICA ISLANDICA*.

Abstract

The potential of *Arctica islandica* to provide high-resolution radiocarbon measurements within the marine environment is explored through a pilot study of ^{14}C incorporation from a shallow water specimen from Irvine Bay, UK. The increase in atmospheric radiocarbon in the 1950s associated with the testing of thermonuclear devices provided researchers a way to track the uptake of the carbon by tracing "bomb pulse" ^{14}C. This area is also affected by discharge from the Sellafield nuclear power and reprocessing plant. Results show that the ^{14}C signals overlap, with elevated pre-bomb ^{14}C concentrations likely to relate to Sellafield discharges. With only a single specimen in this study, further work is required.

7.1 Introduction

Arctica islandica has the potential to provide a high temporal resolution record of ^{14}C variations. This chapter presents the results of a pilot project measuring ^{14}C fluctuations in a live-collected specimen from Irvine Bay, west coast of Scotland from the 1950s to the present day.

In the 1950s, the atmospheric denotation of thermonuclear weapons, prior to the Nuclear Test Ban Treaty in August 1963, produced large numbers of neutrons that generated a distinctive "peak" of radiocarbon known as the "bomb pulse" (e.g. Hesshaimer *et al.*, 1994; Levin and Kromer, 1997; Levin and Hesshaimer, 2000).
However, Irvine Bay may also be affected by discharge from the Sellafield nuclear facility on the Cumbrian coast (Figure 7.1), which has been in operation since the 1950s. The discharges into the Irish Sea were not initially monitored, which together with a number of accidental discharges, has meant the quantity and extent of the area affected by radioactive material, including ^{14}C is unknown. Thus, this pilot project explores whether influences from Sellafield nuclear and reprocessing plant can be identified, independent of increases due to the bomb pulse. A comprehensive survey of *A. islandica* ^{14}C along the West coast of Britain could compare ^{14}C variation with increasing distance from Sellafield in order to separate bomb pulse effects and discharge from Sellafield. This is beyond the present study but rather this chapter explores the potential for such a study in the future.

7.1.1 Sellafield facility

Sellafield facility was put into commission in 1950. Sellafield has had several recorded accidents, including one in 1983 when high discharge concentrations of nuclear waste in the Irish Sea lead to the closure of beaches >20 km north and south

of Sellafield (Martiniussen, 2001). The discharge of medium-level radioactive liquors containing nuclides such as ^{14}C, ^{99}Tc, and ^{129}I increased between 1985 and 1995 due to the processing of these materials instead of storage onsite. This discharge is now reduced by ~75% (Royal Irish Academy, 2002). Discharge of ^{99}Tc is shown on Figure 7.2 (no data was available on ^{14}C).

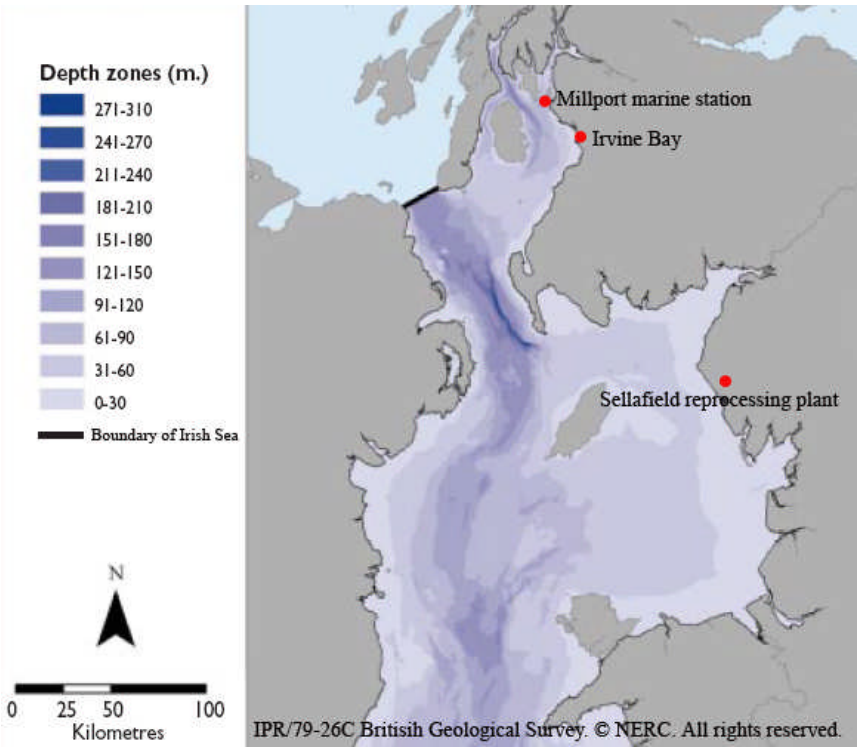

Figure 7.1: Map of the locations of Sellafield reprocessing plant together with Irvine Bay, and Millport Marine station (modified from Lieberknecht *et al.*, 2004 with permission from the Geological Survey).

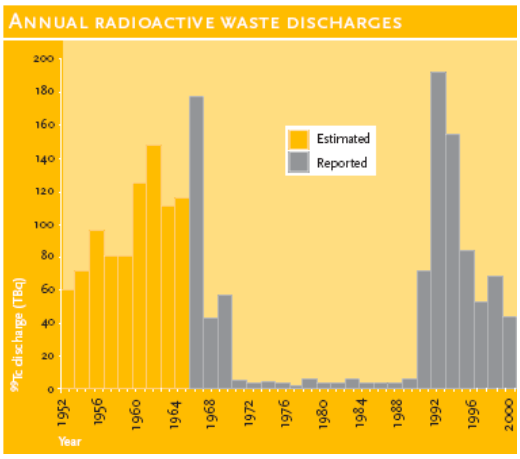

Figure 7.2: Discharge from Sellafield of ^{99}Tc published by Royal Irish Academy (2002) (Data compiled from Gray *et al*. (1995) and BNFL (1980-2001)).

7.1.2 Bomb pulse

In the Northern Hemisphere, the peak in atmosphere bomb-produced ^{14}C occurred in 1963 compared to ~1965 in the Southern Hemisphere with radiocarbon concentrations about 100% above normal concentrations in the troposphere (Nydal *et al.*, 1979; Nydal and Lövseth, 1983; Taylor, 1987). The amount of local and global fallout after each explosion was initially unknown (Nydal, 2000). The increase in radiocarbon is recorded within both terrestrial and marine records with the magnitude and speed of the migration of the bomb pulse reflecting the rate of exchange between carbon reservoirs. In the Northern Hemisphere, elevated radiocarbon concentrations were found in the terrestrial system within about three weeks (Nydal, 2000).

The concentration of bomb radiocarbon recorded in the oceans is far from uniform. Higher concentrations are recorded in temperate regions and the North Atlantic, compared with the Antarctic and North Pacific, due to lateral transport from upwelling regions (Broecker *et al.*, 1985). Thus, the movement of radiocarbon provides a tracer to test models of oceanic circulation and to quantify the oceanic

invasion of excess CO_2 produced by anthropogenic deforestation and fossil fuel consumption (Bard *et al.*, 1989).

7.1.3 Reporting changes in radiocarbon, post-bomb

Changes in radiocarbon post-bomb are often defined as $\Delta^{14}C$. This is derived from A_{SN}/A_{abs} where A_{SN} is the normalised sample activity and A_{abs} is the absolute international standard activity which is 95% of activity in 1950 AD of the NBS (National Bureau of Standards) oxalic acid normalised to $\delta^{13}C$ (see Stuiver and Polach, 1977). The disadvantage of this system is that a sample grown for example in 1962 will give a different $\Delta^{14}C$ if measured today compared to 1962 (Reimer *et al.*, 2004). The difference between the two is presently very small (Reimer *et al.*, 2004). Data quoted from other papers are reported as presented, (i.e. without correction). Results from ^{14}C work presented here are reported as % modern, which is defined as: A_{SN}/A_{ON}, where A_{ON} is the activity of the international standard (oxalic acid). This implicitly corrects for isotopic fractionation ($\delta^{13}C$ values corrected to –25 ‰), decay of the standard (oxalic acid II in this case) from 1950 to the year of measurement decay of the sample, and from year of collection to year of measurement.

7.1.4 Reconstructing the bomb pulse

Research on the bomb pulse has focused heavily on land-based (e.g. tree rings) reconstruction of ^{14}C concentrations. This has produced numerous datasets that show the uptake of radiocarbon in the terrestrial system to be very similar, with no significant latitude dependence (Goodsite *et al.*, 2001). Unfortunately, marine datasets are much more limited, with one of the constraints being the identification of suitable marine material for radiocarbon measurement.

Corals from low latitudes, which can provide sub-annual records, have therefore been extensively studied. Coral ^{14}C records from Belize and Florida show nearly identical uptake of bomb-pulse ^{14}C. Those from the Galapagos, Pacific however, show a lower ^{14}C bomb pulse. This results from the upwelling of subsurface water which lowers the $\Delta^{14}C$ by >100 ‰ (Druffel and Suess, 1983; Druffel, 1996). The change of $\Delta^{14}C$ due to the incorporation of non-contemporary ^{14}C is known as the "reservoir effect." Upwelling water, which has been isolated from the atmosphere long enough to result in ^{14}C decay, changes the $\Delta^{14}C$ of the surface water.

Belize and Florida corals record a maximum of ^{14}C uptake in 1966, a few years after the peak in the atmosphere. The time delay results from the time required for the ocean to reach a steady state with respect to $^{14}CO_2$ exchange, i.e. the time it takes for carbon in the atmosphere to exchange with the ocean and be incorporated into the coral to form $CaCO_3$.

A more rapid decline in ^{14}C sea surface concentrations occurs at higher ocean latitudes, due to a more frequent exchange with the deep ocean. However, apart from the two sets of radiocarbon measurements taken by research cruises in the North Atlantic (GEOSECS 1972-1973) and Transient Tracer in the Ocean (TTO, 1981-1982) (Ostlund and Grall, 1987), no further real-time data were collected at the higher latitudes. Thus, there is a need for reconstruction of the dispersal of bomb-pulse at higher latitudes, using archives such as *A. islandica*.

7.2 Uptake of ^{14}C in A. islandica

Molluscs build up shells with carbon from two sources; bicarbonate dissolved in seawater (DIC) and food particles (Mangerud *et al.*, 2006). Most food particles will have the same reservoir age, as they are normally part of the marine food chain that

started with phytoplankton assimilating carbon. However Tanaka *et al*. (1986) showed that in a coastal setting, up to 60% of the carbon within mollusc shell $CaCO_3$ was derived from food consisting of remnants of terrestrial plants, sewage particles etc. This has lead to the term "food reservoir age" (Mangerud *et al.*, 2006). However *A. islandica* are filter feeders and hence should derive their carbon directly from seawater dissolved inorganic carbon (Cage *et al.*, 2006). Work by Ascough *et al*. (2005) found no significant offset in radiocarbon concentrations between different mollusc species, despite utilising a different variety of food.

7.2.1 Existing data on A. islandica

Researchers have already carried out a number of analyses on *A. islandica*. These are detailed in Table 7.1, with the locations shown on Figure **7.**3.

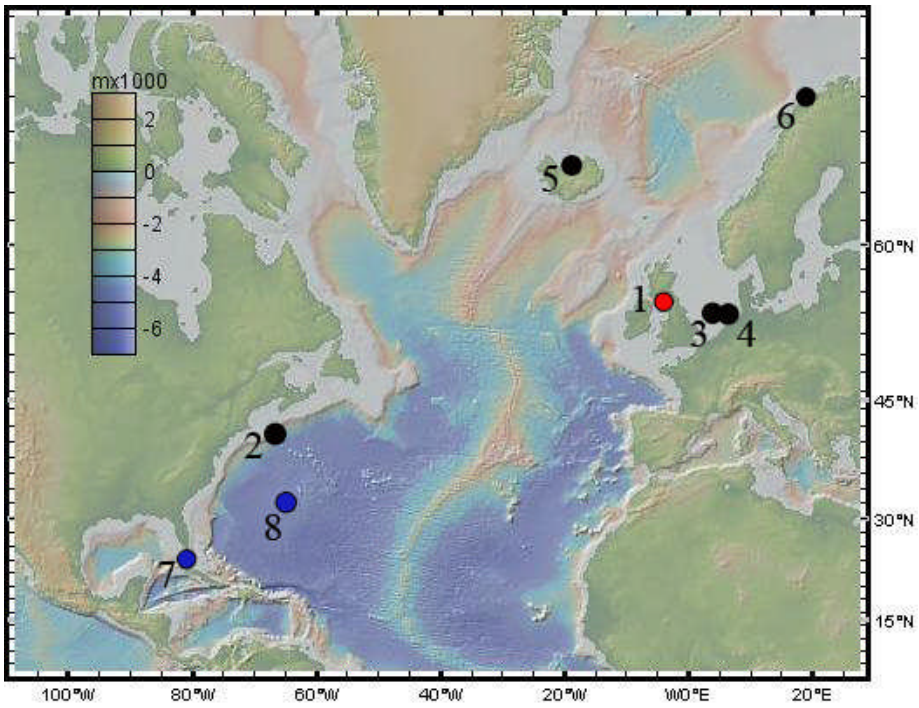

Figure 7.3: Map of *A. islandica* sites with published ^{14}C studies. *A. islandica* sites are shown in black, with red depicting the site of present study. The blue spots mark data from coral sites. The numbering refers to that given in Table 7.1.

Weidman and Jones (1993) used a live-collected specimen from the Georges Bank off the coast of North America to reconstruct bomb ^{14}C at a resolution of 1-2 years. Comparison with the low latitude corals of Bermuda and Florida showed that the exchange at Georges Bank was more rapid occurring 1-2 years earlier, but more suppressed. This can be explained by waters in the region being supplied by a deep (depleted) source, but with a fast exchange on a shallow shelf (Weidman and Jones, 1993). In addition, the "Great Salinity Anomaly" which occurred throughout the northern North Sea (1968-1982) is reflected in the $\Delta^{14}C$ concentrations, showing the link between deepwater formation and surface salinity in the high-latitude North Atlantic (Weidman and Jones, 1993).

Weidman (1993) used multiple shells to illustrate that, although the bomb pulse arrived relatively synchronously across the North Atlantic, its magnitude varied. Iceland has the smallest amplitude increase (~120 ‰), with the North Sea the largest (~320 ‰). The variation in ^{14}C enrichment a function of local and regional mixed layer depth (Weidman, 1993). *A. islandica* samples from the Oyster Bank show a ^{14}C peak much earlier than those from Georges Bank. This is due to a strong tidal front in the North Sea that increases vertical transport (Witbaard *et al.*, 1994; Witbaard, 1997). Thus, radiocarbon analysis can provide strong evidence of water circulation within a region.

7.3 Samples

A. islandica samples were collected live from Irvine Bay, NW Scotland in May 2001. This shallow marine site (6 m below O.D.) is likely to have a rapid exchange with the atmosphere. Thus, ^{14}C measurements would be expected to show a high ^{14}C shortly after the bomb pulse, followed by a rapid decline. Apparent slower

exchange could be attributed to the carbon coming from a secondary source (e.g. exchange with deeper water). In addition, this site (Figure **7.**1) is ~150 km north of the Sellafield. Hence, reconstructions of ^{14}C movement and concentrations using *A. islandica* would have value in providing estimates of the environmental impact of the Sellafield site over time.

A number of samples were sectioned along the line of maximum growth and replicate peels were taken (see section 1.2.2 for more details). The number of annual bands and position were noted. Specimens from Irvine Bay were found to be typically 30-40 years old, which was younger than had been initially expected from their size (those in Fladen Ground of similar size are typically 150 years+). The oldest sample collected was 50 years old (shell 389), and therefore this was used for analysis. As the bands in the first five years of growth were too narrow to enable sampling by microcorer, the oldest sampling corresponded to 1957. An alternative sampling method- micromilling was attempted to sample the youngest years to increase the number of years sampled, however the narrowness of the bands and the high risk of contamination from inner layers/ later growth prohibited this. The earliest part of the shell was more intensely cored in order to provide the most detail during these earlier growth bands and to pick up as much pre-bomb and bomb pulse as possible.

Samples were collected by microcorer from shell 389. Coring has the advantage that it provides a solid sample, which can be etched at the AMS lab just prior to the sample being hydrolysed. Thus, it would provide a pristine sample. Initial work on the stability of aragonite in *A. islandica* had highlighted the possibility of exchange with modern CO_2 due to the conversion of the sample to calcite. The effect of micromilling and possible exchanges with the atmosphere are explored extensively in Chapter 5. A 3.7 Ma year old *A. islandica* specimen was also sampled; the ^{14}C

concentrations should be below the limits of detection to determine if there was any exchange with modern CO_2. In addition, it was specified that the sample should cover a single year (Austin, Pers. Comm. 2005). The samples were stored under argon prior to analysis at SUERC radiocarbon laboratory, East Kilbride, UK.

	Sample type	Site location	Latitude	Longitude	Water depth (m)	No. of specimens	Years covered (maximum extend)	Reference
1	*Arctica islandica*	Irvine Bay, Irish Sea	55° 45'N	4° 54'W	6	1	1956-1993	Current study
2	*Arctica islandica*	Georges Bank, Labrador Sea	41°N	67°W	76	1	1939-1990	Weidman & Jones, 1993
3	*Arctica islandica*	Oyster Bank,North Sea	54°N	4°E	30-50	4	1826-1988	Witbaard, 1997
4	*Arctica islandica*	German Bight, North Sea	54°N	6°E	~37	2	1948-1990	Weidman, 1993
5	*Arctica islandica*	Siglufjodur, Iceland	66°N	19°W	22	3	1872-1991	Weidman, 1993
6	*Arctica islandica*	Tromsø, Norway	70°N	19°E	3	1	1940-1993	Weidman, 1993
7	coral	Florida	24°N	81°W	4			Druffel et al 1989
8	coral	Bermuda	32°N	65°W	10			Druffel et al 1989
	Atmospheric	central Eastern North Atlantic			n/a			compiled by Weidman, 1993

Table 7.1: Details of radiocarbon specimens discussed in this chapter.

7.4 Method

7.4.1 Microcoring

The microcorer provides a stable platform from which a small core (maximum length ~2 mm, with variable width- typically 0.5 mm) can be taken (Figure 7.4). The microcorer tip rotates around a central axis, with a motor attached to the geological stage so it also rotates at high speed. Material is gradually removed, leaving a central column exposed, which can then be removed (Figure 7.5). The width of the axis of rotation will determine the top core width. As the depth increases however, the size of the crater around the core increases. This results in the loss of progressively larger amounts of the surrounding material. In order to compensate for this, a core for each of the 18 aliquots were taken, and then sampling for the 2nd set of cores were taken (i.e. sampling for the first aliquot was done again after a short core had been taken for all the other aliquots) and the material summed into a single aliquot.

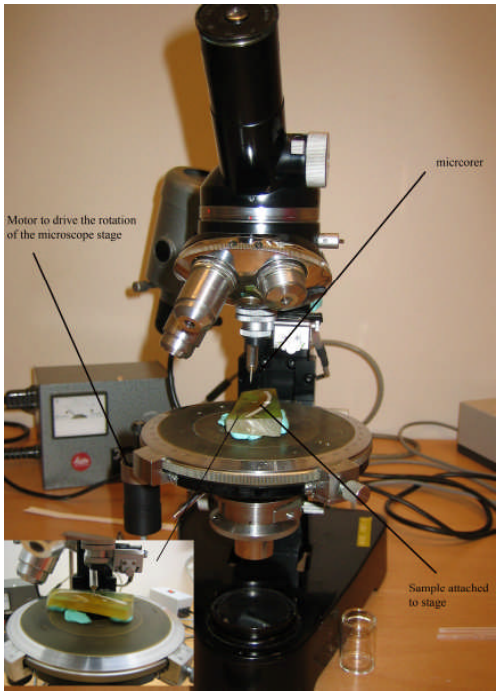

Figure 7.4: Photograph of Microcorer sample with a sample attached.

Despite doing this, the aliquots were below the minimum sample size of 6 mg required at SUERC radiocarbon facility UK. Therefore, adjacent cores had to be combined to provide some indication of radiocarbon fluctuations within the shell giving nine ^{14}C analyses (see Table 7.2). This was unfortunate but no further material was available from this shell. It was also not possible to etch the samples prior to analysis. In addition to the samples, two further cores were taken: one from Iceland Spar Calcite (laboratory standard, age is >100 ka), and a second core from a 3.7 Ma year old *A. islandica* specimen from Tjörnes Bed, Iceland. These provide checks on contamination during processing and storage of the sample prior to analysis, since neither should have measurable ^{14}C.

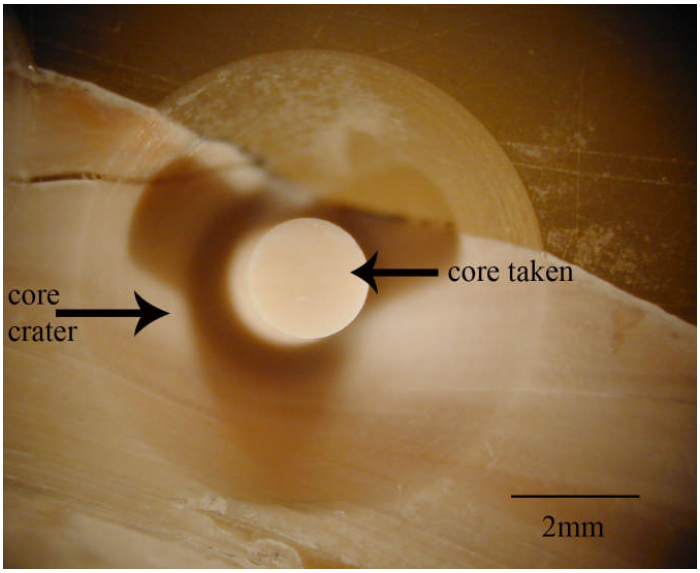

Figure 7.5: Reflected light micrograph showing the core sample from 389. The size of the crater is 2-3x the width of the core. The shell is in the lower half of the image, with the epoxy resin in the upper half.

7.4.2 Radiocarbon Analysis

Radiocarbon samples were processed and analysed by SUERC AMS facility, East Kilbride, UK, using the following procedure. Samples were hydrolysed to form CO_2 using 85% orthophosphoric acid at 25 °C. The CO_2 was condensed, vaporised and then converted to graphite by Fe/Zn reduction (Slota *et al.*, 1987). Graphite was pressed into aluminium cathodes and analysed using the SUERC 5MV NEC AMS (Ertunç, Pers. Comm. 2006).

7.5 Results and Discussion

The results of the ^{14}C analysis of the Iceland Spar calcite (Table 7.2) showed it was statistically indistinguishable from the NERC radiocarbon laboratory's inorganic background, indicating no contamination of ^{14}C during analysis (Gulliver, Pers. Comm. 2006). However, the 3.7 Ma year old *A. islandica* specimen shows slightly elevated concentrations of radiocarbon. It is not possible to discount the possibility of exchange of carbon with atmospheric CO_2, but the study of $\delta^{18}O$ (see Chapter 5) suggests that is not the case. The $\delta^{18}O$ values of the otoliths showed that there was no shift in the $\delta^{18}O$ values, indicating that there was no exchange with the atmosphere. Although radiocarbon aliquots were taken using coring rather than micromilling, it is likely that these findings are also applicable to coring (as like micromilling it uses a drill bit to remove the material). The slightly elevated concentrations of ^{14}C may be attributed to epoxy within the pores of the specimen as epoxy was seen to have impregnated the shell, which due to its age was highly porous. Samples of epoxy analysed in the mass spectrometer showed the presence of CO_2 on reaction with phosphoric acid. Shell 389 did not show any visual evidence of epoxy impregnation

and therefore the risk of contamination is likely to be minimal. Further analysis would be required to confirm this finding.

The AMS data show ^{14}C maxima between 1971-1974 in the Irvine Bay specimen (Table 7.2). Atmospheric central Atlantic data shows the $\Delta^{14}C$ maxima at 750 ‰ in 1964 (Figure 7.6). The bomb pulse initially appearing about 1959 (± 1 year) in North Atlantic *A. islandica* $\Delta^{14}C$ records, followed by a steep rise during the early to mid-1960s, with a maxima in the late 1960s to the late 1970s (Weidman, 1993). Although the Irvine Bay sample also shows a steep-rise in the early 1960s, with a maximum in the early 1970s there are two crucial differences to the results of Weidman (1993) and Witbaard (1997). The first is that the values of $\Delta^{14}C$ in the Irvine Bay samples are much higher than would be expected pre-1960. All other marine samples show values <0 ‰, whereas Irvine Bay samples show >30 ‰.

Atmospheric data indicate that the elevated concentrations of $\Delta^{14}C$ shown in the shells pre-1960 (see Figure 7.6) could be due to rapid exchange with the atmosphere, but this is unlikely for two reasons. Firstly, the maximum $\Delta^{14}C$ values found within *A. islandica* from Irvine Bay do not significantly exceed those from other sites. In other words, if the exchange with the atmosphere were extremely rapid, the maximum $\Delta^{14}C$ found in these specimens would be significantly higher than those in other *A. islandica* sites, as the ^{14}C concentrations would be less affected by ^{14}C-depleted water. Secondly, Weidman *et al*. (1994) found the $\Delta^{14}C$-bomb signature of Norwegian specimens to be weaker than that of deep water specimens of Witbaard (1997) despite being sampled at 3 m. These data show that the local hydrography plays an important role. Another hypothesis is that the coastal setting of the Irvine Bay samples may result in elevated ^{14}C concentrations, due to terrestrial input. However, as discussed earlier, *A. islandica* derives its carbonate from DIC (Cage *et*

al., 2006). Terrestrial ^{14}C is also unlikely to be the cause of the continued elevated concentrations after the bomb peak (i.e. post 1970). Therefore, it would suggest that Sellafield provided significant (>30 ‰) ^{14}C to the *A. islandica* specimen prior to the bomb pulse.

Another explanation for the presence of ^{14}C prior to other *A. islandica* sites could be due to errors in the sclerochronology. Independent analysis of the sclerochronology at the umbo put the age at 47 + 3-5 years for ligament correction (the ligament correction is applied to compensate for the fact that early growth years that are eroded). This would place the specimen at a minimum of 50 years (our age estimate was 50 years). It could therefore be that 2-3 bands in the outer shell prismatic layer (classified as sub-annual/disturbance lines) may in fact be annual bands, actually increasing the age of the specimen. Typically, errors in the sclerochronology for this age of specimen would be 2-3 years. Therefore, the increase in *A. islandica* prior to the other sites is most likely due to Sellafield discharge.

The maximum in ^{14}C is reached between 1965 and 1972, which is generally consistent with other *A. islandica* ^{14}C data (e.g. Weidman and Jones, 1993; Witbaard, 1997) (see Figure 7.7). Unfortunately, the poor resolution of data makes it impossible to ascribe a precise date to this maximum. The ^{14}C peak is higher than that of any of the other sites from which ^{14}C in *A. islandica* data have been reported (by ~15 ‰). It is likely the actual peak in ^{14}C was higher, especially given the initial offset between the Irvine Bay and other samples was >30 ‰. In addition, the continued elevated values of ^{14}C in the Irvine Bay data, suggests that Sellafield discharges influence the ^{14}C concentrations in this region. There are no primary data on ^{14}C output from Sellafield but estimates of ^{99}Tc discharge show significant flux from 1952-1969 but a sharp decrease 1970-1990 (Figure 7.2). These data, combined with the ^{14}C

measurements, could indicate that Sellafield was discharging material containing both ^{99}Tc and ^{14}C. However, perhaps more likely, the coincidence may reflect prevailing management attitudes to the discharge of medium-level radioactive waste into the environment. The period from 1990 onwards shows an increase of ^{99}Tc discharge due to increased processing of medium radioactive waste onsite. It is therefore likely that significant discharges of ^{14}C from Sellafield are superimposed on the bomb signature. This can be seen particularly post-1970s when all other *A. islandica* records show a decrease in radiocarbon, but whereas the specimen from Irvine Bay continues to show elevated radiocarbon concentrations. Further samples would be required to deconvolute these components further.

The use of the microcorer for sampling had severe drawbacks. It was designed to provide a better sampling technique than milling, as the sample surface could be etched prior to ^{14}C analysis. However, the coring was a difficult sampling technique to use, with the large crater and short cores meaning that a lot of surrounding sample material was lost, and therefore reducing the temporal resolution that could be obtained. In addition, the long extraction time (typically 1-2 days) increased the likelihood of cross contamination. It addition because material is removed around each core, it produces significant hiatuses in the data. Thus, the use of the micromill, which would produce a continuous record, would have been much better.

SUERC sample identifier	core reference	Years (A.D.)*		Average year (A.D.)	^{14}C enrichment (% modern)	±1σ	^{14}C Enrichment (% Modern absolute)	±1σ	$\delta^{13}C_{VPDB}$‰ ±0.1
SUERC-9926	Core 1	1956.0	1956.0	1956.5	103.81	0.45	103.14	0.45	2.60
	Core 2	1957.0	1957.0						
SUERC-9927	core 3	1957.0	1957.0	1957.5	104.17	0.45	103.49	0.45	2.50
	Core 4	1958.0	1958.0						
SUERC-9928	core 5	1958.5	1959.5	1959.2	104.38	0.45	103.70	0.45	2.30
	core 6	1960.0	1960.0						
SUERC-9929	core 7	1961.0	1961.0	1962.0	107.61	0.47	106.91	0.47	2.10
	core 8	1962.0	1963.0						
SUERC-9932	core 9	1963.0	1963.0	1964.5	116.41	0.51	115.65	0.51	2.00
	core 10	1966.0	1966.0						
SUERC-9933	core 11	1970.0	1970.0	1971.5	126.13	0.55	125.31	0.55	1.80
	core 12	1973.0	1973.0						
SUERC-9934	core 13	1978.0	1979.0	1982.0	124.15	0.54	123.34	0.54	1.20
	core 14	1984.0	1986.0						
SUERC-9935	core 15	1986.0	1989.0	1989.5	124.10	0.54	123.30	0.54	1.20
	core 16	1991.0	1993.0						
SUERC-9936	Core from *Arctica islandica* specimen			3.7 Ma	0.46	0.45	0.45	0.01	1.5
SUERC-9937	Iceland spar calcite core				0.10	0.10	0.10	2.00	2.0

Table 7.2: Sample details and results for *A. islandica* from Irvine Bay. The sample years are those determined by sclerochronology. * ages were adjusted from those originally logged after a revision in the sclerochronology. Note the ^{14}C enrichment (% modern absolute) is the ^{14}C measurement corrected for the ^{14}C decay of the standard (in this case Oxalic acid II) from 1950 to the year of measurement (2006). The years are estimated for each core, and the combined estimate of the date is shown as the "average year." The years selected for coring were intended to provide the most detail during the earliest part of the shell.

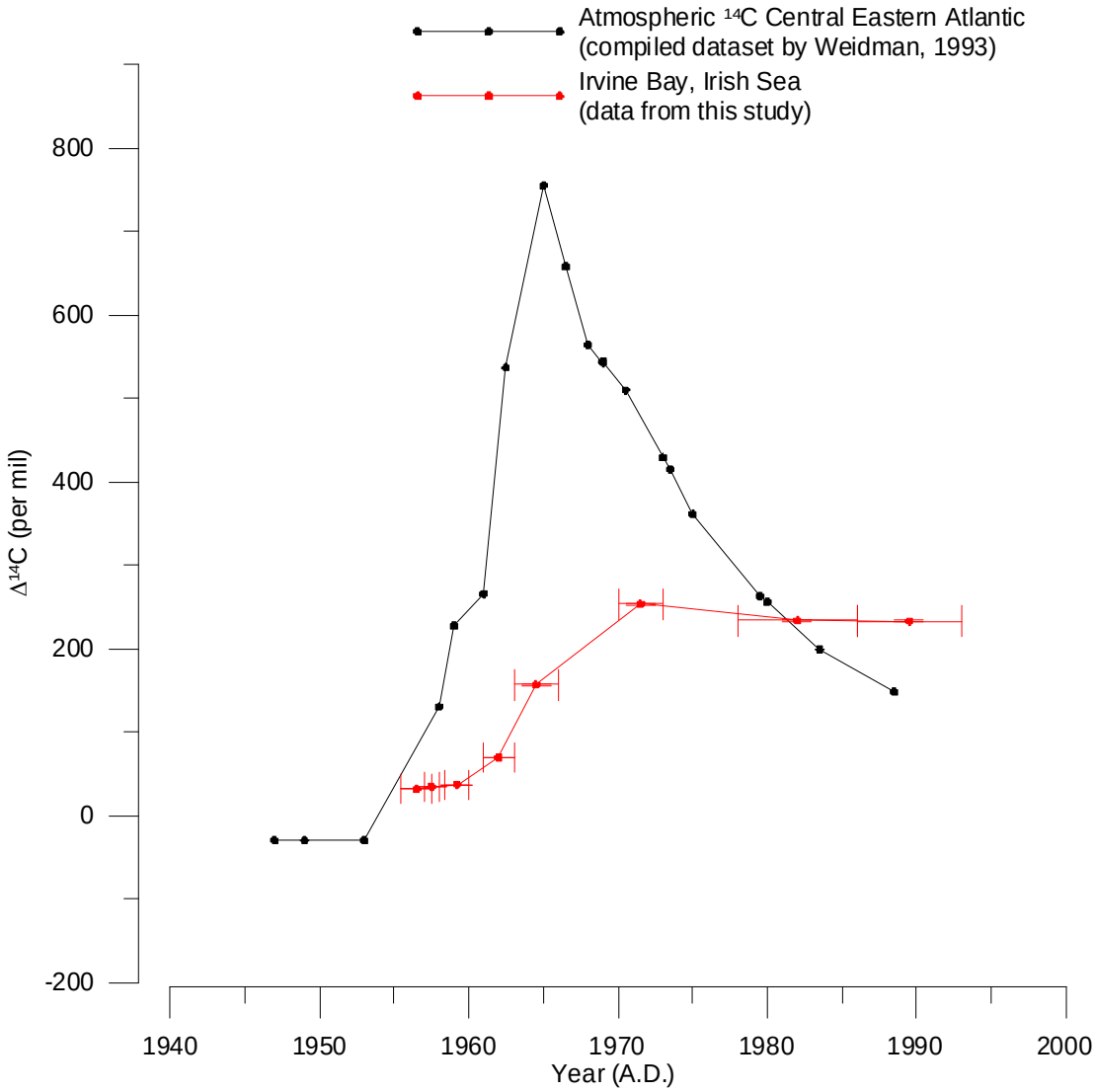

Figure 7.6: Plot of the ^{14}C results from this study (with 1σ error bar) compared to atmospheric central East Atlantic (errors in measurements were not noted by Weidman, 1993). Note that ^{14}C data cover for *A. islandica* specimen multiple but not continuous years (see Table 7.2 for more information).

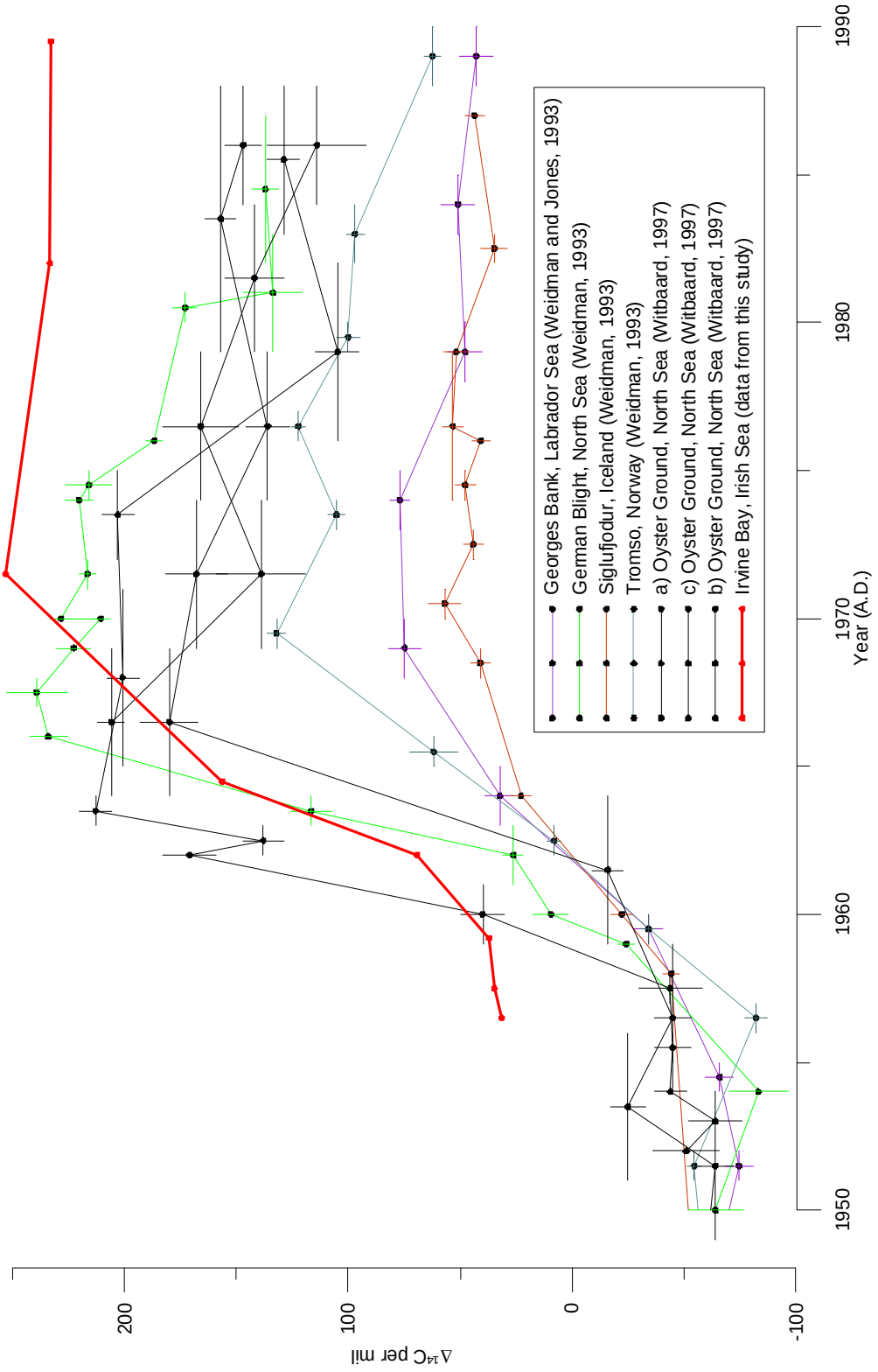

Figure 7.7: Plot of ^{14}C results from *A. islandica*, Irvine Bay compared to existing *A. islandica* datasets from 1950 onwards. Note that Irvine Bay data cover multiple but not continuous years (see Table 7.2 for more information). 1σ error is too small to be shown for Irvine Bay specimen (see Table 7.2).

7.6 Conclusion

The ^{14}C data can be interpreted in a number of ways but there is strong evidence that this site is influenced by discharge of ^{14}C from Sellafield as well as the bomb-pulse ^{14}C. Comparison to other *A. islandica* samples suggests that the elevated concentrations (of >30 ‰.) seen in pre-1960, and continued elevated concentrations throughout the sample were due to discharges from Sellafield. Further samples, such as those at different distances from Sellafield would be required to separate the bomb pulse from the discharges from Sellafield. Additional shells would also provide further confirmation of the timing of such events.

In hindsight, the microcoring was very slow since samples typically taking 2 days to core. Thus, the procedure may carry a higher risk of contamination than conventional micromilling due to longer exposure with atmospheric CO_2. The multiple cores taken with the microcoring provide an innovative way of increasing the sample size, but it would perhaps have been more appropriate to make multiple sections from which to take a core. However, the risk of a hiatus and the large craters suggest that despite the problems with handling powdered samples, micromilling (such as that used in this PhD for $\delta^{18}O$ analysis) would have been much more appropriate. Given the modern age of the samples, contamination by modern ^{14}C is less of an issue. Further work would be required to see if the slightly elevated concentrations of ^{14}C in the 3.7 Ma year old specimen were due to problems with epoxy in the micropores or due to exchange with the atmospheric carbon.

This pilot study has shown that *A. islandica* along the west coast of Britain might be an useful archive of ^{14}C from thermonuclear testing of the 1950s and from the Sellafield reprocessing plant.

Acknowledgements

This project was under the supervision of Dr. W. Austin, supported by NERC grant code 981.0402. The 3.7 Ma year old *A. islandica* specimen from Iceland was kindly provided by Jon Eiriksson, (Earth Science Institute, University of Iceland). Personal thanks are given to Tanya Ertunç and Pauline Gulliver for their invaluable support and to Philippa Ascough for her valuable comments on the chapter.

CHAPTER 8: THE POTENTIAL OF HIGH RESOLUTION PALAEOCLIMATE RECONSTRUCTION FROM *ARCTICA ISLANDICA*.

Abstract

The long-lived marine bivalve *Arctica islandica* has the potential to provide (sub-annual) high resolution palaeoclimate data. This potential has been explored during this thesis using a suite of different techniques including X-ray Absorption Spectroscopy (XAS), Secondary Ion Mass Spectrometry (SIMS), Inductively Coupled Plasma Mass Spectrometry (ICPMS), Scanning Electron Microscope (SEM) and stable oxygen and carbon isotopes with the aim of better understanding how *Arctica islandica* may encode aspects of the environment.

The three trace elements (Sr, Mg, Ba) measured show heterogeneity within the same growth band (i.e. at the same temporal position) in the prismatic layer. In the umbo, the concentrations increase away from the maximum growth axis whereas within the outer shell they decrease e.g. in the outer shell the offset is ~45% for Sr/Ca, ~30% for Mg/Ca, and ~25% for Ba/Ca for a lateral change of 750 μm.

Despite Sr being ideally substituted for Ca within aragonite, Sr/Ca fluctuations are not dominated by temperature, but rather by other controls such as changes in crystal nucleation and propagation, crystal growth rate and vital effects. Sr in *Arctica islandica* is therefore unlikely to be suitable as a palaeoenvironmental proxy of temperature.

X-ray Absorption Near Edge Structure (XANES) indicate Mg is hosted by organics and thus the manner in which Mg partitioning is modelled using inorganic equilibrium thermodynamics is flawed. Mg/Ca content in the shell results from interaction between overall organic content and Mg partitioning into the organic matrix.

Ba/Ca shows low concentrations with sporadic increases to over five times this. The timing and magnitude of these maxima correspond between the prismatic

layer of the outer shell layer and umbo region despite the lateral change in concentration. The timing of Ba peaks is inconsistent in position within the growth band and the timing between the shells differs. Low Ba/Ca may reflect Ba/Ca concentrations of seawater. Further work is required with improved precision to determine whether there is a lateral offset at low Ba/Ca concentrations.

Data from sample 248 show that $\delta^{18}O$ fluctuates between 0.6 and 2.6 ‰; which, assuming constant salinity, gives a growth temperatures of ~+5 to +13 ºC using the equation of Grossman and Ku (1986). This temperature range differs by ~2.1 ˚C from the sea surface temperature measured at the nearby Millport marine station. However, modelling of $\delta^{18}O$ is most successful when contributions from temperature, salinity and changes in temporal resolution in sampling (resulting from changes in growth rate) are employed. Since growth rate is a significant component, it is necessary to establish how variable growth seasons are, not only when comparing $\delta^{18}O$ within the same shell, but also when comparing shells from different regions or times. $\delta^{13}C$ fluctuations show a strong ontogenetic effect in all three shells sampled (with a decrease of >2.0 ‰ during the lifespan of the organism (shell 405)), but no lateral variation was found. Vital effects play an important role in the $\delta^{13}C$ behaviour, with damage in one sample (248) marked by a sharp decrease in $\delta^{13}C$ of >0.5 ‰.

Radiocarbon measurements within *Arctica islandica* show that high ^{14}C values from material formed before global nuclear testing. This is inferred to result from discharges from Sellafield nuclear reprocessing plant, values of which were enhanced by ^{14}C from the testing of thermonuclear weapons.

8.1 Introduction

This thesis studies the potential of *Arctica islandica* to reconstruct palaeoenvironmental conditions and in particular the use of trace elements using a multi-technique approach. This chapter compares trace element and stable isotope results from the prismatic layer of the umbo and outer shell region of the same individuals and interprets the data in the light of XAS data and Secondary Electron images. Further interpretation of the controls of trace element uptake is presented, as well as a discussion of the accuracy of $\delta^{18}O$ reconstructions.

8.2 Comparison of trace element fluctuations in the prismatic layer of the umbo and outer shell

Quantitative data of the composition of the prismatic layer of the umbo and shell outer layer were collected using SIMS and ICPMS respectively. Standardisation between these two methods to allow direct comparison of the data is therefore imperative. Analysis using SIMS and LA-ICPMS was carried out on a single OKA chip using both methods, the results of which are shown on Table 4.7. An offset occurs in the calculated concentration of SIMS compared to LA-ICPMS. The latter provides values that are >24% greater for Sr/Ca, >15% greater for Mg/Ca, and >20% less for Ba/Ca with respect to data collected by SIMS. These offsets are likely to be due to the different matrices of the standards used in calculating absolute values within *A. islandica*. LA-ICPMS concentrations were estimated with respect to rhyolite glass (NIST610) standards whereas SIMS data were calculated using relative ion yields from an OKA calcite standard. Neither set of standards comply with the matrix of the *A. islandica*, an aragonite intimately mixed with varying amounts of organic material,

and hence systematic matrix offsets (between LA-ICPMS and SIMS data and between both datasets and 'true values') are to be expected. This offset needs to be taken into consideration when comparing the two regions of the shell. All SIMS and LA-ICPMS data are presented here without correction.

Understanding how trace element behaviour may differ between the two regions of the shell is important as it provides insights into the controls on trace element uptake e.g. growth rate, nature and amount of organics etc. As discussed in Chapter 3 and 4, a lateral compositional gradient is present within the prismatic layer. However, the umbo shows an increase away from the maximum growth, while the outer shell layer shows a *decrease*. If the lateral change of both regions is driven by the same mechanism, shell growth rate can be discounted as the cause.

Lateral changes in the shell architecture, may influence trace element uptake. For example, changes in organic concentration may influence directly Me^{2+} if it is hosted by the organics e.g. Mg (Chapter 2). Organic content may have a further, indirect effect by exerting a control over the nucleation and propagation of the crystal and with the matrix acting as nucleation surface and predefined mould, determining size and orientation of the crystals (Watabe and Wilbur, 1960; Belcher *et al.*, 1996; Mann and Ozin, 2003; De Yoreo and Dove, 2004; Heinemann *et al.*, 2006). It has been noted in calcite that different faces having different affinities for trace elements, resulting in zoning within the crystal (Reeder and Grams, 1987; Paquette and Reeder, 1995; Reeder *et al.*, 2001). This partitioning may be more marked in aragonite as it has a lower symmetry than calcite and therefore potentially a greater number of crystallographically distinct crystal faces (Allison and Finch, 2004).

As seen in the Secondary Electron (SE) images of the outer shell prismatic layer (Figure 4.23), changes in concentration of organic components occur laterally.

The organics are more distinct at the growth check, but lateral changes also occur during the growth bands, with the crystals becoming less well aligned further from the periostracum. Therefore, changes in organics may result in lateral changes in trace element uptake.

Rosenberg and Hughes (1991) inferred from higher S/Ca concentrations that the slow-growing sections of *Mytilus edulis* of high curvature had higher organic concentrations. Therefore, in the prismatic layer of the umbo, the organic concentrations may become higher towards the margins, but in the outer shell prismatic layer, the organics become less well defined away from the periostracum suggesting lower concentrations. Thus, it could explain the apparent paradox.

Changes in the trace element (Me) concentrations to calcium (Me^{2+}/Ca) in the EPF as the shell grows may also explain lateral changes in trace element concentrations. During periods of rapid growth, Wada and Fujinuki (1976) found in three of the four types bivalves that Sr/Ca ratios in the central EPF were more concentrated. Conversely, Sr/Ca was more dilute during periods of slow or no shell growth. The fourth sample studied by Wada and Fujinuki (1976) however showed the opposite trend, suggesting that the controls on Sr/Ca within the EPF are complex. Klein *et al*. (1996a) hypothesised that lateral variation found within the calcite layer of *Mytilus trossulus* was due to changes in metabolic activity, with higher Sr/Ca and $\delta^{13}C$ at the lateral margins. However, $\delta^{13}C$ aliquots taken across the bands in *A. islandica* PL228 show no lateral variability, suggesting that the EPF is well mixed, and therefore this mechanism of trace elemental partitioning is unlikely to occur.

Although a full explanation of the driving mechanism of the lateral variation has not been determined, the presence of the lateral variation indicates that the trace elements are unlikely to be suitable as palaeoproxies from which quantitative

environmental reconstructions can be routinely obtained. In particular, it shows that the trace element composition is not independent of lateral distance from the maximum growth axis. In addition, initial findings indicate that Mg/Ca varies with depth, with an increase in concentration (of >40%) after the sample was repolished (a depth of ~125 μm).

The extent of the lateral change is not constant, affecting higher concentrations more significantly. However, if the lateral offset is significantly smaller than fluctuations that encode environmental change, some qualitative information may be obtained. For example, Ba/Ca changes laterally by ~25% but the sporadic increases can be >500% of the typical value. Ba/Ca sporadic increases can be easily distinguished, delimited by low Ba/Ca concentrations. The timing of Ba/Ca peaks may therefore be identified. The lateral variation for Sr/Ca and Mg/Ca is >50% of the annual variation and therefore confidentially identifying a specific environmental signal is difficult.

A better understanding of the controls on trace element uptake can be achieved by comparing transects taken closest to the maximum growth in the umbo and outer shell layer within the same shell (see Figure 1.2). Understanding the behaviour of trace elements and controls is important not only for *A. islandica* but also has relevance to studies of other taxa in which these trace elements are applied for palaeoenvironmental reconstructions. It is crucial, for example, to determine whether the controls on trace elements are constant throughout the lifespan of the organism.

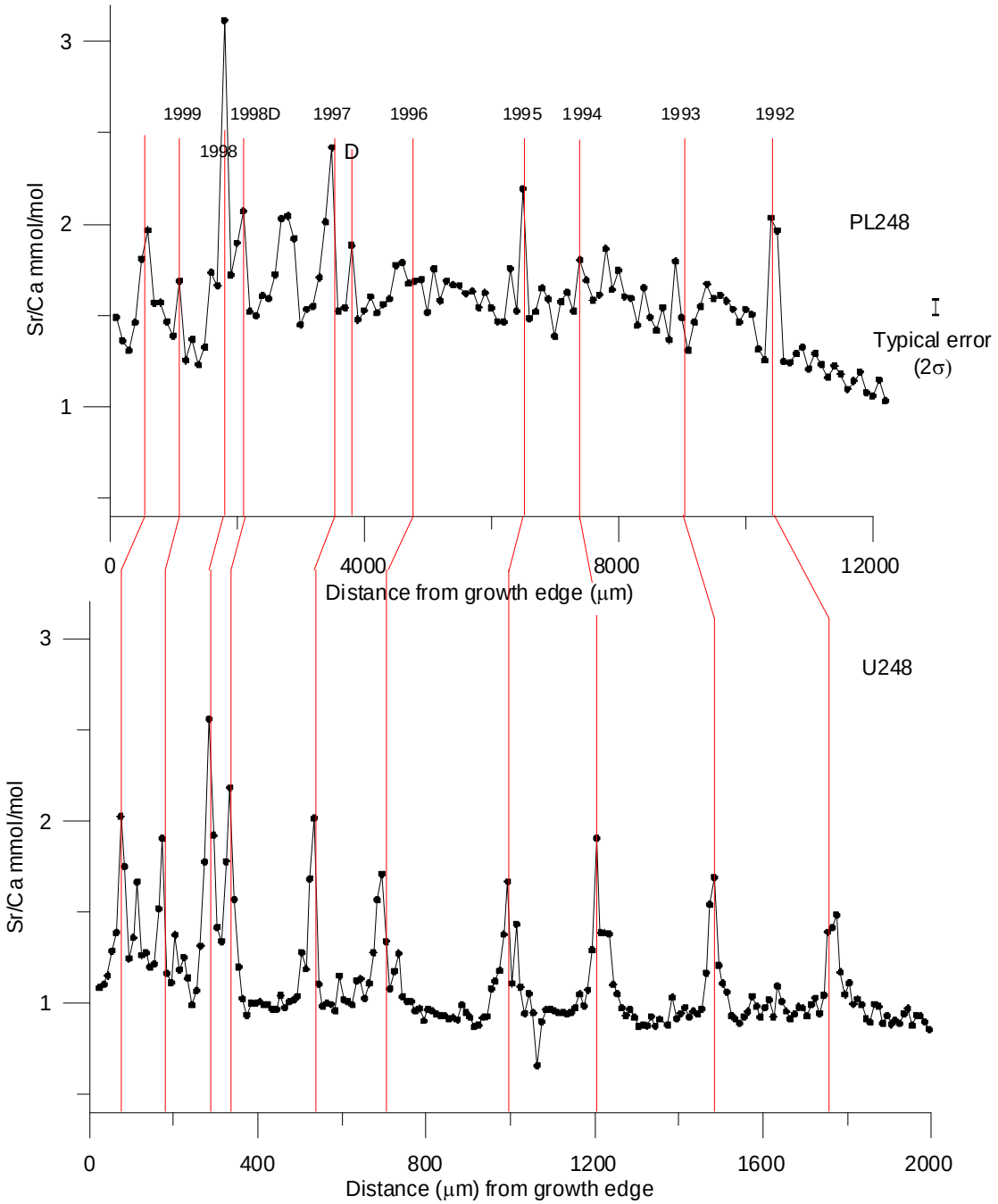

Figure 8.1a: Sr/Ca fluctuations in *A. islandica* specimen 248: comparison between the prismatic layer of the umbo and outer shell. Errors for U248 (not shown as too small) were 0.9% (2 S.E.). Note that standardisation to the same OKA chip analysed showed that Mg/Ca calculated by LA-ICPMS were >24% less than equivalent values from SIMS.

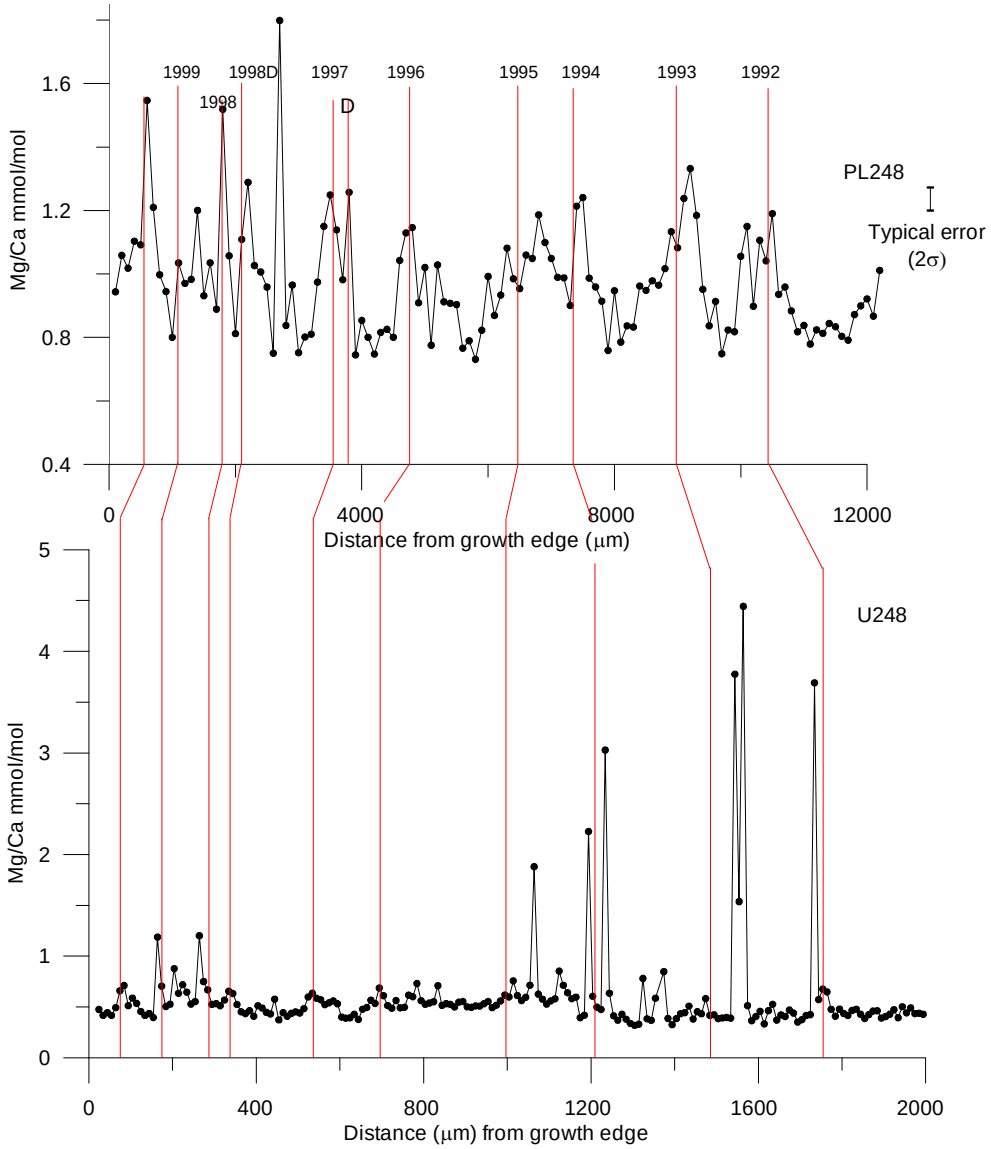

Figure 8.1b: Mg/Ca fluctuations in *A. islandica* specimen 248: comparison between prismatic layer of the umbo (unfiltered data) and outer shell layer. U248 error from standard was too small to be shown 5.1% (2 S.E). Mg/Ca concentrations measured by spot analyses, to the maximum concentration measured of 1.0 mmol/mol showed no evidence of superficial contamination. Higher concentrations may however, be affected by superficial contamination with Mg/Ca linescan data correlating significantly with Si/Ca. Note that standardisation to the same OKA chip analysed showed that the Mg/Ca calculated LA-ICPMS were >15% less than equivalent values from SIMS.

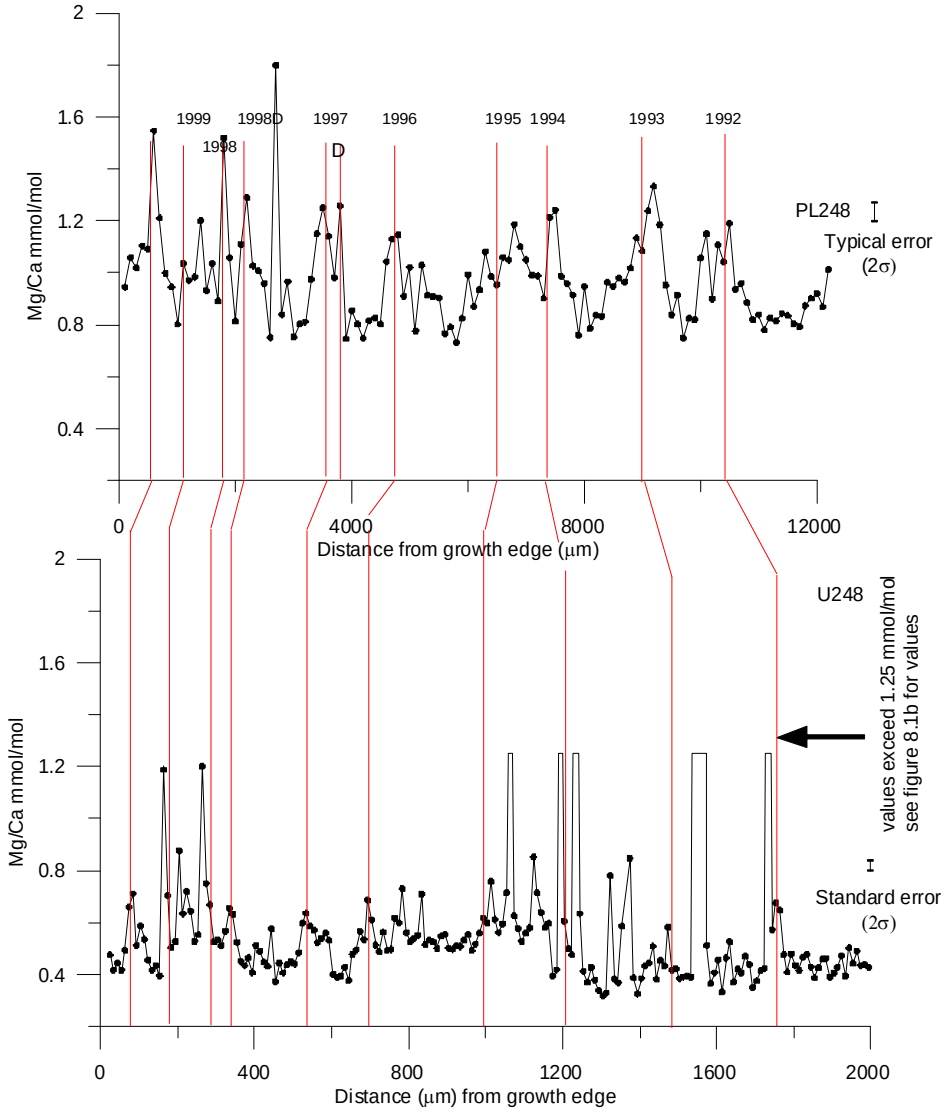

Figure 8.1c: Mg/Ca fluctuations in *A. islandica* shell 248: using the same scale for prismatic layer of the umbo and outer shell. Mg/Ca concentrations measured by spot analyses, to the maximum concentration measured of 1.0 mmol/mol showed no evidence of superficial contamination. Higher concentrations may however, be affected by superficial contamination with Mg/Ca linescan data correlating significantly with Si/Ca. Despite concerns about contamination of Mg/Ca within the umbo, the values are lower than the outer shell layer (in which no contamination indicators were found). Note that standardisation to the same OKA chip analysed showed that the Mg/Ca calculated LA-ICPMS were >15% less than equivalent values from SIMS.

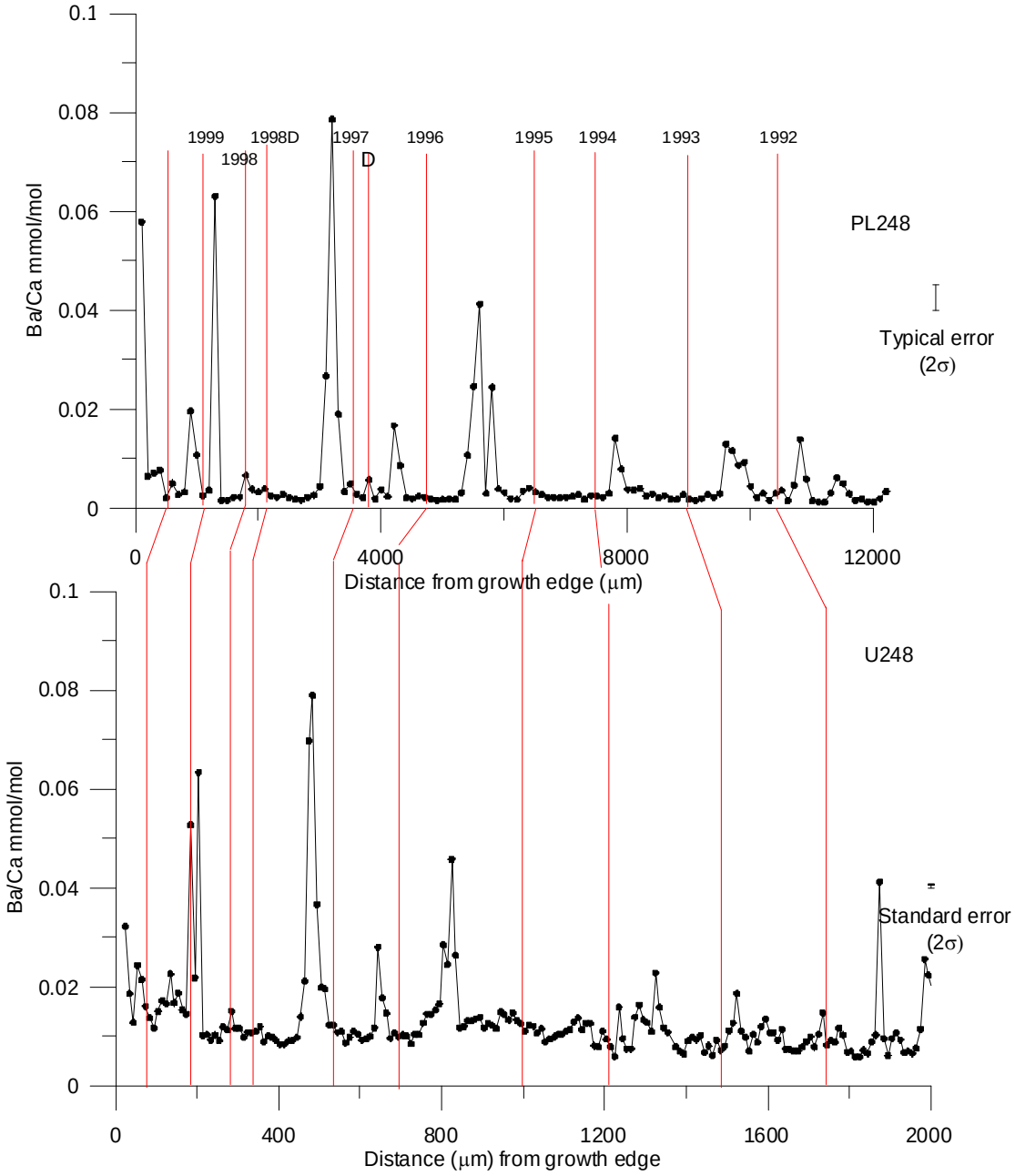

Figure 8.1d: Ba/Ca fluctuations in *A. islandica* specimen 248: comparison between the prismatic layer of the umbo and outer shell layer. Note that standardisation to the same OKA chip analysed showed that the Ba/Ca calculated LA-ICPMS were >20% more than equivalent values from SIMS. Note that low Ba/Ca measurements (<0.01 mmol/mol) in the umbo were sensitive to contamination, showing significant correlation with Si/Ca.

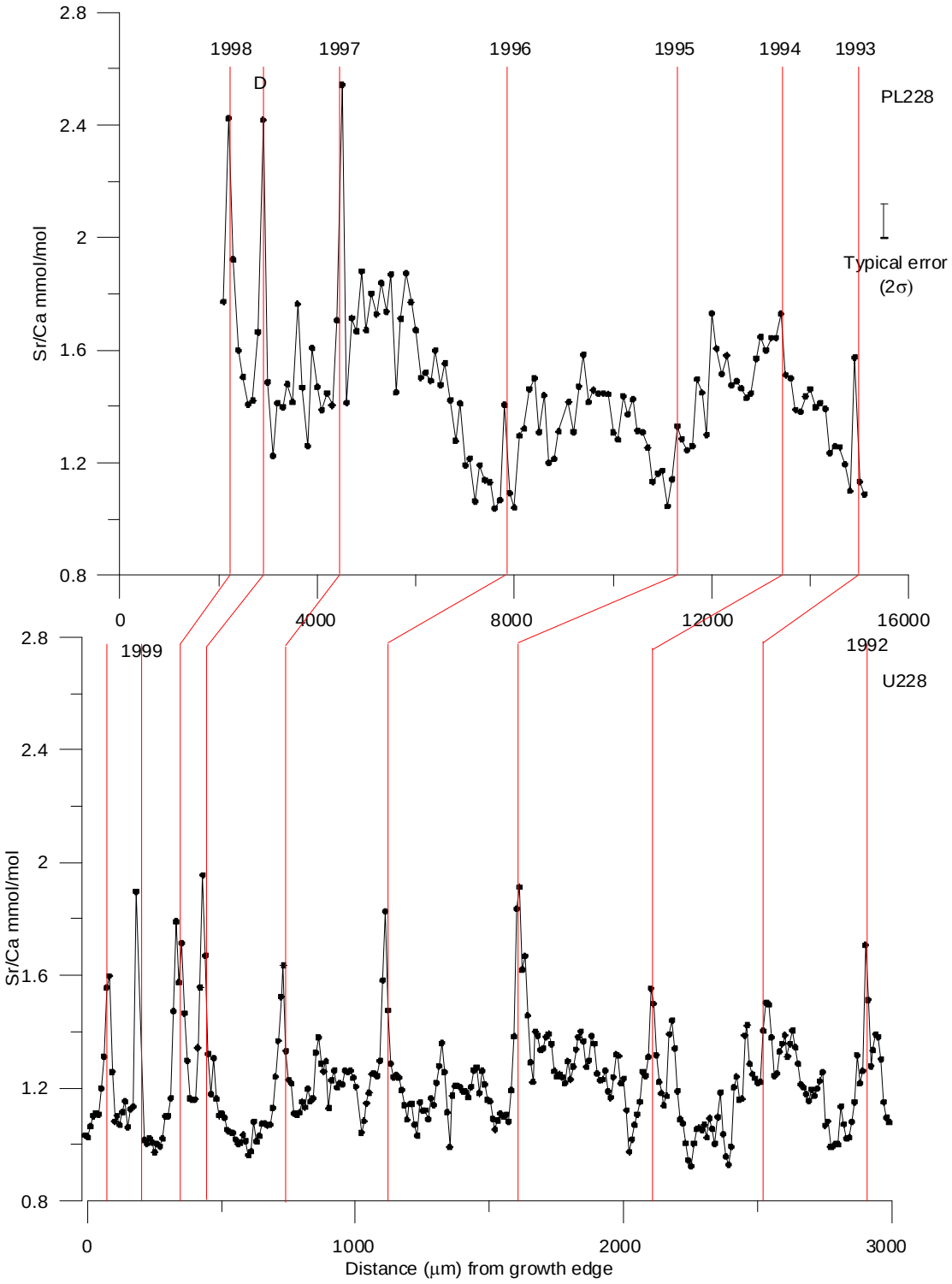

Figure 8.2a: Sr/Ca fluctuations in *A. islandica* specimen 228: comparison between the prismatic layer of the umbo and the outer shell layer. U228 error from standard was too small to be shown 0.9% (2 S.E.). Note that standardisation to the same OKA chip analysed showed that the Sr/Ca calculated LA-ICPMS were >24% less than equivalent values from SIMS.

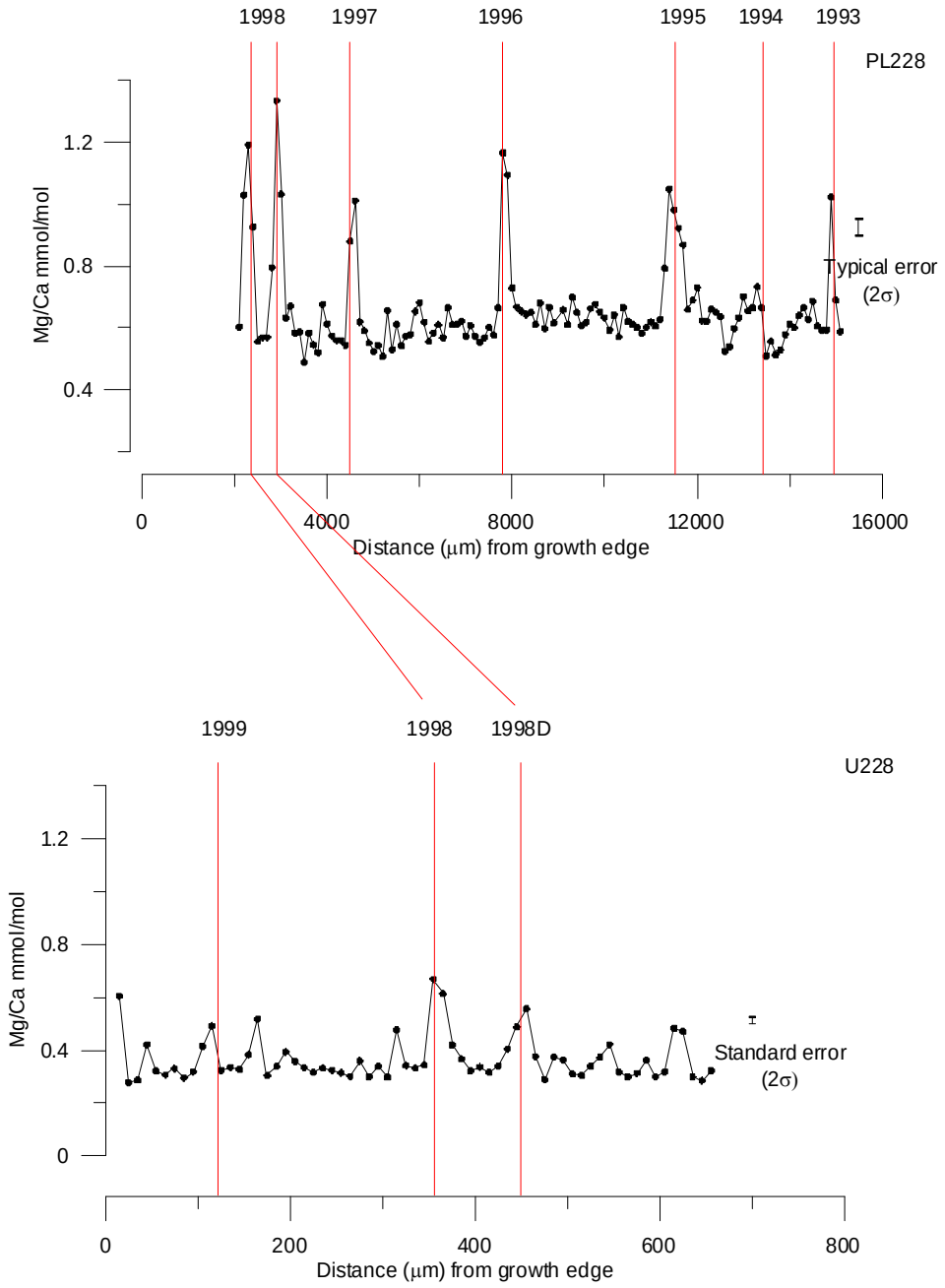

Figure 8.2b: Mg/Ca in *A. islandica* specimen 228: comparison between the prismatic layer of the umbo and outer shell layer. Note only a short transect was analysed on U228. Mg/Ca measurements of the umbo may be sensitive to contamination. Mg/Ca concentrations measured by spot analyses, to the maximum concentration measured of 1.0 mmol/mol showed no evidence of superficial contamination. Note that standardisation to the same OKA chip analysed showed that the Mg/Ca calculated LA-ICPMS were >15% less than equivalent values from SIMS.

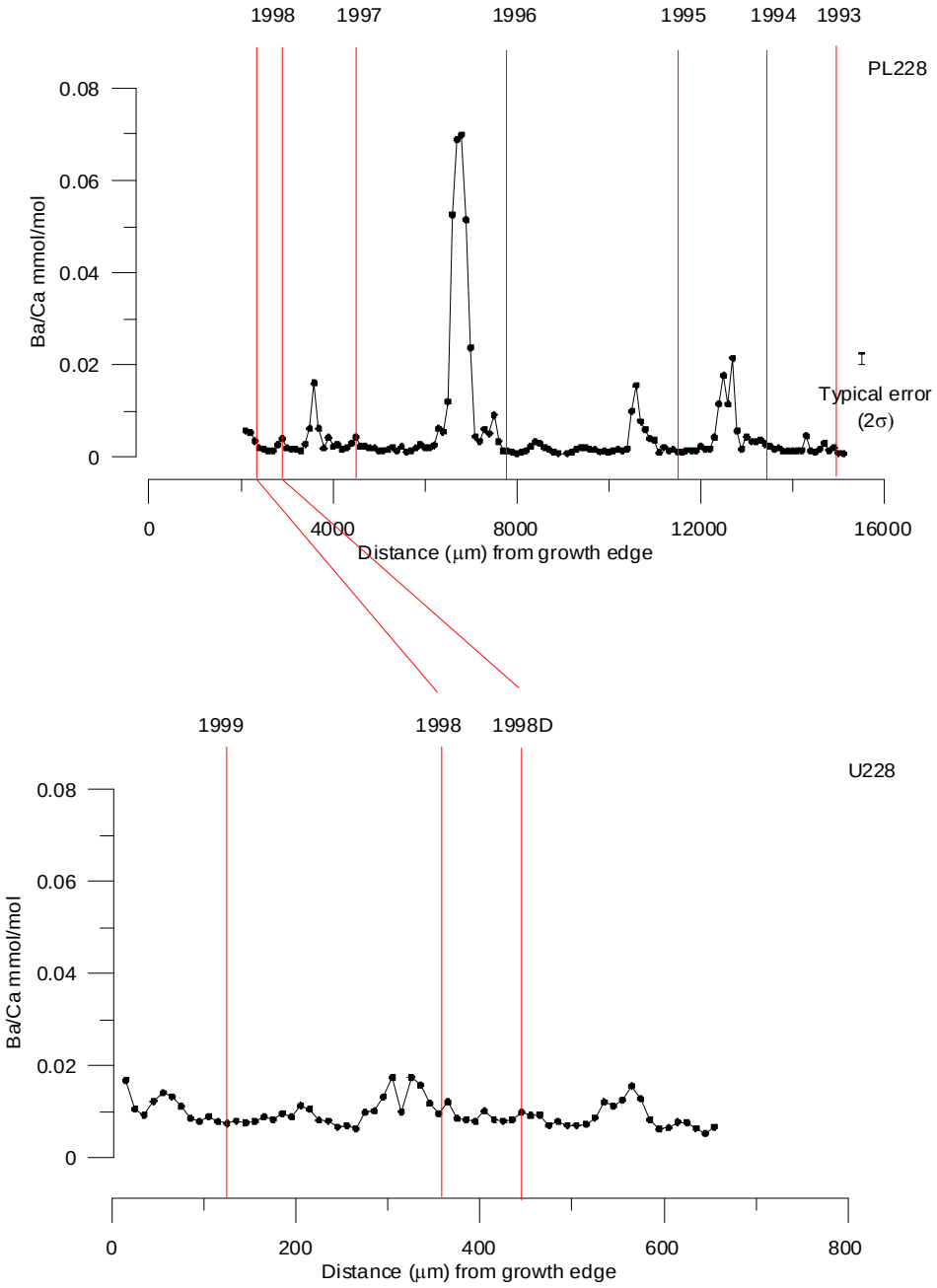

Figure 8.2c: Ba/Ca in *A. islandica* specimen 228: comparison between the prismatic layer of the umbo and the outer shell. Note only a short transect was analysed on U228. U228 error from standard was too small to be shown 1.8% (2 S.E.). Note that low Ba/Ca measurements (<0.01 mmol/mol) in the umbo was sensitive to contamination, showing significant correlation with Si/Ca. Note that standardisation to the same OKA chip analysed showed that the Mg/Ca calculated LA-ICPMS were >20% more than equivalent values from SIMS.

8.2.1 Sr behaviour

Sr/Ca behaviour in the two shells (Figure 8.1a and Figure 8.2a) shows similarity in the overall profile. High Sr/Ca peaks become less and less evident with increasing distance from the growth edge (i.e. more juvenile). However, high Sr/Ca maxima at the growth check are generally found when the shell growth rate is <~2000 μm/yr in the prismatic layer rather than related to a specific age in the shell. Sr/Ca increases at the growth checks are seen through most of the prismatic layer analyses of the umbo, although in U248 when growth rate >1500 μm, no Sr peak occurs at the growth check. Hence, high Sr/Ca within the growth checks occurs only within the latter few years of the outer shell whereas it is found through the majority of the umbo. These Sr/Ca peaks are higher within the outer shell layer with increases >2.4 mmol/mol compared to ~2.0 mmol/mol, and when the offset between LA-ICPMS and SIMS is accommodated the difference is >40%.

The average Sr/Ca fluctuations in the outer shell prismatic layer of 248 is ~0.5 mol/mol (without correction), which with compensation for the offset equates to ~60% higher than in the prismatic layer of the umbo. In shell 228 there was a much less marked difference between the two, with there only being an offset in the last few years of growth, but as LA-ICPMS underestimates values with respect to the ion probe by >24%, concentrations in the outer shell prismatic layer are notably higher than in the prismatic layer of the umbo.

The aragonite of the shell precipitates from a highly regulated water-soluble proteins (Belcher *et al.*, 1996; Falini *et al.*, 1996), with trace element composition of the precipitate, modelled by the empirical equation:

$$[Me/Ca]_{carbonate} = D_{me}[Me/Ca]_{H_2O}$$

where $[Me/Ca]_{carbonate}$ is the composition, D_{me} is the partition coefficient and [Me/Ca] is the concentration of the trace element in the water (Boyle, 1988; Morse and Bender, 1990; Lea and Spero, 1992; Lea and Spero, 1994). In an equilibrium thermodynamic system:

$$\ln (D_{Me}) = - \Delta G_f/RT$$

where ΔG_f is the Gibbs free energy of formation of the solid, R is the molar gas constant and T is temperature. However, in practise, many studies call upon a variety of other factors to control the observed coefficient including salinity, metal site, crystal growth rate, shell architecture and vital effects. Note that when such factors are invoked to explain trace element variability, it is implicit that the system is not at thermodynamic equilibrium. Thus, the observed Sr behaviour (D_{obs}) can be written as:

D_{obs} = f(Sr_{water}). f(host). f(temperature). f(growth rate). f(shell architecture). f(vital effects)

The relative impacts of each of these functions on D_{obs} are discussed in the following section.

f(Sr_{water})

As discussed in earlier chapters, salinity has been shown to have negligible effect on Sr concentrations in bivalves when salinity is >~10 (Dodd and Crisp, 1982). de Villiers *et al*. (1995) however showed that Sr content of water did vary by ~2% with change of latitude between 10ºS to 30ºN.

f(host)

Analysis of the synchrotron data (in Chapter 2) shows Sr substitution within *A. islandica* fits well with the model of ideal substitution for Ca in aragonite, i.e. Sr is found randomly within the Ca sites. Aragonite has one Ca site and hence there is no partitioning between different crystallographically non-equivalent sites.

f(temperature)

As Sr is ideally substituted in aragonite within *A. islandica* shells, substitution can in principal, obey the thermodynamic models (in which log [Sr]) is inversely proportional to absolute temperature (Kinsman and Holland, 1969; Dietzel *et al.*, 2004; Gaetani and Cohen, 2006). However, temperature variation only accounts for ~0.039 mmol/mol/ºC (Kinsman and Holland, 1969; Gaetani and Cohen, 2006), which corresponds to approximately one third of the Sr/Ca fluctuations seen (using temperature measurements from nearby Millport marine data station). Comparison to the $\delta^{18}O$ record measured within the same shell provides an indication of the timing of temperature variation. If Sr/Ca is controlled by seawater temperature, stronger correlations between Sr/Ca and $\delta^{18}O$ may be expected over correlations between Sr/Ca and instrumental temperature records. This is because $\delta^{18}O_{shell}$ indicates the temperature only during periods when the shell was growing, in contrast to instrumental SST measurements that also contain data lost in growth hiatuses, and data available was for SST rather than water temperatures at 6 m. It also provides a good comparison of the impacts of changes in temporal resolution ($\delta^{18}O$ was sampled at 75 μm, with LA-ICPMS every 100 μm). Comparison of the timing of Sr/Ca fluctuations shows no correlation with the $\delta^{18}O$ record (see for example Figure 8.3). Comparison to the instrumental record also showed not covariation, indicating that the

effect temperature has on Sr incorporation is obscured by other factors. Indirectly, temperature may control factors such as the growth rate, since it is likely there is a strong correlation between temperature, shell growth and metabolism (Lewis and Cerrato, 1997; Heilmayer *et al.*, 2004).

f(growth rate)

A number of researchers have hypothesised growth rate of the shell influences trace element incorporation (e.g. Pilkey and Goodell, 1963; Dodd and Crisp, 1982; Stecher *et al.*, 1996; Takesue and van Geen, 2004). However, inorganic aragonite precipitation experiments such as Kinsman and Holland (1969); Mucci *et al*. (1989) and Zhong and Mucci (1989) have shown that incorporation of Sr^{2+} is independent of precipitation rates over range of 10-500 μmol/m^2/h. However, rate-dependence in other inorganic carbonates is well established (e.g. Lorens, 1981; Rimstidt *et al.*, 1998). Corals precipitate at 3,000-25,000 μmol/m^2/h (Clausen and Roth, 1975a, b), six times faster than the inorganic experiments (de Villiers *et al.*, 1994). In the sections analysed in *A. islandica* (i.e. not the whole shell), growth rate of the prismatic layer varied from the slowest in the umbo (<100- 1500 μm/yr) to the outer shell layer (<500- 3500 μm/yr), with a precipitation rate of 400-14,000 μmol/m^2/h. Thus, analogies drawn from fast-growing coral may be applicable to *A. islandica* (particularly during the faster parts of growth). Carré *et al*. (2006)'s study of the bivalves *Mesodesma donacium* and *Chione subrugosa* attributed up to 74% of Sr/Ca variations to crystal growth rate, with higher growth rates showing higher Sr/Ca. Typically the linear growth rate of the shell is considered to reflect the crystal extension rate (e.g. Klein et al., 1996a; Gillikin et al., 2005a). Carré *et al*. (2006) extended this model by assuming that the crystal growth direction may not be aligned

to the shell growth direction. Non-parallel growth can be seen in SE images of *A. islandica* (Figure 4.23). However, neither of these scenarios considers whether increased nucleation could cause increased shell growth rate, as it is inherently assumed that crystal growth rate and shell growth rate are linked. The possible impact of increased nucleation is discussed within the f(shell architecture) section.

Gaetani and Cohen (2006) used the surface growth entrapment model developed by Watson (1996, 2004) to explain why both compatible and incompatible trace elements were found in higher concentrations at the inorganic aragonite crystal surface compared to the fluid. Crystal growth rate and diffusivity prevent equilibrium with the fluid in this model. They applied these findings to explain Sr/Ca seasonal fluctuations in the skeletal composition of *Diploria labyrinthiformis* (brain coral), concluding that Sr/Ca fluctuations were due to a combination of growth entrapment and what they termed "precipitation efficiency." This term describes the mass fraction of aragonite precipitated from the calcifying fluid from a given volume of fluid. This is important as the partition coefficient for Sr is greater than Ca in aragonite and thus the Sr/Ca ratio of the calcifying fluid decreases over time (Gaetani and Cohen, 2006).

. If however we consider the linear shell growth rate, it would be expected that during a year, the fastest rate would occur within the growth band. Measurements of Sr/Ca reach a maximum mid-way through the growth band in the outer shell prismatic layer (e.g. PL248 1993-1995) initially suggesting that there is a growth control. However, these variations can be explained by changes in the shell shape during the year, which effectively change the lateral distance from the periostracum. As discussed in Chapter 3, it is difficult to determine the exact position of the maximum growth in the umbo, and therefore Sr/Ca changes result from lateral changes in the sampling position. It is estimated that the distance from the measurement transect to

the maximum growth axis could be >500 μm (see Figure 3.4b, c). Transects ~750 μm apart showed changes in Sr/Ca of >45%, with changes in Sr/Ca during the growth bands being ~30% suggesting that lateral changes can account for a significant proportion of Sr/Ca variation.

Comparison of the concentration of Sr/Ca in the prismatic layer of the umbo and shell outer layer however show that the latter is higher, e.g. in PL248 by ~0.4 mmol/mol. This nominal value is in reality higher due to offset between values calculated by SIMS and LA-ICPMS. This therefore could suggest that the average Sr/Ca is affected by shell growth rate. Comparison however, of the Sr/Ca in the outer shell prismatic layer of 228 and 248, shows that the latter has the faster shell growth rate shows a lower Sr/Ca.

Modelling of the $\delta^{18}O$ profile is consistent with significant changes in shell growth rate through the year and in particular, that there are two growth seasons per year. Such changes in shell growth rate are likely to be linked to changes in crystal growth rate. No relationship between Sr/Ca fluctuations and the changes in shell growth rate was found, indicating that Sr/Ca is independent of shell growth rate.

Thus, it appears that any shell growth rate effect is relatively minor, with lateral variation accounting for changes during the growth band. There is no significant ontogenetic effect in Sr/Ca. Further work is however, required in the umbo to separate out the result of lateral changes from other effects, and determine the *in situ* crystal growth rate, which was may not be directly attributed to shell growth rate.

f(shell architecture)

The shell architecture is not constant through the shell. In the outer shell prismatic layer, the crystals close to the periostracum are interlocking crystals, aligned with

growth direction whereas further away from the periostracum there is no clear alignment (Figure 4.23). The organics in the SE image closest to the periostracum can be clearly discerned whereas ~1000 μm from the periostracum it is much harder.

The manner in which biominerals grow affects the uptake of the trace elements as different faces of the crystals have different affinities for trace elements (Reeder and Grams, 1987; Paquette and Reeder, 1995; Reeder *et al.*, 2001). In non-biogenic crystals (of speleothems), data presented by Finch *et al.*, (2003b) clearly infers a change of ~50% across a single aragonite crystal. A change in crystal habit may therefore be reflected in the Sr/Ca values. Partitioning of trace elements within biogenic crystals such as that found in *A. islandica* and non-biogenic crystals such as that found in a speleothems may however differ. In other words, whether partitioning in biogenic crystals could be significant enough to be the sole driving factor behind Sr/Ca increases at the growth checks, which can be >100% is unclear. However, it could explain why Carré *et al*. (2006) found for the same crystal growth rate higher Sr/Ca in the curved sections, with increased nucleation with shorter crystals likely to occur during these sections.

Rosenberg and Hughes (1991) measured the changes in S/Ca in *Mytilus edulis* in the outer calcitic layer bivalve, and found that S/Ca values along the slow-growing sections were 1.25 higher than along rapidly growing axes of low curvature. S/Ca were interpreted as an index of matrix content, as S is primarily concentrated in various acid mucopolysaccharides and amino acids within the shell (Rosenberg and Hughes, 1991). Thus, such changes in organics could influence Sr/Ca partitioning, with shorter crystals likely to provide greater affinity for Sr.

f(vital effects)

Some researchers have cited metabolic efficiency as a control on Sr/Ca (e.g. Klein *et al.*, 1996a; Purton *et al.*, 1999). Klein *et al*. (1996a) demonstrated that lower Sr/Ca at lateral margins (which are more curved) in the calcitic section of the bivalve *Mytilus trossulus* which were associated with changes in $\delta^{13}C$, and concluded that lateral variation resulted from lateral changes in metabolic activity. Results presented in this thesis show that Sr/Ca lateral variation is not associated with $\delta^{13}C$ changes. While some researchers (e.g. Mook and Vogel, 1968; Fritz and Poplawski, 1974; Buchardt and Simonarson, 2003) concluded that $\delta^{13}C$ variation was the product of dissolved inorganic carbon in the water column, $\delta^{13}C$ in *A. islandica* is, at least in part, influenced by changes in metabolic activity. This can be seen clearly in Figure 6.9a which shows a sharp change in $\delta^{13}C$ of >0.5 ‰ after a shell damage event. It is difficult to envisage an abiogenic mechanism that could account for such an isotopic shift, indicating that the damage triggered a long-term change in the metabolic rate of the organism. Therefore, the lack of lateral change in $\delta^{13}C$ across the bands is likely to indicate that EPF is well mixed, and lateral variation across the bands is not due to heterogeneity within the EPF.

High Sr/Ca is found within the growth checks (with increases of >0.5 mmol/mol) during the latter years of growth. They are however, generally present when the growth rate is <2000 μm/yr in the outer shell prismatic layer (see Chapter 4). In the prismatic layer of the umbo, the picture is less clear, with Sr/Ca peaks occurring at the growth checks of U228 during most of the shell. In U248 however, Sr/Ca peaks do not occur when the growth rate is >1500 μm/yr. Epplé (2004) also found high Sr/Ca peaks at the growth check in *A. islandica*, but Toland *et al*. (2000) found a minimum in Sr/Ca at the annual growth checks. However, the latter

only sampled the youngest part of the shell and never covered a period when the growth rate was slow. This is further consistent with the hypothesis that high Sr/Ca concentrations are associated with slow growth (which generally occurs in the latter years).

As discussed in Chapter 3 and 4, three pathways are considered for Ca^{2+} transport through the calcifying mantle;

1) Passive non-selective intercellular pathway (direct exchange with seawater).
2) Active (energy consuming) selective intracellular pathway involving Ca^{2+}-ATPase enzymes (Ca^{2+}-pump) (Klein *et al.*, 1996a; Gillikin *et al.*, 2005a).
3) Calcium channels (Carré *et al.*, 2006). Ca^{2+}-ATPase enzymes may be an important control for Sr/Ca at the growth checks.

Increased activity of enzyme Ca^{2+}-ATPase increases the calcification rate. As Ca^{2+}-ATPase has a higher affinity for Ca^{2+}, it results in a decrease in the proportion of Sr^{2+}; conversely, at lower calcification rates, the proportion of Sr^{2+} increases (Gillikin *et al.*, 2005a). However, Sr peaks at the growth check are typically only seen when the growth rate is <~2000 μm in the prismatic layer, indicating either that the Ca^{2+}-ATPase pathway is not a controlling factor, that the uptake pathway changes, or that another mechanisms become more dominant during the lifetime of the bivalve.

Carré *et al*. (2006) showed that the ion fluxes through either the passive or the active pathway were not sufficient for biomineralisation in a bivalve (with a daily growth rate of 20 μm/day). Therefore, they proposed the use of calcium channels for the ion fluxes. A calcium channel is an aqueous pore facilitating Ca^{2+} diffusion (Carré *et al.*, 2006) and can support very high ionic fluxes (Sather and McCleskey, 2003).

The gradient in Ca^{2+} caused by mineralisation drives the ion flux, and thus as mineralisation rate increases, Sr^{2+} ions cross the pores more easily (Carré *et al.*, 2006). They suggested however that the model would not be applicable to "very slow" growing specimens ("very slow" is not defined), as they may not involve Ca^{2+}-channels in ionic transport. Thus, the uptake channels could change during the lifetime of *A. islandica*. However, if partitioning in the Ca^{2+} during growth were a controlling factor, it would require that separate pathways were invoked for biomineralisation in the umbo to the outer shell despite both being the same prismatic layer, as the presence of high Sr/Ca relates to the slower growth rate, and not to a specific annual band within the shell. $\delta^{13}C$ data indicate the EPF is relatively well mixed prior to deposition in the outer shell prismatic layer, suggesting such pathways cannot result in lateral changes. Whether differing pathways could occur for deposition of the prismatic layer in the umbo compared to the outer shell requires further research.

Preliminary research presented by Nägler *et al*. (2006) found that Sr/Ca and $^{44}Ca/^{40}Ca$ are highly correlated for the three years analysis 1956-1958 (r=0.92 for 1957) This provides more data to understand the controls on Sr behaviour, as it suggests that controls (and hence uptake pathways) for Sr is similar to that which control Ca fractionation.

The aragonitic *M. arenaria* and the calcitic *M. mercenaria* are both long-lived bivalves and show a strong Sr/Ca peak within the growth check (Palacios *et al.*, 1994; Thorn *et al.*, 1995). The former has a lifespan of <28 yr (MacDonald and Thomas, 1980) and <50 yr respectively thus suggesting that the longevity of the species may play a role.

Overall findings on Sr

A number of possible controls on Sr behaviour have been discussed, including how Sr is hosted, changes in temperature and salinity, growth rate (both shell and crystal), changes in shell architecture (in particular how it influences crystal propagation), and vital effects. Changes in crystal nucleation and propagation as well as crystal growth rate and vital effects could be significant controls on Sr/Ca. Wada and Fujinuki (1976) found that the EPF in bivalves did not greatly differ from seawater suggesting Sr^{2+} discrimination occurred during shell crystallisation. High Sr/Ca at the growth checks may relate to a biological effect associated with the slowing of the shell growth rate. No relationship between temperature and Sr/Ca is found despite Sr being ideally substituted, indicating that other controls are dominant.

8.2.2 Mg behaviour

XANES of Mg within *A. islandica* indicate that Mg is hosted in the shell by organics and not aragonite. Mg/Ca counts by SIMS in the umbo are partly compromised by superficial contamination and thus comparison of the compositional data between the umbo and the outer shell layer (by LA-ICPMS) should be treated with caution. In the outer shell prismatic layer, no evidence for contamination was found with good replication of the pattern of Mg/Ca fluctuations, though the absolute values decreased laterally across the band. In addition, preliminary research suggested that there is also a change in Mg/Ca with depth, which could not be accounted for by lateral variation with a change in depth of ~125 μm (after repolishing) showing a >40% change in Mg/Ca concentration.

In the outer shell prismatic layer, Mg/Ca increases within the annual growth check, which is as expected, with increased organics found during the growth checks.

This concurs with Takesue and van Geen (2004) who found 52% less Mg in the aragonitic bivalve *Protothaca staminea*, when the organic fraction was removed. The XANES profile from *A. islandica* is consistent with the dominant host for Mg being organic material. This profile shows no discrepancy when compared with the organic standard that would indicate the presence of a secondary phase, notably aragonite. Therefore, it is inferred that Takesue and van Geen (2004)'s estimate of the organic content hosting Mg is an underestimate.

However, the relationship of high Mg/Ca at the growth check is not straightforward, with some growth checks not associated with high Mg/Ca. Mg/Ca concentration is sometimes higher in the growth band than in the growth check. Epplé (2004) reported a similar observation in *A. islandica* from the German Bight. It suggests that the organics vary significantly within the growth bands or that, while Mg is hosted by organics, there is no linear relationship between organic content and Mg. In other words, Mg content is not a simple function of total organics within the structure, but that vital effects may modify Mg uptake by the organics. Further work is required to determine the controls on Mg, but it is clearly not a simple, quantitative environmental proxy. Application of inorganic-based equilibrium models to organically-hosted Mg in *A. islandica* is unlikely to provide a route for accurate palaeoenvironmental reconstruction. Those attempts that have been applied (e.g. Takesue and van Geen, 2004) are probably erroneous and demonstrate a weakness in the largely empirical approaches to environmental reconstruction widely used. X-ray absorption spectroscopy may find an important niche in "ground truthing" environmental proxies in a manner similar to that applied here.

8.2.3 Ba behaviour

Ba/Ca shows similar profiles in the prismatic layer of the umbo and outer shell layer, with low average values (e.g. in the U228 <0.02 mmol/mol), and sporadic increases of as much as 500%. There is good agreement between the timing of these events between the umbo and outer shell layer in the prismatic layer of the same shell. The magnitude is at higher Ba/Ca concentrations within error (i.e. Ba/Ca >0.025 mmol/mol) despite the lateral offset (using data from 248). Ba/Ca low values in the outer shell prismatic layer are lower, but low Ba/Ca counts in the umbo (<0.1 mmol/mol) were affected by contamination, approximately one-third of counts at the lower concentration. Comparison between the timing of Ba/Ca peaks in different individuals (PL228 and PL248) show that these maxima are not synchronous.

Research in inorganic aragonite has found Ba is more dependent on temperature than Sr (e.g. Dietzel *et al.*, 2004; Gaetani and Cohen, 2006). Little is known about the mechanisms of Ba substitution in the shell and XAS was not possible in the present study due to the low concentrations. Ba maybe ideally substituted in carbonate, or maybe precipitated as secondary minerals such as barite ($BaSO_4$). Ba may also be trapped in crystal defects or adsorbed on crystal surfaces.

Filter feeding bivalves, such *A. islandica*, may uptake Ba directly (through dissolved Ba in the seawater) or by the ingestion of Ba rich particles associated with diatom blooms, as phytoplankton or barite particulates (Stecher *et al.*, 1996; Putten *et al.*, 2000; Toland *et al.*, 2000; Torres *et al.*, 2001; Lazareth *et al.*, 2003; Gillikin *et al.*, 2006). Primary productivity and barite formation are closely associated (e.g. Dehairs *et al.*, 1987). The pattern of high sporadic Ba/Ca maxima from low Ba/Ca concentrations has been noted in bivalves by numerous researchers (e.g. Stecher *et al.*,

1996; Putten *et al.*, 2000; Lazareth *et al.*, 2003; Gillikin *et al.*, 2006) as well as within corals (Sinclair, 2005). These similarities hint at a common source.

Laboratory and field tests by Gillikin *et al*. (2006) found a linear correlation with $[Ba/Ca]_{water}$ and background $[Ba/Ca]_{shell}$, but this differed between the laboratory and field experiments. Gillikin *et al*. (2006) suggested the difference in the equations related to inaccuracies in the field measurements or stress induced by handling in the laboratory experiments. Differences in Ba/Ca between the two experiments may however also relate to temperature differences, with inorganic experiments (Dietzel *et al.*, 2004; Gaetani and Cohen, 2006) as well as [Ba/Ca] in corals showing a temperature relationship (Allison and Finch, 2007). Comparison of $[Ba/Ca]_{shell}$ within *A. islandica* to that reported by Gillikin *et al*. (2006) for *Mytilus edulis* (a calcite bivalve) show similar concentrations. However, it is unclear whether a lateral variation also occurs at lower concentrations (measurements were within error). Analysis with an instrument with a higher precision at lower concentrations would be required to determine that the background $[Ba/Ca]_{shell}$ was unaffected by lateral changes in concentration.

The cause of the sporadic increases in Ba/Ca in *A. islandica* remains unclear with the timing of these increases differing between years. The timing also differed between the two shells. Replication of the peaks in the prismatic layer of the umbo and shell outer layer however suggests that the increase in Ba/Ca occurs is mediated by the EPF, and is not the result of local incorporation of Ba-rich detritus. Comparison of Ba/Ca fluctuations to the $\delta^{18}O$ and $\delta^{13}C$ from PL228 (with the split aliquots) also fails to reveal any relationship (Figure 8.3). Gillikin *et al*. (2006) tentatively concluded that the Ba/Ca increases relate to the ingestion of barite crystals.

Further research on such a hypothesis is required to measure *in situ* Ba/Ca concentrations and possible sources.

Ba/Ca data presented in this thesis indicate a slight decline in the Ba/Ca peaks during the latter years, but the numbers of peaks are too few to be fully conclusive. However, Ba/Ca fluctuations in other bivalves (e.g. Putten *et al.*, 2000; Lazerth *et al.*, 2003) as well as in other *A. islandica* specimens (e.g. Epplé, 2004) all showed an ontogenetic decrease.

Thus, in summary, Ba/Ca sporadic fluctuations are recorded within different regions of the prismatic layers are the same, but the timing between the two individuals measured is different. Developments in instrumentation, notably the opening of the DIAMOND facility at the Rutherford Appleton Laboratories in Oxfordshire, may provide more brilliant X-ray sources that will allow the coordination of Ba (and other trace elements currently below detection limits) to be explored. Further research is required to determine the controls on Ba/Ca.

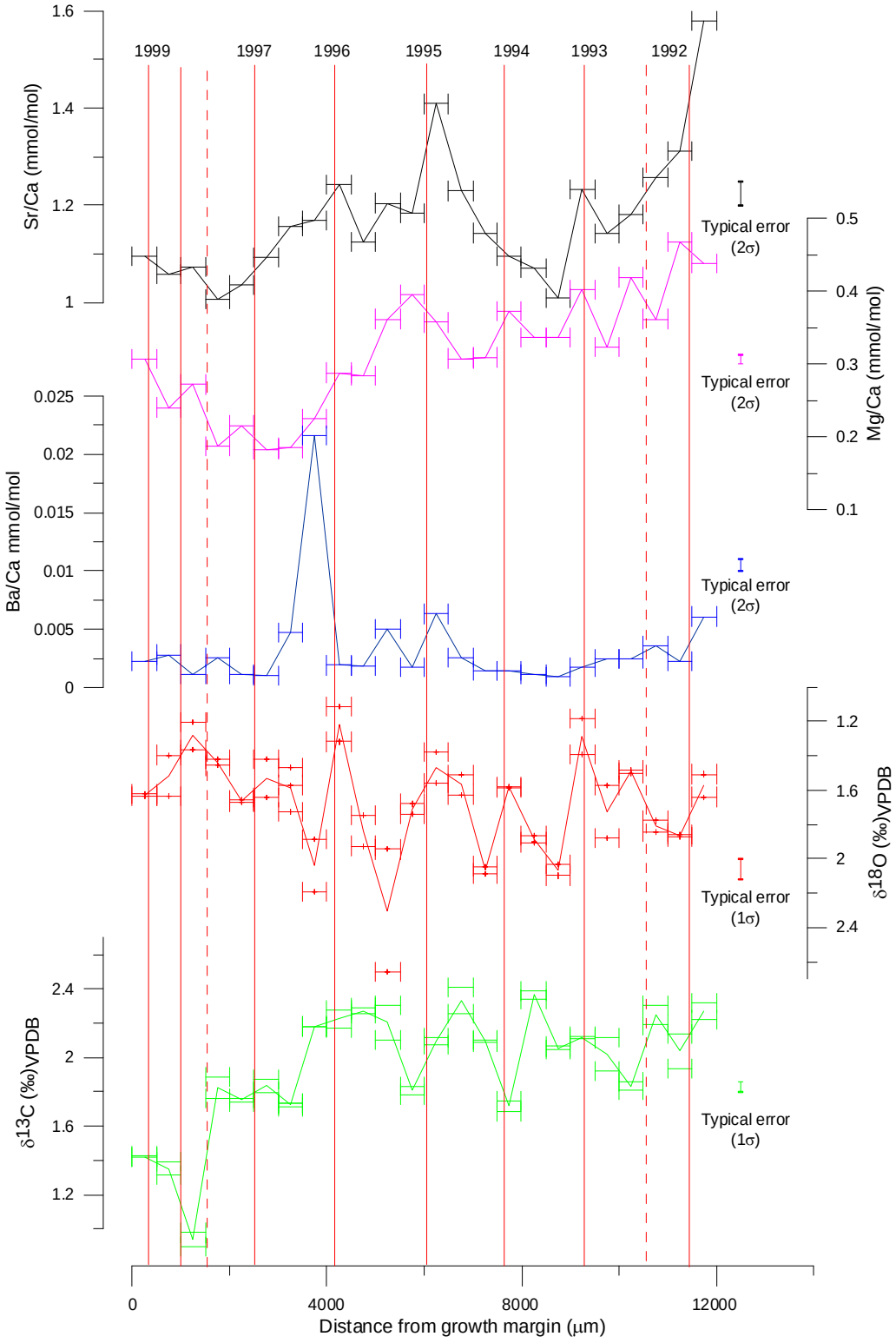

Figure 8.3: Comparison of the trace element fluctuations measured during solution-ICPMS to $\delta^{18}O$ and $\delta^{13}C$ fluctuations from outer shell prismatic layer of shell 228. Note the horizontal errors bars represent the area milled. The red lines mark the annual termination bands.

8.3 Reconstruction using stable isotopes

The use of oxygen isotopes to reconstruct temperature fluctuations is widely used within sclerochronology. However, concerns about the impacts of micromilling on the oxygen isotopes have been raised by Aharon (1991) and Gill *et al*. (1995). XRD of *A. islandica* and cod otoliths show that aragonite converts to calcite during milling and drilling. $\delta^{18}O$ measurements of aliquots taken from cod otoliths reared at a constant temperature however show that any changes in $\delta^{18}O$ could be accounted for by variation in salinity. Thus, within the precision of the mass spectrometer, any impacts of sample modification during micromilling on $\delta^{18}O$ values are negligible.

Aliquots for $\delta^{13}C$ and $\delta^{18}O$ were extracted using a fixed platform drill and a micromill. The former provides discrete sampling providing some indication of fluctuations in $\delta^{18}O$ and $\delta^{13}C$, although with hiatuses in the data. The micromill is much superior, providing a more continuous higher resolution sampling.

Oxygen isotopes are dependent on both temperature and salinity, with the latter often assumed constant. $\delta^{18}O$ profiles within the outer shell prismatic layer of shell 248 (PL248) were compared to SST measurements from nearby Millport Marine station. Data from PL248 show that $\delta^{18}O$ fluctuates between 0.6 and 2.6 ‰; which assuming a constant salinity suggests growth temperatures of ~+5 to +13 ºC using the equation of Grossman and Ku (1986) Measured SST at Millport Marine station for the same period were between +6.3 and +15.6 ˚C. The maximum fluctuation of the salinity during the year is 1.2 (determined from Irvine bay measurements of salinity profiles at 7 m in a water depth of >30 m). The salinity variations at Millport give rise to uncertainties in the estimated from $\delta^{18}O$ of ~2.1 ˚C, i.e. if we assume a constant salinity, this gives an error of ±1.1 °C. Assuming that the lowest salinity occurs

during the coldest months, the lowest reconstructed temperature would be within error (of 1.2 °C the standard deviation (2σ) found between the snapshot Irvine Bay data and that of Millport). Conversely the maximum temperature would be reduced, and therefore not show the extremes shown in the SST measurements at Millport. This may reflect the fact that the sea surface is particularly susceptible to diurnal warming during the summer (with seawater temperatures typically >0.8 ˚C cooler in Irvine Bay *in situ* measurements taken at 7 m). It could also, as the constructed model suggests, result from a growth slowdown or shutdown during the summer months. Discrepancies could also result from differences in local water circulation of Millport vs. Irvine Bay, inaccuracies with the measurements at Millport station due to the use of the "bucket method," or inaccuracies of the equation of Grossman and Ku (1986).

To study further the relative importance of temperature, salinity and growth rate on $\delta^{18}O$, a simple model was produced. The effect growth rate has on the $\delta^{18}O$ profile is particularly significant, as it shows that changes in temporal resolution of sampling significantly impact the $\delta^{18}O$ data. Modelling shows that the relative importance of changes in the growth rate on temporal resolution was 0.8 compared to 0.7 for the seawater temperature and 0.1 for salinity (the other two modelled components). Thus indicating that changes in temporal resolution significantly impact on the $\delta^{18}O$ profile. Such findings concur with those of Goodwin *et al*. (2003), who modelled $\delta^{18}O$ fluctuations in the bivalve *Chione Cortezi*, and concluded that isotopic amplitudes and averages may reflect decreases in growth rate rather than direct environmental fluctuations (i.e. temperature and salinity).

While this has lead to "adaptive sampling" for ontogenetic changes (e.g. Schöne *et al.,* 2004c), the model highlights that intra-annual variations in the growth season are also important.

The model suggests that salinity has a relatively small impact and therefore assuming a constant value, even within shallow water sites is valid. This fits well with the instrumental measurements, which shows that fluctuations in salinity from Irvine Bay are 1.2 with a mean of 33 (1990-1996) equating to a maximum temperature error of ~2.1 ˚C using the equation of Ganssen (unpublished, cited in Witbaard *et al.*, 1994) to reconstruct $\delta^{18}O_{seawater}$ with the equation of Grossman and Ku (1986) for the temperature reconstruction.

Further development of the $\delta^{18}O$ model would allow a better understanding of how changes in temporal resolution of sampling of trace elements would impact on the concentrations measured within the prismatic layer of both the outer shell and the umbo. This may provide further insights and discussions into the controls of trace elements. Initial comparison of the modelled changes in shell growth rate, failed to show any significant correlation, though further, more detailed analyses may provide some additional insights.

Research by Ghosh *et al*. (2006) has shown that the temperature of formation of calcium carbonate may be determined independently of the salinity, by measuring the state of ordering of ^{13}C and ^{18}O i.e. bound together vs. separated into different CO_3^{2-} units. In addition, by comparing these results with bulk $\delta^{18}O$ measurements, a calculation of the *in situ* $\delta^{18}O_{water}$, rather than an approximation from salinity measurements, can be made. This could be especially helpful in intertidal zones where there is significant salinity variation. The precision however of this technique at present is ca. ±2 °C (1σ) (Ghosh *et al.*, 2006) compared to ±1.2 °C (1σ) using a bulk $\delta^{18}O$ determination and a constant salinity used in *A. islandica* (Weidman *et al.*, 1994). The technique of Ghosh *et al*. (2006) may however become more common with improved precision and development.

Another technique being developed is the use of SIMS to measure $\delta^{18}O$ fluctuations on microvolumes within the shell. It has recently been successfully applied to corals using the Cameca-1270 series instruments with spot sizes of ~30 μm diameter at precisions of 0.2 ‰ (Allison *et al*., unpublished; Rollion-Bard *et al.*, 2007) Further development of SIMS instrument will allow microscale fluctuations to be examined, vastly increasing the temporal resolution.

Analysis of $\delta^{13}C$ shows a decline in ontogeny in all three shells sampled (405, 228 and 248) (Figure 6.7, 6.8, and 6.9a respectively). This was contrary to findings by Schöne *et al*. (2005a) whom found no ontogenetic trend and Witbaard *et al*. (1994) who found an increase. $\delta^{13}C$ measurements within *A. islandica* from Irvine Bay show a maximum $\delta^{13}C$ of 3 ‰ (PL405), suggesting that $\delta^{13}C_{shell}$ could be depleted relative to $\delta^{13}C_{DIC}$ in the water. During and after damage to the outer shell prismatic layer in shell 248 a sharp decrease of >0.5 ‰ was seen. This observation is a strong indication that metabolic rate has a key influence. McConnaughey *et al*. (1997) proposed that metabolic carbon can account for ~10% of the $\delta^{13}C$ signal in molluscs, and findings from Owen *et al*. (2002); Lorrain *et al*. (2004); and Gillikin *et al*. (2005b) supported this conclusion. However, the results presented here suggest that in times of stress, this percentage can be considerably higher, with $\delta^{13}C$ in PL248 showing a decrease of >50% after damage to the shell occurred. Thus, indicating that >50% of carbon is metabolic. This observation, combined with an ontogenetic change in these faster growing specimens, suggests that metabolic activity plays an important role. However, it does not explain why specimens presented in this thesis showed the opposite ontogenetic trend to that reported by Witbaard *et al*. (1994).

8.4 Using fluctuations in radiocarbon

A. islandica has the potential to reconstruct recorded fluctuations in radiocarbon concentrations. The pilot project shows elevated concentrations of ^{14}C occurred prior to the bomb-^{14}C pulse that is attributed to discharges from the Sellafield Nuclear and Reprocessing plant. ^{14}C concentrations remain more elevated than in other regions, such as the North Sea, which is ascribed to renewed discharge of ^{14}C from reprocessing at the Sellafield plant after 1985. Ideally, a comparison of sites, close to Sellafield and further from the effects of Sellafield (but with similar water depth) would allow greater deconvolution of radiocarbon fluxes attributable to Sellafield discharge and from testing of the thermonuclear weapons. The latter would also provide data that may be used to calibrate marine radiocarbon dates post-bomb. The present study shows that *A. islandica* is a suitable archive to record ^{14}C in the marine environment. In addition, the use of microcoring should not be used, but rather continuous micromilling (as used in the stable isotope work) is more appropriate.

Summary and future directions

A key aim of this thesis is to understand the potential of *Arctica islandica* for climate reconstruction, in order that findings from this study on live-collected specimens can be applied to dead collected specimens in future studies. The study of trace elements shows that the uptake is complex and cannot, at present, be readily used for quantitative palaeoenvironmental reconstruction. Findings on the behaviour of trace elements within *Arctica islandica* provide insights into processes that may occur not only in other bivalves but also for other aragonitic systems.

The trace elements Sr, Mg and Ba showed heterogeneity within the prismatic layer, with the umbo showing increases in concentration of Sr and Ba away from the maximum growth line (Mg in the umbo was affected by contamination), whereas in the outer shell layer an increase of Sr, Mg and Ba was found.

Sr EXAFS shows that it is substituted for Ca in the aragonite skeleton, indicating that thermodynamic equations and inorganic temperature experiments such as that of Kinsman and Holland (1969) are applicable. Temperature is however not a dominant control in this system, but rather other factors dominant. This may include crystal nucleation and propagation, crystal growth rate (but not shell growth rate) and vital effects. Analysis of changes and impacts on crystal growth could be investigated using critical point drying, which would allow the structure to maintain integrity once etched. This would allow changes in the organic concentration and composition and possible impacts on the crystal shape and propagation also to be understood better, as well as the possibility to accurately measure crystal growth. Particularly when SE images are combined with *in situ* quantitative analysis (either LA-ICPMS or SIMS), it will allow the controls on Sr uptake to be more fully understood.

Of the other trace element systems, XANES analysis indicates that Mg is hosted by organics and inorganic-based thermodynamics are inapplicable to this system. Quantitative analysis of Mg in the umbo by SIMS was complicated by superficial contamination, but the outer shell prismatic layer shows increases spatially associated with increased concentration of organic components at the growth checks consistent with XANES data. However, the relationship between Mg content and organics does not appear to be linear but rather is consistent with vital effects playing a dominant role in controlling Mg uptake into organics. The outlook for Mg as an environmental proxy for temperature is unpromising.

Ba/Ca variation shows sporadic increases in both shells and in both prismatic shell regions- the umbo and the outer shell layer and, although the timings between shells are not identical, those within a single shell are. The cause of sporadic increases in Ba/Ca is unknown but background Ba/Ca may reflect Ba/Ca concentrations within the seawater. Further research with an instrument capable of higher precision Ba/Ca measurements is required to determine if lateral variation occurs at low concentrations.

The oxygen isotope data show the greatest potential of all the proxies in *Arctica islandica* in the present thesis. Concerns about the effect milling and drilling may have on $\delta^{18}O$ is unfounded and any changes in isotopic ratio caused by sampling are within analytical precision.

$\delta^{18}O$ results from *Arctica islandica* show good agreement with the range of SST data (within 2.1 ºC) from Millport marine station, the correlation of individual years with SST is less clear. As modelling highlights, changes in temporal resolution of the sampling, due to changes in the shell growth can significantly affect the $\delta^{18}O$ profile. In particular, changes in growth intra-annually is important, and may be

important in comparing shells where there has been a significant change in the growth season or in examining the impact of vital effects such as growth rate. The $\delta^{13}C$ is strongly influenced by metabolic carbon.

Results from the radiocarbon pilot study show that *Arctica islandica* is a suitable archive of changes in radiocarbon and, in principle, can be used to distinguish discharges of radiocarbon from nuclear reprocessing (in this case the Sellafield plant) and ^{14}C from the testing of thermonuclear weapons. Sampling however should be done using a micromill.

In summary, the future of palaeoenvironmental reconstruction using trace elements fluctuations recorded within *Arctica islandica* is unclear. Trace element incorporation has been shown to be complex, and the study of multiple shells from the same location may yet yield some data on environmental controls. *Arctica islandica* is not however alone in demonstrating complex trace element uptake mechanisms in which vital effects and growth rate play a role. Most aragonitic proxies (e.g. corals, speleothems) have initially appeared simple however, detailed microanalytical studies have in every case demonstrated greater complexity e.g. in speleothems, Holmgren *et al*. (2001) compared to Finch *et al*. (2003b); in corals, Tudhope *et al*. (2001) compared to Allison *et al*. (2005). Nonetheless there are a number of temperature reconstructions from corals using Sr/Ca, which have been published, despite the vital controls (e.g. Beck *et al.*, 1992; Alibert and McCulloch, 1997; Stephans *et al.*, 2004).

Using the average variation of trace element uptake in multiple shells, a technique similar to that used to study coral colonies (Stephans *et al.*, 2004) and trees (see Stokes and Smiley, 1996) may help to extract climate data. However, the costs of such analyses may prohibit this, and insights into environmental controls may be better achieved by examining changes in the width of the growth bands, which can

show growth synchrony (e.g. Thompson *et al.*, 1980a; Marchitto *et al.*, 2000; Schöne *et al.*, 2003).

Ba/Ca peaks are extremely interesting as they are within error for the outer shell prismatic layer and umbo (comparing transects closest to the maximum growth axis). They may provide environmental information as the presence of Ba/Ca peaks in other taxon suggests that there may be a common driving mechanism (Stecher *et al.*, 1996; Putten *et al.*, 2000; Lazareth *et al.*, 2003; Sinclair, 2005; Gillikin *et al.*, 2006). Low Ba/Ca also has the potential to reconstruct Ba/Ca concentrations within the water (e.g. Gillikin *et al.*, 2006). Studies on a larger number of *Arctica islandica* specimens and perhaps other bivalves from the same location will help to understand better the controls on Ba/Ca.

$\delta^{18}O$ measurements show that reconstructed temperatures are within a 2.1 ºC range of SST measurements from Millport. Continuing improvements in understanding the growth season, temporal resolution of sampling, including *in situ* analysis with the ion probe will provide improvements in temporal resolution.

$\delta^{13}C$ measurements show evidence of stress events, which could be used to examine the timing of particular events, such anoxic events (which could be combined with visual analysis to examine shell damage). This may be of particular interest in areas where mass extinction of *Arctica islandica* (or other bivalves) has occurred as it may help to interpret the cause e.g. was it a long-term stress or did it occur through a single event. In addition, further research into the metabolic controls may also help to yield information on the relative uptake of metabolic vs. seawater DIC. The deconvolution of these signals may yield further environmental data, with $\delta^{13}C$ providing important information about DIC within the water column, which is

influenced by variations in primary productivity, upwelling and mixing (Killingley and Berger, 1979; McConnaughey *et al*., 1997; Purton and Brasier, 1997).

References

Aharon P. (1991) Recorders of reef environment histories: stable isotopes in corals, giant clams, and calcareous algae. *Coral Reefs* **10**, 71-90.

Alibert C. and McCulloch M. T. (1997) Strontium/Calcium ratios in modern Porites corals from the Great Barrier Reef as a proxy for sea surface temperature: Calibration of the thermometer and monitoring of ENSO. *Palaeoceanography* **12**, 345-363.

Allison N. and Austin W. E. N. (2003) The potential of ion microprobe analysis in detecting geochemical variations across individual foraminifera tests. *Geochemistry Geophysics Geosystems* **4**(2), 8403, doi:10.1029/2002GC000430.

Allison N. and Finch A. A. (2004) High-resolution Sr/Ca records in modern *Porites lobata* corals: Effects of skeletal extension rate and architecture. *Geochemistry Geophysics Geosystems* **5**(5), Q05001, doi: 1029/2004GC000696.

Allison N., Finch A. A., Tudhope A. W., Newville M., Sutton S. R., and Ellam R. M. (2005) Reconstruction of deglacial sea surface temperatures in the tropical

Pacific from selective analysis of a fossil coral. *Geophysical research letters* **32**, doi:10.1029/2005GL023183.

Allison N. and Finch A. A. (2007) High temporal resolution Mg/Ca and Ba/Ca records in modern *Porites lobata* corals. *Geochemistry Geophysics Geosystems* **8**(5), Q05001, doi:10.1029/2006GC001477.

Ambrose W. G., Carroll M., Greenacre M., Thorrold S. R., and McMahon K. W. (2006) Variation in *Serripes groenlandicus* (Bivalvia) growth in a Norwegian high-Arctic fjord: evidence for local- and large-scale climatic forcing. *Global Change Biology* **12**, 1595-1607.

Amiel A. J., Friedman G. M., and Miller D. S. (1973) Distribution and nature of incorporation of trace elements in modern aragonite corals. *Sedimentology* **20**, 47-64.

Ascough P. L., Cook G. T., Dugmore A. J., Scott E. M., and Freeman S. P. H. T. (2005) Influence of mollusk species on marine delta-R determination. *Radiocarbon* **47**(3), 443-440.

Bard E., Arnold M., Toggweille J. R., Maurice P., and Duplessy L.-C. (1989) Bomb ^{14}C in the Indian Ocean measured by Accelerator Mass Spectrometry: Oceanographic Implications. *Radiocarbon* **31**(3), 510-522.

Beck J. L., Edwards L., Ito E., Taylor F., Recy J., Rougerie F., Joannot P., and Henin C. (1992) Sea surface temperature from coral strontium-calcium ratios. *Science* **257**, 644-647.

Beck J. W., Recy J., Taylor F., Edwards R. L., and Cabioch G. (1997) Abrupt changes in early Holocene tropical sea surface temperature derived from coral records. **385**(6618), 705-707.

Belcher A. M., Wu X. H., Christensen R. J., Hansma P. K., Stucky G. D., and Morse D. E. (1996) Control of crystal phase switching and orientation by soluble mollusc-shell proteins. *Nature* **381**, 56-58 doi:10.1038/381056a0.

Bennett J. T., Turekian K. K., Shaul. W. J., and Ropes J. W. (1982) Using natural radionuclides to measure shell growth rates and ages of the bivalves *Arctica islandica* (Linne) and *Panope generosa* (Gould). *Journal of Shellfish Research* **2**(1), 88-89.

Bice K. L., Arthur M. A., and Maincovich L. J. (1996) Late Paleocene Arctic Ocean shallow-marine temperatures from mollusc stable isotopes. *Paleoceanography* **11**, 241-249.

Bijma J., Spero H. J., and Lea D. W. (1999) Reassessing foramaniferal stable isotope geochemistry: impact of the oceanic carbonate system (experimental results). In *Use of Proxies in Paleoceanography: Examples from the South Atlantic*, (ed. G. Fischer and G. Wefer), pp. 489-512. Springer-Verlag, Berlin.

Bishop J. K. B. (1988) The barite-opal-organic carbon association in oceanic particulate matter. *Nature* **332**, 341-343.

Bohm F., Joachimski M. M., Dullo W.-C., Eisenhauer A., Lehnert H., Reitner J., and Worheide G. (2000) Oxygen isotope of marine aragonite of coralline sponge. *Geochimica et Cosmochimica Acta* **64**, 1695-1703.

Borchardt T. (1985) Physiological energetics of marine molluscs. In *Mollusca* (ed. A. S. M. Saleuddin and K. M. Wilbur), pp. 407-415. Academic Press, New York.

Boyle E. A. (1988) Cadmium: Chemical tracer of deepwater paleoceanography. *Paleoceanography* **3**, 471-489.

Brousseau D. J. (1978) Spawning cycle, fecundity, and recruitment in a population of soft-shell clams, *Mya arenaria*, from Cape Ann, Massachusetts. *Fishery Bulletin* **76**, 155-166.

Buchardt B. and Simonarson L. A. (2003) Isotope paleotemperatures from the Tjörnes beds in Iceland: evidence of Pliocene cooling. *Palaeogeography, Palaeoclimatology, Palaeoecology* **189**, 71-95.

Bunker G. (1997) Elements of XAFS. http://gbxafs.iit.edu/training/xafsoverview.pdf Last Accessed: 11th July 2006

Cage A. G., Heinemeier J., and Austin W. E. N. (2006) Marine radiocarbon reservoir ages in Scottish coastal and fjordic waters. *Radiocarbon* **48(1)**, 31-43.

Campana S. E. (1999) Chemistry and composition of fish otoliths pathways, mechanisms and applications. *Marine Ecology Progress Series* **188**, 263-297.

Carré M., Bentaleb I., Blamart D., Ogle N., Cardenas F., Zevallos S., Kalin R. M., Ortlieb L., and Fontugne M. (2005a) Stable isotopes and sclerochronology of the bivalve *Mesodesma donacium*: Potential application to Peruvian paleoceanographic reconstructions. *Palaeogeography Palaeoclimatology Palaeoecology* **228**, 4-25.

Carré M., Bentaleb I., Fontugne M., and Lavalleé D. (2005b) Strong El Nino events during the early Holocene: stable isotope evidence from Peruvian sea-shells. *The Holocene* **15**, 42-47.

Carré M., Bentaleb I., Bruguier O., Ordinola E., Barrett N. T., and Fontugne M. (2006) Calcification rate influence on trace element concentrations in aragonitic bivalve shells: Evidences and mechanisms. *Geochimica et Cosmochimica Acta* **70**(19), 4906-4920.

Carriker M. R., Swann C. P., Prezant R. S., and Counts C. L. (1991) Chemical elements in the aragonitic and calcitic microstructural groups of shell of the oyster *Crassostrea virginica*: A proton probe study. *Marine Biology* **109**(2), 287-297.

Carriker M. R., Swann C. P., Ewart J., and Counts I., Clement L. (1996) Ontogenetic trends of elements (Na to Sr) in prismatic shell of living *Crassostrea virginica* (Gmelin) grown in three ecologically dissimilar habitats for 28 weeks: a proton probe study. *Journal of Experimental Marine Biology and Ecology* **201**(1-2), 87-135.

Charlier B. L. A., Ginibre C., Morgan D., Nowell G. M., Pearson D. G., Davison J. P., and Ottley C. J. (2006) Methods for the microsampling and high-precision analysis of strontium and rubidium isotopes at single crystal scale for petrological and geochronological applications. *Chemical Geology* **232**, 114-133.

Clark G. R. I. (1980) Techniques for observing the organic matrix of molluscan shells. In *Skeletal Growth in Aquatic Organisms* (ed. D. C. Rhoads and R. A. Lutz), pp. 607-612. Plenum, New York.

Clausen C. D. and Roth A. A. (1975a) Estimation of coral growth-rates from laboratory ^{45}Ca-incorporation rates. *Marine Biology* **33**, 85-91.

Clausen C. D. and Roth A. A. (1975b) Effect of temperature and temperature adaptation on calcification rate in hermatypic coral *Pocillopora damicornis*. *Marine Biology* **33**, 93-100.

Cohen, A. L. and McConnaughey, T. A., 2003. Geochemical perspectives on coral mineralisation. In *Biomineralization, Reviews in Mineralogy and Geochemistry*, **54**, (ed. P. M. Dove, J.J. De Yoreo and S. Weiner), pp 151-187. Mineralogical Society of America.

Coplen T. B., Kendall C., and Hopple J. (1983) Comparison of stable isotope reference samples. *Nature* **302**, 236-238.

Craven J. (2007) Secondary Ion Mass Spectrometry (SIMS). http://www.geos.ed.ac.uk/facilities/ionprobe/SIMS4.pdf Last Accessed: 1st March 2007

Crenshaw M. A. and Neff J. M. (1969) Decalcification at Mantle-Shell Interface in Molluscs. *American Zoologist* **9**(3), 881-889.

Crenshaw M. A. (1980) Mechanisms of Shell Formation and Dissolution. In *Skeletal growth of aquatic organisms* (ed. D. C. Rhoads and R. A. Lutz), pp. 115-132. Plenum Press, New York.

Cross T. S. and Cross B. W. (1983) U, Sr and Mg in Holocene and Pleistocene corals *A.palmata* and *M.annularis*. *Journal of Sedimentary Petrology* **53**(2), 587-594.

Dachille F. and Roy R. (1960) High-pressure phase transformations in laboratory mechanical mixers and mortars. *Nature* **186**, 34, 71.

de Villiers S., Shen G. T., and Nelson B. K. (1994) The Sr/Ca-temperature relationship in coralline aragonite: Influence of variability in $(Sr/Ca)_{seawater}$ and

skeletal growth parameters. *Geochimica et Cosmochimica Acta* **58**(1), 197-208.

de Villiers S., Nelson B. K., and Chivas A. R. (1995) Biological controls on coral Sr/Ca and $\delta^{18}O$ reconstructions of sea surface temperature. *Science* **269**, 1247-1249.

De Yoreo J. J. and Vekilov P. G. (2003) Principles of crystal nucleation and growth. In *Biomineralization, Reviews in Mineralogy and Geochemistry*, **54**, (ed. P. M. Dove, J.J. De Yoreo and S. Weiner), pp 151-187. Mineralogical Society of America.

De Yoreo J. J. and Dove P. M. (2004) Shaping Crystals with Biomolecules. *Science* **306**(5700), 1301-1302.

Dehairs F., Lambert C. E., Chesselet R., and Risler N. (1987) The biological production of marine suspended barite and the barium cycle in the Western Mediterranean Sea. *Biogeochemistry* **4**, 119-139.

Dettman D. L. and Lohmann K. C. (1995) Microsampling carbonates for stable isotope and minor element analysis: physical separation of samples on a 20 micrometer scale. *Journal of Sedimentary Research* **65**, 566-569.

Dettman D. L., Reische A. K., and Lohmann K. C. (1999) Controls on the stable isotope composition of seasonal growth bands in aragonitic fresh-water bivalves (unionidae). *Geochimica et Cosmochimica Acta* **63**(7-8), 1049-1057.

Dietzel M., Gussone N., and Eisenhauer A. (2004) Co-precipitation of Sr^{2+} and Ba^{2+} with aragonite by membrane diffusion of CO_2 between 10 and 50 °C. *Chemical Geology* **203**(1-2), 139-151.

Dodd J. R. and Crisp E. L. (1982) Non-linear variation with salinity of Sr/Ca and Mg/Ca ratios in water and aragonitic bivalve shells and implications for palaeosalinity studies. *Palaeogeography, Palaeoclimatology, Palaeoecology* **38**, 45-56.

Drever R. R. (1980) The geochemistry of natural waters: Englewood Cliffs, 388pp. New Jersey, Prentice-Hall. *Cited in*: Hendry, J.P., Perkins, W.T., Bane, T. 2001 Short-term environmental change in a Jurassic lagoon deduced from geochemical trends in aragonite bivalve shells, *Geological Society of America Bulletin*, **113(6)**, 790-798.

Druffel E. R. M. and Suess H. E. (1983) On the radiocarbon record in banded corals: exchange parameters and net transport of $^{14}CO_2$ between atmosphere and surface ocean. *Journal of Geophysical Research* **88**(C2), 1271-1280.

Druffel E. R. M. (1996) Post-bomb radiocarbon records of surface corals from the tropical Atlantic Ocean. *Radiocarbon* **38**(3), 563-572.

Dugal L. P. (1939) The use of calcareous shell to buffer the product of anaerobic glycolysis in *Venus mercenaria*. *Journal of Cellular and Comparative Physiology* **13**, 235-251.

Dunbar R. B. and Wefer G. (1984) Stable isotope fractionation in benthic foraminifera from the Peruvian continental margin. *Marine Geology* **59**, 215-225.

Elliot M., DeMenocal P. B., Linsley B. K., and Howe S. S. (2003) Environmental controls on the stable isotopic composition of *Mercenaria mercenaria*: potential application to paleoenvironmental studies. *Geochemistry Geophysics Geosystems* **4**, doi:10.1029/2002GC000425.

Epplé V. M. (2004) High-resolution climate reconstruction for Holocene based on growth chronologies of bivalve *Arctica islandica* from the North Sea. PhD Thesis, University of Bremen, pp90.

Epplé V. M., Brey T., Witbaard R., Kuhnert H., and Patzold J. (2006) Sclerochronological records of *Arctica islandica* from the inner German Bight. *The Holocene* **16**(5), 763-769.

Epstein S. and Mayeda T. K. (1953) Variations of the $^{18}O/^{16}O$ ratio in natural waters. *Geochimica et Cosmochimica Acta* **4**, 213-224.

Fairbanks R. G. (1982) The origin of continental shelf and slope water in the New York Bight and Gulf of Maine: Evidence from $H_2{}^{18}O/H_2{}^{16}O$ ratio measurements. *Journal of Geophysical Research* **87**, 5796-5808.

Fairchild I. J., Smith C. L., Baker A., Fuller L., Spötl C., Mattey D., McDermott F., and E.I.M.F. (2006) Modification and preservation of environmental signals in speleothems. *Earth and Planetary Science Letters* **75**, 105-153.

Falini G., Albeck S., Weiner S., and Addadi L. (1996) Control of aragonite or calcite polymorphism by mollusk shell macromolecules. *Science* **271**, 67-69.

Fallon S. J., McCulloch M. T., and Guilderson T. P. (2005) Interpreting environmental signals from the corralline sponge *Astrosclera willeyana*. *Palaeogeography Palaeoclimatology Palaeoecology* **228**, 58-69.

Ferrier-Pagès C., Boisson F., Allemand D., and Tambutté E. (2002) Kinetics of strontium uptake in the scleractinian coral *Stylophora pistillata*. *Marine Ecology Progress Series* **245**, 93-100.

Finch A. A., Shaw P. A., Weedon G. P., and Holmgren K. (2001) Trace element variation in speleothem aragonite: potential for palaeoenvironmental reconstruction. *Earth and Planetary Science Letters* **186**(2), 255-267.

Finch A. A., Allison N., Sutton S. R., and Newville M. (2003a) Strontium in coral aragonite: 1. Characterisation of Sr coordination by EXAFS. *Geochimica et Cosmochimica Acta* **67**(23), 4519-4527.

Finch A. A. and Allison N. (2003) Strontium in coral aragonite: 2. Sr coordination and the long-term stability of coral environmental records. *Geochimica et Cosmochimica Acta* **67**(23), 4519-4527.

Finch A. A., Shaw P. A., Holmgren K., and Lee-Thorp J. (2003b) Corroborated rainfall records from aragonitic stalagmites. *Earth and Planetary Science Letters* **215**, 265-273.

Finch A. A., Allison N., Foster L. C., and Wilson L. (in prep.) Magnesium in palaeoenvironmental carbonates.

Fleming R. (2000) Secondary Ion Mass Spectrometry Theory Tutorial. http://www.me.ust.hk/~mejswu/MECH343/intro%20to%20SIMS.pdf Last Accessed: 15th June 2006

Fritz L. W. (1991) Seasonal condition change, morphometrics, growth and sex ratio of the ocean quahog *Arctica islandica* (Linneaus, 1767) off New Jersey (U.S.A). *Journal of Shellfish Research* **10**(1), 79-88.

Fritz P. and Poplawski S. (1974) ^{18}O and ^{13}C in the shells of freshwater mollusks and their environments. *Earth and Planetary Science Letters* **24**, 91-98.

Fuge R., Palmer T. J., Pearce N. J. G., and Perkins W. T. (1993) Minor and trace element chemistry of modern shells: A laser ablation inductively coupled plasma mass spectrometry study. *Applied geochemistry* **2(Suppl.)**, 111-116.

Gaetani G. A. and Cohen A. L. (2004) Thermodynamic and kinetic controls on element incorporation into aragonite. *Eos Trans. AGU*, **85(47)**, Fall Meeting Supplement, Abstract B14B-01 American Geophysical Union, San Francisco.

Gaetani G. A. and Cohen A. L. (2006) Element partitioning during precipitation of aragonite from seawater: A framework for understanding paleoproxies. *Geochimica et Cosmochimica Acta* **70**(18), 4617-4634.

Gaffey S. J., Kolak J. K., and Bronnimann C. E. (1991) Effects of drying, heating, annealing, and roasting on carbonate skeletal material, with geochemical and diagenetic implications. *Geochimica et Cosmochimica Acta* **55**, 1627-1640.

Galuska A. A. and Morrison G. H. (1987) Distribution analysis of major and trace elements through semiconductor layers of changing matrix using secondary ion mass spectrometry (SIMS). *Pure and applied Chemistry* **59**(2), 229-244.

Gauldie R. W. (1996) Biological factors controlling the carbon isotope record in fish otoliths: principles and evidence. *Comparative Biochemistry and Physiology-Part B: Biochemistry and Molecular Biology* **115B**, 201-208.

Ghosh P., Adkins J., Affek H., Balta B., Guo W. F., Schauble E. A., Schrag D., and Eller J. M. (2006) C-13-O-18 bonds in carbonate minerals: A new kind of paleothermometer. *Geochimica et Cosmochimica Acta* **70**(6), 1439-1456.

Gill I., Olson J. J., and Hubbard D. K. (1995) Corals, paleotemperature records, and the aragonite-calcite transformation. *Geology* **23**(4), 333-336.

Gillikin D. P., Lorrain A., Navez J., Taylor J. W., André L., Keppens E., Baeyens W., and Dehairs F. (2005a) Strong biological controls on Sr/Ca ratios in aragonitic marine bivalve shells. *Geochemistry Geophysics Geosystems* **6**(5), Q05009, doi:10.1029/2004GC000874.

Gillikin D. P., De Ridder F., Ulens H., Elskens M., Keppens E., Baeyens W., and Dehairs F. (2005b) Assessing the reproducibility and reliability of estuarine bivalve shells (*Saxidomus giganteus*) for sea surface temperature reconstruction: Implications for paleoclimate studies. *Palaeogeography Palaeoclimatology Palaeoecology* **228**, 70-85.

Gillikin D. P., Dehairs F., Lorrain A., Steenmans D., Baeyens W., and Andre L. (2006) Barium uptake into the shells of the common mussel (*Mytilus edulis*)

and the potential for estuarine paleo-chemistry reconstruction. *Geochimica et Cosmochimica Acta* **70**(2), 395-407.

Gischler E., Lomando A. J., Alhazeem S. H., Fiebig J., Eisenhauer A., and Oschmann W. (2005) Coral climate proxy data from a marginal reef area, Kuwait, northern Arabian-Persian Gulf. *Palaeogeography Palaeoclimatology Palaeoecology* **228**, 86-95.

Goldschmidt V. M. (1954) Geochemistry. (ed A. Muir), pp730. Clarendon Press, Oxford.

González-Muñoz M. T., Fernández-Luque B., Martínez-Ruiz F., Chekroun K. B., Arias J. M., Rodríguez-Gallego M., Martínez-Cañamero M., Concepción de Linares, and Paytan A. (2003) Precipitation of Barite by *Myxococcus xanthus*: Possible implications of the Biogeochemical cycle of Barium. *Applied and Environmental Microbiology* **69**(9), 5722-5725.

Goodkin N. F., Hughen K. A., and Cohen A. L. (2007) A multicoral calibration method to approximate a universal equation relating Sr/Ca and growth rate to sea surface temperature. *Paleoceanography* **22**, doi:10.1029/2006PA001312.

Goodsite M. E., Rom W., Heinemeir J., Lange T., Ooi S., Appleby P. G., Shotyk W., van der Kannp W. O., Lohse C., and Hansen T. S. (2001) High-resolution AMS ^{14}C dating of post-bomb peat archives of atmospheric pollutants. *Radiocarbon* **43**(2B), 495-515.

Goodwin D. H., Schöne B. R., and Dettman D. L. (2003) Resolution and fidelity of oxygen isotopes as paleotemperature proxies in bivalve mollusk shells: models and observations. *Palaois* **18**, 110-125.

Gordon J. and Carriker M. R. (1978) Growth lines in a bivalve mollusk: Subdaily patterns and dissolution of the shell. *Science* **202**, 519-521.

Gray J., Jones S. R., and Smith A. D. (1995) Discharges to the environment from the Sellafield site, 1951-1992. *Journal of Radiological Protection* **15**(2), 99-131.

Grossman E. L. and Ku T.-L. (1986) Oxygen and carbon isotope fractionation in biogenic aragonite: Temperature effects. *Chemical Geology: Isotope Geoscience section* **59**, 59-74.

Guillong M. (2004) Laser Ablation Inductively Coupled Plasma Mass Spectrometry: Laser ablation system developments and investigations on elemental fractionation. Diplomierter Chemiker der ETH Zurich, pp. 190.

Gunther D. and Heinrich C. A. (1999) Enhanced sensitivity in laser ablation-ICP mass spectrometry using helium-argon mixtures as aerosol carrier. *Journal of Analytical Atomic Spectrometry* **14**, 1363-1368.

Hare P. E. (1983) Amino Acids in the Proteins from Aragonite and Calcite in the Shells of *Mytilus californianus*. *Science* **139**, 216-217.

Hart S. R. and Blusztajn J. (1998) Clams as recorders of ocean ridge volcanism and hydrothermal vent field activity. *Science* **280**, 883-886.

Heilmayer O., Brey T., and Portner O. (2004) Growth efficiency and temperature in scallops: A comparative analysis of species adapted to different temperatures. *Functional Ecology* **18**, 641-647.

Heinemann F., Treccani L., and Fritz M. (2006) Abalone nacre insoluble matrix induces growth of flat and oriented aragonite crystals. *Biochemical and Biophysical Research Communications* **344**(1), 45-49.

Hendry J. P., Perkins W. T., and Bane T. (2001) Short-term environmental change in a Jurassic lagoon deduced from geochemical trends in aragonite bivalve shells. *Geological Society of America Bulletin* **113**(6), 790-798.

Herman A., Addadi L., and Weiner S. (1988) Interactions of sea-urchin skeleton macromolecules with growing calcite crystals- a study of intracrystalline proteins. *Nature* **331**(6156), 546-548.

Hesshaimer V., Heimann M., and Levin I. (1994) Radiocarbon evidence for a smaller oceanic carbon dioxide sink than previously believed. *Nature* **370**(6486), 201-203.

Hinton R. W. (1995) Ion microprobe analysis in geology. In *Microprobe Techniques in the Earth Sciences* (ed. P. J. Potts, J. F. W. Bowles, S. J. B. Reed, and M. R. Cave), pp. 235-290. Chapman and Hall, London.

Holmgren K., Tyson P. D., Moberg A., and Svanered O. (2001) A preliminary 3000-year regional temperature reconstruction for South African. *South African Journal of Science* **97**, 49-51.

Iguchi Y. and Senna M. (1985) Mechanochemical polymorphic transformation and its stationary state between aragonite and calcite I. Effects of preliminary annealing. *Powder Technology* **43**(2), 155-162.

Israelson C. and Buchardt B. (1991) The isotopic composition of oxygen and carbon in some fossil and recent bivalve shells from East Greenland. *LUNDQUA report* **33**, 117-123.

Jarvis I. and Jarvis K. E. (1992) Plasma spectrometry in the Earth Sciences: techniques, applications and future trends. *Chemical Geology* **95**, 1-33.

Jones D. S. (1980) Annual cycle of shell growth increment formation in two continental shelf bivalves and its palaeoecologic significance. *Paleobiology* **6**(3), 331-340.

Jones D. S., Williams D., and Romanek C. S. (1986) Life history of symbiont-bearing clams from stable isotope profiles. *Science* **231**, 46-48.

Kalish J. M. (1989) Otolith microchemistry: validation of the effects of physiology, age and environment of otolith composition. *Journal of Experimental Marine Biology and Ecology* **132**, 151-178.

Kalish J. M. (1991) C-13 and O-18 isotopic disequilibria in fish otoliths: metabolic and kinetic effects. *Marine Ecology Progress Series* **75**, 191-203.

Killingley J. S. and Berger W. H. (1979) Stable isotopes in a mollusk shell: detection of upwelling events. *Science* **205**, 186-188.

Kinsman D. J. J. and Holland H. D. (1969) The co-precipitation of cations with $CaCO_3$-IV. The co-precipitation of Sr^{2+} with aragonite between 16 ºC and 96 ºC. *Geochimica et Cosmochimica Acta* **33**, 1-17.

Klein R. T., Lohmann K. C., and Thayer C. W. (1996a) Sr/Ca and $^{13}C/^{12}C$ ratios in skeletal calcite of *Mytilus trossulus*: Covariation with metabolic rate, salinity, and carbon isotopic composition of seawater. *Geochimica et Cosmochimica Acta* **60**(21), 4207-4221.

Klein R. T., Lohmann K. C., and Thayer C. W. (1996b) Bivalvia skeletons record sea-surface temperature and $\delta^{18}O$ via Mg/Ca and $^{18}O/^{16}O$ ratios. *Geology* **24**, 415-418.

Krantz D. E., Williams D., and Jones D. S. (1987) Ecological and paleoenvironmental information using stable isotope profiles from living and fossil molluscs. *Palaeogeography Palaeoclimatology Palaeoecology* **58**, 249-266.

Kraus M. G., Beal B. F., Chapman S. R., and McMartin L. (1992) A comparison of growth rates in *Arctica islandica* (Linnaeus, 1767) between field and laboratory populations. *Journal of Shellfish Research* **11**(2), 289-294.

Kucera M., Rossell-Melé A., Schneider R., Waelbroeck C., and Weinelt M. (2005) Multiproxy approach for the reconstruction of the glacial ocean surface (MARGO). *Quaternary Science Reviews* **24**, 813-810.

Land L. S., Lang J. C., and Barnes D. J. (1975) Extension rate: A primary control on the isotopic composition of West Indian (Jamaican) scleractinian reef coral skeletons. *Marine Biology* **33**, 221-233.

Lazareth C. E., Putten E. V., Andre L., and Dehairs F. (2003) High-resolution trace element profiles in shells of the mangrove bivalve *Isognomon ephippium*: a record of environmental spatio-temporal variations? *Estuarine, Coastal and Shelf Science* **57**(5-6), 1103-1114.

Lea D. W., Shen G. T., and Boyle E. A. (1989) Coralline barium records temporal variability in equatorial Pacific upwelling. *Nature* **340**, 373–376.

Lea D. W. and Spero H. J. (1992) Experimental determination of barium uptake in shells of the planktonic foraminifera *Orbulina universa* at 22 °C. *Geochimica et Cosmochimica Acta* **56**(7), 2673-2680.

Lea D. W. and Spero H. J. (1994) Assessing the reliability of paleochemical tracers: Barium uptake in the shells of planktonic foraminifera. *Geochimica et Cosmochimica Acta* **56**, 2673-2680.

Levin I. and Kromer B. (1997) Twenty years of high precision atmospheric $^{14}CO_2$ observations at Schauinsland station, Germany. *Radiocarbon* **39(**2), 205-218.

Levin I. and Hesshaimer V. (2000) Radiocarbon- a unique tracer of global carbon cycle dynamics. *Radiocarbon* **42**(1), 69-80.

Lewis D. E. and Cerrato R. M. (1997) Growth uncoupling and the relationship between shell growth and metabolism in the soft shell calm *Mya arenaria*. *Marine Ecology Progress Series* **158**, 177-189.

Liberknecht, L. M., Carwardine, J., Connor, D., Vincent, M. A., Atkins, S. M., and Lumb, C. M. (2004) The Irish Sea Pilot- Report on the identification of nationally important marine area in the Irish Sea, **Report 347**, pp. 176. Joint Nature Conservation Committee.

Longerich H. P., Jackson S. E., and Gunther D. (1996) Laser ablation inductively coupled plasma mass spectrometry analysis of geological samples: a critical evaluation on case studies. *Chemical Geology* **83**, 105-118.

Loosanoff V. L. (1953) Reproductive cycle in *Cyprina islandica*. *Bulletin of Marine Biology Laboratory, Woodshole* **104**, 146-155.

Lorens R. B. (1981) Sr, Cd, Mn, and Co distribution coefficients in calcite as a function of calcite precipitation rate. *Geochimica et Cosmochimica Acta* **45**, 553-561.

Lorrain A., Paulet Y. M., Chauvaud L., Dunbar R. B., Mucciarone D., and Fontugne M. (2004) $\delta^{13}C$ variation in scallop shells: increasing metabolic carbon contribution with body size. *Geochimica et Cosmochimica Acta* **68**, 3509-3519.

Lorrain A., Gillikin D. P., Paulet Y. M., Chauvaud L., Le Mercier A., Navez J., and Andre L. (2005) Strong kinetic effects on Sr/Ca ratios in the calcitic bivalve *Pecten maximus*. *Geology* **33**(12), 965-968.

Lutz R. A. and Rhoads D. C. (1977) Anaerobiosis and a theory of growth line formation. *Science* **198**, 1222-1227.

Lutz R. A. and Rhoads D. C. (1980) Growth Patterns within the Molluscan Shell: an overview. In *Skeletal growth of aquatic organisms: biological records of*

environmental change (ed. D. C. Rhoads and R. A. Lutz), pp. 203-254. Plenum Press, New York.

Lutz R. A. (1981) Electron probe analysis of strontium in mussel (Bivalvia, Mytilidae) shells: Feasibility of estimating water temperature. *Hydrobiologia* **83**, 377-382.

Lutz R. A., Mann R., Goodsell J. G., and Castagna, M. (1982) Larval and early post-larval development of *Arctica islandica*. *Journal of Marine Biological Association, UK* **62**, 745-769

MacDonald B. A. and Thomas M. L. H. (1980) Age determination of the soft-shell clam *Mya arenaria* using shell internal growth lines. *Marine Biology* **58**, 105-109.

Mangerud J., Bondevik S., Gulliksen S., Hufthammer A. K., and Hoisaeter T. (2006) Marine ^{14}C reservoir ages for 19th century whales and molluscs from the North Atlantic. *Quaternary Science Reviews* **25**(24-24), 3228-3245.

Mann K. O. (1992) Physiological, environmental, and mineralogical controls on Mg and Sr concentrations in *Nautilus*. *Journal of Paleontology* **66**(4), 620-636.

Mann S. and Ozin G. A. (2003) Synthesis of inorganic materials with complex form. *Science* **261**, 1286-1292.

Marchitto T., Jones G. A., and Goodfriend G. A. (2000) Precise temporal correlation of Holocene Mollusk shells using sclerochronology. *Quaternary Research* **53**, 236-246.

Marin F. and Luquet G. (2004) Molluscan shell proteins. *Comptes Rendus Palevol* **3**(6-7), 469-492.

Martiniussen. (2001) Sellafield Reprocessing plant in Great Britain, pp. 53. Bellona, Oslo.

McConnaughey T. A. (1989) ^{13}C and ^{18}O isotopic disequilibrium in biological carbonates: 2. in vitro simulation of kinetic isotope effects. *Geochimica et Cosmochimica Acta* **53**, 163-171.

McConnaughey T. A., Burdett J., Whelan J. F., and Paull C. K. (1997) Carbon isotopes in biological carbonates: respiration and photosynthesis. *Geochimica et Cosmochimica Acta* **61**, 611-622.

Miheliç A. (2002) XANES spectroscopy. http://www.p-ng.si/~arcon/xas/xanes/xanes-theory.pdf Last Accessed: 7th December 2006

Mitsuguchi T., Matsumoto E., Abe O., Uchida T., and Isdale P. J. (1996) Mg/Ca Thermometry in Coral Skeletons. *Science* **274**(5289), 961-963.

Mook W. G. and Vogel J. C. (1968) Isotopic equilibrium between shells and their environment. *Science* **159**, 874-875.

Morse J. W. and Bender M. L. (1990) Partition coefficients in calcite: examination of factors influencing the validity of experimental results and their application to natural systems. *Chemical Geology* **82**, 265-277.

Mosselmans F. (2004) X-ray Absorption Fine Structure (XAFS) The basics. http://srs.dl.ac.uk/XRS/courses/summer_files/frame.htm Last Accessed: 7th December 2006

Mosselmans F. (2005) An introduction to X-ray spectroscopy. http://www.srs.dl.ac.uk/xrs/Stations/basics/basic_EXAFS.htm Last Accessed: 27th January 2007

Mucci A. (1987) Influence of temperature on the composition of magnesian calcite overgrowths precipitated from seawater. *Geochimica et Cosmochimica Acta* **51**, 1977-1984.

Mucci A., Canuel R., and Zhong S. (1989) The solubility of calcite and aragonite in sulfate-free seawater and the seeded growth kinetics and composition of the precipitates at 25 °C. *Chemical Geology* **74**(3-4), 309-320.

Murawski S. A., Ropes J. W., and Serchuk F. M. (1982) Growth of the ocean quahog, *Arctica islandica* in the middle Atlantic Bight. *Fishery Bulletin* **80**(1), 21-34.

Nägler T. F., Hart S. R., and Hippler D. (2006) Seasonal Sr/Ca, and $^{44}Ca/^{40}Ca$ co-variation in *Arctica islandica*. *Geophysical Research Abstracts*, **8**, 02256 EGU, Vienna. European Geosciences Union.

Newville M.(2004) XANES spectroscopy

http://cars9.uchicago.edu/xafs/xas_fun/xas_fundamentals.pdf

Last Accessed: 7th December 2006

Nicol D. (1951) Recent species of the Veneroid pelecypod *Arctica*. *Journal of the Washington Academy of Science* **41**, 102-106.

Nydal R., Lövseth K., and Gulliksen S. (1979) A survey of radiocarbon variation in nature since the test ban treaty. *Proceedings of the 9th International Radiocarbon conference*, University of California, Los Angeles.

Nydal R. and Lövseth K. (1983) Tracing bomb ^{14}C in the atmosphere 1962-1980. *Journal of Geophysical Research* **88**(C6), 3621-3642.

Nydal R. (2000) Radiocarbon in the ocean. *Radiocarbon* **42**(1), 81-98.

Oeschger R. (1990) Long-term anaerobiosis in sublittoral marine invertebrates from the western Baltic Sea: *Halicryptus spinulosus* (Priapulida), *Astarte borealis* and *Arctica islandica* (Bivalvia). *Marine Ecology Progress Series* **59**, 133-143.

Oomori T., Kaneshima H., Maezato Y., and Kitano Y. (1987) Distribution coefficient of Mg^{2+} ions between calcite and solution at 10-50 °C. *Marine Chemistry* **20**, 327-336.

Ostermann D. R. and Curry W. B. (2000) Calibration of stable isotopic data: An enriched $\delta^{18}O$ standard used for source gas mixing detection and correction. *Paleoceanography* **15**(3), 353-360.

Ostlund H. G. and Grall C. (1987) North and Tropical Atlantic tritium and radiocarbon; Tritium Laboratory Data Report, pp. 277. R.S.M.A.S.University of Miami.

Owen R., Kennedy H., and Richardson C. (2002) Experimental investigation into partitioning of stable isotopes between scallop (*Pecten maximus*) shell calcite and sea water. *Palaeogeography Palaeoclimatology Palaeoecology* **185**, 163-174.

Palacios R., Orensanz J. M., and Armstrong D. A. (1994) Seasonal and Life-long Variation of Sr/Ca Ratio in Shells of *Mya arenaria* from Grays Harbor (Washington)- an Ancillary Criterion in Demographic Studies. *Estuarine, Coastal and Shelf Science* **39**(4), 313-327.

Paquette J. and Reeder R. J. (1995) Relationship between surface-structure, growth mechanism, and trace element incorporation in calcite. *Geochimica et Cosmochimica Acta* **59**, 735-749.

Patterson W. P., Smith G. R., and Lohmann K. C. (1993) Continental paleothermometry and seasonality using the isotopic composition of aragonitic otoliths of freshwater fishes. *Geophysical Monograph* **78**, 191-202.

Peacock J. D., Graham D. K., Robinson J. E., and Wilkinson I. (1977) Evolution and chronology of Lateglacial marine environments at Lochgilphead, Scotland. In

Studies in the Scottish Lateglacial Environment. (ed. J. M. Gray and J. J. Lowe), pp. 89-100. Pergamon Press, Oxford.

Pearce N. J. G., Perkins W. T., Westgate J. A., Gorton M. P., Jackson S. E., Neal C. R., and Chenery S. P. (1997) A compilation of new and published major and trace element data for NIST SRM 610 and NIST SRM 612 glass reference materials. *Geostandards Newsletters* **21**(115-144).

Pilkey O. H. and Goodell H. G. (1963) Trace element in Recent mollusc shells. *Limnology and Oceanography* **8**, 137-148.

Plummer L. N. and Busenberg E. (1987) Thermodynamics of aragonite-strontianite solid solutions: Results from stoichiometric solubility at 25 and 76 ºC. *Geochimica et Cosmochimica Acta* **51**(6), 1393-1411.

Purton L. M. A. and Brasier M. D. (1997) Gastropod carbonate $\delta^{18}O$ and $\delta^{13}C$ values record strong seasonal productivity and stratification shifts during the late Eocene in England. *Geology* **25**(10), 871-874.

Purton L. M. A., Shields G. A., Brasier M. D., and Grime G. W. (1999) Metabolism controls Sr/Ca ratios in fossil aragonitic mollusks. *Geology* **27**(12), 1083-1086.

Putten E. V., Dehairs F., Keppens E., and Baeyens W. (2000) High resolution distribution of trace elements in the calcite shell layer of modern *Mytilus edulis*: environmental and biological controls. *Geochimica et Cosmochimica Acta* **64**(6), 997-1011.

Reeder R. J. and Grams J. C. (1987) Sector zoning in calcite cement crystals: Implications for trace element distribution in carbonates. *Geochimica et Cosmochimica Acta* **51**, 187-194.

Reeder R. J., Nugent M., Tait C. D., Morris D. E., Heald S. M., Beck K. M., Heiss W. P., and Lanzirotti A. (2001) Coprecipitation of uranium (VI) with calcite: XAFS, micro-XAFS and luminescence characterization. *Geochimica et Cosmochimica Acta* **65**(20), 3491-3503.

Rege S., Jackson S. E., Griffin W. L., Davies R. M., Pearson N. J., and O'Reilly S. Y. (2005) Quantitative trace-element analysis of diamond by laser ablation inductively coupled mass spectrometry. *Journal of Analytical Atomic Spectrometry* **20**(7), 601-611.

Reimer P. J., Brown T. A., and Reimer R. W. (2004) Discussion: reporting and calibration of post-bomb ^{14}C data. *Radiocarbon* **46**(3), 1299-1304.

Richardson C. (2001) Molluscs as archives of environmental change. *Oceanography and Marine Biology* **39**, 103-164.

Rimstidt J. D., Balog A., and Webb J. (1998) Distribution of trace elements between carbonate minerals and aqueous solutions. *Geochimica et Cosmochimica Acta* **62**(11), 1851-1863.

Rollion-Bard C., Mangin D., and Champenois M. (2007) Development and Application of Oxygen and Carbon Isotopic Measurements of Biogenic Carbonates by Ion Microprobe. *Geostandards and Geoanalytical Research* **31**(1), 39-50.

Romanek C. S., Grossman E. L., and Morse J. W. (1992) Carbon isotopic fractionation in synthetic aragonite and calcite: Effects of temperature and precipitation rate. *Geochimica et Cosmochimica Acta* **56**(1), 419-430.

Ropes J. W., Jones D. S., Murawski S. A., Serchuk F. M., and Jearld J. A. (1984) Documentation of annual growth lines in ocean quahog, *Arctica islandica*. *Fishery Bulletin* **82**(1), 1-20.

Rosenberg G. D. and Hughes W. W. (1991) A metabolic model for the determination of shell composition in the bivalve mollusc, *Mytilus edulis*. *Lethaia* **24**, 83-96.

Rosenheim B. E., Swart P. K., and Thorrold S. R. (2005) Minor and trace elements in sclerosponge *Ceratoporella nicholsoni*: Biogenic aragonite near the inorganic endmember? *Palaeogeography Palaeoclimatology Palaeoecology* **228**, 109-129.

Rosenthal Y. and Katz A. (1989) The applicability of trace elements in freshwater shells for paleogeochemical studies. *Chemical Geology* **78**, 65–76.

Rosenthal Y., Boyle E. A., and Slowey N. (1997) Temperature control on the incorporation of magnesium, strontium, fluorine, and cadmium into benthic foraminiferal shells from Little Bahama Bank: Prospects for thermocline paleoceanography. *Geochimica et Cosmochimica Acta* **61**, 3633-3643.

Royal Irish Academy. (2002) Making sense of Sellafield. *Royal Irish Academy Conference*, Dublin, Ireland.

http://www.ria.ie/news/presentations/sellafield%20programme.pdf

Last accessed: 1st March 2007.

Sather W. A. and McCleskey E. W. (2003) Permeation and selectivity in calcium channels. *Annual Review of Physiology* **65**(1), 133-159.

Sato K., Kumagai Y., Kogure T., Watari K., and Tanaka J. (2006) Polymorph and orientation controls of calcium carbonate crystals achieved by organic matrices. *Journal of the Ceramic Society of Japan* **114**(1333), 754-759.

Schöne B. R., Oschmann W., Rossler J., Castro A. D. F., Houk S. D., Kroncke I., Dreyer W., Janssen R., Rumohr H., and Dunca E. (2003) North Atlantic Oscillation dynamics recorded in shells of a long-lived bivalve mollusk. *Geology* **31**(12), 1037-1040.

Schöne B. R., Castro A. D. F., Fiebig J., Houk S. D., Oschmann W., and Kroncke I. (2004a) Sea surface water temperatures over the period 1884-1983 reconstructed from oxygen isotope ratios of a bivalve mollusk shell (*Arctica islandica*, southern North Sea). *Palaeogeography Palaeoclimatology Palaeoecology* **212**(3-4), 215-232.

Schöne B. R., Dunca E., Mutvei H., and Norlund U. (2004b) A 217-year record of summer air temperature reconstructed from freshwater pearl mussels (M-margarifitera, Sweden). *Quaternary Science Reviews* **23**(16-17), 1803-1816.

Schöne B. R., Freyre Castro A. D., Fiebig J., Houk S. D., Oschmann W., and Kroncke I. (2004c) Sea surface water temperatures over the period 1884-1983

reconstructed from oxygen isotope ratios of a bivalve mollusk shell (*Arctica islandica*, southern North Sea). *Palaeogeography, Palaeoclimatology, Palaeoecology* **212**(3-4), 215-232.

Schöne B. R., Fiebig J., Pfeiffer M., Gless R., Hickson J., Johnson A. L. A., Dreyer W., and Oschmann W. (2005a) Climate records from a bivalved Methuselah (*Arctica islandica*, Mollusca; Iceland). *Palaeogeography Palaeoclimatology Palaeoecology* **228**(1-2), 130-148.

Schöne B. R., Houk S. D., Castro A. D. F., Fiebig J., Oschmann W., Kroncke I., Dreyer W., and Gosselck F. (2005b) Daily growth rates in shells of *Arctica islandica*: Assessing sub-seasonal environmental controls on a long-lived bivalve mollusk. *Palaios* **20**(1), 78-92.

Schöne B. R., Pfeiffer M., Pohlmann T., and Siegismund F. (2005c) A seasonally resolved bottom-water temperature record for the period AD 1866-2002 based on shells of *Arctica islandica* (Mollusca, North Sea). *International Journal of Climatology* **25**, 947-962.

Scourse J., Richardson C., Forsythe G., Harris I., Heinemeier J., Fraser N., Briffa K., and Jones P. (2006) First cross-matched floating chronology from the marine

fossil record: data from growth lines of the long-lived bivalve mollusc *Arctica islandica*. *The Holocene* **16**(7), 967-974.

Sharma T. and Clayton R. N. (1965) Measurement of $^{18}O/^{16}O$ ratios of total oxygen of carbonates. *Geochimica et Cosmochimica Acta* **29**, 1347-1353.

Sharp Z. D. (2004) Terminology, standards and mass spectrometry. http://epswww.unm.edu/facstaff/zsharp/505/final%20chapter%202.htm Last Accessed: 15th December 2006

Sinclair D. J., Kinsley L. P. J., and McCulloch M. T. (1998) High resolution analysis of trace elements in corals by laser ablation ICP-MS. *Geochimica et Cosmochimica Acta* **62**(11), 1889-1901.

Sinclair D. J. (2005) Non-river flood barium signals in the skeletons of corals from coastal Queensland, Australia. *Earth and Planetary Science Letters* **237**(3-4), 354-369.

Slota P. J., Jull A. J. T., Linick T. W., and Toolin L. J. (1987) Preparation of small samples for ^{14}C acceleration targets by catalytic reduction of CO. *Radiocarbon* **29**, 303-306.

Stecher I., H. A., Krantz D. E., Lord I., C. J., Luther I., G. W., and Bock K. W. (1996) Profiles of strontium and barium in *Mercenaria mercenaria* and *Spisula solidissima* shells. *Geochimica et Cosmochimica Acta* **60**(18), 3445-3456.

Stephans C. L., Quinn T. M., Taylor F. W., and Correge T. (2004) Assessing the reproducibility of coral-bases climate records. *Geophysical research letters* **31**, doi:10.1029/2004GL020343.

Stokes M. and Smiley T. L. (1996) *An Introduction to Tree-Ring Dating*, 73 pp., University of Arizona Press, Arizona.

Stolarski J. and Mazur M. (2005) Nanostructure of biogenic versus abiogenic calcium carbonate crystals. *Acta Palaeontologica Polonica* **50**(4), 847-865.

Stroobants N., Dehairs F., Goeyens L., Vanderheijden N., and van Grieken R. (1991) *Marine Chemistry* **35**, 411.

Stuiver M. and Polach H. A. (1977) Discussion; reporting of C-14 data. *Radiocarbon* **19**(3), 355-363.

Surge D. and Walker K. J. (2005) Oxygen isotope composition of modern and archaeological otoliths from the estuarine hardhead catfish (*Ariopsis felis*) and

their potential to record low-latitude climate change. *Palaeogeography Palaeoclimatology Palaeoecology* **228**, 179-191.

Swan E. F. (1956) The meaning of strontium- calcium ratios. *Deep Sea Research* **4**, 71.

Swart P. K. and Leder J. (1996) Corals, paleotemperature records, and the aragonite-calcite transformation: Comment and Reply. *Geology* **24**(1), 91-93.

Szulczewski M. D., Helmke P. A., and W.F. B. (1997) Comparison of XANES Analyses and Extractions to determine Chromium Speciation in Contaminated Soils. *Environmental Science and Technology* **31**, 2954-2959.

Takesue R. K. and van Geen A. (2004) Mg/Ca, Sr/Ca, and stable isotopes in modern and Holocene *Protothaca staminea* shells from a northern California coastal upwelling region. *Geochimica et Cosmochimica Acta* **68**(19), 3845-3861.

Tanaka N., Monaghan M. C., and Rye D. (1986) Contribution of metabolic carbon to mollusc and barnacle shell carbonate. *Nature* **320**, 520-523.

Tarutani T., Clayton R. N., and Mayeda T. K. (1969) The effects of polymorphism and magnesium substitution on oxygen isotope fractionation between calcium carbonate and water. *Geochimica et Cosmochimica Acta* **33**, 987-996.

Taylor A. C. and Brand A. R. (1975) Effects of hypoxia and body size on the oxygen consumption of the bivalve *Arctica islandica* (L.). *Journal of Experimental Marine Biology and Ecology* **19**, 187-196.

Taylor A. C. (1976) Burrowing behaviour and anaerobiosis in the bivalve *Arctica islandica* (L.). *Journal of Marine Biological Association, UK* **56**, 95-109.

Taylor R. E. (1987) *Radiocarbon dating: an Archaeological perspective*. Academic Press.

Theede H., Ponat A., Hiroki K., and Schlieper C. (1969) Studies on the resistance of marine bottom invertebrates to oxygen deficiency and hydrogen sulphide. *Marine Biology* **2**, 325-337.

ThermoFinnigan. (2001) Element2 Operator Manual.

Thompson I., Jones D. S., and Dreibelbis D. (1980a) Annual internal growth banding and life history of the ocean quahog, *Arctica islandica* (Mollusca: Bivalvia). *Marine Biology* **57**, 25-34.

Thompson I., Jones D. S., and Ropes J. W. (1980b) Advanced age for sexual maturity in the ocean quahog *Arctica islandica* (Mollusca: Bivalvia). *Marine Biology* **57**, 35-39.

Thórarinsdóttir G. G. (1990) Lifespan of two long lived bivalves *Arctica islandica* and Panopea generosa. *Phuket Marine Biological Center Special Publication, no.* **9(1)**, 41-46. *Cited In*: Sabatini, M. & Pizzola, P.F., 2004. *Arctica islandica*. Icelandic cyprine. Marine Life Information Network: Biology and Sensitivity Key Information Sub-programme [on-line]. Plymouth: Marine Biological Association of the United Kingdom. [cited 16/09/2004]. Available from: <http://www.marlin.ac.uk/species/Arcticaislandica.htm>.

Thorn K., Cerrato R. M., and Rivers M. L. (1995) Elemental distributions in marine bivalve shells as measured by synchrotron X-ray fluorescence. *Biological Bulletin* **188**, 57-67.

Toland H., Perkins W. T., Pearce N. J. G., Keenan F., and Leng M. J. (2000) A study of sclerochronology by laser ablation ICP-MS. *Journal of Analytical Atomic Spectrometry* **15**, 1143-1148.

Toole C. L. and Nielsen R. L. (1992) Effects of microprobe precision on hypotheses related to otolith Sr: Ca ratios. *Fishery Bulletin* **90**, 421-427.

Torres M. E., Barry J. P., Hubbard D. A., and Suess E. (2001) Reconstructing the history of fluid flow at cold seep sites from Ba/Ca ratios in *Vesicomyid* clam shells. *Limnology and Oceanography* **46**, 1701-1708.

Tripati A., Partington J., Elderfield H., Scourse J., Richardson C., Forsythe G., Fraser N., Harris I., Jones P., Briffa K. R., and Heinemeier J. (2004) Controls on Sr/Ca ratios in the aragonite shell of the long-lived clam *Arctica islandica*. *8th International Conference on Paleoceanography, Conference abstracts*, Biarritz, France.

Tudhope A. W., Chilcott C. P., McCulloch M. T., Cook E. R., Chappell J., Ellam R. M., Lea D. W., Lough J. M., and Shimmield G. B. (2001) Variability in the El Niño-Southern oscillation through a glacial-interglacial cycle. *Science* **291**, 1511-1571.

Turekian K. K., Cochran J. K., Nozaki Y., Thompson I., and Jones D. S. (1982) Determination of shell deposition rates of *Arctica islandica* form the New York Bight using natural ^{228}Ra and ^{228}Th bomb produced ^{14}C. *Limnology and Oceanography* **27**(4), 737-741.

Urey H. C. (1947) The thermodynamic properties of isotopic substances. *Journal of Chemical Society (London)*, 562-581.

van Achterbergh E., Ryan C., Jackson S. E., and Griffin W. L. (2001) Data reduction software for LA-ICPMS. In *Laser Ablation-ICPMS in the Earth Sciences*, Vol. 29 (ed. P. Sylvester), pp. 239-243. Mineralogical Association of Canada, Ottawa.

Wada K. and Fujinuki T. (1976) Biomineralization in bivalve molluscs with emphasis on the chemical composition of the extrapallial fluid. In *The Mechanisms of Mineralisation in the Invertebrates and Plants* (ed. T. Watanabe and K. M. Wilbur), pp. 175-190. University of South Carolina Press, Columbia.

Watabe N. and Wilbur K. M. (1960) Influence of the Organic Matrix on Crystal Type in Molluscs. *Nature* **188,** 334, doi:10.1038/188334a0.

Watson E. B. (1996) Surface enrichment and trace-element uptake during crystal growth. *Geochimica et Cosmochimica Acta* **60**(24), 5013-5020.

Watson E. B. (2004) A conceptual model for near-surface kinetic controls on the trace-element and stable isotope composition of abiogenic calcite crystals. *Geochimica et Cosmochimica Acta* **68**(7), 1473-1488.

Wefer G. and Berger W. H. (1991) Isotope paleontology: growth and composition of extant calcareous species. *Marine Geology* **100**, 207-248.

Weidman C. R. and Jones G. A. (1993) A shell-derived time history of bomb ^{14}C on Georges Bank and its Labrador Sea implications. *Journal of Geophysical Research* **98**(C8), 14577-14588.

Weidman C. R. (1993) Development and application of the mollusc *Arctica islandica* as a paleoceanographic tool for the North Atlantic ocean, PhD Thesis, MIT. pp 203.

Weidman C. R., Jones G. A., and Lohmann, K.C. (1994) The long-lived mollusc *Arctica islandica*: a new paleoceanographic tool for the reconstruction of bottom temperatures for the continental shelves of the northern North Atlantic Ocean. *Journal of Geophysical Research* **99**(C9), 18305-18314.

Welberry T. R. (2004) *Diffuse X-Ray Scattering and Models of Disorder*. International Union of Crystallography Monographs on Crystallography, pp. 280. Oxford University Press, Oxford.

Wilbur K. M. (1984) Many minerals, several phyla, and a few considerations. *American Zoologist* **24**, 839-845.

Williams P. (1992) Quantitative analysis using sputtering techniques: secondary ion and sputtered neutral mass spectrometry, In *Practical surface analysis (2nd Ed) Vol 2: Ion and Neutral Spectroscopy*, (ed. D. Briggs, and M. P. Seah), pp 177-228. J. Wiley and Sons, New York.

Witbaard R., Jenness M. I., van de Borg K., and Ganssen G. (1994) Verification of annual growth increments in *Arctica islandica* L. from the North Sea by means of oxygen and carbon isotopes. *Netherlands Journal of Sea Research* **33**, 91-101.

Witbaard R. (1997) Tree of the Sea: the use of the internal growth line in the shell of *Arctica islandica* (Bivalvia, Mollusca) for the retrospective assessment of marine environmental change. PhD Thesis, University of Groningen. pp. 157.

Witbaard R. and Bergman M. J. N. (2003) The distribution and population structure of the bivalve *Arctica islandica* L. in the North Sea: what possible factors are involved? *Journal of Sea Research* **50**, 11-25.

Witbaard R., Jansma E., and Sass Klaassen U. (2003) Copepods link quahog growth to climate. *Journal of Sea Research* **50**, 77-83.

Yu X. and Inesi G. (1995) Variable stoichiometric efficiency of Ca^{2+} and Sr^{2+} transport by the sarcoplasmic-reticulum ATPase. *Journal of Biological Chemistry* **270**, 4361–4367.

Zhong S. and Mucci A. (1989) Calcite and aragonite precipitation from seawater solutions of various salinities: Precipitation rates and overgrowth compositions. *Chemical Geology* **78**(3-4), 283-299.

Zhou G.-T. and Zheng Y.-F. (2003) An experimental study of oxygen isotope fractionation between inorganically precipitated aragonite and water at low temperatures. *Geochimica et Cosmochimica Acta* **67**(3), 387-399.